AD NUMBER

AD020687

NEW LIMITATION CHANGE

TO

Approved for public release, distribution unlimited

FROM

Distribution authorized to U.S. Gov't. agencies and their contractors; Administrative/Operational Use; 31 AUG 1953. Other requests shall be referred to Office of Naval Research, Arlington, VA 22203.

AUTHORITY

26 Oct 1972, ST-A per ONR ltr

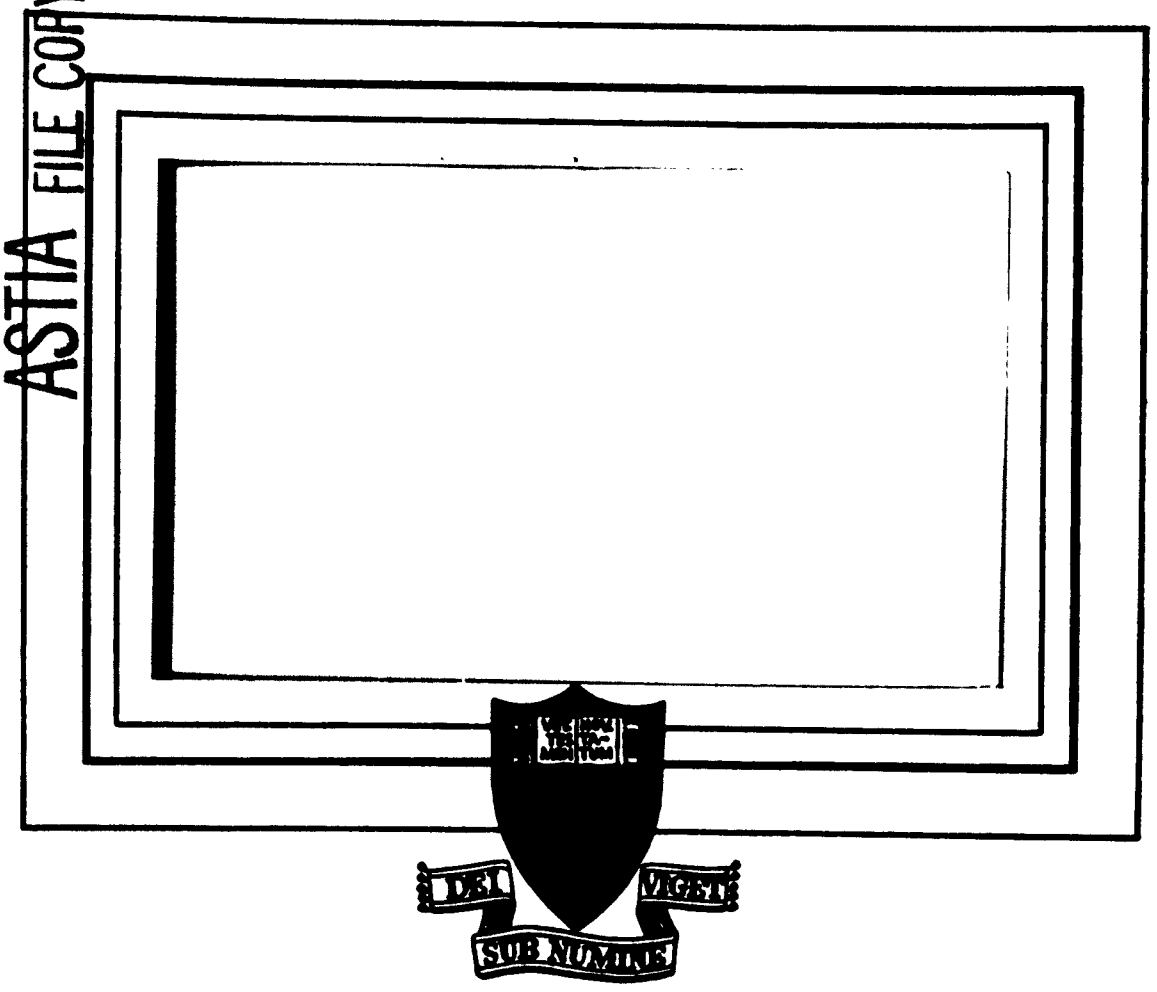

PRINCETON UNIVERSITY

DEPARTMENT OF AERONAUTICAL ENGINEERING

CIRCULATION CONTROL BY MEANS OF TRAILING EDGE SUCTION

(final report)

by

D. C. Hazen
T. E. Sweeney
R. F. Lehnert
F. C. Ringleb

Report No. 239

August 31, 1953

Office of Naval Research
Contract No. N6-onr-27016
Project No. NR 212-011

TABLE OF CONTENTS

LIST OF SYMBOLS AND COEFFICIENTS

α angle of attack, degrees

S area of model, ft.^{2}

V free stream velocity, ft./sec.

Q suction quantity, ft.^{3}/sec.

q free stream dynamic pressure, lbs./ft.^{2}

H_D total pressure in duct, lbs./ft.^{2}

H_o total pressure in free stream, lbs./ft.^{2}

c_l two dimensional lift coefficient

c_d two dimensional drag coefficient

$c_{mc/4}$ two dimensional pitching moment coefficient about the quarter chord point

c_p slot pressure coefficient = $\frac{H_o - H_D}{q}$

c_{dw} two dimensional wake drag coefficient

c_{dm} two dimensional momentum drag coefficient = $2c_q$

c_{de} two dimensional equivalent drag coefficient = $c_q(c_p - 1)$

c_{dt} two dimensional total drag coefficient = $c_{dw} + c_{de}$

c_q suction quantity coefficient = $\frac{Q}{VS}$

Other engineering symbols defined in text.

SUMMARY

A theoretical and experimental investigation of the primary characteristics of trailing edge suction is reported. The theoretical study results in a mathematical method for the prediction of the performance of such a system under limited conditions. The experimental study confirms the theory and extends the investigation to the determination of the effect of suction slot geometry on the lift, drag, pitching moment and power requirement for such a system. In addition, an attempt has been made to relate the significant geometry of the airfoil-slot combination to the measured lift increase.

INTRODUCTION

One of the operational requirements limiting the over-all performance of an aircraft is the necessity of designing for reasonably safe landing speeds. As aircraft maximum speeds have increased the speed range of the airplane has not, in general, kept pace. This has necessarily resulted in pushing the landing speed to the highest acceptable limits and perhaps in several instances even beyond these limits. Of course, this is well recognized and designers have made extensive use of high lift devices to achieve even the marginal landing speeds that are now accepted. However, as operational aircraft grow heavier and faster and retain the same limits on size (as in the case of carrier borne aircraft) the landing speed generally must increase.

For Naval operations, the significant speed is that of deck touch-down and since this speed has about reached its upper limit, a new approach for safe carrier landings is desirable. One means would be to build the carrier larger and faster. The alternative, of course, is to provide the airplane with a lower landing speed. Since compromise dominates every phase of airplane design and operation, it is probable that a compromise will be reached here to make the future carrier compatible with the future naval aircraft.

If present trends hold, wing loadings will continue to increase. This, of course, suggests that a solution to the problem is to find a means of increasing the airplane lift coefficient beyond that achieved with flaps and/or slots. Several schemes designed to increase the lift coefficient of a profile, at a given angle of attack, have been advanced over the years and they have generally involved either blowing across some portion of the wing or suction at some station on the profile. In both systems, the boundary layer is affected, either energized with blowing or removed with suction. A combination of blowing and suction has been used and seems to have some advantage. There is, however, a limit to the amount of influence blowing or suction may have upon the boundary layer. Beyond this limit lift continues to increase at a lower rate, for the case of a trailing edge suction slot, seemingly due to the direct influence of the sink upon the adjacent free streamlines. For this reason, the term circulation control or, more recently, super circulation has been applied to these devices. A lift increase caused by the removal of some portion of the boundary layer is equivalent to an increased circulation. Therefore, strictly speaking, it seems improbable that the two types of lift increase can be separated and the system is finally one of increasing circulation by one means or another. Thus small amounts of suction remove the boundary layer, or some portion of the boundary layer, thereby permitting the bordering streamlines to follow more closely the pattern of potential flow resulting in increased circulation. Larger quantities of suction seem to influence the adjacent streamlines directly, inducing a greater downward component to the flow which again provides greater lift and, of course, more circulation.

Princeton University became interested in this phase of low speed flight research with a suggestion from the Office of Naval Research, Air Branch, that

the validity of the early Regenscheit[1] work, in the field of boundary layer control by trailing edge suction slots, be investigated. This was formalized by Contract Number N6-onr-27016 in March of 1951 between the Office of Naval Research, Air Branch and Princeton University, to conduct a general investigation of trailing edge suction.

The program of investigation subsequently setup was both extensive regarding slot shape and location and intensive with respect to the thousands of individual measurements of lift, drag, pitching moment, suction quantity and power requirement of the various configurations tested. Since the effects of the several variables of a trailing edge suction slot were largely unknown quantities, it was decided to limit the study to the airfoil without a flap. Future experiments are to be made, however, which will include a flap study.

This report deals with the problem of trailing edge suction both theoretically and experimentally. The principal aim has been to understand and evaluate the mechanics of the suction slot geometry. Since any system of circulation control must be evaluated with respect to a given design, the results reported here should be helpful in such an evaluation.

1. Reference 1.

DISCUSSION

I. THEORY OF TRAILING EDGE SUCTION

In order to understand the basic mechanics of increased circulation due to trailing edge suction, it is first necessary to examine the possible flow patterns. When these flows are understood, it becomes possible to arrive theoretically at an expression relating ΔC_l , C_Q and a suction slot parameter.

A. Determination of the Type of Flow:

A study of the flow pattern necessarily requires that consideration be given to the location of the stagnation points. In general, it may be stated that a stagnation point leaves the lower lip of the trailing edge for the free stream if the suction coefficient exceeds a certain value. This can be, and has been, visualized in a smoke tunnel study. The lift and the suction quantity at the instant the stagnation point leaves the profile can be determined theoretically. This point may be considered the combination of two stagnation points, one of them being located on the trailing edge satisfying the Kutta-Joukouski condition, and the other located between the sink and the trailing edge (See Figure 1-a and 1-b). The stagnation point T moves aft with increasing suction until it reaches the trailing edge where it is combined with T_2 . Any increase in suction coefficient forces this combined stagnation point to the free stream (see Figure 1-c and 1-d).

Figures 2-a, 2-b, and 2-c illustrate flow conditions that are theoretically possible and predictable under certain circumstances. In these T continues to move around the trailing edge to the lower surface of the profile. The case is shown (Figure 2-b) where T meets the stagnation point T_1 moving aft on the under surface. An increase of suction coefficient at this point causes this combined stagnation point to jump to the free stream as shown in Figure 2-c. The motion of the stagnation points can be studied analytically in the following way. The function

$$z = f(\zeta)$$

yields a one to one conformal representation of the area $|\zeta| > 1$ into the outside of the profile (in the z-plane) in such a way that

$$f(\infty) = \infty , \quad \left(\frac{dz}{d\zeta}\right)_{\zeta=\infty} = 1$$

so that $\zeta = 1$ corresponds to the trailing edge of the profile. This flow, having a sink at the point corresponding to $\zeta = e^{i\beta}$, can be represented by the complex potential function

$$\chi = w_0\left(e^{-i\alpha}\zeta + \frac{e^{i\alpha}}{\zeta}\right) + \frac{Q + \Gamma_1}{2\pi}\ln\zeta - \frac{Q}{\pi} - e^{i\beta} \qquad (1)$$

For a stagnation point ζ is valid

$$\frac{dz}{d\zeta} = \omega_0\left(e^{-i\alpha} - \frac{e^{i\alpha}}{\zeta^2}\right) + \frac{Q+\Gamma i}{2\pi}\frac{1}{\zeta} - \frac{Q}{\pi}\frac{1}{\zeta - e^{i\beta}} = 0 \qquad (2)$$

For the stagnation point on the trailing edge $\zeta = 1$

$$\omega_0\left(e^{-i\alpha} - e^{i\alpha}\right) + \frac{Q+\Gamma i}{2\pi} - \frac{Q}{\pi}\frac{1}{1-e^{i\beta}} = 0 \qquad (3)$$

Subtracting (3) from (2) yields:

$$\omega_0 e^{i\alpha}\left(1 - \frac{1}{\zeta^2}\right) - \frac{Q+\Gamma i}{2\pi}\left(1 - \frac{1}{\zeta}\right) - \frac{Q}{\pi}\frac{1-\zeta}{(1-e^{i\beta})(\zeta - e^{i\beta})} = 0$$

Dividing thru by $\zeta - 1$ results in

$$\omega_0 e^{i\alpha}\frac{\zeta+1}{\zeta^2} - \frac{Q+\Gamma i}{2\pi}\frac{1}{\zeta} + \frac{Q}{\pi}\frac{1}{(1-e^{i\beta})(\zeta - e^{i\beta})} = 0$$

Multiplication by $(\zeta - e^{i\beta})\zeta^2$

$$\left(\omega_0 e^{i\alpha} - \frac{Q+\Gamma i}{2\pi} + \frac{Q}{\pi}\frac{1}{1-e^{i\beta}}\right)\zeta^2 + \qquad (4)$$

$$\left[\omega_0 e^{i\alpha}(1-e^{i\beta}) + \frac{Q+\Gamma i}{2\pi}e^{i\beta}\right]\zeta - \omega_0 e^{i(\alpha+\beta)} = 0$$

It follows from (3) that

$$\frac{Q+\Gamma i}{2\pi} = \frac{Q}{\pi}\frac{1}{1-e^{i\beta}} - \omega_0\left(e^{-i\alpha} - e^{i\alpha}\right)$$

Substituting in (4) yields

$$\omega_0 e^{-i\alpha}\zeta^2 - \omega_0 e^{i(\alpha+\beta)} +$$

$$\left[\omega_0 e^{i\alpha}(1-e^{i\beta}) + \frac{Q}{\pi}\frac{e^{i\beta}}{1-e^{i\beta}} - \omega_0(e^{-i\alpha} - e^{i\alpha})e^{i\beta}\right]\zeta = 0$$

or

$$\zeta^2 + \left(e^{2i\alpha} - e^{i\beta} + \frac{Q}{\pi\omega_0}\frac{e^{i(\alpha+\beta)}}{1-e^{i\beta}}\right)\zeta - e^{i(2\alpha+\beta)} = 0$$

This may be re-written as

$$\left[e^{-i(\alpha+\beta/2)}\zeta\right]^2 +$$

$$\left[e^{i(\alpha-\beta/2)} - e^{-i(\alpha-\beta/2)} + \frac{Q}{\pi\omega_0}\frac{e^{i\beta/2}}{1-e^{i\beta}}\right]\left[e^{-i(\alpha+\beta/2)}\zeta\right] - 1 = 0$$

or

$$\left[e^{-i(\alpha+\beta/2)}\zeta\right]^2 + i\left[2\sin(\alpha-\beta/2) + \frac{Q}{2\pi\omega_0}\frac{1}{\sin\beta/2}\right]\left[e^{-i(\alpha+\beta/2)}\zeta\right] - 1 = 0 \quad (5)$$

In addition to the stagnation point $\zeta = 1$ there are two other stagnation points as solutions of equation (5). By denoting

$$S = \sin(\alpha-\beta/2) + \frac{Q}{4\pi\omega_0}\frac{1}{\sin\beta/2} \quad (6)$$

the solutions become

$$\zeta = e^{i(\alpha+\beta/2)}\left(-iS \pm \sqrt{1-S^2}\right) \quad (7)$$

For fixed values of α, β, ω_0 the values of S are variable with the amount of suction Q. This variation is such that S increases with Q if $\beta > 0$. If $|S|<1$, then

$$|\zeta| = \left|iS \pm \sqrt{1-S^2}\right| = 1 \quad (8)$$

which means that both stagnation points are located on the circle $|\zeta|=1$. To these correspond, due to $z = f(\zeta)$, two stagnation points on the profile surface. If, however, $|S|>1$ then

$$\zeta = ie^{i(\alpha+\beta/2)}\left(-S \pm \sqrt{S^2-1}\right)$$

or

$$\zeta = e^{i(\pi/2+\alpha+\beta/2)}\left(-S \pm \sqrt{S^2-1}\right) \quad (9)$$

One of these points is outside the circle (see Figure 3) $|\zeta| = 1$, on the radius which is inclined at the angle $\alpha + \beta/2$ from the negative η axis, the distance being $S + \sqrt{S^2-1}$ from O. The other point is situated inside the circle on the same radius, the distance, in this case, being

$S - \sqrt{S^2-1}$ from O. Only the first of these is of interest since it corresponds to a stagnation point outside the profile in the z-plane. With increasing suction (Q) this point moves toward infinity in the free stream and the condition for its existance is

$$|S| > 1 \quad (10)$$

Obviously, the determination of which of these flow patterns can be expected is of basic importance to the understanding of trailing edge suction. A smoke tunnel experiment (See Figure 4) clearly proved that the free stream stagnation point of Figure 1-d is the solution with physical significance. With a stagnation point of this type, flow around the lower trailing edge occurs which greatly reduces the effect of trailing edge suction. Hence, unless measures are taken to prevent this motion of the stagnation points, the value of suction coefficient which causes the two stagnation points to combine

at the trailing edge can be considered the practical upper limit for this means of increasing lift.

B. Lift Increase due to Trailing Edge Suction:

The theoretical developments presented in this section are based upon a normal wing profile with a small suction slot located on the upper surface. It will be assumed that this slot has parallel straight walls and that suction is produced by a sink S situated within the slot. To satisfy continuity requirements, a source of equal strength must be assumed to be located at infinity. It is further assumed that the profile is at an angle of attack α in a uniform flow field having the velocity w_∞ at infinity. Figure 5 indicates the resulting flow field for a moderate suction quantity. For this suction quantity a stagnation point P appears on the upper surface of the profile between the suction slot and the trailing edge. (This is also illustrated by Figure 6). The flow leaves the trailing edge smoothly, indicating the presence of a stagnation point attached to the profile at this point and hence the Kutta-Joukowski condition is satisfied as in the case of no suction. A third stagnation point is, of course, situated near the nose of the profile.

The two-dimensional potential flow of an incompressible fluid satisfying these conditions can be determined in the classical manner. To do this, the outside of the profile in the $z = x + iy$ plane is transformed conformally to the outside of a circle of unit radius in the $\zeta = \xi + i\eta$ plane in such a way that the infinite points of the two planes correspond and that the size and position of the profile in the z plane is such that $dz/d\zeta = 1$ for $\zeta = \infty$ and $\zeta = 1$ corresponds to the trailing edge of the profile. (See Figure 5). Under these conditions, the transformation is determined uniquely and the region outside of the circle $|\zeta| = 1$ has an expansion of the form

$$z = f(\zeta) = \zeta + \frac{c_1}{\zeta} + \frac{c_2}{\zeta^2} + \cdots \tag{11}$$

Under the restrictions of the transformation, the x-axis corresponding to $\alpha = 0$ is at the same time the axis of zero lift without suction. The length of the profile is determined by the transformation and has a value approximately equal to four.

As a result of the transformation, a well defined point, $\zeta = e^{i\beta}$, where β is the arc of the circle between the points corresponding to the trailing edge and the slot, corresponds to the slot exit on the profile. More rigorously, the point determined by β corresponds to the sink within the slot, and the slot walls correspond to two small arcs adjacent to β if the inside of the slot is included in the transformation. If, however, the slot is considered infinitesimally small, β defines a point which corresponds to the slot including the sink as a limit.

The flow under discussion is determined by the complex potential function:

$$\chi = w_\infty \left(\zeta e^{-i\alpha} + \frac{1}{\zeta e^{-i\alpha}}\right) + \frac{\Gamma i}{2\pi} \ln \zeta + \frac{Q}{2\pi}\left[\ln \zeta - 2\ln(\zeta - e^{i\beta})\right] \tag{12}$$

The first term represents the parallel flow at an angle of attack α around the circle, the second term a circulation (vortex) around the circle with strength Γ. The third term results from a source with the strength Q at $\zeta=0$, a source of equal strength at $\zeta=\infty$ and sink with the strength -2Q at $\zeta = e^{i\beta}$ so that the strength of this sink with respect to the flow outside the circle is equal to -Q, where Q is measured in units of volume per unit span and time. The source at $\zeta=0$ inside the circle is added in order to obtain the contour of the circle as a streamline. The flow represented by $z = z(\zeta)$ is transformed by $z = f(\zeta)$ to a flow with corresponding singularities in the plan of the profile.

The complex velocity function may be expressed as

$$\frac{dz}{dz} = \frac{1}{f'(\zeta)}\frac{dz}{d\zeta} = w e^{-i\theta} \tag{13}$$

where $f'(\zeta) = \frac{dz}{d\zeta}$, w is the velocity and θ is the direction of the flow at a point in the z plane. Thus, for a stagnation point in the z plane $\frac{dz}{dz} = 0$.

Hence, for a point $\zeta = e^{i\gamma}$ to correspond to a stagnation point on the profile, $\frac{dz}{d\zeta}$ must equal zero at the point, with the further condition that $f'(\zeta) = \frac{dz}{d\zeta}$ is not zero or is at least of smaller order than $\frac{dz}{d\zeta}$.

Differentiation of equation (12) yields:

$$\frac{dz}{d\zeta} = w_0\left(e^{-i\alpha} - \frac{e^{i\alpha}}{\zeta^2}\right) + \frac{\Gamma i}{2\pi}\frac{1}{\zeta} + \frac{Q}{2\pi}\left(\frac{1}{\zeta} - \frac{2}{\zeta - e^{i\beta}}\right)$$

For a stagnation point $\zeta = e^{i\gamma}$ on the circle $|\zeta|=1$ it is necessary that $\frac{dz}{d\zeta} = 0$. Therefore;

$$w_0\left(e^{-i\alpha} - e^{i(\alpha-2\gamma)}\right) + \frac{\Gamma i}{2\pi}e^{-i\gamma} + \frac{Q}{2\pi}\left(e^{-i\gamma} - \frac{2}{e^{i\gamma} - e^{i\beta}}\right) = 0$$

Multiplying by $e^{-i\gamma}$:

$$w_0\left(e^{i(\gamma-\alpha)} - e^{-i(\gamma-\alpha)}\right) + \frac{\Gamma i}{2\pi} + \frac{Q}{2\pi}\left(1 - \frac{2}{1 - e^{i(\beta-\gamma)}}\right) = 0$$

or

$$w_0\left(e^{-i(\alpha-\gamma)} - e^{i(\alpha-\gamma)}\right) + \frac{\Gamma i}{2\pi} - \frac{Q}{2\pi}\frac{1+e^{i(\beta-\gamma)}}{1-e^{i(\beta-\gamma)}} = 0$$

now

$$e^{i(\alpha-\gamma)} - e^{-i(\alpha-\gamma)} = 2i\sin(\alpha-\gamma)$$

and $$\frac{e^{i\frac{\beta-\gamma}{2}} + e^{-i\frac{\beta-\gamma}{2}}}{e^{i\frac{\beta-\gamma}{2}} - e^{-i\frac{\beta-\gamma}{2}}} = -i\cot\frac{\beta-\gamma}{2}$$

Therefore
$$\Gamma = 4\pi\omega_0 \sin(\alpha-\gamma) + Q\cot\frac{\beta-\gamma}{2} \tag{14}$$

where the angle γ determines the position of any stagnation point. Since the point $\zeta=1$ (i.e. $\gamma=0$) is supposed to be a stagnation point in accordance with the Kutta-Joukowski condition, the relationship simplifies to

$$\Gamma = 4\pi\omega_0 \sin\alpha + Q\cot\beta/2 \tag{15}$$

Thus the circulation is determined by the velocity ω_0, the angle of attack α, the position β and the strength Q of the sink.

The suction coefficient c_Q is generally defined as

$$c_Q = \frac{Q}{\omega_0 S} \tag{16}$$

where S is the wing area, ω_0 the free stream velocity and Q the volume of suction per unit time. In the preceeding discussion, a unit span has been assumed, thus if C is the profile chord length, c_Q may be defined as

$$c_Q = \frac{Q}{C\omega_0} \tag{16a}$$

where C is approximately equal to four. If Γ is now eliminated from equation 15 and 16, one obtains the coefficient

$$c_Q = \frac{-4\pi\sin(\alpha-\gamma) - \sin\alpha}{C\cot\frac{\beta-\gamma}{2} - \cot\frac{\beta}{2}}$$

which simplifies to

$$c_Q = \frac{8\pi}{C}\cos(\alpha-\gamma/2)\sin\beta/2\cdot\sin\frac{\beta-\gamma}{2} \tag{17}$$

From this relation one can determine how the stagnation point between the suction slot and the trailing edge, defined by γ, moves with changing c_Q.

As previously explained, a case of special interest occurs when c_Q is increased sufficiently to cause this stagnation point to reach the trailing edge. In this case γ reaches the limit zero and one obtains the value

$$c_Q^* = \frac{8\pi}{C}\cos\alpha\cdot\sin^2\beta/2 \tag{18}$$

where c_Q^* is the highest suction coefficient for which trailing edge suction is practical.

The components, X and Y, of the force acting on the outside of the profile due to the pressures produced by the flow, can be determined from Blasius' equation:

$$Y + iX = -\rho/2 \oint_C \left(\frac{dw}{dz}\right)^2 dz \tag{19}$$

where ρ is the density of the fluid. In this particular case, the curve of integration C which must be considered, is the surface contour of the profile up to the slot, the parallel sides of the slot and a perpendicular connection between the sides of the slot. When transformed into the ζ-plane equation 19 becomes

$$Y + iX = -\rho/2 \oint_K \left(\frac{dw}{d\zeta}\right)^2 \Big/ \frac{dz}{d\zeta}\, d\zeta \tag{20}$$

The curve of integration K now consists of the circle $|\zeta| = 1$ up to a small half circle excluding the point $\zeta = e^{i\beta}$ from the outside region and of this small half circle itself which corresponds to the connection of the slot walls. This curve K can be deformed into a large circle around $\zeta = 0$ because there are no singularities of the integrand outside K except those at infinity.

Differentiation and simplification of equation 12 yields:

$$\frac{dw}{d\zeta} = w_0\left(e^{-i\alpha} - \frac{e^{i\alpha}}{\zeta^2}\right) + \frac{Q + \Gamma i}{2\pi}\,\frac{1}{\zeta} - \frac{Q}{\pi}\,\frac{1}{\zeta - e^{i\beta}}$$

Expanding this expression into a power series of $\frac{1}{\zeta}$ using the expansion

$$\frac{1}{\zeta - e^{i\beta}} = \frac{1}{\zeta}\left(1 + \frac{e^{i\beta}}{\zeta} + \frac{e^{2i\beta}}{\zeta^2} + \cdots\right)$$

results in

$$\frac{dw}{d\zeta} = w_0 e^{-i\alpha} + \frac{\Gamma i - Q}{2\pi}\,\frac{1}{\zeta} - \left(w_0 e^{i\alpha} + e^{i\beta}\right)\frac{1}{\zeta^2} + \cdots$$

and

$$\left(\frac{dw}{d\zeta}\right)^2 = w_0^2 e^{-2i\alpha} + \frac{w_0}{\pi} e^{-i\alpha}\left(\Gamma i - Q\right)\frac{1}{\zeta} + \cdots$$

The function $\frac{dz}{d\zeta} = f'(\zeta)$ has the expansion

$$\frac{dz}{d\zeta} = 1 - \frac{c_1}{\zeta^2} - \frac{2c_2}{\zeta^3} - \cdots$$

Equation 20 yields then

$$Y + iX = -\rho/2 \oint_K \left[\omega_0^2 e^{-2i\alpha} + \frac{\omega_0}{\pi} e^{-i\alpha}(\Gamma i - Q)\frac{1}{\zeta} + \ldots\right] \cdot \left[1 + \frac{c_1}{\zeta^2} + \ldots\right] d\zeta$$

or

$$Y + iX = -\rho/2 \oint_K \left[\omega_0^2 e^{-2i\alpha} + \frac{\omega_0}{\pi} e^{-i\alpha}(\Gamma i - Q)\frac{1}{\zeta} + \ldots\right] d\zeta$$

or

$$Y + iX = \rho\omega_0(\Gamma + Qi)e^{-i\alpha} \tag{21}$$

The components of this force parallel and perpendicular to the free stream direction are the drag, d, and the lift, ℓ; therefore,

$$\ell + id = (Y + iX)e^{i\alpha}$$
$$= \rho\omega_0(\Gamma + Qi)$$

Thus

$$\ell = \rho\omega_0\Gamma, \qquad d = \rho\omega_0 Q \tag{22}$$

This result has been derived by C. B. Smith[1]. Substituting the value of Γ from equation 15 into equation 22, one obtains

$$\ell = \rho\omega_0(4\pi\omega_0 \sin\alpha + Q\cot\beta/2) \tag{23}$$

By definition the lift coefficient is

$$C_\ell = \frac{\ell}{\rho/2\, c\, \omega_0^2} \tag{24}$$

Substituting equations 23 and 16-a in equation 24 yields

$$C_\ell = \frac{8\pi}{c}\sin\alpha + 2C_Q\cot\beta/2 \tag{25}$$

An examination of equation (25) reveals that the lift coefficient consists of $\frac{8\pi}{c}\sin\alpha$, as predicted for the zero suction case by classical aerodynamics, plus a term

$$\Delta C_\ell = 2C_Q\cot\beta/2 \tag{26}$$

due to suction. When the stagnation point, P, reaches the trailing edge, the expression for the lift increase becomes

1. See Reference 2.

$$\Delta C_{\ell}^{*} = 2\pi \cos\alpha \sin\varepsilon \qquad (27)$$

which represents the upper practical limit for trailing edge suction.

C. The Determination of β in the Case of Trailing Edge Suction.

If the suction slot is small and enters the surface of a profile with parallel walls, the value of β can be found by the conformed mapping of the profile into a circle as previously described. If, however, as is usually the case of trailing edge suction, the end of the profile has been cut off so that the edges of the upper and lower surfaces form the slot entrance, then the conformal mapping of the original profile will not lead to a correct determination of β. This arrangement has now to be treated as an entirely new profile like that of Figure 7, the location of the real slot being indicated by an arrow.

For this condition the following procedure is proposed. The edge of the longer lip of the trailing edge (usually the lower lip) is connected by a straight line to the mid point of the radius connecting the center of curvature of the leading edge to the leading edge. This straight line is then considered a slot and the region surrounding it is transformed conformally to the region outside a circle. If the straight line connects the points $z = -R$ and $z = +R$ in the plane of the profile, the transformation to be applied is the inverse transformation of

$$z = \tfrac{1}{2}\left(\zeta + \frac{R^2}{\zeta}\right) \qquad (28)$$

(the Joukowski transformation) or

$$\zeta = z + \sqrt{z^2 - R^2} \qquad (29)$$

This transformation is frequently applied in order to transform a profile into a nearly circular curve. The numerical computation of $\zeta = \xi + i\eta$ as a function of $z = x + iy$ can be performed by expressing ζ in terms of polar coordinates

or $$\zeta = r e^{i\phi}$$

and substituting this in equation 28 yielding

$$z = \tfrac{1}{2}\left(r e^{i\phi} + \frac{R^2}{r} e^{-i\phi}\right)$$

By separating the real and imaginary parts

$$\left.\begin{aligned} x &= \tfrac{1}{2}\left(r + \frac{R^2}{r}\right)\cos\phi \\ y &= \tfrac{1}{2}\left(r - \frac{R^2}{r}\right)\sin\phi \end{aligned}\right\} \qquad (30)$$

Substituting in equation 30 for r

$$r = R e^{\theta}$$

where Θ is a new variable, results in

$$X = R \cosh \Theta \cdot \cos \phi$$

$$Y = R \sinh \Theta \cdot \sin \phi$$

and

$$\frac{X^2}{R^2 \cosh^2 \Theta} + \frac{Y^2}{R^2 \sinh^2 \Theta} = 1 \tag{31}$$

Replacing $\sinh^2 \Theta$ in equation 31 by $(\cosh^2 \Theta - 1)$, one obtains an algebraic equation of second order in $\cosh^2 \Theta$. The solution of this equation yields

$$\cosh^2 \Theta = \tfrac{1}{2}\left(\frac{X^2+Y^2}{R^2} + 1\right) + \sqrt{\tfrac{1}{4}\left(\frac{X^2+Y^2}{R^2} + 1\right)^2 - \frac{X^2}{R^2}} \tag{32}$$

Knowing $\cosh \Theta$, the relation

$$\cos \phi = \frac{X}{R \cosh \Theta} \tag{33}$$

may be applied and

$$\gamma = R e^{\Theta} \tag{34}$$

then

$$\xi = \gamma \cos \phi \qquad \eta = \gamma \sin \phi \tag{35}$$

Figure 8 shows the transformed profile points of figure 7 where the trailing edge of a NACA 23015 airfoil has been cut off 10% on the upper side and 5% on the lower side. The transformed profile is now approximated by two tangential circular arcs, one ending at the upper edge A and the other ending at the point $\xi = R$. Both arcs are tangent at a point C somewhere near the point corresponding to the profile leading edge. A third circle, orthogonal to these two, passing through A and C is now considered. This circle (in this example a straight line) intersects the upper arc RC at the point B. The arc AB now corresponds to a curve in the z-plane which closes the profile by connecting the edge of the upper lip with a point on the line between -R and +R forming the upper boundary of the lower lip. This connection is perpendicular to both lips and can, as an approximation, be replaced by a small circular arc. On this connection the slot entrance S (sink) with parallel sides is assumed as indicated by the arrow in Figure 8. This configuration corresponds very closely to the normal geometry of a profile with trailing edge suction.

A transformation by reciprocal radius with C as the center is now used to map the outside of the area bounded by the three arcs into a half plane

with a rectangular step. (See Figure 9) This stepped half plane can be conformally transformed by use of the Schwartz-Christoffel transformation into a half plane. If $t = t_1 + i t_2$ is the complex coordinate in the half plane as indicated by Figure 9, the transformation is

$$s = \int_0^t \sqrt{\frac{t+1}{t}}\, dt \quad .$$

$t = 0$ and $t = -1$ are the points corresponding to the corners of the step. Integration of this expression yields

$$s = \sqrt{t+t^2} + \ln\left(\sqrt{t} + \sqrt{1+t}\right) \tag{36}$$

From this, one sees that $s = 0$ corresponds to $t = 0$ and $s = \frac{\pi}{2} i$ to $t = -1$.

In order to compute this transformation, it is convenient to introduce a new complex variable Υ defined by the relation

$$\sqrt{t} + \sqrt{1+t} = \Upsilon \tag{37}$$

So:

$$\sqrt{t} = \tfrac{1}{2}\left(\Upsilon - \frac{1}{\Upsilon}\right) \quad , \qquad \sqrt{1+t} = \tfrac{1}{2}\left(\Upsilon + \frac{1}{\Upsilon}\right)$$

and

$$t = \tfrac{1}{4}\left(\Upsilon - \frac{1}{\Upsilon}\right)^2$$
$$s = \tfrac{1}{4}\left(\Upsilon^2 - \frac{1}{\Upsilon^2}\right) + \ln \Upsilon \tag{38}$$

By letting

$$\Upsilon = \sigma e^{i\epsilon} \tag{39}$$

one obtains the expressions

$$s_1 = \tfrac{1}{4}\left(\sigma^2 - \frac{1}{\sigma^2}\right)\cos 2\epsilon + \ln \sigma \tag{40a}$$

$$s_2 = \tfrac{1}{4}\left(\sigma^2 + \frac{1}{\sigma^2}\right)\sin 2\epsilon + \epsilon \tag{40b}$$

and

$$t_1 = \tfrac{1}{4}\left(\sigma^2 + \frac{1}{\sigma^2}\right)\cos 2\epsilon - \tfrac{1}{2} \tag{41a}$$

$$t_2 = \tfrac{1}{4}\left(\sigma^2 - \frac{1}{\sigma^2}\right)\sin 2\epsilon \tag{41b}$$

The values of S corresponding to real values of $\tau \geq 0$ can be found directly from equation 36 and are plotted in Figure 10. In order to obtain the values of σ which correspond to points on the straight line $s_1 = 0$, equation 40a must be used to compute ϵ as a function of σ. The other three expressions, equations 40b and 41a and b yield the values s_2, τ_1, and τ_2 as functions of the same parameter, σ. Figure 11 presents values of τ_1 and τ_2 plotted as functions of s_2. This figure, together with Figure 10, contains sufficient information for the determination of β.

The τ-half plane is now transformed into the region outside of a circle in such a way that infinity of the z-plane corresponds to the infinite point of the new plane. This can be done by a transformation by reciprocal radius with C' as a center, where C' is the point corresponding to C after the step transformation (Figure 8). In this manner, the real τ axis is transformed into a circle K.

The two inversions and the step transformation have to be constructed or computed for only the original points R and S (corresponding to the sink). If R' and S' are the images on the circle K with the center M, then

$$\beta = \angle R'MS'$$

For the example of Figure 7 where the end of the NACA 23015 airfoil has been cut off from 90% chord on the upper surface to 95% on the lower, the above method yields

$$\Delta c_l = 2 c_Q \cot \beta/2 = 12.3 c_Q$$

In Figure 13, this theoretical result is compared with experimental pressure distribution measurements for $\alpha = 0°$. The actual trailing edge 1b used in these measurements is shown in Figure 12. If trailing edge 1a of this figure, where the lower lip reaches the trailing edge and the upper lip is maintained at 90% chord, is used, the theory yields

$$\Delta c_l = 8.05 c_Q$$

A balance measurement for $\alpha = 0°$ is compared for this case with the theoretical result in Figure 14. In both cases the maximum Δc_l values attained are considerably lower than the corresponding Δc_l^* values, from which it may be concluded that the stagnation point P did not reach the trailing edge in these tests.

D. Computation of the Pressure Distribution:

The methods described in the previous section may also be used to compute the pressure distribution. In this case, all the points of the profile transformed by the inverse Joukowski transformation, shown in Figure 8, must be further transformed by the reciprocal radius and step transformations. These transformations yield a set of points in the

neighborhood of the circle K. By any of the well known transformations, these points may be transformed into points on the circle K itself.

A simpler and as accurate a method is to use the conformal transformation of the original profile and to locate a suction slot at the point corresponding to $\zeta = e^{i\beta}$ as found by the preceding method. It is advisable to use this method particularly if the conformal transformation of the original profile is known as in the case of many of the NACA profiles.

In order to find the velocity of the flow, the expression

$$w = \left|\frac{dz}{d\zeta}\right|$$

may be computed by differentiating and simplifying equation 12, yielding

$$\frac{dz}{d\zeta} = w_0\left(e^{-i\alpha} - \frac{e^{i\alpha}}{\zeta^2}\right) + \frac{Q+\Gamma i}{2\pi}\frac{1}{\zeta} - \frac{Q}{\pi}\frac{1}{\zeta - e^{i\beta}}$$

The values of the points on the profile correspond to

$$\zeta = e^{i\phi}$$

Thus

$$\frac{dz}{d\zeta} = w_0\left(e^{-i\alpha} - e^{i(\alpha-2\phi)}\right) + \frac{Q+\Gamma i}{2\pi}e^{-i\phi} - \frac{Q}{\pi}\frac{1}{e^{i\phi}-e^{i\beta}}$$

multiplied by $e^{i\phi}$ results in

$$e^{i\phi}\frac{dz}{d\zeta} = w_0\left(e^{-i(\alpha-\phi)} - e^{i(\alpha-\phi)}\right) + \frac{Q+\Gamma i}{2\pi} - \frac{Q}{\pi}\frac{e^{i\phi}}{e^{i\phi}-e^{i\beta}}$$

$$= w_0\left(e^{-i(\alpha-\phi)} - e^{i(\alpha-\phi)}\right) + \frac{\Gamma i}{2\pi} + \frac{Q}{2\pi}\left(1 - \frac{2e^{i\phi}}{e^{i\phi}-e^{i\beta}}\right)$$

Now

$$1 - \frac{2e^{i\phi}}{e^{i\phi}-e^{i\beta}} = -\frac{e^{i\phi}+e^{i\beta}}{e^{i\phi}-e^{i\beta}} = -\frac{e^{i\frac{\phi-\beta}{2}} + e^{-i\frac{\phi-\beta}{2}}}{e^{i\frac{\phi-\beta}{2}} - e^{-i\frac{\phi-\beta}{2}}} = i\cot\frac{\phi-\beta}{2}$$

Therefore

$$e^{i\phi}\frac{dz}{d\zeta} = -2iw_0\sin(\alpha-\phi) + \frac{\Gamma i}{2\pi} + \frac{Q}{2\pi}i\cot\frac{\phi-\beta}{2}$$

Replacing Γ by Q using equation 15 yields

$$\frac{1}{i}e^{i\phi}\frac{dz}{d\zeta} = 2w_0\sin(\phi-\alpha) + 2w_0\sin\alpha + \frac{Q}{2\pi}\left(\cot\frac{\phi-\beta}{2} + \cot\frac{\beta}{2}\right)$$

By introducing C_Q (from equation 16a) in place of Q in the above expression and by letting $C = 4$ as an approximation, this equation yields

$$\left|\frac{dz}{d\zeta}\right| = w_0\left|2(\sin(\phi-\alpha) + \sin\alpha) + \frac{2C_Q}{\pi}\left(\cot\frac{\phi-\beta}{2} + \cot\frac{\beta}{2}\right)\right| \qquad (42)$$

Now

$$\omega = \left|\frac{dx}{dz}\right| = \frac{1}{|f'(\zeta)|}\left|\frac{dx}{d\zeta}\right| \qquad (43)$$

Combining equations 42 and 43 results in

$$\frac{\omega}{\omega_0} = \frac{1}{|f'(\zeta)|}\left|2[\sin(\phi-\alpha)+\sin\alpha] + \frac{2c_a}{\pi}\left(\cot\frac{\phi-\beta}{2} + \cot\frac{\beta}{2}\right)\right| \qquad (44)$$

In this equation ϕ is the amplitude of the point $\zeta = e^{i\phi}$ corresponding to the profile point under consideration. It should be noted that the equation has been developed on the assumption that the chord c is equal to 4. Using this assumption, it is possible to express the ordinate as

$$x = 2\cos\phi$$

with only a small error. If the velocity distribution ω/ω_0 of the profile is known for the case without suction ($c_a = 0$) for a given angle of attack α, the value of $|f'(\zeta)|$ can be found for any point $x = 2\cos\phi$ on the profile by use of equation 44. This equation can then be used to obtain the velocity distribution ω/ω_0 for any c_a, β and α. The pressure distribution is then obtained from the equation

$$\frac{\Delta p}{q} = 1 - \left(\frac{\omega}{\omega_0}\right)^2.$$

In this manner, the computed pressure distributions of Figures 15 and 16 have been obtained for comparison with the experimental measurements.

II. THEORY OF SUCTION SLOT DESIGN.

The magnitude of the lift produced by suction through a slot is mainly dependent on the position of the sink which replaces the slot. However, the economy of the lift producing device, assuming a fixed position of the sink, will depend on the shape of the suction slot. In order to produce a laminar flow within and near the slot, it is necessary to determine the correct slot shape so that there is no decrease in flow velocity along the slot walls in the direction of the flow. The hodograph method is used to determine this shape for the case of a trailing edge suction slot.

A. Analysis of the Problem:

The trailing edge of the original profile is assumed to be formed by two planes including the angle β (Figure 17). This trailing edge is cut off so that the lower surface has the end point $o = c$ and the upper surface the end point A. The trace of the slot in the x-y plane is formed by the straight line ending at $o = c$ as the lower wall and an undetermined wall connecting point A with point B, the latter being the theoretical infinite point of the lower wall. The flow entering the slot will have a stagnation point S on the lower wall and will leave the edge $o = c$ smoothly according to the Kutta-Joukowski condition which is valid in this case.

The wall AB has to be designed in such a way that the flow has increasing velocities from M to A, from S to B and from S to $O=C$ and a constant velocity along the wall AB. These conditions are imposed in order to prevent flow separation since it is known that avoiding an adverse pressure gradient prevents separation on a flat plate. It is by no means clear, however, that the avoidance of an adverse pressure gradient has the same effect in regions of high curvature. In Figure 17 the flow directions are indicated by arrows and numbers. The slot width is designated by δ and M denotes the point on the upper surface where the flow has the lowest velocity. The sink is located at B. The function

$$t = \ln \frac{dx}{dz} = \ln w \mp i\vartheta$$

represents the logarithmic hodograph, x being the complex potential function, w the flow velocity and ϑ the direction of the flow for the point $z = x + iy$. The flow in the z-plane corresponds then to the flow represented by Figure 18 in the t plane. The notations for corresponding points and flow directions are the same as in the z-plane. The constant velocity along the wall AB is denoted by w_1 , the finite velocity at C by w_0 and the velocity minimum at M by w_M.

A one to one conformal transformation of the flow area in the z-plane into the upper half of the $\zeta = \xi + i\eta$ plane is represented by Figure 19. Again, the corresponding points and flow directions are denoted by the same symbols. The transformation is accomplished in such a way that $\zeta = \infty$ corresponds to the infinity outside the trailing edge in the z-plane and that the points $\zeta = -1$ and $\zeta = +1$ correspond respectively to the points A and B. The abscissas ξ of the real points corresponding to M, S, and C are denoted by m, s, c. The flow in the ζ-plane has a source at infinity, a sink at $\zeta = 1$ and stagnation points of first order at $\zeta = s$ and $\zeta = c$.

B. Transformation of the ζ-Plane Into the t-Plane:

The flow area in the t-plane is a polygon. The conformal transformation of the upper ζ half plane into this polygon can be determined, therefore, by Schwartz-Christoffel's equation. This yields

$$t_0 = C_0 \int \frac{\zeta - m}{(\zeta - s)\sqrt{\zeta^2 - 1}}\, d\zeta + C_1 \qquad (45)$$

where C_0 and C_1 are constants to be determined.

The integral can be evaluated and gives

$$t = C_0 \ln \frac{(\zeta + \sqrt{\zeta^2-1})(\zeta - s)^{\frac{s-m}{\sqrt{s^2-1}}}}{\left(s\zeta - 1 + \sqrt{\zeta^2-1}\sqrt{s^2-1}\right)^{\frac{s-m}{\sqrt{s^2-1}}}} + C_1 \qquad (46)$$

The logarithm is real for real values of $\zeta \geq s$. Starting with a large positive value of ζ and passing over S the function t is augmented by

$$C_0 \frac{s-m}{\sqrt{s^2-1}} \pi i = \pi i$$

therefore

$$C_0 = \frac{\sqrt{S^2-1}}{S-m} \tag{47}$$

Passing with ζ over $\zeta = +\infty$ the function t is augmented by

$$\frac{\sqrt{S^2-1}}{S-m}\,\pi i = \beta i$$

therefore

$$\frac{\beta}{\pi} = \frac{\sqrt{S^2-1}}{S-m} \tag{48}$$

An inspection of equations 47 and 48 shows that

$$C_0 = \frac{\beta}{\pi} \tag{49}$$

Thus C_0 is determined by β. Assuming a given value for S, it follows from equation 48 that

$$m = S - \frac{\pi}{\beta}\sqrt{S^2-1} \tag{50}$$

So the position of the velocity maximum is determined too.

Approaching $\zeta = +1$ along the real ζ axis from the right side, we find

$$t = \pi i + C_1 = \ln w_1 + \pi i$$

Multiples of $2\pi i$ to be added to t eventually are without importance because $\frac{dx}{d\tau} = e^{\tau}$. Thus

$$C_1 = \ln w_1 \tag{51}$$

and the result is

$$t = \ln\left[w_1 \frac{(\zeta+\sqrt{\zeta^2-1})^{\beta/\pi}(\zeta-S)}{S\zeta-1+\sqrt{S^2-1}\sqrt{\zeta^2-1}}\right] \tag{52}$$

valid for $|\zeta| \geq 1$.

For $|\zeta| \leq 1$ equation 45 is replaced by

$$t = C_0 \int \frac{\zeta-m}{(\zeta-S)\sqrt{1-\zeta^2}}\,d\zeta + C_1 \tag{53}$$

and by evaluating the integral for real values of ζ and using equation (48), which is valid for this case

$$t = C_0\left[\arcsin\zeta + \frac{2}{\beta}\pi \arctan\sqrt{\frac{S+1}{S-1}}\sqrt{\frac{1-\zeta}{1+\zeta}}\right] + C_1 \tag{54}$$

For $\zeta = +1$

$$t = \frac{\pi}{2} C_0 + C_1 = \ln \omega_1 + \pi i$$

and for $\zeta = -1$

$$t = C_0 \left(-\frac{\pi}{2} + \frac{\pi^2}{\beta}\right) + C_1 = \ln \omega_1 + \beta i$$

therefore

$$C_0 = -\frac{\beta}{\pi} i \tag{55}$$

and

$$C_1 = \ln \omega_1 + (\pi + \beta/2) i \tag{56}$$

Thus the result

$$t = \ln \omega_1 + i \left[\pi + \beta/2 - \frac{\beta}{\pi} \arcsin \zeta - 2 \arctan \sqrt{\frac{\zeta+1}{\zeta-1}} \sqrt{\frac{1-\zeta}{1+\zeta}}\right] \tag{57}$$

is valid for $|\zeta| \leq 1$. Equation 57 may be rewritten as

$$t = \ln \omega_1 + i h(\zeta) \tag{58}$$

where

$$h(\zeta) = \pi + \beta/2 - \frac{\beta}{\pi} \arcsin \zeta - 2 \arctan \sqrt{\frac{\zeta+1}{\zeta-1}} \sqrt{\frac{1-\zeta}{1+\zeta}} \tag{59}$$

C. Determination of the Complex Potential Function:

The complex potential function of the flow in the upper ζ half plane has the form

$$\chi = A\zeta^2 + B\zeta + \frac{Q}{2\pi} \ln(\zeta - 1) \tag{60}$$

where Q is the strength of the total sink located at $\zeta = 1$ and its sign is negative. A source of equal strength is located at infinity giving χ the required singularities. Now

$$\frac{d\chi}{d\zeta} = 2A\zeta + B + \frac{Q}{2\pi} \frac{1}{\zeta - 1} \tag{61}$$

becomes zero for two values of ζ . If A and B are determined so that these values coincide with $\zeta = C$ and $\zeta = S$, the potential χ represents the desired flow. Then

$$\left.\begin{aligned} 2AC + B + \frac{Q}{2\pi} \frac{1}{C-1} &= 0 \\ 2AS + B + \frac{Q}{2\pi} \frac{1}{S-1} &= 0 \end{aligned}\right\} \tag{62}$$

and

$$\left.\begin{aligned} A &= \frac{Q}{4\pi} \frac{1}{(C-1)(S-1)} \\ B &= -\frac{Q}{2\pi} \frac{S+C-1}{(C-1)(S-1)} \end{aligned}\right\}$$

With these values, equation 61 becomes

$$\frac{d\chi}{d\zeta} = \frac{Q}{2\pi} \frac{(c-\zeta)(s-\zeta)}{(c-1)(s-1)(\zeta-1)} \tag{64}$$

Before determining the shape of the slot a generalization of this result is in order.

The preceding investigation has been based upon a consideration of the flow near the trailing edge only. Without a suction slot, the flow is identical to the stagnation point flow represented by Figure 20. This is an approximation for the flow at the trailing edge of a profile and no influence due to change in angle of attack is provided for. For larger angles of attack where this influence has to be taken into account, a stagnation point s_0 can be added to the flow on the lower surface so that the flow in Figure -20 would become that of figure -21. There must be added a third order term of ζ to the right side of the complex potential function χ of equation 60. If ζ_0 is the ζ value corresponding to s_0, one obtains instead of equation 64 the generalization

$$\frac{d\chi}{d\zeta} = \frac{Q}{2\pi} \frac{(c-\zeta)(s-\zeta)(s_0-\zeta)}{(c-1)(s-1)(s_0-1)(\zeta-1)} \tag{65}$$

Of course the hodograph is more complicated in this case, however, the considerations of the preceding section can be generalized for this also. As long as the angle of attack is not extremely high and the forward stagnation point of the profile is still situated in the vicinity of the leading edge, this generalized solution will not be necessary.

D. Determination of the Shape of the Slot:

The hodograph relation $\tau = \ln \frac{d\chi}{dz}$

yields

$$\frac{d\chi}{dz} = e^{\tau} \tag{66}$$

Combining equations 64 and 66 results in

$$\frac{dz}{d\zeta} = \frac{Q}{2\pi} \frac{(c-\zeta)(s-\zeta)}{(c-1)(s-1)(\zeta-1)} e^{-\tau} \tag{67}$$

The function $t\ (\zeta)$ is known from part B of this section, so z can be found as a function of ζ from the above equation.

Substituting into equation 67 the value of t as obtained by equation 52 yields

$$\frac{dz}{d\zeta} = -\frac{Q}{2\pi w_1} \frac{c-\zeta}{(c-1)(s-1)} \frac{\zeta s - 1 + \sqrt{s^2-1}\sqrt{\zeta^2-1}}{(\zeta+\sqrt{\zeta^2-1})^{s/\pi}} \frac{1}{\zeta-1} \tag{68}$$

for $|\zeta|=1$. In the vicinity of $\zeta=1$ this function behaves according to

$$-\frac{Q}{2\pi\omega_1}\,\frac{1}{\zeta-1}$$

Passing over $\zeta=1$ within the upper ζ half-plane from a real value $\zeta>1$ to a real value $\zeta<1$ the function z is augmented by

$$-\frac{Q}{2\pi\omega_1}\cdot\pi i=-\frac{Q}{2\omega_1}\,i$$

The slot width is then

$$\delta=-\frac{Q}{2\omega_1} \tag{69}$$

The same expression for δ results if one uses equation 57 for t and passes over $\zeta=1$ from a value $\zeta<1$ to a value $\zeta>1$.

For the computation of the shape of the slot and the velocity distribution along the slot walls, the following expressions can be used which result from equations 67 with 52 or 57:

If $|\zeta|\geq 1$

$$\frac{dz}{d\zeta}=-\frac{Q}{2\pi\omega_1}\,\frac{(c-\zeta)(\zeta s-1+\sqrt{s^2-1}\sqrt{\zeta^2-1}}{(c-1)(s-1)(\zeta-\sqrt{\zeta^2-1})^{\beta/\pi}(\zeta-1)} \tag{70}$$

and if $|\zeta|\leq 1$

$$\frac{dz}{d\zeta}=\frac{Q}{2\pi\omega_1}\,\frac{(c-\zeta)(s-\zeta)}{(c-1)(s-1)(\zeta-1)}\left[\cos h(\zeta)-i\sin h(\zeta)\right] \tag{71}$$

where

$$h(\zeta)=\pi+\beta/2-\beta/\pi\ \arcsin\zeta-2\arctan\sqrt{\frac{\zeta+1}{\zeta-1}}\sqrt{\frac{1-\zeta}{1+\zeta}}$$

The function $z=f(\zeta)$ for the above equations has to be determined by graphical or numerical integration. the z-values of the curved wall of the slot corresponds to real values of ζ with $|\zeta|\leq 1$.

The velocity distribution along the walls follows from equation 66

$$\omega=\left|\frac{dx}{dz}\right|=|e^{t}|$$

which yields together with equations 52 and 57 for $|\zeta|\geq 1$

$$\frac{\omega}{\omega_1}=\left|\frac{(\zeta+\sqrt{\zeta^2-1})^{\beta/\pi}(\zeta-s)}{\zeta s-1+\sqrt{s^2-1}\sqrt{\zeta^2-1}}\right| \tag{72}$$

and for $|\zeta|\leq 1$

$$\frac{\omega}{\omega_1}=1 \tag{73}$$

Figure 22 shows a suction slot computed for the trailing edge of the NACA 23015 profile. The slot width δ has been chosen equal to unity. Thus $-\frac{Q}{\Sigma w_i} = 1$ from equation 69. The angle $\beta = 17.2^\circ$ and the parameters C and S have been chosen,

$$C = S = 2 .$$

Their choice determines the length of the lower lip of the slot and the location of the stagnation point S'. For the case $C = S$ the stagnation point has its rearmost position and is ready to leave the profile with an increased amount of suction.

III. DESCRIPTION OF EXPERIMENTAL APPARATUS

A. Wind Tunnel and Allied Apparatus:

All of the quantative measurements of lift, drag, pitching moment and pressure readings were taken in the Princeton University 3½' x 5' subsonic wind tunnel. In its original configuration this tunnel was three dimensional, however in this program the tunnel was converted to the two dimensional by the construction of a new contraction section, test section and diffuser. It was the construction of the diffuser that presented the first real problem in that flow separation from the walls could not be avoided and the location of the initial separation point could not be maintained constant. This resulted in a tunnel with a quite low energy ratio (which could be tolerated in this investigation) and with severe velocity fluxuations in the test section. Of course the test velocity varation was unacceptable. The first attempt at a "cure" was the splitter configuration as shown in figure 23. This showed a very definite improvement in the steadiness of the flow in the test section. However the problem was still largely unsolved. Further attempts with slats to direct the diffuser flow to the walls and spoilers to fix the position of the stall proved unsatisfactory.

In order to bring the operating characteristics of the two dimensional test section up to an acceptable level in as little time as possible two approaches were made simultaneously. They were: (1) the design of vortex generators from data supplied by the United Aircraft Corp. and (2) the design, construction and installation of a new low angle diffuser equipped with cusps at the down stream end. The vortex generators were finished last but not installed by the time the new diffuser with cusps was completed. This arrangement was found to be wholly satisfactory and the tunnel was operated in this configuration throughout the test program. (See Figure 24).

The wind tunnel balance is a six component, oil dampened, pneumatic system indicating forces and moments directly on large differential pressure gages. For this investigation, however, only the components of lift, drag and pitching moment had significance. Drag is discussed in a later section,

---

1. Reference 3

however, it was found desirable to use a wake rake in order to determine drags by momentum considerations. This rake is of the differentiating type and is located in the test section approximately one and one half chord lengths behind the trailing edge of the model. The total head and static tubes in the rake were connected to a multiple manometer equipped with lights and a graflex camera. Thus all wake drag data and all other pressure data were taken by means of photography.

B. Smoke Tunnel:

Early in the investigation of trailing edge suction it was realized that a number of unknown qualities of the flow, associated with this type of high lift device, might be revealed by a smoke study. This realization eventually led to the purchase of a 3'x5' smoke tunnel designed by Dr. A. Lippisch and built by Collins Radio Corp. of Cedar Rapids, Iowa. It was felt that there would be a considerable time delay in the delivery of such an apparatus and the decision was made to build a small smoke tunnel[1] in order to solve some of the more immediate problems of circulation control systems.

The smoke tunnel as used in this study is purely a means for obtaining qualitative information since the flow velocities were so small that neither force or pressure reading could be taken to indicate lift or drag. Except for this the tunnel is well instrumented with a means for determining flow velocities and suction quantities. This instrumentation offered a basis for accurate comparison of the flows studied.

C. Models:

The primary model used in this study of trailing edge suction is a NACA 23015 profile of rectangular planform complete with end plates. This model is hollow and is constructed entirely of brass. It is equipped with 22 chordwise pressure taps and with nozzle like ends outboard of the end plates through which the air removed via the suction slot is withdrawn. This model has an 18" span between the end plates and a base chord of 8", however the after 20% of the chord was made removable for the attachment of trailing edge suction slots (see figure 25 & 26). A total of ten different combinations of upper and lower suction slots were attached to this model and completely tested. In addition a series of experiments were made with a variable trailing edge also made of brass and adjustable between wind tunnel runs. In addition to the brass 23015 airfoil two 16 inch chord wood models (see figure 27) were built and tested both by force and pressure measurements. A 15 percent thick elliptical model was also built to obtain preliminary information on the behavior of the bent up lower lip as finally used in configuration 4-f. The data taken with this model is reported in Reference 7. Other models used in the study were 5 inch chord 2 inch span profiles built for testing in the smoke tunnel. These were geometrically similar in trailing edge configuration to the pressure distribution models (see figure 28).

1. Reference 4

D. Suction System:

For the wind tunnel tests of all models, except those built for the smoke tunnel, suction was obtained by using an auxilliary stage compressor taken from an Allison V-1710 engine. This compressor, driven by a 40 HP D.C. motor was located outside the wind tunnel and air was ducted from the model by the system shown in figure 29. In order to avoid affecting the balance readings by introducing loads from the air ducting, a special coupling consisting of two ball and socket joints, connected by piping containing a slip joint, was employed. Flexible piping was used to connect this coupling to the ducts. Properly located (according to the ASME power test code) in the duct is a box which permits insertion of several different size orifice plates for measuring the flow or amount of suction. Control of the amount of suction is obtained by varying the speed of the D. C. motor and/or by changing the valve position of the hydraulic coupling between the power input to the compressor and the compressor wheel.

IV. METHODS OF DATA REDUCTION

This section will deal with the methods and techniques used to reduce the raw wind tunnel data to coefficient form and the corrections applied to this data in order to make a clear and accurate presentation.

A. Force Measurements

All force measurements (lift, drag, and pitching moment) were reduced to coefficient form on the basis of the actual chord of the model tested and not upon the base chord. Similarly the pitching moment coefficient is based upon the quarter chord length of the actual chord and not the base chord of the profile.

Wind tunnel test section velocities were calibrated with a pitot-static tube for each model tested. This was accomplished by setting the model at zero degrees angle of attack with the pitot tube, located in the middle of the tunnel over the model, mid way between the model and the top of the test section. A calibration was made between the pitot-static readings and the difference in static pressure between the settling chamber and contraction section. These latter pressures were obtained by means of wall taps in the respective sections. This yielded a calibration curve for q plotted against tunnel differential pressure and all subsequent speeds were measured by this ΔP reading. The slope of this calibration curve together with data taken during the tests yielded a simple method for reduction of force measurements to coefficient form. The wind tunnel balance was initially calibrated[1] and the results plotted so that each of the forces (i.e. lift, drag, side force) and the moments (pitch, roll, yaw) appear as a straight line with force or moment vs. gage reading. Thus the slope of each of these balance calibration curves multiplied by the difference in wind off and wind on gage readings yields the force or moment directly. Therefore the expression for lift

1. Reference 3

coefficient

$$C_L = \frac{L}{qS}$$

can be changed to

$$C_L = \frac{\Delta L_R K_1}{\Delta P K_2 S} = \frac{\Delta L_R K_L}{\Delta P S}$$

where ΔL_R = the difference between wind on and wind off lift gage readings

K_1 = slope of lift calibration curve

ΔP = wind tunnel differential pressure

K_2 = slope of q calibration curve

$K_L = \frac{K_1}{K_2}$ = overall lift constant

In a similar manner the expression for drag and pitching moment coefficients are derived, resulting in

$$C_D = \frac{\Delta D_R K_D}{\Delta P S}$$

and

$$C_M = \frac{\Delta P_{iR} K_P}{\Delta P S}$$

It is, of course, of great importance to properly evaluate the tares for any wind tunnel test. The force model was, in this installation, mounted on end plates having a diameter somewhat greater than the chord. Balance readings indicated excessively high drag coefficients but quite normal lift coefficients[1] in good agreement with the published NACA results. These lift values were obtained with the conventional sharp trailing edge with, of course, no suction. Other tests performed in the same wind tunnel, which were part of a project being carried out concurrently with the subject of this report, indicated that leakage into the wind tunnel at the model mounts had a detrimental effect. This effect was not noticed with the circulation control force model at zero suction coefficient. However, it seemed reasonable to expect a greater leakage where suction was applied with the possibility of introducing some error. Means were not available at the time to evaluate properly the effect of this leakage. However, partial pressure distributions taken about the model with the end plates

1. This is explained in more detail in section V-A of the discussion.

sealed and not sealed indicates the lift results are conservative by a few percent. The continuing experiments with this model, which combines flaps with trailing edge suction, will include a study to evaluate the tares with suction. As previously mentioned the balance drag readings were excessively high. As an expedient solution the drags were determined by means of pressure surveying the wake[1].

Since the force measurements were taken with the model mounted at the 50% base chord point the pitching moment coefficients were, of course, about this point. These data were, however, converted to the 25% actual chord point of each configuration by means of the following expression, the significance of which is easily understood by reference to the accompaning diagram.

$$C_{m\,c/4} = C_{m\,c/2} - \frac{\bar{X}}{c} C_L \cos\alpha - \frac{\bar{X}}{c} C_d \sin\alpha$$

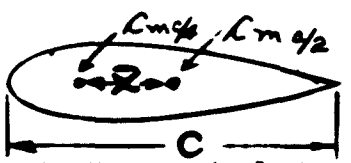

The term, base chord, refers to the original chord of the unmodified NACA 23015 profile while the actual chord refers to the profile with the sharp trailing edge removed and suction slots installed.

B. Pressure Measurements

1. Pressure Distributions:

The experience gained in testing and analyzing the results of the force measurement model answered some questions about trailing edge suction but created many new ones. The question of the type of pressure distribution in the vicinity of the slot and the effect of the increased circulation (pressurewise) led to the construction and testing of two 16" chord models equipped with pressure taps. The results of these tests are discussed in section VI.

These pressure distributions were plotted in a direct manner (Fig. 30 shows a typical plot for trailing edge 1-b). Since the data were taken by photographing a multiple manometer, the manometer readings themselves were plotted versus the chord length (in inches). This yielded an area proportional to lift. Mechanical integration of the area enclosed by the curve was accomplished by use of a planimeter. This area multiplied by a constant relating square inches under the curve to pounds of lift resulted in the determination of the lift coefficient. When the pressure distribution is plotted in this manner one must be careful to establish the ordinate of the leading edge stagnation point. This is accomplished by plotting a straight horizontal line having the ordinate of the test section static pressure. The algebraic addition of tunnel q to this static pressure

1. This is discussed more fully in the next section.

yields the ordinate of the stagnation point. For the example shown in Figure 30 the tunnel static pressure was -6.70 in. H_2O (gage) and tunnel q was 4.31 in. H_2O. The stagnation point, therefore, is represented by the ordinate 2.39 in. of H_2O. Thus the stagnation point corresponds to a c_p of +1.0 and the horizontal line representing test section static pressure corresponds to $c_p = 0$. This method, rather than the more conventional transfer of the data to pressure coefficients, was used because it eliminated a great deal of routine computation. Since the pressure distributions made numbered in the hundreds a significant amount of time was saved.

2. Equivalent Power Drag Coefficient

In order to compare the slot efficiencies of the several configurations the following procedure was undertaken: A kiel tube located within the model was used to determine the total pressure on the down stream side of the slot. The external total pressure was determined by a pitot tube placed in the free stream. Thus a pressure coefficient, $\Delta p/q$, was evaluated, for a range of c_Q's, for each trailing edge slot. The drop in total pressure across the slot is a function of its drag and hence the power requirement for a given c_Q. An equivalent power drag coefficient c_{de} was evaluated by means of the following expression[1]

$$c_{de} = c_Q(c_p - 1).$$

3. Profile Drag Coefficient by Wake Survey

The profile drag coefficients presented in this report were obtained by a pressure survey of the wake[2]. A differentiating wake rake located in the wake of the model was used in combination with a multiple manometer. Manometer readings were taken by means of photography yielding an instantaneous picture of the reduced total head within the wake. The method of reduction of these data follows the procedure outlined in Reference 6 which results in the expression for drag coefficient.

$$c_d = \frac{y_w}{c} - \frac{1}{q_0 c}\int q\, dy$$

where:

y_w = wake width

c = profile chord

q_0 = free stream dynamic pressure

q = dynamic pressure within the wake

dy = incremental distance between the wake dynamic pressure readings.

1. Reference 5
2. Reference 6

The shape of the wake pressures when seen on a multiple manometer is best described as a bell shape curve which tends to spread out and flatten with increasing angle of attack. This occurs in a manner so that the area under this curve constantly increases but at a slower rate than the wake width increases.

With increasing suction the wake width and the area under the bell curve both decrease but the decrease in wake width is the more pronounced.

Early in the circulation control study the procedure for solving the wake drag equation utilized the mechanical integration of the integral $\int q\,dy$ by means of a planimeter. The results of this method were somewhat disappointing in that a great deal of scatter of the test points was encountered. In order to arrive at a better way of evaluating the integral, a plot of $x = y^2$ was carefully made between limits which yielded an area of approximately the same magnitude as the experimental area. A mathematical integration of this area was made and used as the standard in a comparison with several other methods of integration. These other methods included:

1. Planimeter, percentage error 1.2%
2. Trapezoidal rule, percentage error 0.72%
3. Simpson's rule, percentage error 0.15%

The percentage error is based upon a zero percentage error for the mathematical integration. While none of the errors look excessive at first glance nevertheless an inspection of the equation 74 shows that the drag coefficient is a small difference of two relatively large numbers. Thus any error involved in evaluating the integral is magnified many times in the drag coefficient. Accordingly, a procedure was set up whereby $\int q\,dy$ could be evaluated automatically on an I.B.M. computing machine set to use Simpson's Rule. In fact it was found to be economically sound to feed all of the wake information into the machine and receive the wake drag coefficients directly.

C. Corrections Made to the Wake Drag Coefficient:

One of the interesting characteristics of trailing edge suction is that it tends to remove the effect of friction. In other words the real flow tends to approach potential flow in some respects. Thus as the suction quantity is increased, more and more of the turbulent wake is swallowed into the suction slot, in fact under some conditions of high C_q it almost entirely disappears and the wake drag coefficient approaches zero. This can only be the profile drag coefficient under one condition and that is the removed air must be returned to the free stream so that there is no change in momentum between the slot and the component in the downstream direction of the discharged air.

If this is not the condition then there must be a correction made to the wake drag to yield the profile drag coefficient. The development of this

correction is as follows: Figure 31 shows a schematic sketch of an airfoil equipped with a trailing edge suction slot. Streamline ψ having a velocity ω_0 at station 1 stagnates at station 2 from 2 it accelerates thru the slot then turns at 3 and flows in a spanwise direction. At point 3 the velocity component in the direction of the free stream is zero.

Therefore:

At station 1 the velocity = ω_0

At station 2 the velocity = 0

At station 3 the velocity = 0

The momentum change between stations 1 and 2 = $\Delta M = \rho Q \omega_0 - \rho Q \omega_2$

The momentum change between stations 2 and 3 = 0

Therefore the increased drag due to momentum change of the removed air is

$$D = \Delta M = \rho Q \omega_0 - \rho Q \omega_2 = \rho Q \omega_0$$

and the increased drag coefficient is

$$C_d = \frac{\rho Q \omega_0}{\rho/2\, S\, \omega_0^2} = \frac{2Q}{\omega_0 S} = 2C_Q$$

D. Measurement and Reduction of Suction Quantity Data:

The procedure by which flow quantities were measured and the data reduced is that outlined in the A.S.M.E. Power Test Code[1]. The sharp edged orifice was selected as the primary element because of its reliability and low cost. It is true that such a metering device is less efficient than a nozzle but an excess of power was available and it appeared more economical to spend power than to suffer the cost of a nozzle.

This method of determining the flow quantity is in essence based upon the fundamental flow equation

$$Q = K\sqrt{\Delta P/\rho} \qquad (75)$$

where ΔP is the pressure drop across the sharp edge orifice. For the test installation vena - contracta pressure taps were used to measure this pressure drop. The actual flow equation used by reference 7 relates mass flow, ω, to the parameters of equation 75. In order to obtain Q

1. Reference 7

(ft.^{3}/sec., tunnel density was obtained by measuring settling chamber static pressure and temperature and dividing this result into the mass flow, ω. This yielded the suction quantity based upon the tunnel conditions rather than upon those of the duct. The A.S.M.E. procedure was carefully followed for a number of tests including various angles of attack and several different slot shapes and dimensions. It was then found that a calibration curve could be constructed relating ΔP across the orifice directly to mass flow thru the orifice and that the error involved in the curve was well within the experimental error of obtaining the data. Such a calibration curve indicates that the density variation with ΔP, at the orifice, was approximately the same regardless of trailing edge geometry. With this calibration established it was then possible to greatly speed up the testing program and the data reduction. The suction quantity was non-dimensionalized into coefficient form by means of the relationship,

$$C_Q = \frac{Q}{\omega_0 S}$$

Here, as in the case of all other coefficients, C_Q was computed on the basis of the actual area tested and not upon the base area of the profile.

V. DESCRIPTION OF EXPERIMENTS

A. Calibration of the Wind Tunnel

As previously mentioned the Princeton 3½'x5' subsonic wind tunnel was modified for this experimental program by the installation of an auxilliary, two dimensional 18" throat. After the initial velocity variation difficulties had been overcome by the installation of the cusped diffuser it became necessary to examine the character of the flow in the new test section in order to make proper corrections to the test data. This investigation was made in four parts:

1. Velocity survey of the test section.

2. Yaw head survey of the region of the test section where the model would be installed.

3. Determination of the turbulence of the wind tunnel.

4. Measurement of the boundary layer on the side walls of the test section in the vicinity of the model.

The velocity survey of the test section was made by probing horizontally with a pitot static tube at different elevations from the bottom of the test section to the top. All of the points tested were outside the boundary layer and the results were considered good since the maximum and minimum values of q were within 1.0% of the average q.

In order to determine the inclination of the flow in the test section a yaw head survey was made across the mid point of the test section. The

average deviation of the flow from the horizontal was approximately one half a degree and the inclination was upward. However, with the model installed at -1° to the horizontal the inclination of the flow was approximately zero degrees. Since the angle of zero lift for the base 23015 profile is -1° and repeated tests with this model gave excellent agreement with the NACA results it was decided that the angularity correction was essentially zero.

The turbulence factor[1] was determined by use of the conventional turbulence sphere fitted with four static pressure taps on the downstream side 22° from the horizontal. The results indicated a critical Reynolds number of 357.200 which yielded a turbulence factor of 1.078. The reason for this rather low turbulence is probably the large contraction ratio (seventeen) of the auxiliary throat and the effect of the cusps in permitting a small angle diffuser.

Information about the thickness and character of the side wall boundary layer was necessary to determine what corrections, if any, would be necessary to obtain the mean dynamic pressure in the test section. This was accomplished by means of a total head survey of the boundary layer at the location of the model in the test section. The assumption of constant static pressure across the boundary layer permits the relating of total head within the boundary layer to the dynamic pressure. The investigation revealed a boundary layer at the model location of approximately one inch in thickness. However, this was a turbulent condition and the difference between the calibrated free stream and the average test section based upon this turbulent layer was of an order of magnitude that could be neglected. Once again the justification for a lack of correction is the excellent agreement between results with this tunnel and those published by the NACA not only for the base 23015 profile but for other profiles more recently tested.

B. Calibration of the Blower:

As mentioned earlier in this report the duct from the wind tunnel to the compressor contained an apparatus permitting the rapid change of orifice plates. Three different orifices were originally used to measure the flow over a wide range of flow quantities. These were 1", 2" and 4.9" in diameter with β ratios of 0.143, 0.286 and 0.70 respectively. After testing several trailing edge configurations thru wide range of angles of attack it was possible to construct the calibration curve discussed in the section on data reduction. As a check on the validity of the calibration a duct was attached to the exhaust part of the blower and the flow in this duct was measured with an anemometer. Pressures and temperatures were taken simultaneously with the velocity readings. From these data mass flow was computed which gave excellent agreement with the calibration for both the 2" and 4.9" orifices. Data taken, however, for the 1-inch orifice was not in good agreement with its calibration. Several explanations for this condition are possible but an investigation would have been necessary to

1. See Reference 6

substantiate any one of them. As an expedient solution it was decided to discard the 1-inch orifice altogether especially since the flow coefficients were not as reliable for this β ratio as for the larger values.

C. Determination of Spanwise Variation of Slot Velocity:

One of the first tests made with the force model was the determination of the spanwise velocity distribution in the suction slot. This was accomplished by the installation of static pressure taps on the lower lip of the slot. It was found that the static pressures across the slot were essentially the same. With the assumption of constant total pressure there was, then, practically no spanwise variation of slot velocity. This was, no doubt, due to the physical relationship of slot size to the large hollow interior of the model and the large ducts. In other words, the greatest pressure drop in the system occurred across the suction slot so this in effect became a severe throttling device, thus tending to automatically distribute the flow. This large pressure drop in some later tests, with very small slot thicknesses, caused severe bending and vibration of the lower slot lip which was solved by the installation of spacers in the slot.

D. Model Testing:

In general the various configurations of the force model were tested in the following manner. With the tunnel doors closed and with zero velocity balance readings were taken of lift, drag and pitching moment for each of the several angles of attack. The model was then returned to the desired angle and the wind tunnel brought up to test velocity. With a suction quantity of zero, readings of lift, drag, and pitching moment were again taken. This process was repeated for approximately fifteen different suction quantities for each angle of attack tested. Concurrently, the wake pressures were photographed on the multiple manometer for each suction quantity for each angle. Additional data taken included the test section and settling chamber static pressures, the settling chamber and duct temperatures and the absolute and differential pressures across the orifice plate in the duct.

A separate series of tests were run on each configuration in order to measure the total pressure drop across the slot. This was done so the pressure leads from the model to the manometer could not influence the force measurements. These total pressures were also photographed for approximately twelve different suction quantities for each angle of attack tested.

A detailed breakdown of the configurations tested and the reasons follow. Figure 32a, b, and c shows the geometry of the various configurations with the exception of a variable trailing edge which will be subsequently discussed in this section and in section VI. Trailing edges 1-a, 1-b, and 1-c were the first three shapes tested. These represented the range of lower lip overhang over which it was felt a detailed investigation was warranted. The upper lip was simply formed with a single radius, for

although it was felt the slot shape would strongly influence the results the theory of such a shape as presented in this report was not at that time completely developed. The test results for these first three models indicated that the geometry of the trailing edge strongly influenced the maximum lift of the section. The highest lift was achieved with trailing edge 1-b which had more overhang than 1-c but less than 1-a as can be seen in Fig. 32. Since the slot thickness varied for each of these cases it was thought that there might be an optimum ratio of overhang to slot thickness. Theory indicates that Δc_l increases as the slot approaches the trailing edge of the base profile. Consequently, it was thought that in the case of 1-c the ratio was far below the optimum. As a result this ratio was increased for trailing edge 2-b.

Trailing edge 2 is the "correct" slot shape as computed by the method outlined in this report. This was first tested with lower lip b and the results were enccuraging in as much as the Δc_l at low angles and low suction quantities was the best that had so far been achieved. The maximum lifts, however, were very disappointing. It was thought that flow around the lower lip might account for this, consequently trailing edges d and e were designed with a longer overhang to overcome this difficulty. It is interesting that again the maximum lifts achieved with the section were with the moderate overhang (trailing edge 2-e).

The amount of air that could be sucked through the slot was, in this case, small compared to the amount for the No. 1 series of trailing edges. It was thought that this might be the result of a flow separation at the slot inlet so trailing edge 2 was modified internally in an attempt to effect a cure. This resulted in trailing edge 4.

It will be noted in Figure 32 that trailing edge 4 has an internal cusp to aid in diffusing the flow inside the model and to prevent any disturbance from working upstream around the inlet contour. The bent up lower lip of configuration 4-f was an attempt to limit the stagnation point travel and provide easy entrance for the air into the slot. The results were mediocre compared to 1-b, although it shows a higher maximum lift than 2-e.

Trailing edge 5-e is another application of the cusp, this time to provide a more efficient inlet contour to the suction slot. The results were not outstanding either in maximum lift achieved or in power required to move the air; however, recent developments indicate that the cusp in trailing edge 5 was improperly designed.

The two configurations, d-a and 1-g, were tested to determine the effect of extreme shapes such as the sharp upper lip in trailing edge d-a. The maximum lift for this profile is poor, but it does compare more favorably with some of the other models at lower c_q's.

The experience of testing these models revealed that there can be a substantial flow around the lower lip into the slot under certain conditions

of angle of attack and c_Q, this forming a free stream stagnation point. Trailing edge 1-g was designed to resist this tendency, but the results indicate that 1-g is not as effective as trailing edge 1-b from which it was formed.

The results of these tests and the general theory indicated that the location of the slot (relative to the trailing edge of the base airfoil) and the amount of overhang had substantial effect upon the Δc_l achieved. In order to experimentally check the overhang portion of this hypothesis a special lower lip was designed and constructed which was adjustable to ten different lengths. This lip in combination with upper lip No. 1 formed trailing edge 1-v. Figure 33 shows the geometry for all ten of the adjustments. Each was tested for lift, drag, and pitching moment as indicated by balance readings. This was in many respects the most interesting experiment of the program because the effect of systematically changing one variable is readily understood.

There were two major pressure distribution studies made during this program. These involved models previously described. One of the pressure models was geometrically similar to configuration 1-b, the other was a typical trailing edge suction model designed I-A. In each case measurements were made following the procedure described for the force model since one of the reasons for these tests was to compare the results of lift by force measurement and pressure distribution. The actual testing to obtain the local static pressures around the profile was again separate from the force tests so that pressure leads would not interfere with balance readings. All the pressures were indicated upon the multiple manometer which was photographed for several suction quantities for each angle of attack tested. A comparison of the results obtained is discussed in the next section.

The third and one of the most revealing series of experiments was that of studies made in a smoke tunnel[1]. This investigation was limited to the three simplest trailing edges tested (1-a, 1-b, and 1-c) because of the small scale to which the profiles were reduced (5½ inch chord). The smoke tunnel results, even though qualitative, are difficult to compare directly with the force model results due to the great difference in Reynolds Number. It was, however, this series of experiments which confirmed the free stream stagnation point under certain conditions of c_Q and angles of attack and showed that this condition can be hastened by shortening the overhang. (see Figure 4)

VI. PRESENTATION AND ANALYSIS OF RESULTS

Detailed plots of all data taken have been prepared although the greater part of these are presented in a separate report[1]. Individual plots of c_l, c_d, $(c_d + 2c_Q)$, $c_{m\,c/4}$ and c_p versus c_Q for each angle

1. Reference 4
1. Reference 8

of attack have been made. From these data summary families of c_l versus angle of attack at several values of c_q have been plotted for each trailing edge configuration and these are presented in Figures 35 thru 46 representing the lifts as obtained by force measurements. Similar families are shown in Figures 47 and 48 but in this case the lift coefficients were obtained by pressure measurements. A comparison will subsequently be drawn between these two figures and Figures 45 and 46.

Also summarized from the detailed data are families of c_d and $c_d + 2c_q$ versus angle of attack for each configuration. These are presented in Figures 49 through 60.

In a similar way curves representing the general variation of $c_{m\ c/4}$ with angle of attack and c_q are presented in Figures 61 through 70. Figures 71 through 80 represent the variation of c_p (based upon total head drop across the slot) with angle of attack for several values of c_q. Five additional figures complete the presentation of the summarized date. These (Figures 81, 82, 83, 84, and 85) compare the characteristics of lift, drag and pitching moment of the various trailing edges tested and figure 85 shows the step by step alteration of the lift coefficient of trailing edge 1-v (variable) as the overhang is systematically increased.

One of the first tests made with the force model was with a plain trailing edge in order to compare the results with those of the NACA for the same profile. Figure 34 shows this comparison, the results being identical up to an angle of attack of 7° where the great difference in Reynolds Numbers between the two tests begins to produce its effect. It was felt that this test was an excellent overall check of the apparatus and technique used.

Table I compares two of the fundamental characteristics of the basic lift curve to those of the lift curve for the several trailing edge configurations. It is interesting to note that the angle of zero lift for each of the configurations tested with the force model, with the exception of 1-g, is identical to the angle of zero lift for the base profile. Trailing edge 1-g has a severely bent down lower lip which would lead one to believe that $\alpha_{z.l.}$ would be lower than for the other cases; however, the flow on the upper surface near the trailing edge is probably badly separated due to both the bent lower lip and the discontinuity of the upper surface. The force measurements taken with the pressure distribution model indicate a slightly lower angle of zero lift than for the force model. This may be due to small differences between the two models, perhaps in the curvature of the mean camber line especially near the trailing edge. The angle of zero lift as obtained from pressure studies is slightly higher than that obtained from force measurements with the same model. This is due to the fact that with force measurements the reaction of the entire model is being measured but a pressure measurement reveals the characteristics at only one spanwise station. It is felt, however, that the agreement, for this case, is quite good. An examination of Table I shows that the slope

TABLE I

BASE AIRFOIL - NACA 23015

	TRAILING EDGE	SLOPE OF LIFT CURVE ($dc_l/d\alpha$)	ANGLE OF ZERO LIFT (DEG.)
	N.A.C.A.	0.108	-1.0
	PLAIN	0.110	-1.0
FORCE MODEL	1-a	0.113	-1.0
	1-b	0.118	-1.0
	1-c	0.124	-1.0
	2-b	0.114	-1.0
	2-d	0.103	-1.0
	2-e	0.123	-1.0
	4-f	0.116	-1.0
	5-e	0.120	-1.0
	d-a	0.105	-1.0
	1-g	0.109	-0.5
PRESS. MODEL	I-A Force	0.099	-1.3
	I-B Force	0.106	-1.5
	I-A Pressure	0.107	-1.2
	I-B Pressure	0.106	-1.0

of the lift curve $(dc_l/d\alpha)$ varies somewhat with the trailing edge configuration; however there does not seem to be enough of a trend to make deductions. The average $(dc_l/d\alpha)$ for the force model is 0.1145 and for the pressure model 0.102. The former is somewhat higher than the slope of the lift curve for the base profile as given by the NACA while the latter is slightly lower. The end plates, which exceeded the chord of the force model, did not completely cover the ends of the larger pressure distribution model. It is possible that normal leakage around the end plates might simulate, to a degree, three dimensional flow which might account for the reduced slope of the lift curve.

Figures 35 thru 44 representing the two dimensional lift characteristics of the several configurations are not consistent with respect to maximum c_q. This is due to some limiting condition, in each case, of the amount of suction that could be applied. There were three conditions thus limiting the scope of the tests. The first was encountered with trailing edges 1-c and 2-b and this was the establishment of a free stream stagnation point after which the lift increments went in the negative direction. Secondly, severe vibration and deflection of the trailing edge was encountered with some of the configurations but this was overcome by the use of spacers between the lips. The third limitation was the size of the slot, the greater the slot thickness the greater the c_q. This last condition limited the majority of the tests and it represents the maximum effort of the system

for each trailing edge geometry. This maximum effort should not be confused with a constant power condition, merely because the compressor controls were in the same approximate setting, since the compressor blades operated at different efficiencies for each slot dimension. In view of this, one would expect that the highest C_Q to be achieved would have been with trailing edge 1-c since it had the largest slot width. This case was, however, limited by a free stream stagnation point due to the short overhang of the lower lip. The highest C_Q was reached with trailing edge 1-b which had the second largest slot width and an overhang long enough to prevent the occurance of the free stream stagnation point. This discussion has so far excluded a comparison with the geometries of trailing edge 1-v which is considered to be a special case. This will be subsequently examined.

The highest lift coefficient measured was with trailing edge 1-b and its value was 2.67. This was only partly due to the fact that 1-b achieved the highest C_Q, since examination of Figures 35, 36, and 44 reveals that this trailing edge (1-b) was more effective at comparable C_Q's and angles than either 1-a or 1-g (it should be remembered that 1-g is 1-b with the lower lip cambered). This indicates that ΔC_L is influenced by the geometry of the trailing edge suction slot. Figure 81 shows a comparison of the different configurations. A study of this figure shows that the effectiveness of any trailing edge depends upon the angle of attack and C_Q. For example, trailing edge 5-e with the external cusp has the highest ΔC_L (0.8) at +1° angle of attack for a C_Q of 0.01 also the value of C_L (1.0) for this suction quantity and angle was the highest tested. For the same C_Q at 13° angle of attack trailing edge d-a indicates the highest lift coefficient (1.5). It is seen that both 1-g and 2-e exceed the above value for d-a but at an angle of 11°. Information on the characteristics of both 2-e and 1-g at 13° angle of attack is not available. However the lift summary curves of Figures 35 thru 44 indicate that these higher angles for the two cases mentioned would be of little interest. The reason that the 11° angle of attack curves of trailing edges 2-e and 1-g compare so favorably with the 13° curve of d-a is because the lift coefficient of d-a at 13° and C_Q = .01 represents the partially stalled condition. Of those configurations that reached a C_Q of .02 the maximum lift was achieved by trailing edge 1-g (C_L = 1.96) at 11°. This is again due to the fact that 1-g had not stalled at 11° with a C_Q = .02 while 1-b, for example, had stalled at 13° with the same C_Q. Of the tests during which a C_Q of .04 or greater was obtained trailing edge 1-b was by far the most effective. Figure 35 indicates that the reason for this is that between a C_Q of .02 and .03 the flow, which had been separated at 13° at lower C_Q's, becomes attached. Thus the effect of suction is not only an upward displacement of the lift curve but is also an extension of the curve. By such behavior trailing edge suction at the higher values of C_Q simulates to a degree the effect of both slots and flaps.

Figures 45 and 47 represent the lift characteristics of trailing edge I-A. This was, as previously explained, a 16" chord pressure distribution model. However force tests were also made with it in order to compare the

results. I-A should not be compared to 1-a since the trailing edge proportions are substantially different. It will be observed in figure 45 that a distinct change in slope of the lift curve occurs at approximately 5° angle of attack. This is shown for c_Q = o and it is for this reason force measurements were not made beyond 5 degrees; however pressure distribution studies were made up to 13 degrees angle of attack and the shape of these curves (Figure 47) are more normal. It is seen that at all angles and c 's the results from the pressure investigation are substantially greater than those of the force measurements. The pressure taps were located at the mid-span of the model and were therefore less influenced by the separation which began at the side walls of the tunnel and worked inward. Of course as soon as this separation began the force measurements were affected and this seems to have started at about 5 degrees angle of attack. The same explanation holds for the pressure and force measurements made with configuration I-B, the results of which are shown in figures 46 and 48. This trailing edge (I-B) is geometrically similar to 1-b but a comparison of the results shows 1-b to be far superior at all angles of attack and suction quantities. Again the explanation for the difference between the 8-inch chord model and the 16-inch chord seems to be the separation which begins at the wall and works inward, this condition being much more severe for the case of the larger chord.

Figures 49 through 60 present the drag characteristics for the several trailing edges. Each of the families of drag curves seem to have the same general behavior with the exception of those of 1-c and 2-b. Figure 49 which represents the drags of trailing edge 1-a is typical. For c_Q = o the c_{dw} vs. α curve is rather flat until an angle of attack of 5 degrees has been reached, at which point the curve abruptly steepens. As the c_Q is increased the whole curve is displaced downward and the increase of drag coefficient with angle of attack is not quite so steep. It can be seen that the wake drag coefficient (c_{dw}) approaches the zero drag condition at the higher of c_Q. As explained in the section on data reduction a value of 2 c_Q was added to the wake drag for momentum considerations. Curves for this are also plotted with the wake drag coefficients. It should be realized that the (c_{dw} + 2c_Q) coefficients are valid only for the condition of discharging the removed free stream and boundary layer air in a spanwise direction. For any other condition the drag is $c_{dw} \pm c_{dm}$ where c_{dm} is the momentum drag coefficient. This may be increased by discharging the air forward and decreased by blowing downstream. In fact c_{dm} may decrease to such a large negative value that the overall drag of the airplane may be negative. Of course to do this the discharged air must be directed downstream and be raised to a momentum level to some degree higher than when sucked into the trailing edge. This last consideration is not seriously suggested as a practical application since the power required to increase the momentum of the discharged air could no doubt be more efficiently utilized in the airplane's propulsive system. This does, however exaggerated, indicate some of the possibilities of drag control since the air must be discharged in some fashion, either blown over some portion of the wing as in the Arado System, or simply thru a discharge duct. If it is thru a duct the

direction could be varied from the minimum drag condition to that of maximum drag thereby permitting L/D control for take off and landing.

The drag characteristics of trailing edges 1-c and 2-b as represented by figures 51 and 52 are erratic in nature. It is significant that these two configurations represent the two instances where a free stream stagnation point occurred. This, no doubt, has a great deal to do with the unorthodox appearance of the drag curves.

Figure 82 compares the drag characteristics of the various trailing edge configurations. The drag coefficient is in this case the wake drag coefficient plus $2C_Q$, $C_{dw} + 2C_Q$. Trailing edges 4-f and 5-e show the lowest drag at zero C_Q for the -1° angle of attack, and 4-f also shows the lowest drag at zero C_Q for the 9° angle of attack. Of those configurations that reached a $C_Q = .02$ practically no difference in drag coefficient can be noted except for 1-c which is much higher. This is because the $2C_Q$ term in the drag coefficient is very large compared with the wake drag except in the case of 1-c which shows a high wake drag coefficient. Of those tests that reached a $C_Q = .03$ and again for $C_Q = .04$ the same is true, pointing out the great influence of the momentum drag.

There is also an equivalent power drag which is a function of the total pressure drop across the slot and hence the power required for suction. This will be discussed in a subsequent section involving the slot C_p, or total pressure drop coefficient

The effect of trailing edge suction on pitching moment is pronounced and seems to be basically a function of shape, overhang and suction quantity. The No. 1 series of trailing edges, as represented by Figures 61, 62, 63, and 70, is characterized by the pitching moment going negative with both increasing angle and increasing suction. As the overhang decreases, there appears a strong tendency for a discontinuity in the pitching moment curve at the higher angles of attack. The pitching moments of the No. 2 and No. 5 series of trailing edges differ somewhat from those of the No. 1 series in that pitching moment goes negative as suction is applied and positive as angle of attack is increased. The net result is that for the range of C_Q tested, the pitching moments are negative except for configuration 1-c, but the slope of the curve is positive. This is illustrated in Figures 64, 65, 66, and 68.

Figure 83 is included to show a comparison of the pitching moments versus C_Q for the several configurations. It is interesting to note the progress in the negative direction of the pitching moments with the exception of the two trailing edges, 1-c and 2-b at 13°, which had the free stream stagnation points. For these two cases the slope of the curve for 13-degrees angle of attack quickly goes positive after starting negative.

In general it appears that the pitching moment characteristics of trailing edge suction are pronounced, although not having downwash information the true severity on the aircraft stability and control problem cannot be

estimated. The maximum moment coefficient measured was -0.455 (Fig. 70, $\alpha = 7.5^{\circ}$, $c_q = 0.05$, $c_l = 1.9$). This value compares favorably to $c_{m(a.c)} = -0.64$ which represents the pitching moment for the base airfoil[1] equipped with 30 percent double slotted flaps at $\delta = 40^{\circ}$ producing the same lift coefficient.

In order to compare the various configurations it is obvious that lift, drag and pitch are but a part of the information needed to gain as clear an idea as possible of the relative merits of the goemetry of the several trailing edges. Some measure of the comparative power requirements is an indenspensible part of such a study. Figures 71 through 80 show the drop in total pressure across the slot as it is affected by angle of attack and suction coefficient. c_p is defined as the total head drop across the slot divided by the free stream dynamic pressure. Without suction ($c_q = o$) the total pressure within the model was equal to the free stream static pressure and, therefore, different from the free stream total pressure by the amount of the dynamic pressure (q). Since, by definition, this difference in total pressure is divided by q to obtain c_p, a plot relating c_p to α for $c_q = o$ is a horizontal straight line ($c_p = 1$) on the figures 71 to 80 regardless of configuration. Thus c_p is a measure of the drag and, therefore, power requirement of the slot.

Figure 84 is a summary presentation of the variation of c_p with c_q and trailing edge for two selected angles of attack. This figure shows that for a $c_q = .02$ and up, trailing edge 1-b suffers the least total pressure drop, however, for lower c_q's 1-a and 1-g rival 1-b at least for one angle of attack. The following tables enable a comparison of the efficiencies of the various slot shapes. Table II has been prepared from Figure 81 and shows the Δc_l for several values of c_q for each slot. Table III is compiled from figure 84 and shows the c_p values corresponding to the Δc_l values of Table II. Table IV has been obtained by dividing the values from Table II by those of Table III.

Table II

Δc_l at 13° angle of attack for several values of c_q

c_q	1-a	1-b	1-c	1-g	2-b	2-d	2-e	4-f	5-e	-a
.01	.64	.63	.06	.36	.08	.76	.41	.08	.12	.22
.02	1.28	1.05	.08	.72	-.05	1.19	.61	1.07	.24	
.03	.30	1.73		.89						
.04	1.46	1.84		.99						

1. Reference 9

Table III

C_p at 13 degrees angle of attack for several values of C_Q

C_Q	1-a	1-b	1-c	1-g	2-b	2-d	2-e	4-f	5-e	d-a
.01	1.9	1.4	1.5	1.4	3.4	2.8	2.7	3.4	5.0	4.0
.02	3.6	2.0	2.5	2.7		10.0		8.0		
.03	6.9	3.3	6.7	4.5						
.04		5.4	10.5	7.0						

Table IV

$\Delta C_e/C_p$ at 13 degrees angle of attack for several values of C_Q

c	1-a	1-b	1-c	1-g	2-b	2-d	2-e	4-f	5-e	d-a
.01	.336	.450	.040	.258	.023	.272	.152	.024	.024	.055
.02	.358	.525	.032	.267		.119		.134		
.03	.043	.525		.198						
.04		.341		.141						

Table IV indicates that trailing edge configuration 1-b was the most efficient one tested with respect to power required to move the air through the slot. A more significant comparison of the efficiencies is presented in figure 84-a in which suction coefficients versus total drag coefficients are plotted for an angle of attack of 90°. The total drag coefficient has been determined by the addition of the profile drag (C_{d_w}) to the equivalent power drag coefficient (see section IV B). Such a definition involves two assumptions:

1. That the momentum drag be zero.
2. That the suction system except for the slot have an efficiency of 100 percent.

The profile drag coefficient of the base airfoil (unmodified NACA 23015) at 9-degrees angle of attack was determined to be 0.02. This value appears as a horizontal straight line on figure 84-a for purposes of comparison. It

is evident from this plot that configuration 1-b is again superior since it shows the minimum drag coefficient (0.011) and also since it shows the greatest spread of c_q (.005 to .018) which yields a total drag coefficient less than that of the base profile at this angle.

The Variable Overhang Trailing Edge

Of the several geometric variables common to the types of trailing edge suction slots studied the amount of lower lip overhang seems to be one of the most significant. For this reason a variable lower lip was constructed and tested in combination with upper lip number one (see Figure 33). Figure 85 shows a comparison of the lift coefficients obtained vs. c_q for each of several angles of attack of the different amounts of overhang tested. The notations 1-v-1 to 1-v-10 designates increasing overhang of the lower lip. Several interesting phenomena are apparent from these plots:

1. As the lower lip is extended there is a gradual decrease in the lift coefficient for the angle of 11 degrees at every value of c_q including $c_q = 0$.

2. As the lower lip is extended there is a decrease in lift coefficient for the angles -1 and 5 degrees for most all values of c_q with the exception of $c_q = 0$.

3. As the lower lip is extended the dip which occurs in the -1° lift curve tends to flatten and this curve finally appears as a straight line.

Figure 86 shows an idealized explanation of the boundary layer removal at a low angle of attack and with a relatively short overhang of the lower lip. Without suction at $\alpha = 0^\circ$ or -1° there is a significant boundary layer thickness on both surfaces of the profile. As suction is added the upper boundary layer tends to be removed first, having an effect upon the lift comparable to an increase in camber, thus producing a lift coefficient corresponding to $c_q = A$. As the suction is increased to B the trailing edge sink apparently has less effect upon the free streamlines than upon the boundary layer on the lower surface. By removing a large portion of the lower surface boundary layer the effect upon lift is comparable to a decrease in camber near the trailing edge. This results in the dip of the c_l vs. c_q curve having a minimum at $c_q = B$. Beyond this suction quantity the free streamlines above the trailing edge of the profile are more and more affected with increasing suction. As the angle of attack increases one would expect a thickening of the upper surface boundary layer and a reduction in thickness of the lower surface boundary layer. This would explain the absence of such a dip in the curve at higher angles. Also as the lower lip is extended there would be less tendency for flow around the trailing edge into the slot, which would explain the lack of the dip in the curve for the greater overhangs. This discussion referring to figure 86 is offered as a suggested explanation for the dip in the c_l versus c_q curve as shown in Figure 85, trailing edge 1-v-1, for an angle of attack of -1 degree. This shape of curve has been observed in other tests made with the force model and pressure model, the detailed data of which are presented in reference 6.

Figure 87 shows the ΔC_l, for several values of C_Q and angle of attack, plotted against the ratio a/c, where a is the chord of the upper surface and c is the chord of the lower surface of the force model fitted with the variable trailing edge. This illustrates the rapid increase of lift coefficient at a given value of C_Q with increasing values of a/c. This of course agrees with theory which calls for an increasing ΔC_l as the slot approaches the trailing edge. It is interesting to note that at the highest angle shown (10 degrees) there is an optimum value for this ratio a/c for two values of C_Q and evidently this optimum value increase with C_Q.

Comparison of Results with those of other Experimenters

Figures 88 and 89 compare some of the results herein reported with those reported by several other experimentalists. The comparison made in Figure 88 is with the optimum trailing edge slot location reported by United Aircraft[1]. Trailing edge configuration 5-e was chosen for this because it produced the greatest ΔC_l at zero angle of attack. It appears to be somewhat more effective than the U.A.C. wing, at this C_Q (.01), but this may be due to the difference in sections. Figure 89 compares trailing edge 1-b with those of Ehlers[2] and Regenscheit[3]. All three represent tests made with the same basic section (N.A.C.A. 23015) but with somewhat different trailing edge slots. Configuration 1-b seems to be inferior at the lower angles of attack but from α = 7.5 degrees and up it is more effective than those reported by both Ehlers and Regenscheit. ΔC_Q = .01 has been selected for this comparison because it is felt that it is in the range of practical application and interest.

Conclusions

It seems possible to deduce the general behavior of subsonic profiles equipped with trailing edge suction slots from this study. The characteristics of lift, drag, pitching moment, power requirement, slot shape and general geometry, as influenced by suction, have been investigated in some detail and it is felt that the following statements are justified for an airfoil without a flap.

1. The lift coefficient of a profile equipped with a trailing edge suction slot can be increased by the application of suction except for the case where a free stream stagnation point occurs; in such an instance the lift increment can become negative.

2. The lift coefficient of such an airfoil in general increases as the sink approaches the trailing edge as shown by theory and experiment. The exception to this statement is the optimum value of the ratio a/c beyond which the opposite is true.

1. Reference 10 Fig. 18, Page 38
2. Reference 11 Fig. 19, Page 39
3. Reference 12 Fig. 12, Page 29

3. The lift coefficient is increased at first (low values of C_Q) by boundary layer removal which permits a flow more nearly approaching that indicated by potential flow theory. At higher values of C_Q the lift increase can be thought of as a result of a circulation increase and sink effect.

4. The lift increase with C_Q is very sensitive to the general geometry of the trailing edge slot but it does not seem at all sensitive to the shape of the upper lip inlet contour unless this shape is extreme.

5. The drag of such a configuration is variable depending upon how the removed air is returned to the free stream. The wake may be practically eliminated with the application of enough suction.

6. Pitching moment is in general negative and moderate increasing in the negative direction with a positive increase of C_Q.

7. The power requirement can be represented by the total pressure loss across the slot and it is a function chiefly of the slot width which determines slot velocity for a given C_Q. It is also a function of angle of attack and slot lower lip overhang.

REFERENCES

1. Regenscheit, B. On a New Application of Suction for the Increase of Lift of an Airfoil, FB 1474 (1941).

2. Smith, C. B. Summary of Analysis of Trailing Edge Suction Slot - United Aircraft Corporation Inter Company Report (1948).

3. Hazen, D. C. Operating Characteristics of Pneumatic Balance System of Princeton University 4'x5' Wind Tunnel (May 1949) Princeton Report No. 145.

4. Hazen, D. C. and Finley, H. B. Operating Characteristics of Princeton University 14"x2" Smoke Tunnel (May 1953 Princeton Report No. 225.

5. Quinn, J. H. Wind Tunnel Investigation of Boundary Layer Control by Suction on the N.A.C.A. 653-418, a $\leq$1.0 Airfoil Section with a 0.29 Airfoil-Chord Double Slotted Flap. N.A.C.A. TN No. 1071 (June 1946)

6. Pope, A. Wind Tunnel Testing, John Wiley and Sons, Inc. (1947).

7. A.S.M.E. Power Test Code, Part 5, Chapter 4, Flow Measurement by Means of Standardized Nozzles and Orifice Plates.

8. Hazen, D. C., Sweeney, T. E., Lehnert, R. F. Circulation Control (Detailed Data Report, (Sept. 1953) Princeton Report No. 241.

9. Abbott and Von Doenhoff, Theory of Wing Sections, McGraw Hill (1949).

10. Goldsmith, J., Effect of Trailing Edge Suction and Pressure Slots, United Aircraft Corporation Report No. R-95374-3 (Feb. 1951).

11. Ehlers, F., On the Influence of Sinks on the Lift and Pressure Distribution of Airfoils with Suction Slots M.A.P. Volkenrode Ref: MAP-VG67-189T.

12. Regenscheit, B., Test on a Wing with Suction at the Trailing Edge, FB 1594 (Jan. 1947).

LIST OF FIGURES

FIG. 1

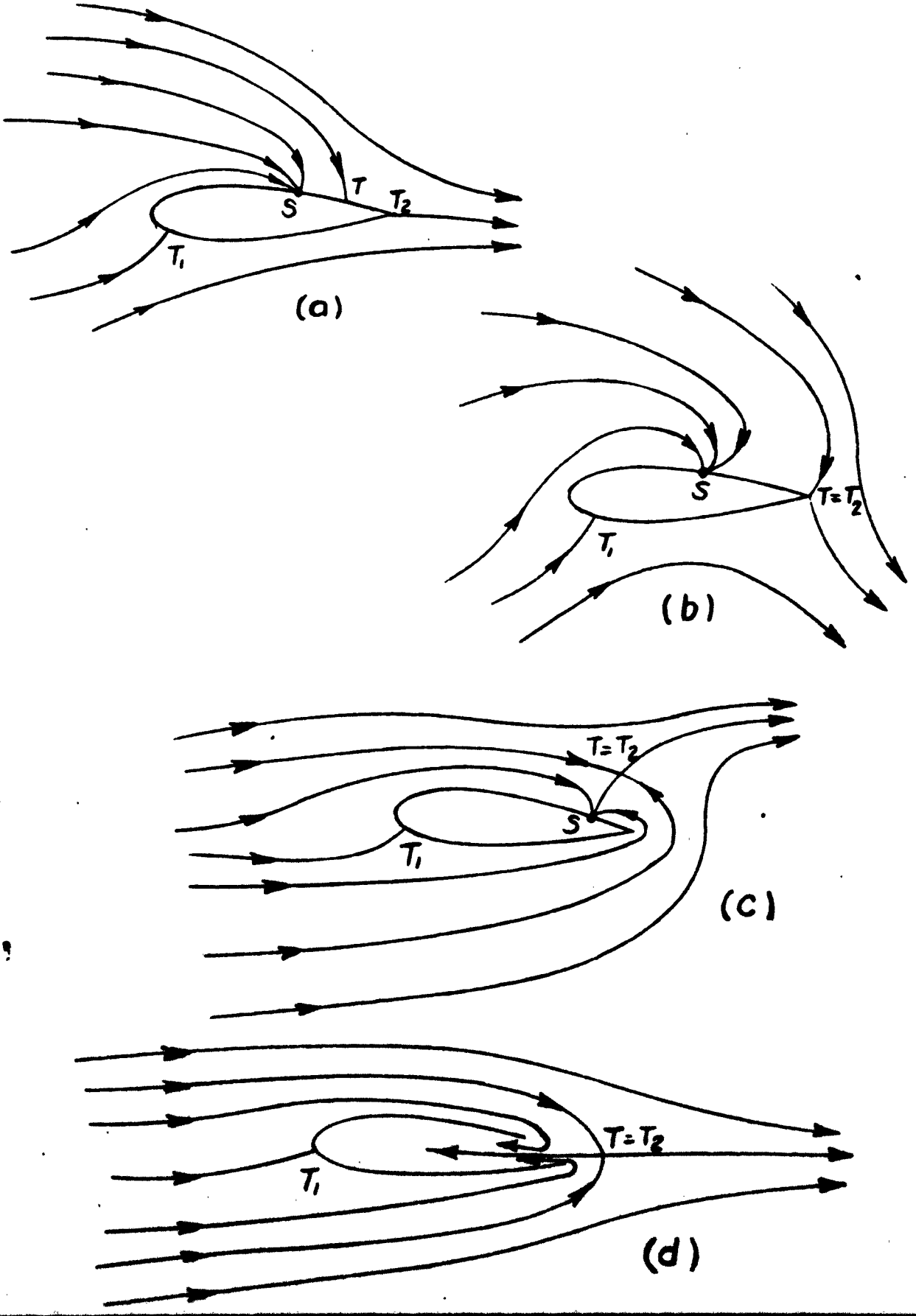

FIG. 2

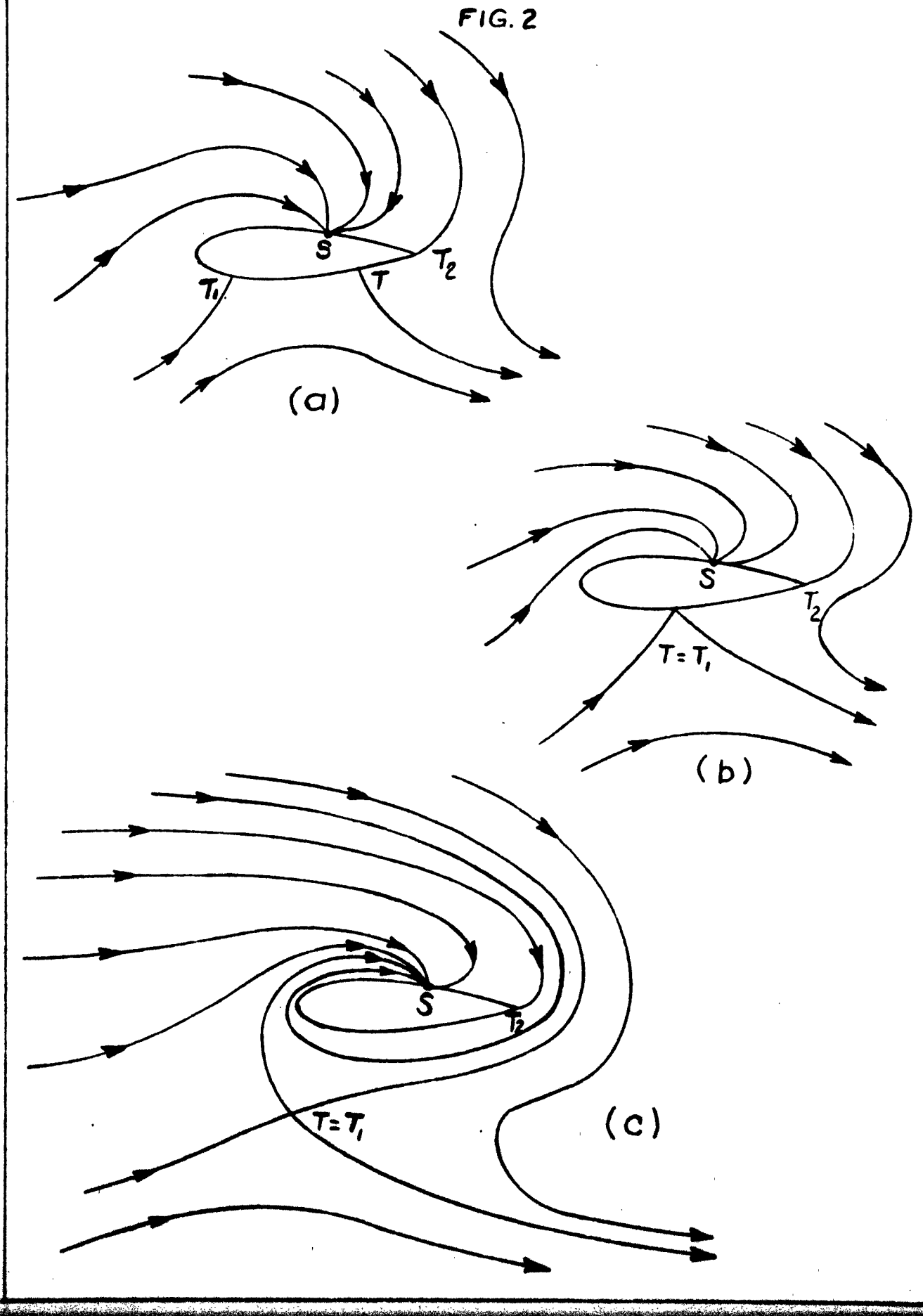

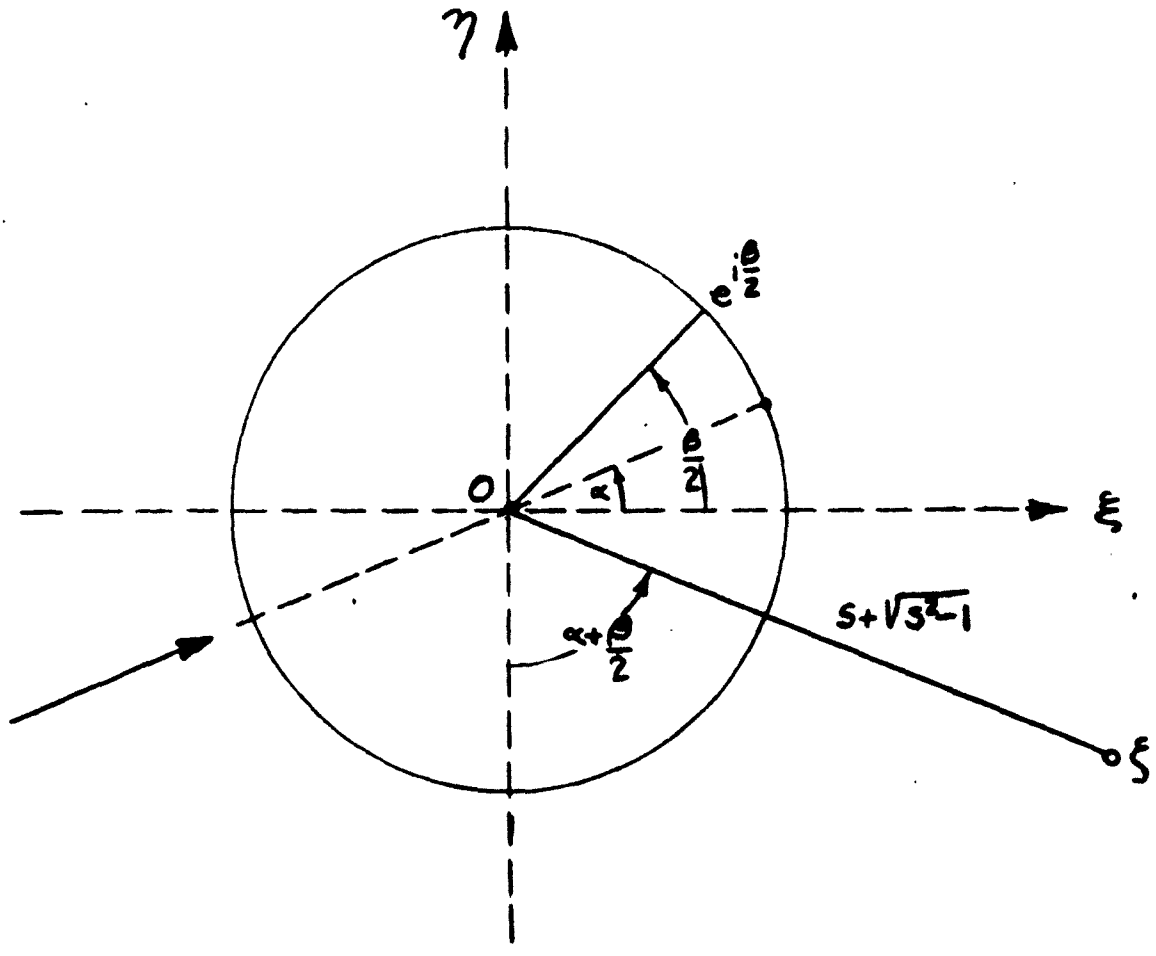
η
ξ
O
α
$e^{i\frac{\theta}{2}}$
$\frac{\theta}{2}$
$\alpha+\frac{\theta}{2}$
$s+\sqrt{s^2-1}$
ξ

FIG. 3

FIG. 4

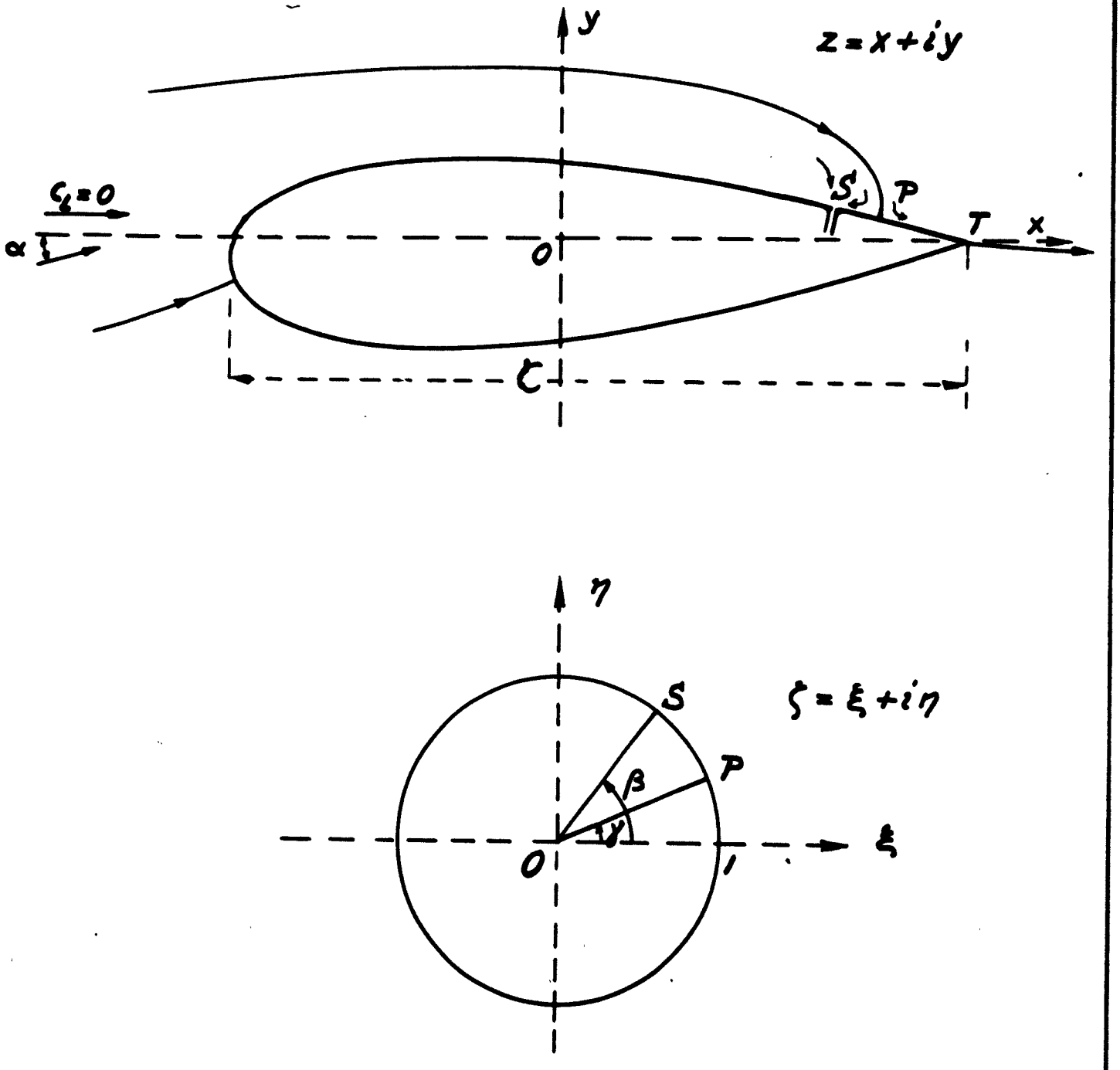

Fig. 5

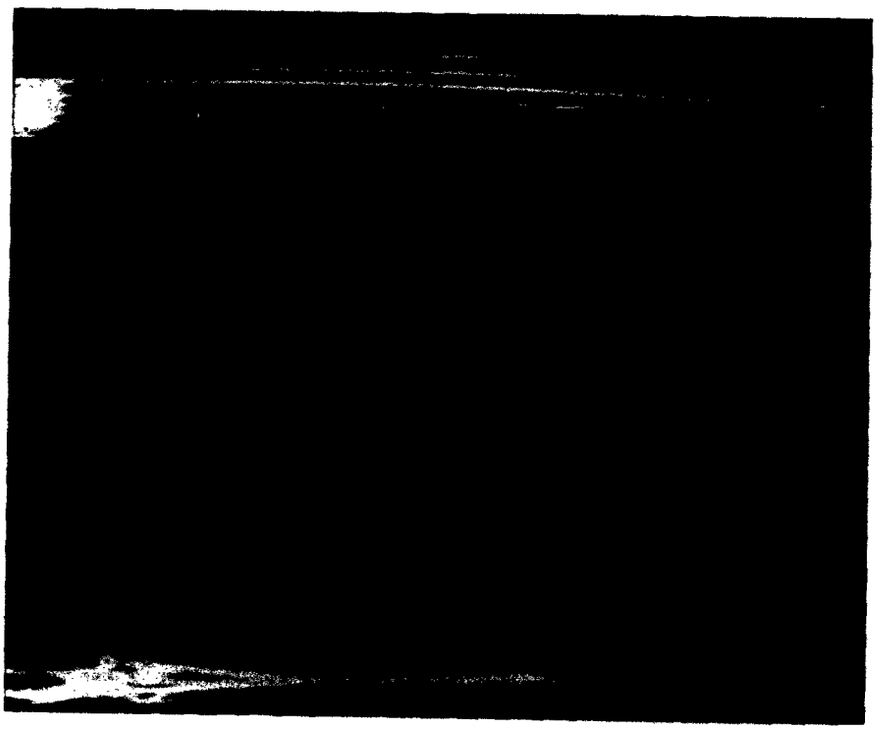

FIG. 6

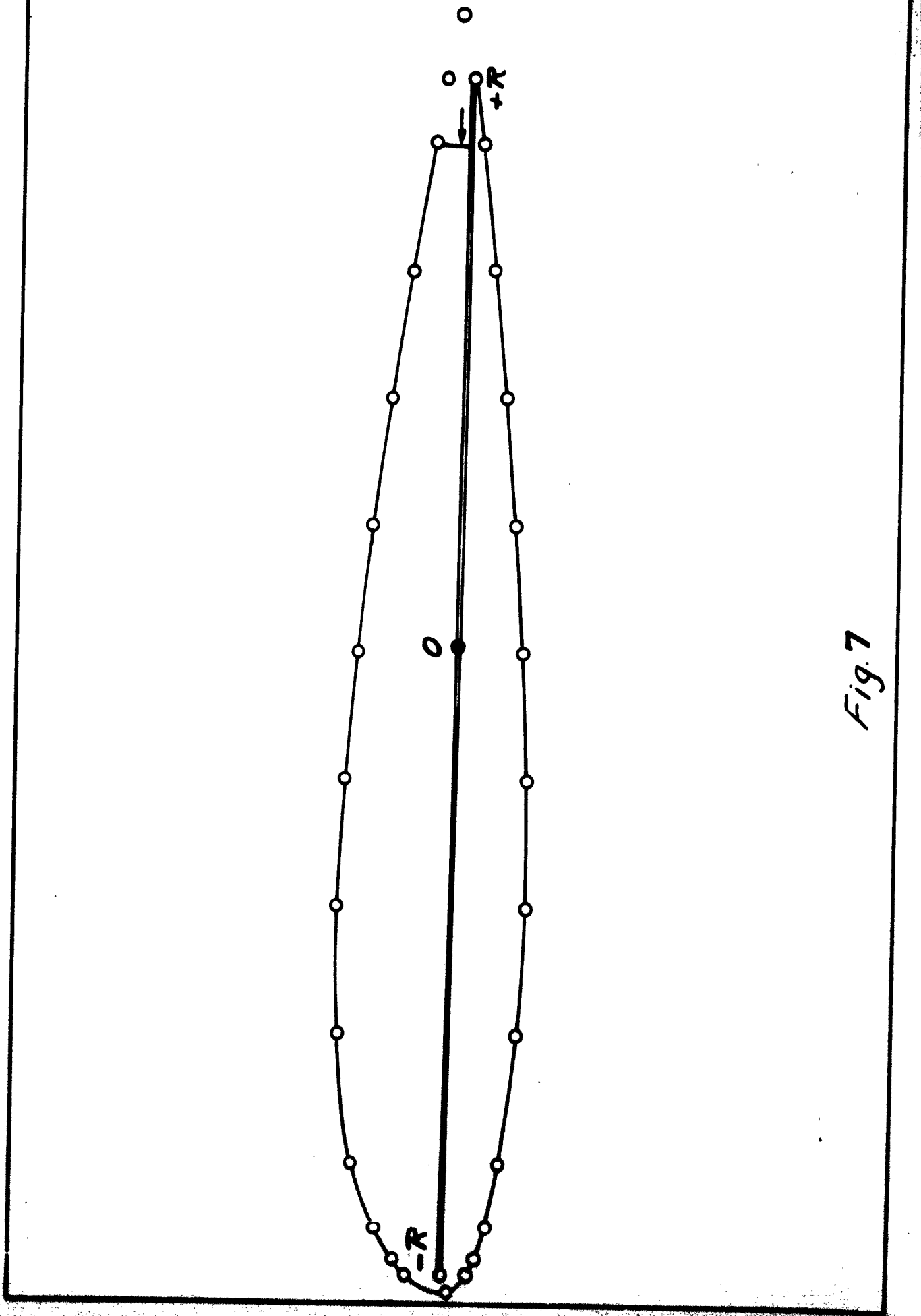

Fig. 7

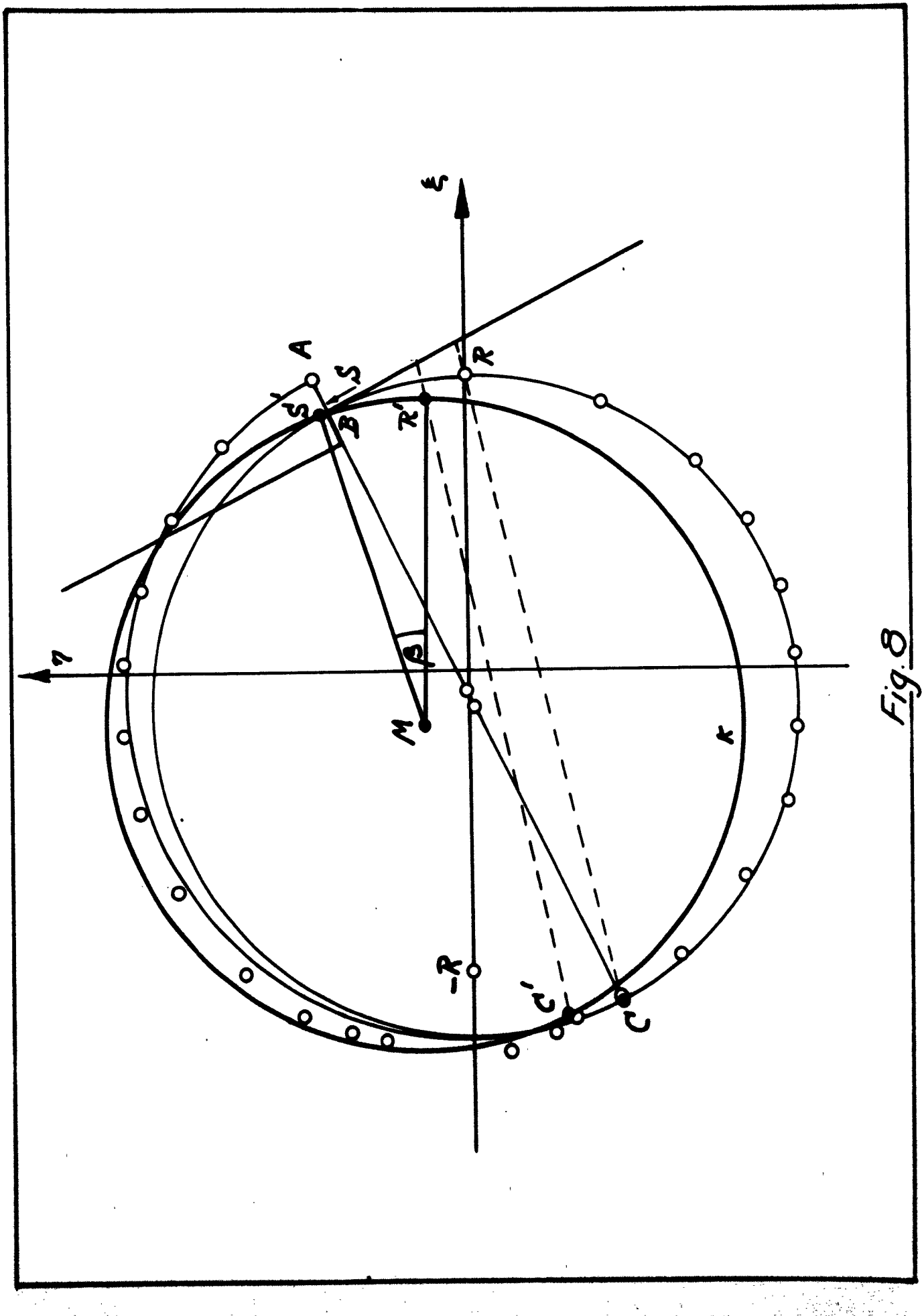

Fig.8

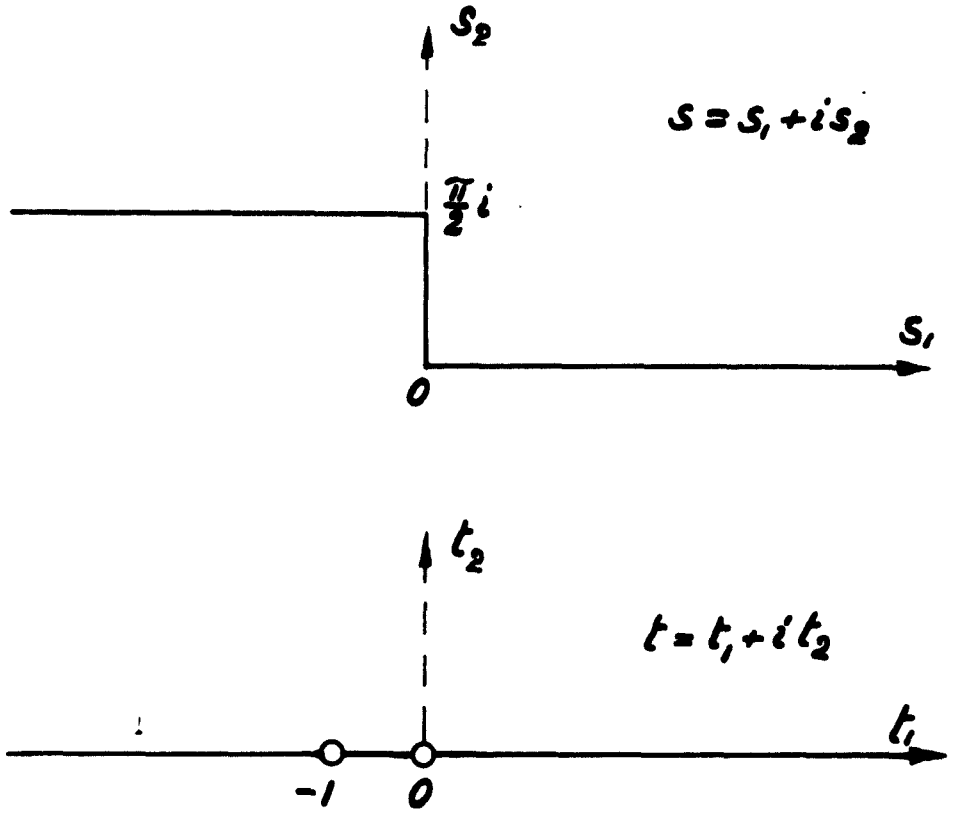

Fig. 9

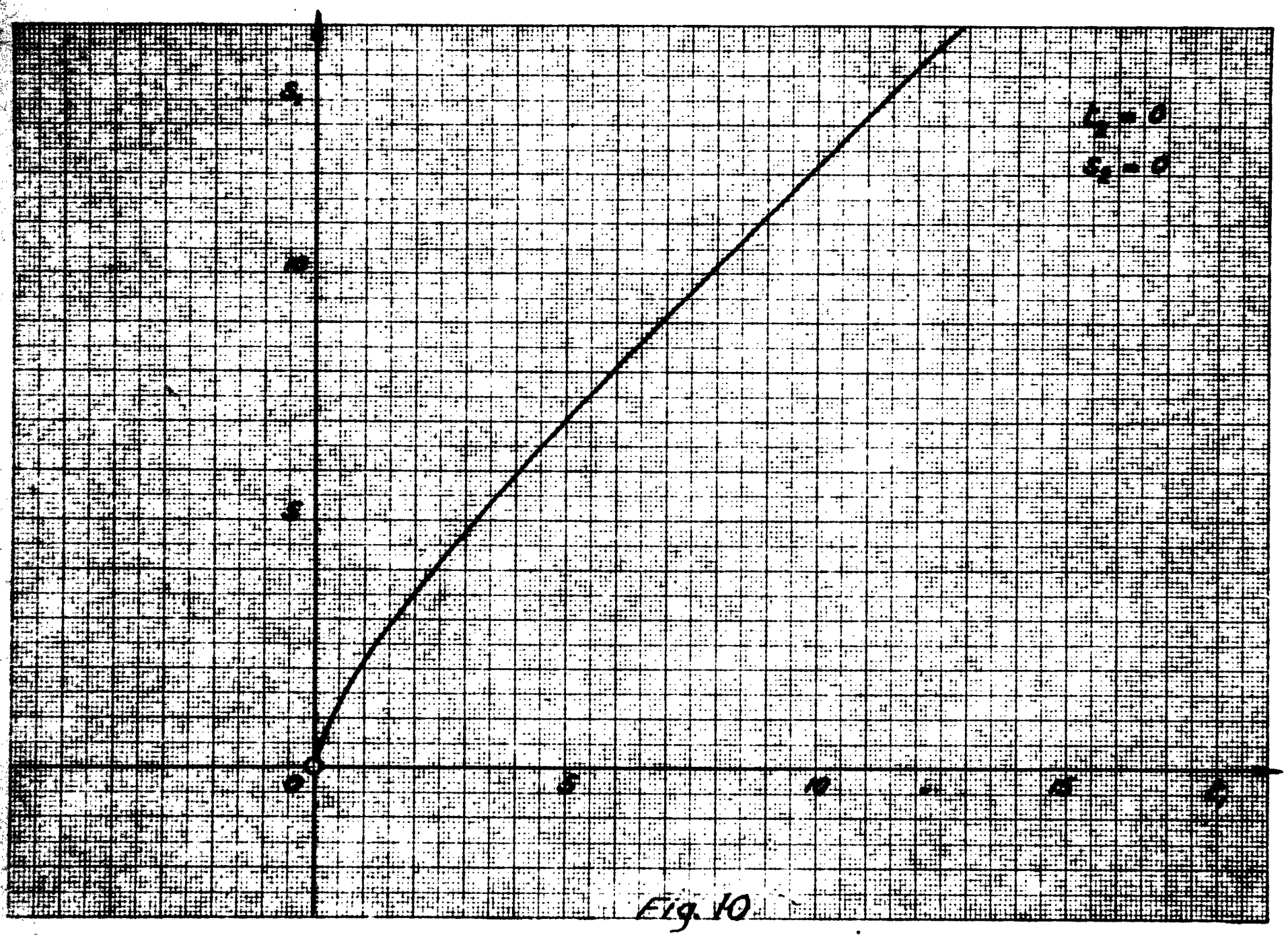

Fig. 10

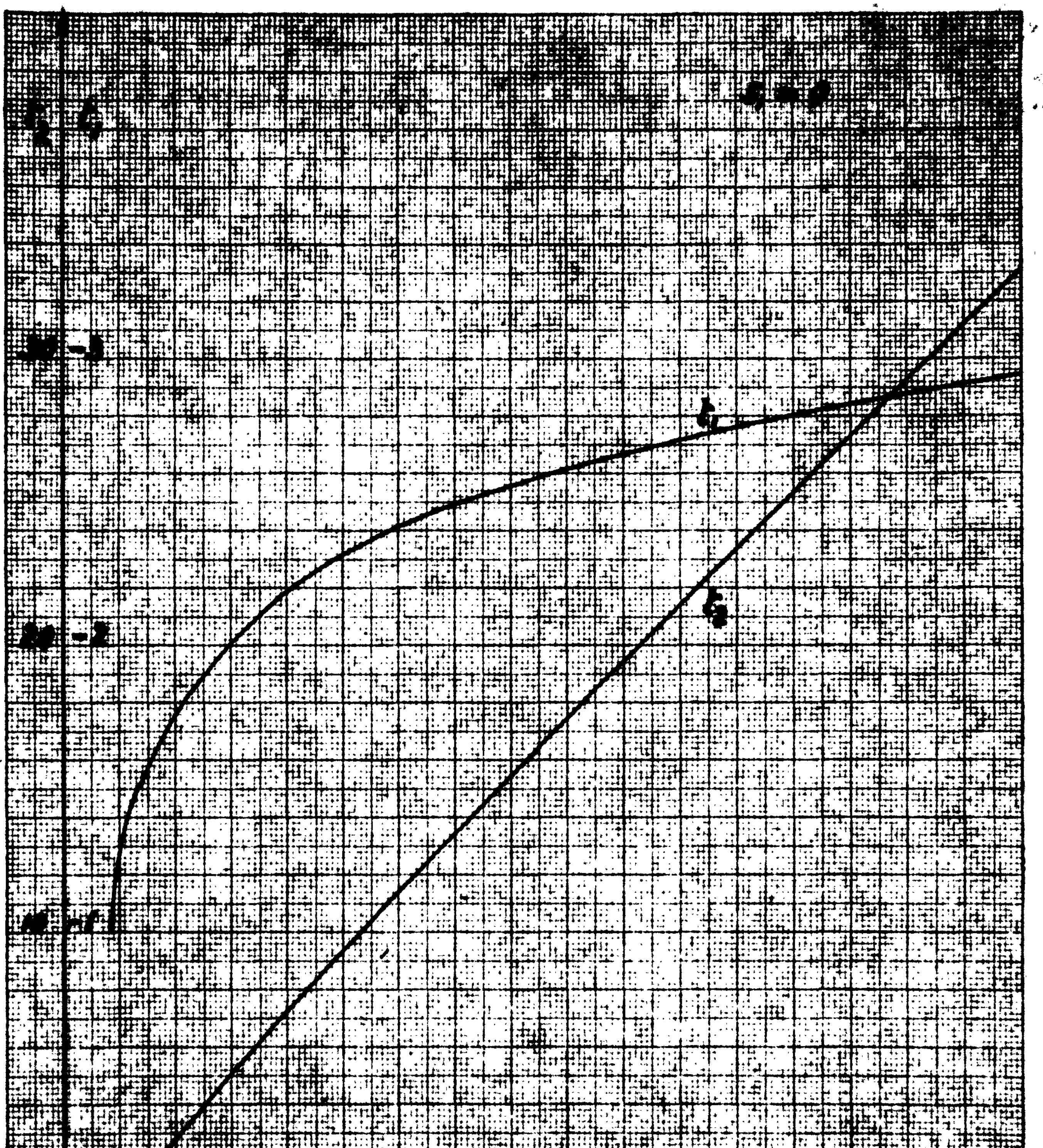

Fig 11

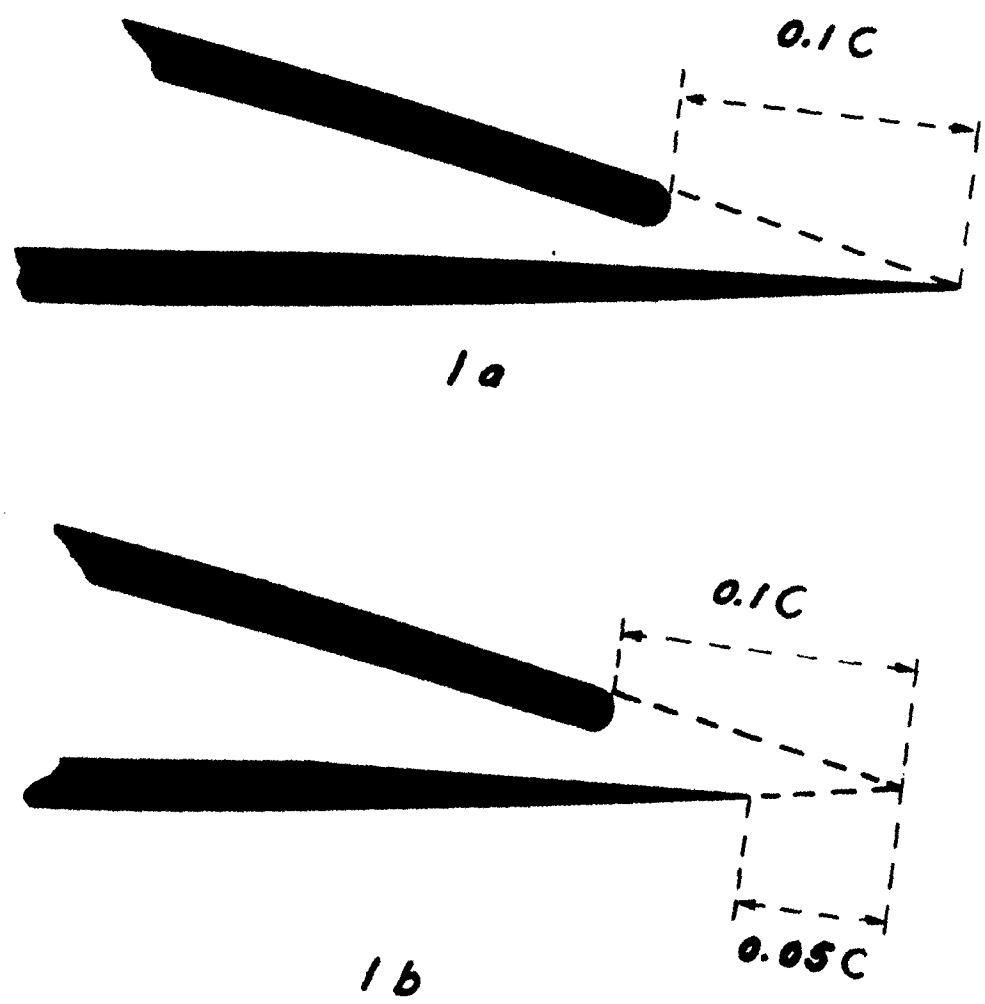

Fig. 12

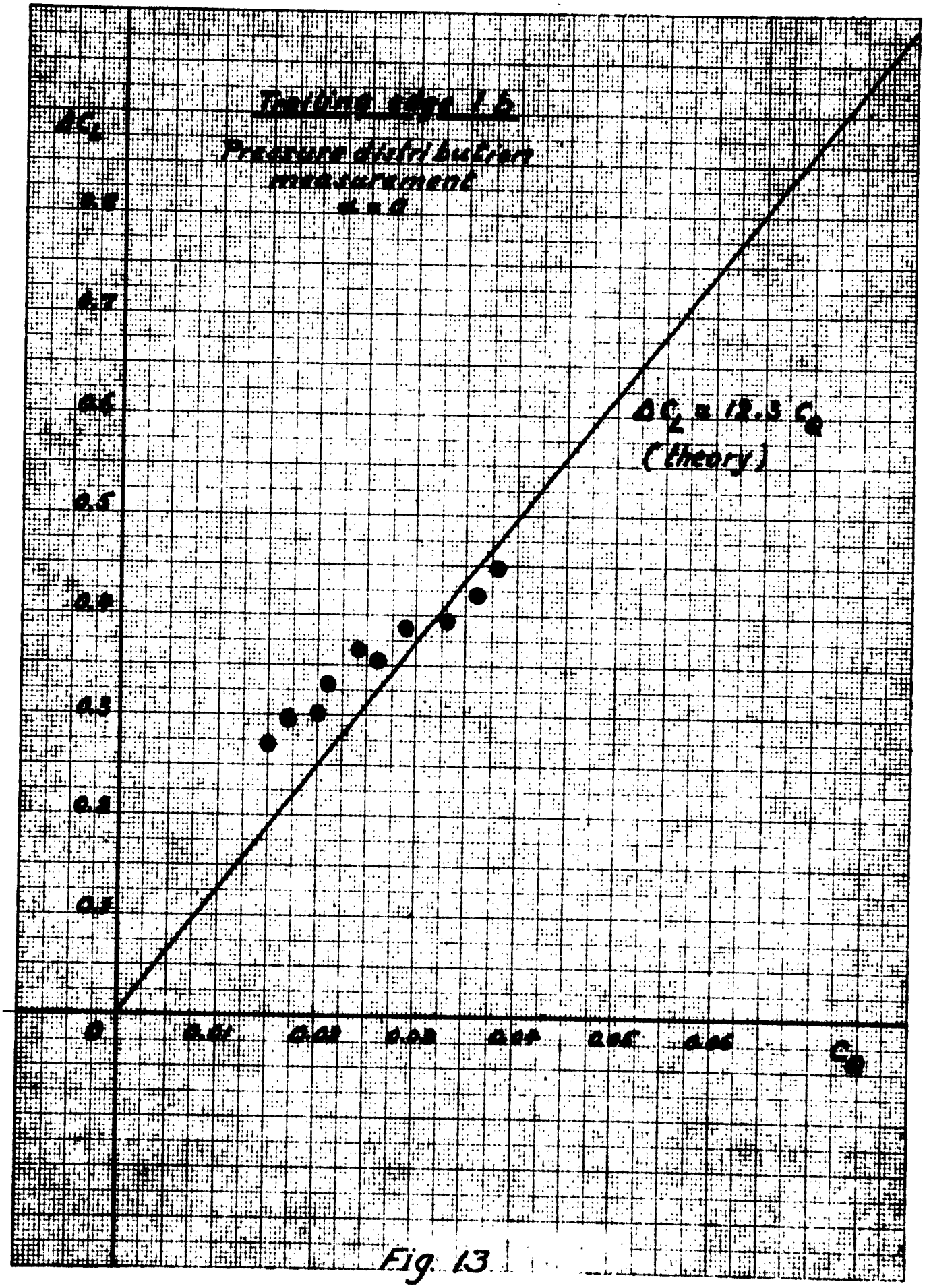

Fig. 13

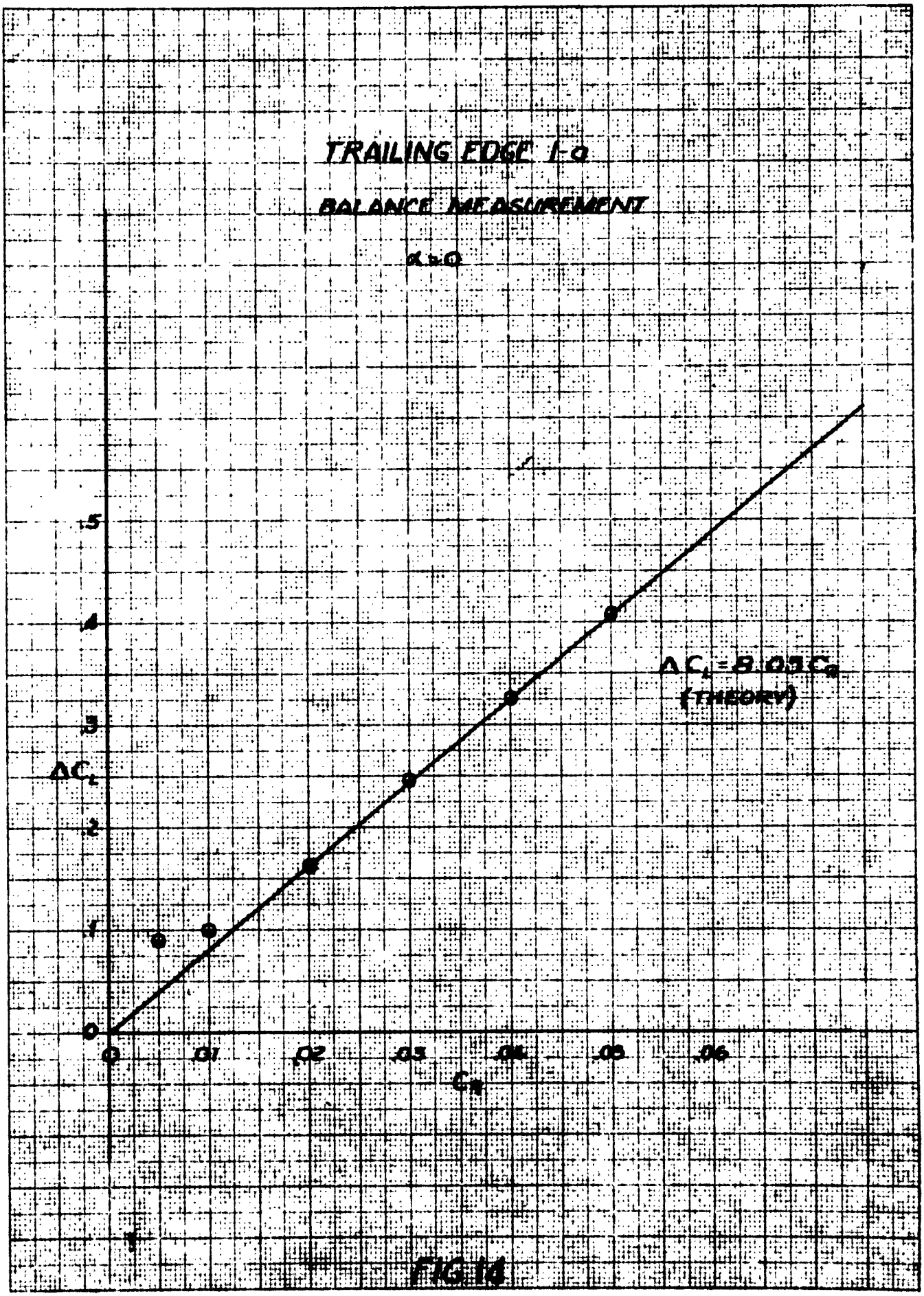
TRAILING EDGE 1-a
BALANCE MEASUREMENT
α = 0
.5
.4
.3
ΔC_L
.2
.1
0
0
.01
.02
.03
.04
.05
.06
C_R
$\Delta C_L = B.03 C_R$
(THEORY)

FIG 14

COMPARISON OF THEORETICAL AND EXPERIMENTAL PRESSURE DISTRIBUTIONS

$\alpha = 0$, $c_a = .0225$, $c_l = 0.387$

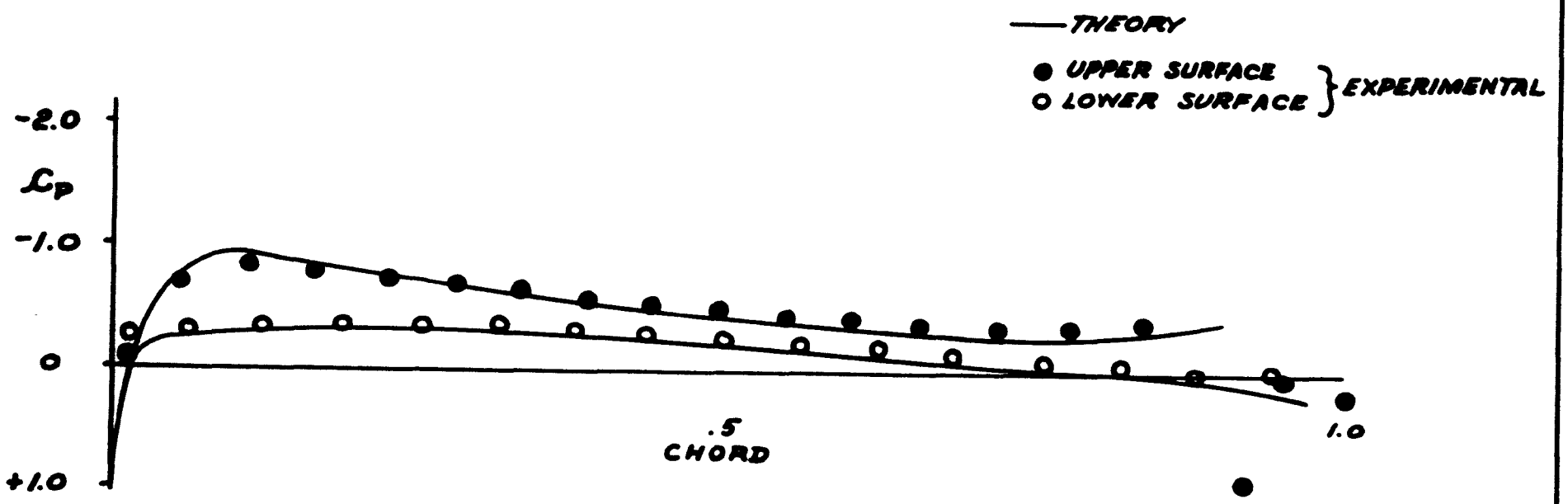

FIG. ~ 15

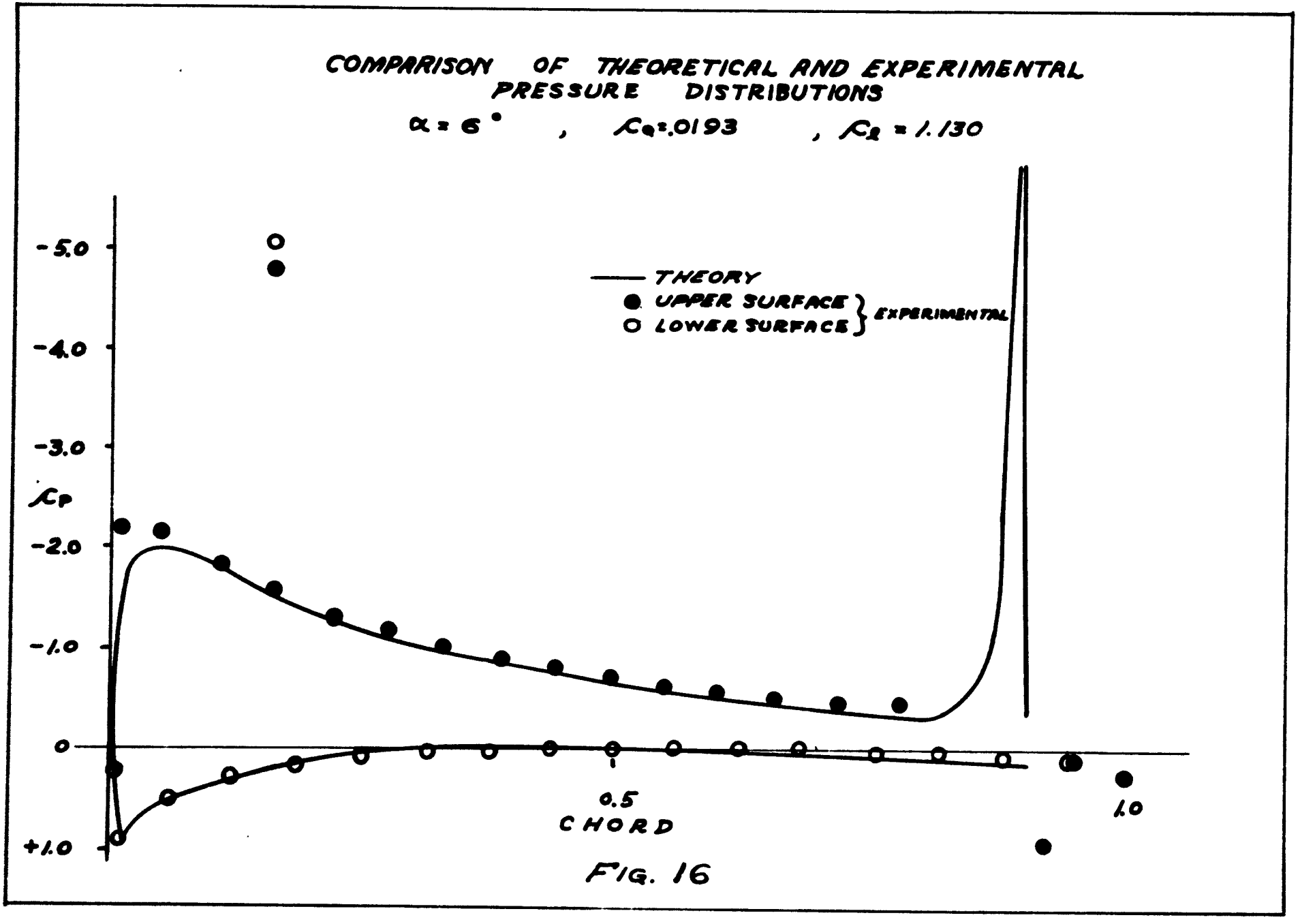
COMPARISON OF THEORETICAL AND EXPERIMENTAL PRESSURE DISTRIBUTIONS
α = 6°, c_{d_0} = .0193, c_l = 1.130
THEORY
UPPER SURFACE
LOWER SURFACE
EXPERIMENTAL
-5.0
-4.0
-3.0
c_p
-2.0
-1.0
0
+1.0
0.5
CHORD
1.0

FIG. 16

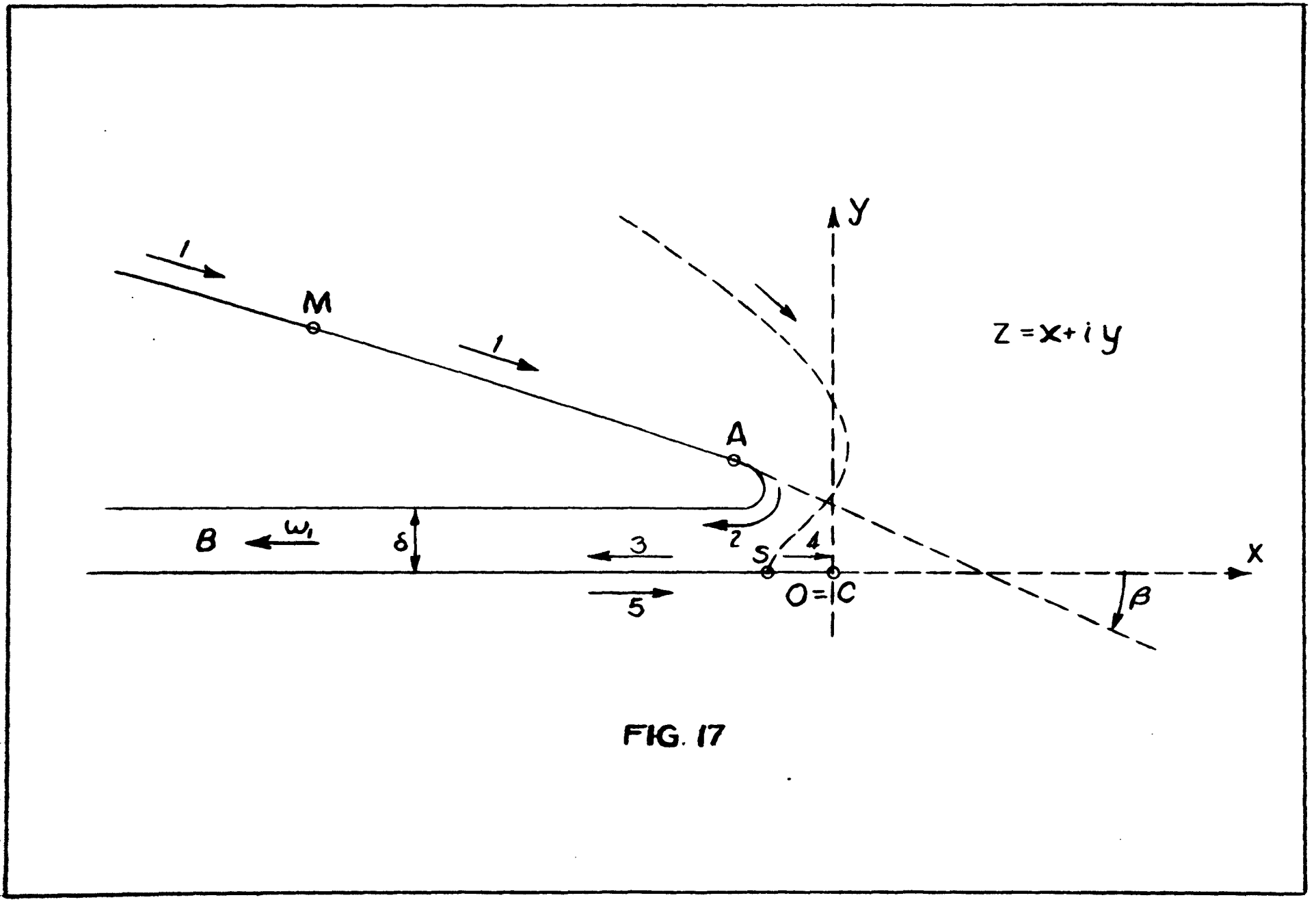

FIG. 17

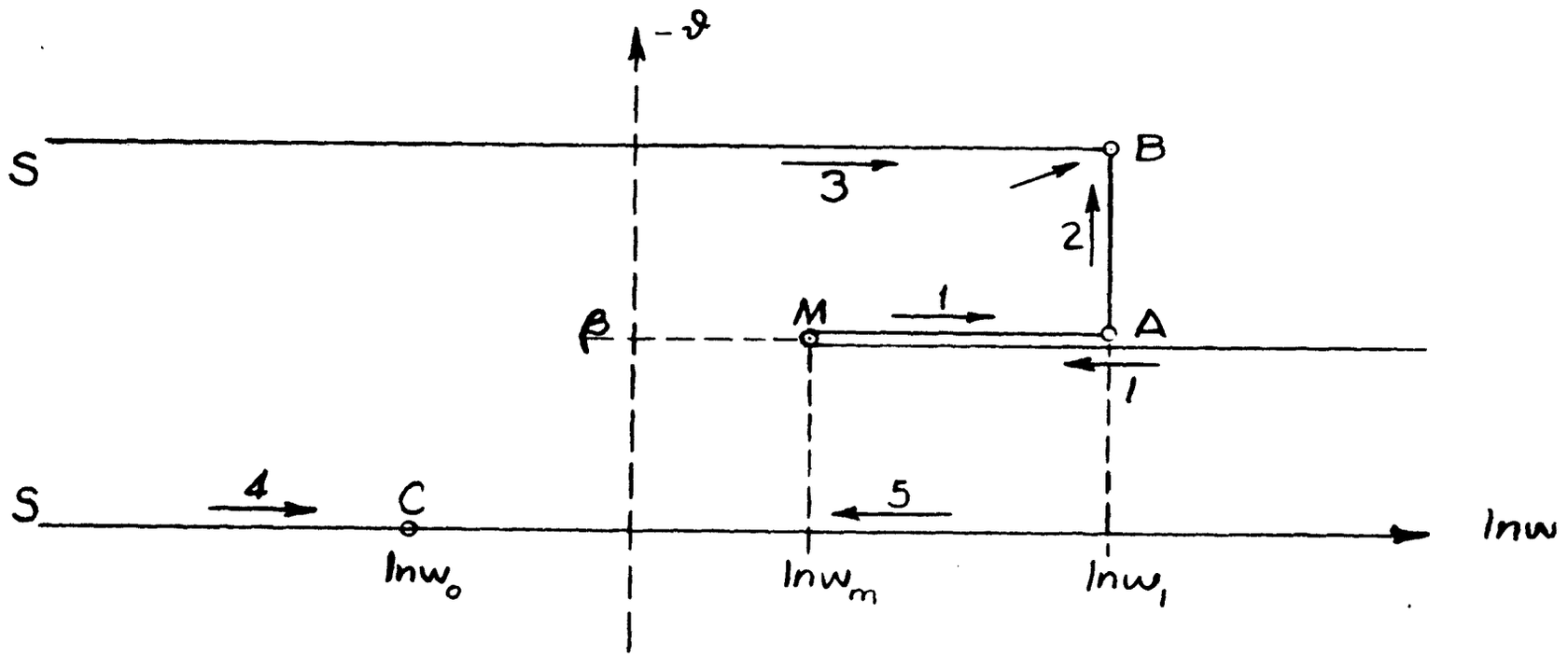

FIG. 18

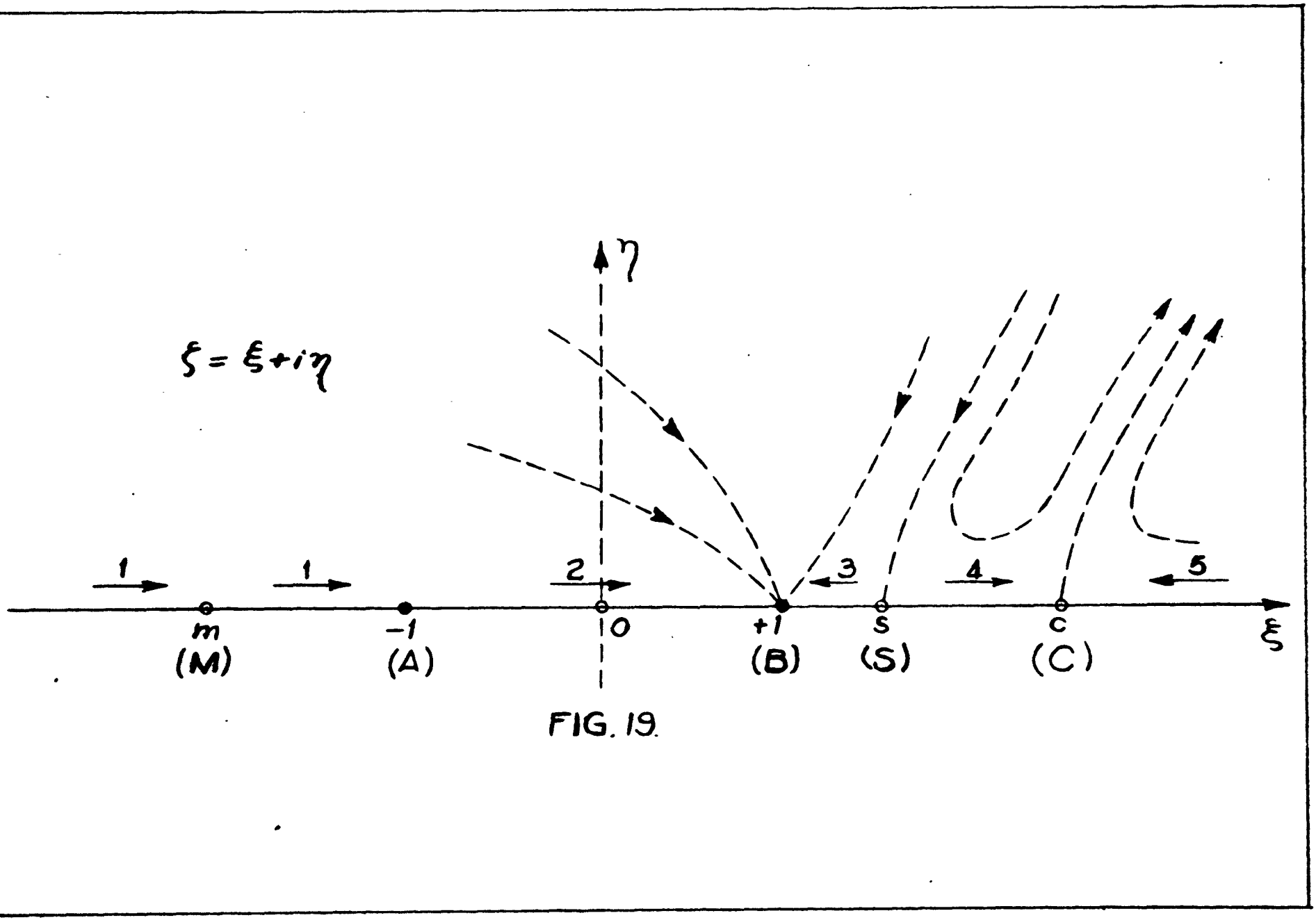

FIG. 19.

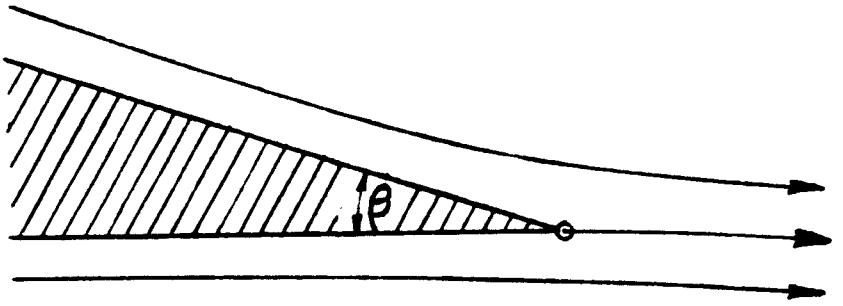

FIG. 20

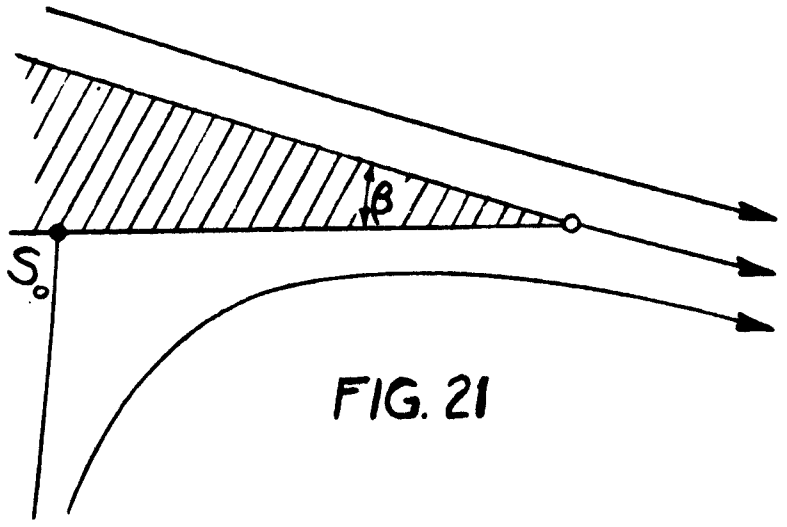

FIG. 21

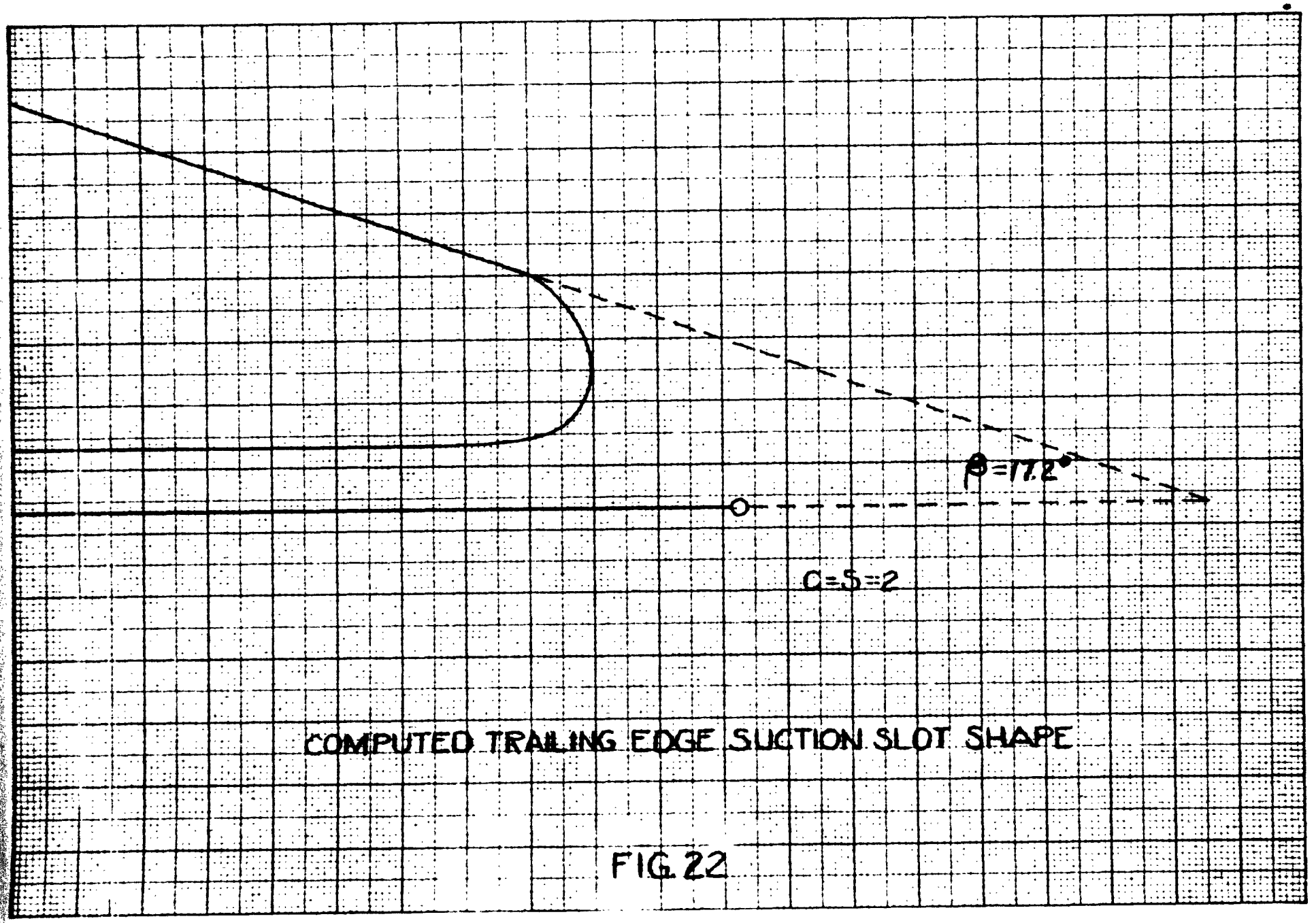

COMPUTED TRAILING EDGE SUCTION SLOT SHAPE

FIG. 22

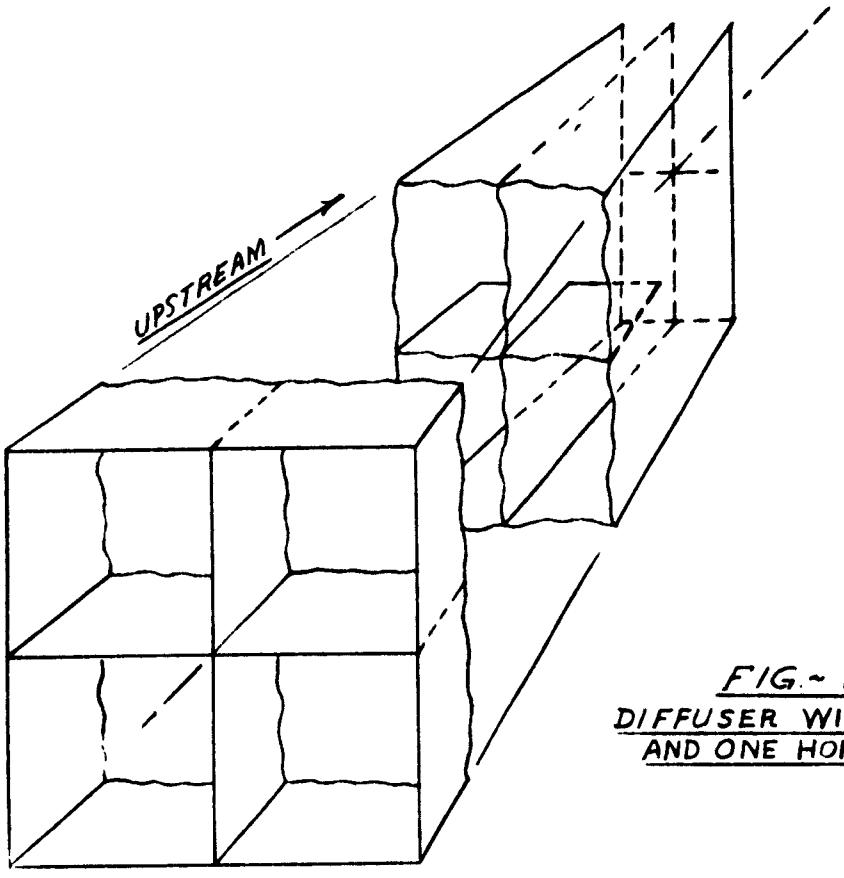

FIG.~ 23a
DIFFUSER WITH ONE VERTICAL AND ONE HORIZONTAL SPLITTER

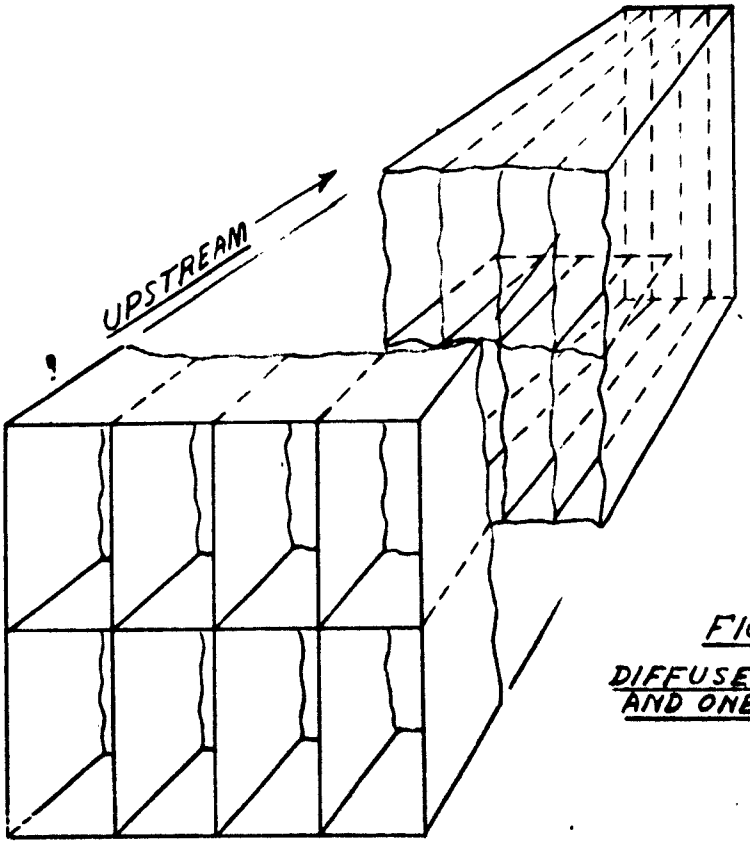

FIG.~ 23b
DIFFUSER WITH THREE VERTICAL AND ONE HORIZONTAL SPLITTER

SCHEMATIC DIAGRAM OF DIFFUSER WITH SPLITTERS

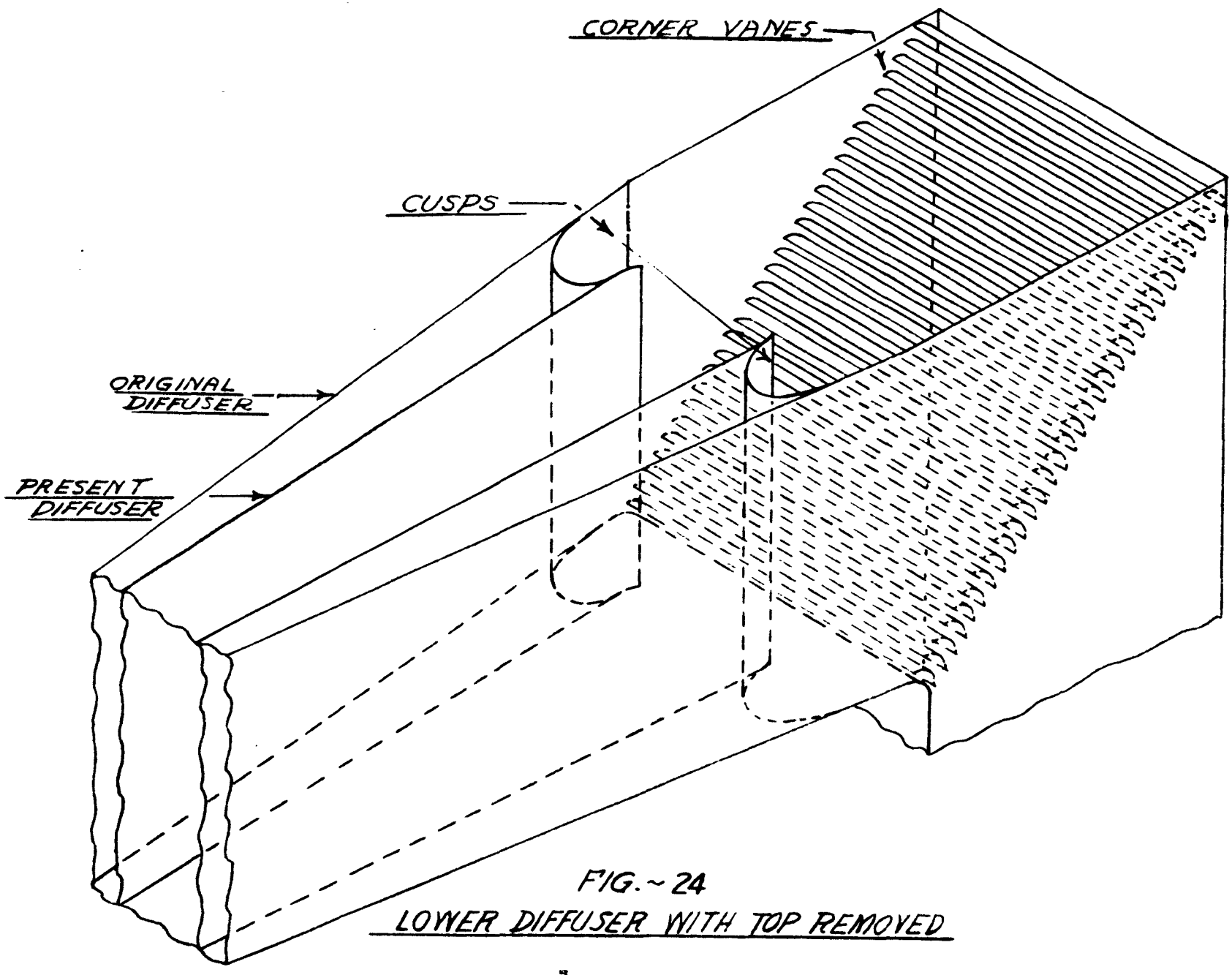

FIG. ~ 24

LOWER DIFFUSER WITH TOP REMOVED

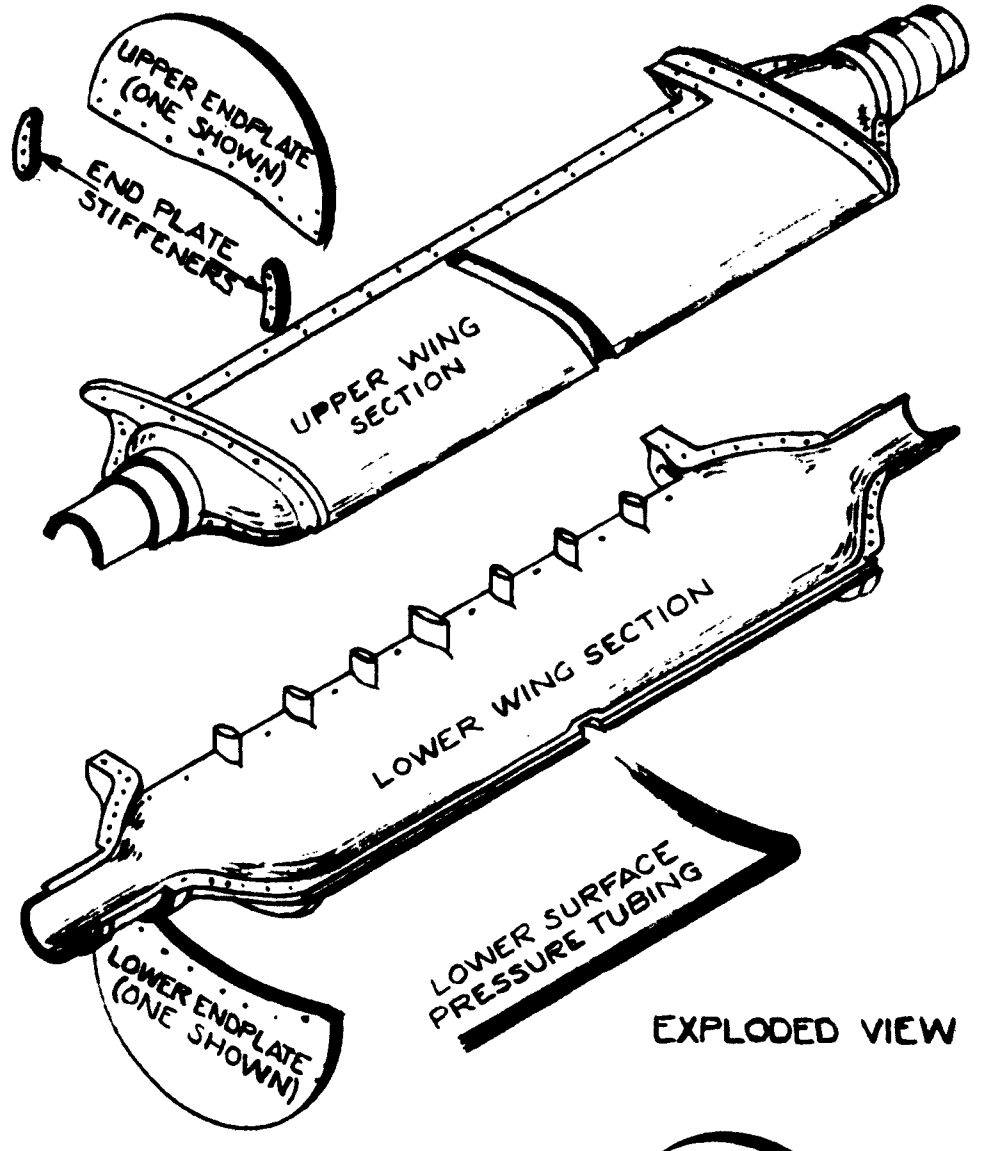

BOUNDARY LAYER CONTROL WIND TUNNEL MODEL

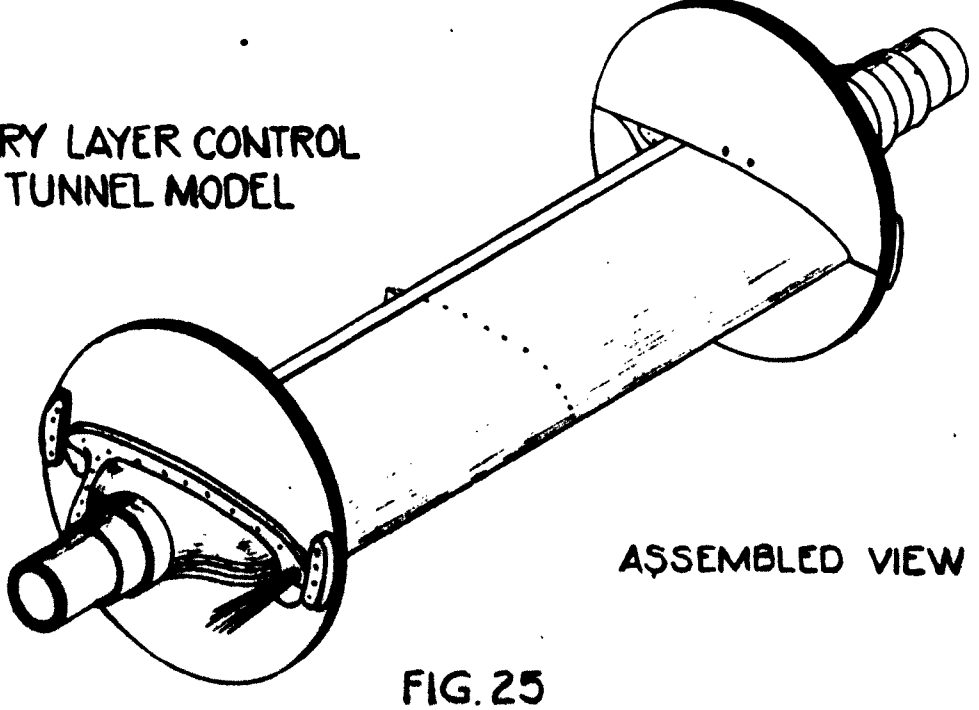

FIG. 25

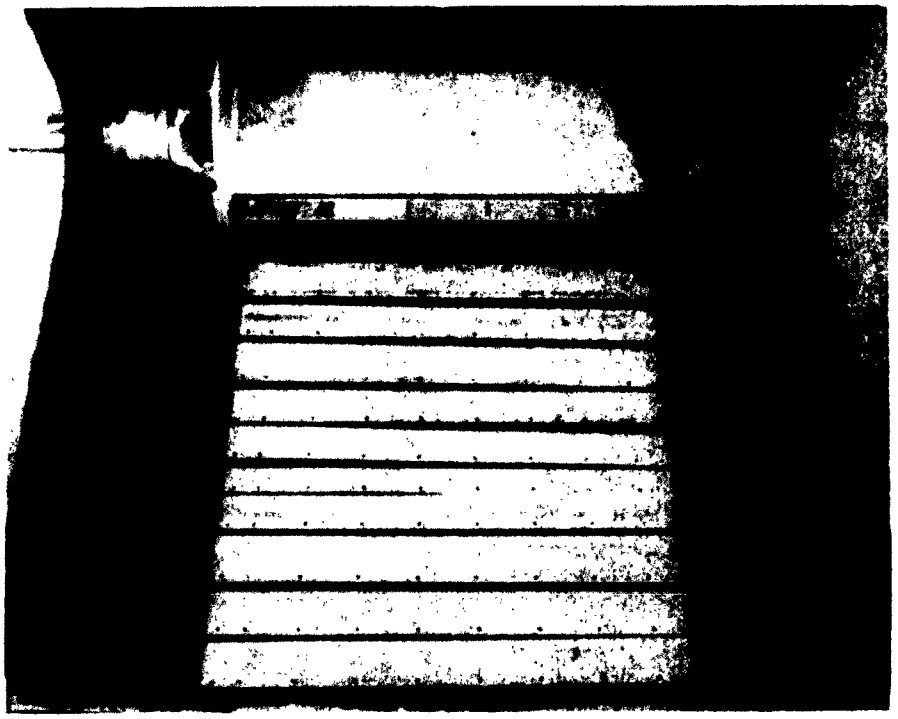

Fig. 26

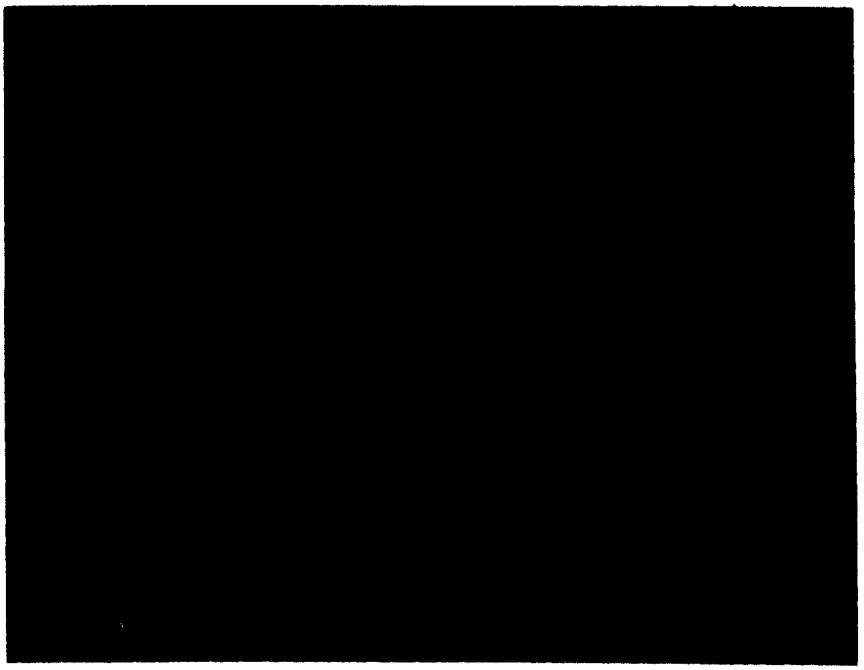

Fig. 27

Fig. 28

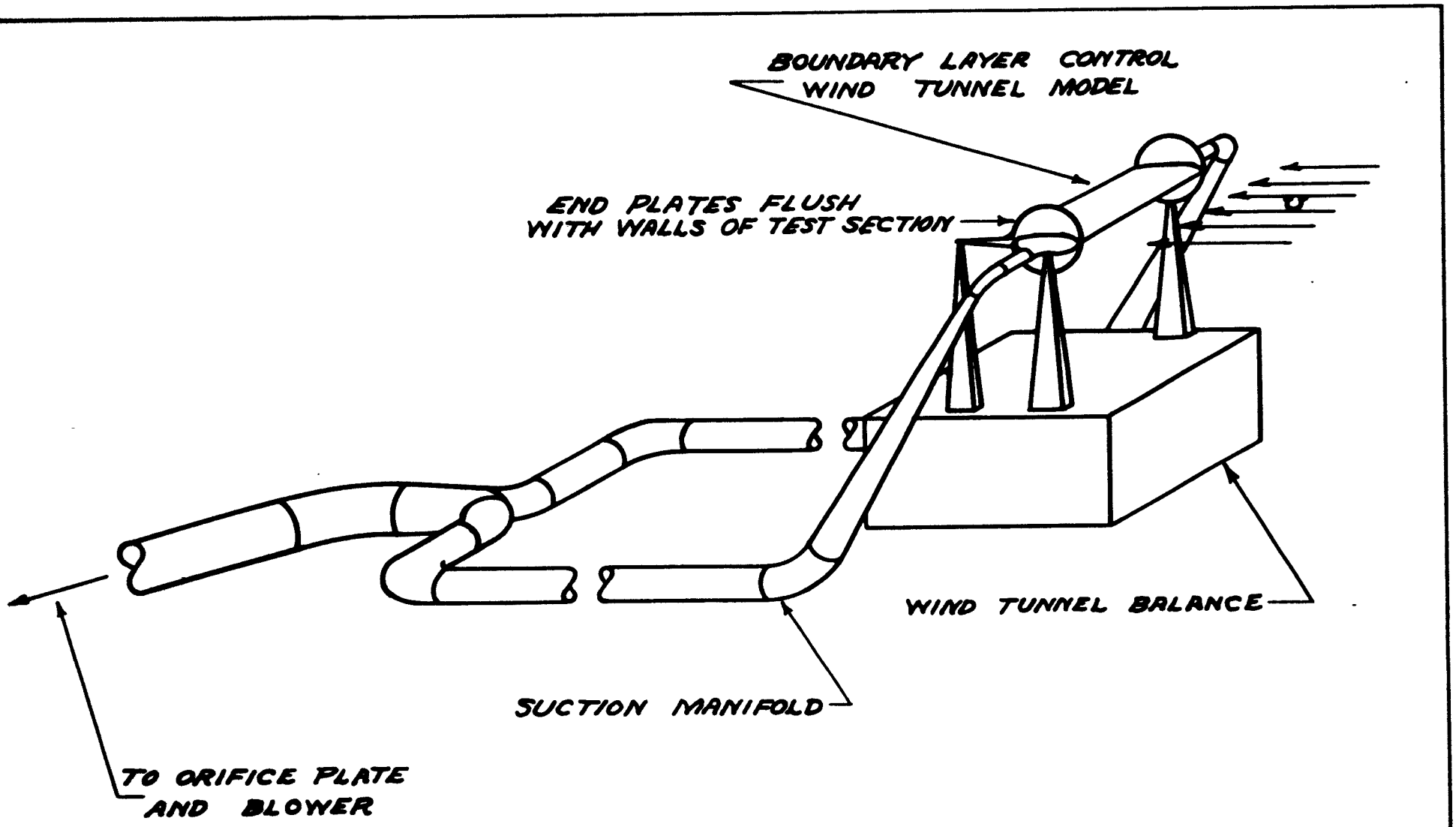

FIG. ~ 29

SCHEMATIC DIAGRAM OF
MODEL, BALANCE AND BLOWER INDUCTION SYSTEM

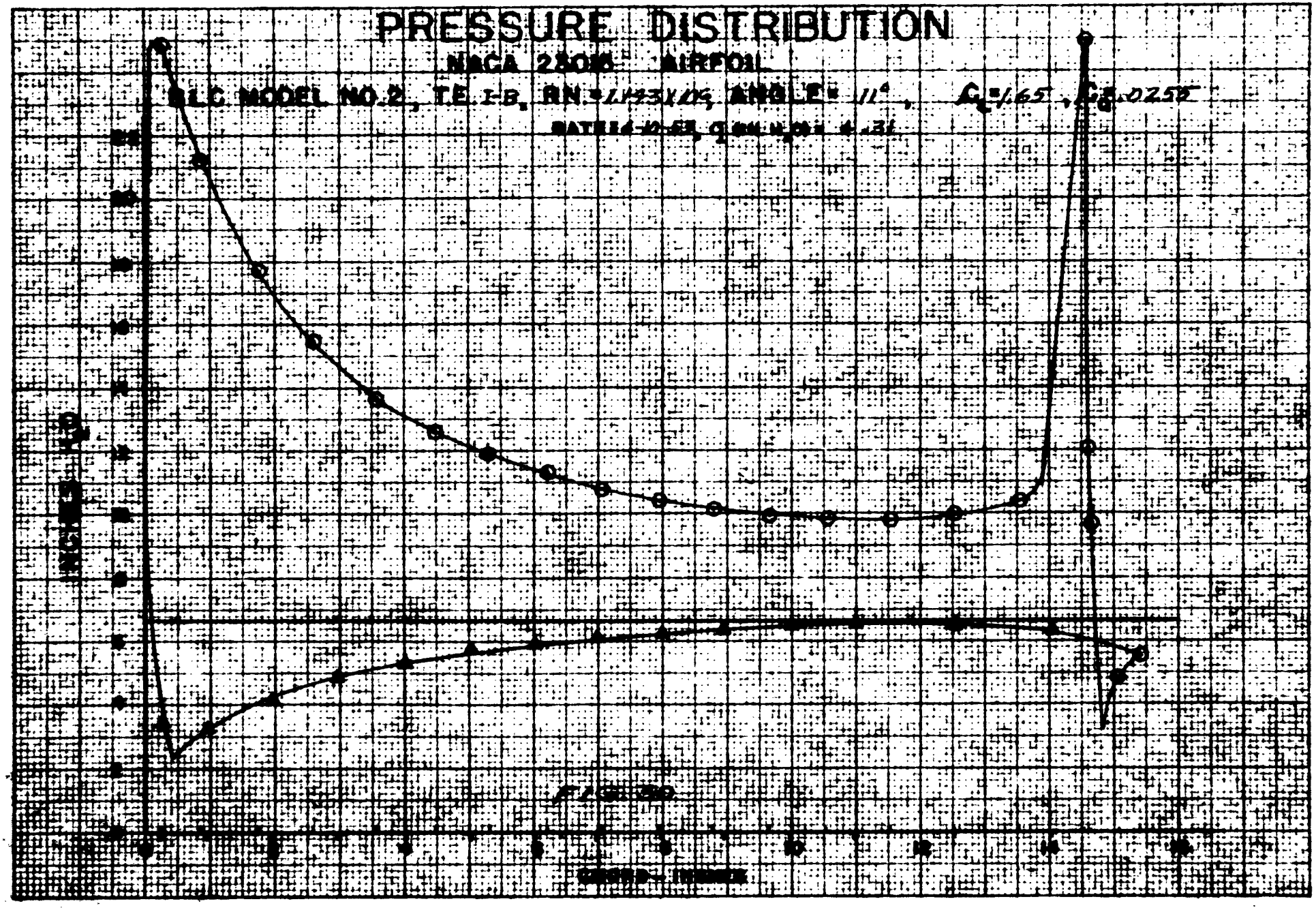

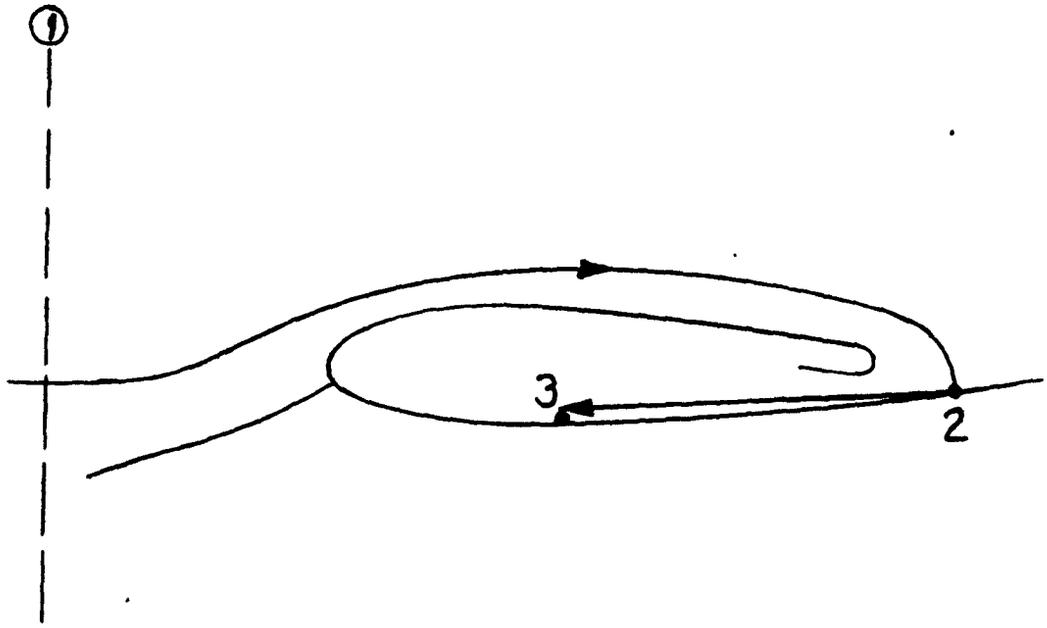

FIG. 31

NACA 23015 AIRFOIL AS MODIFIED FOR TRAILING EDGE SUCTION TESTS

FIG. 32A

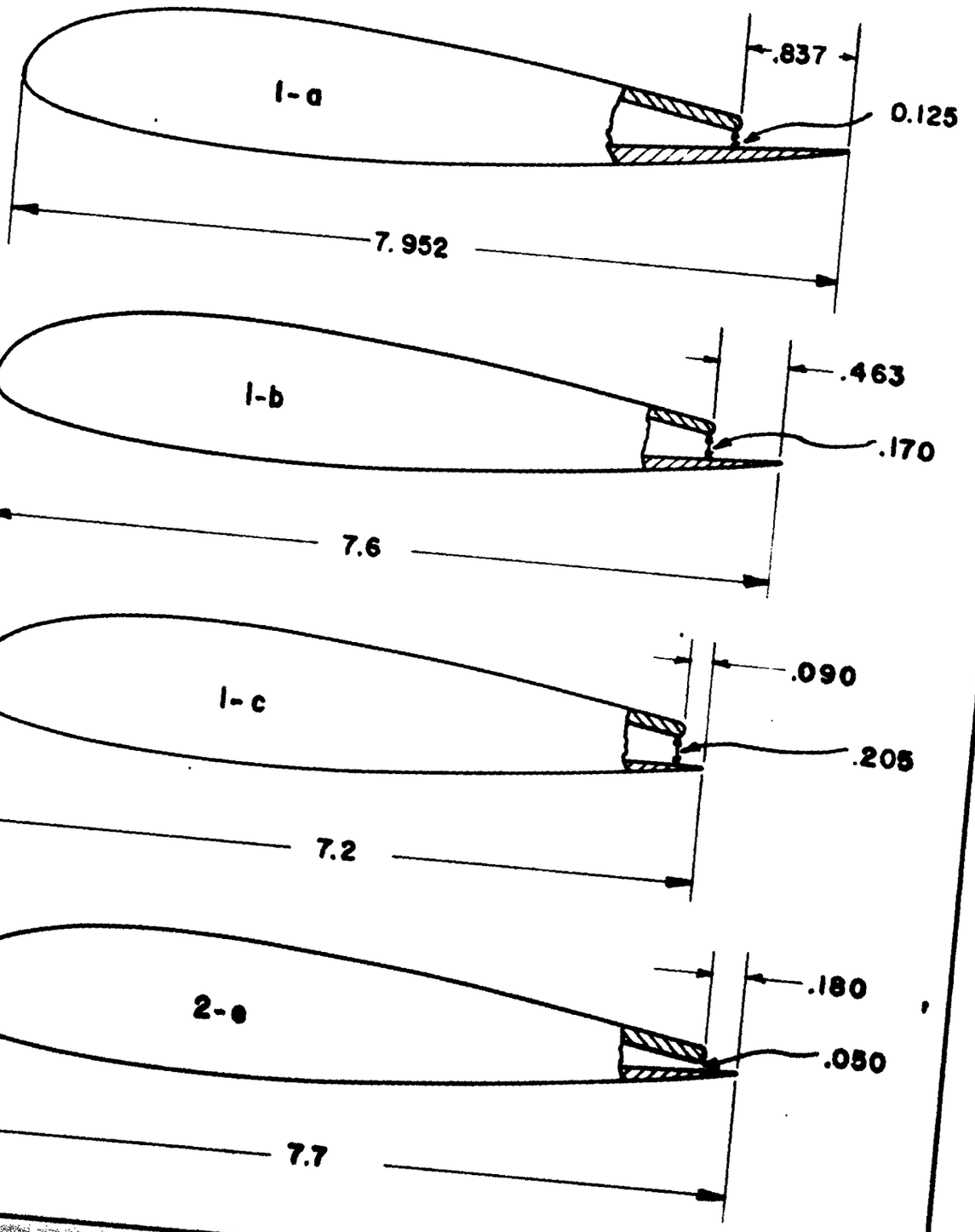

NACA 23015 AIRFOIL AS MODIFIED FOR TRAILING EDGE SUCTION TESTS

FIG. 32 B

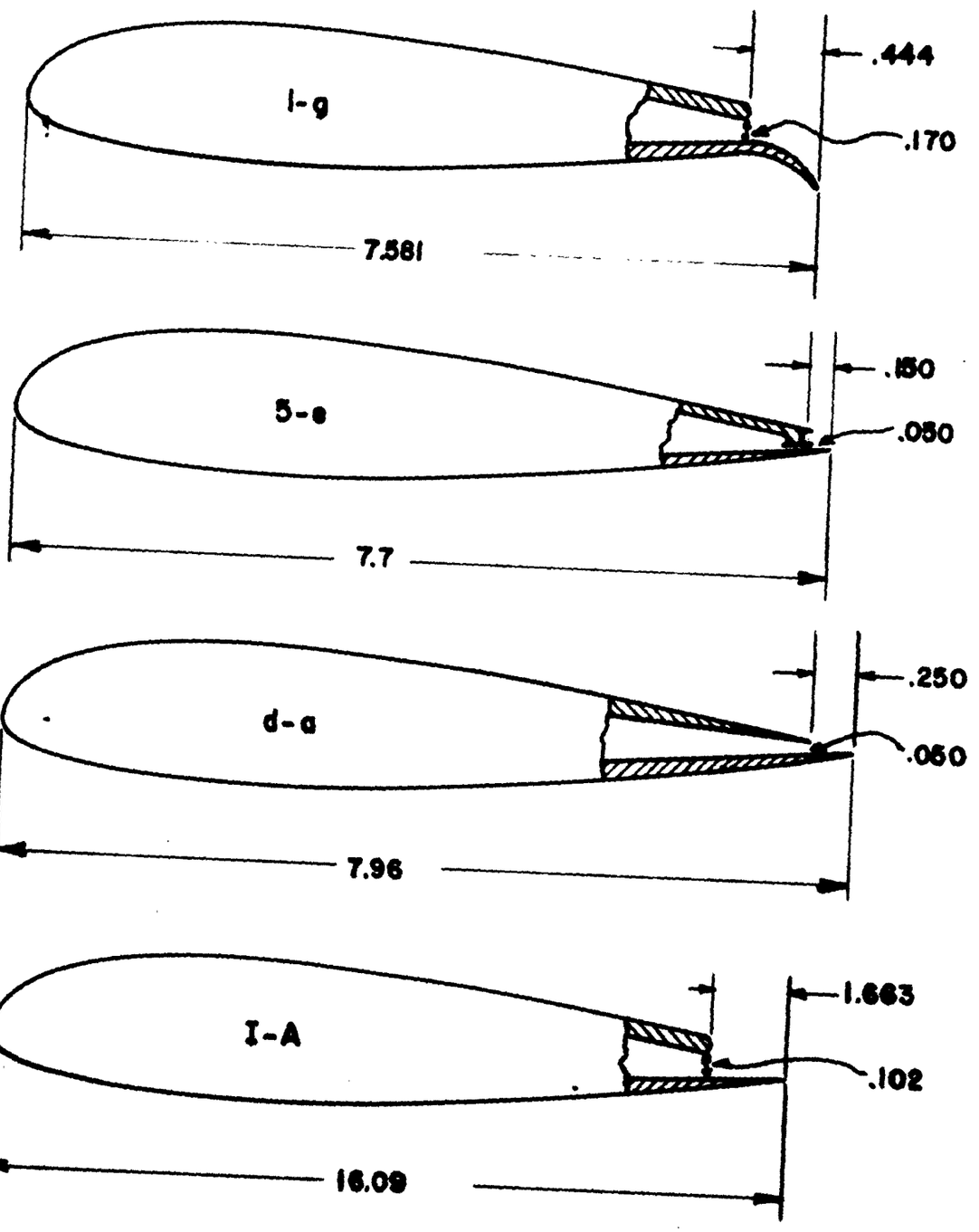

NACA 23015 AIRFOIL AS MODIFIED FOR TRAILING EDGE SUCTION TESTS

FIG. 32 C

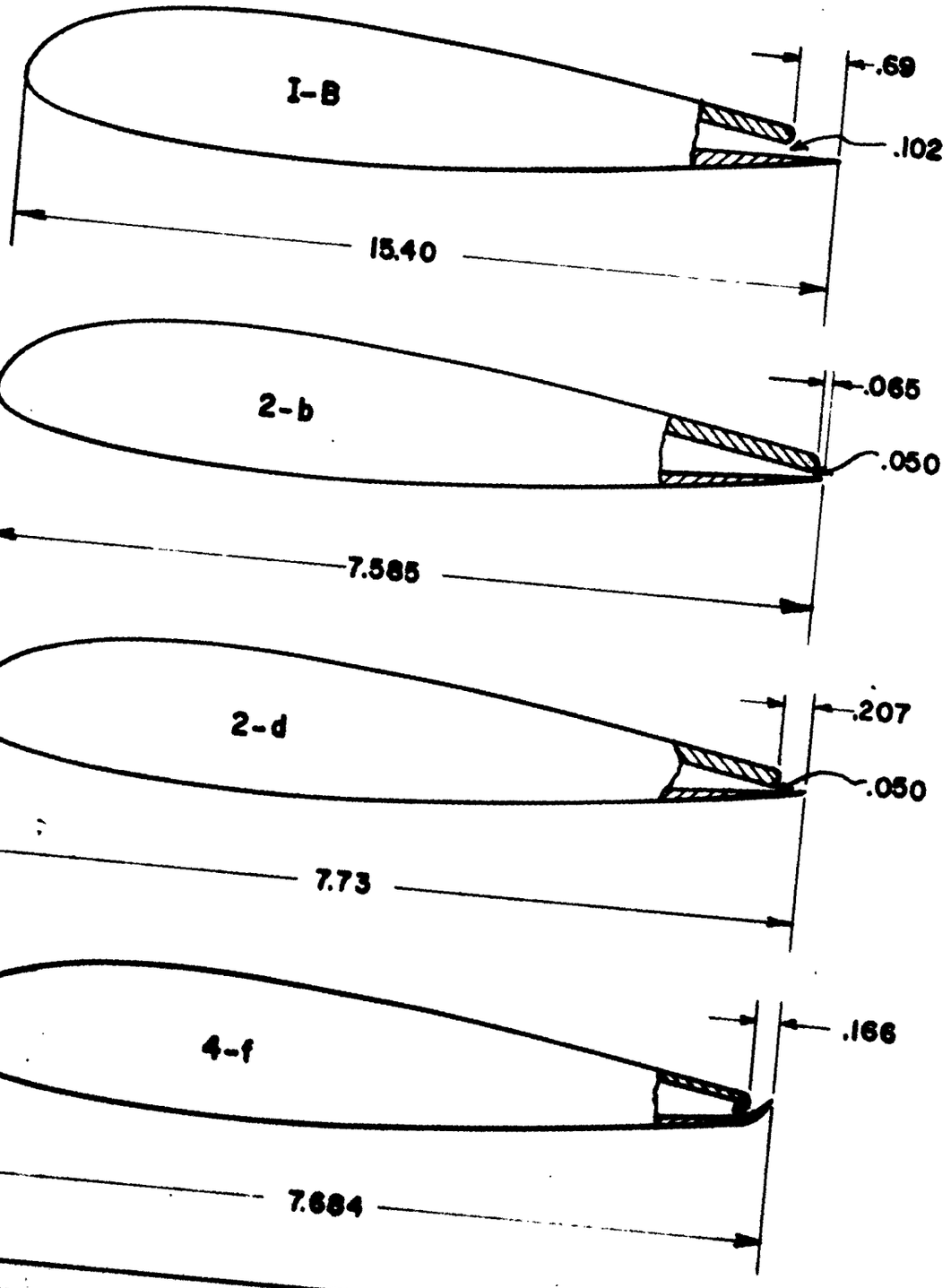

VARIABLE TRAILING EDGE

T.E. 1-V

FIG. 33

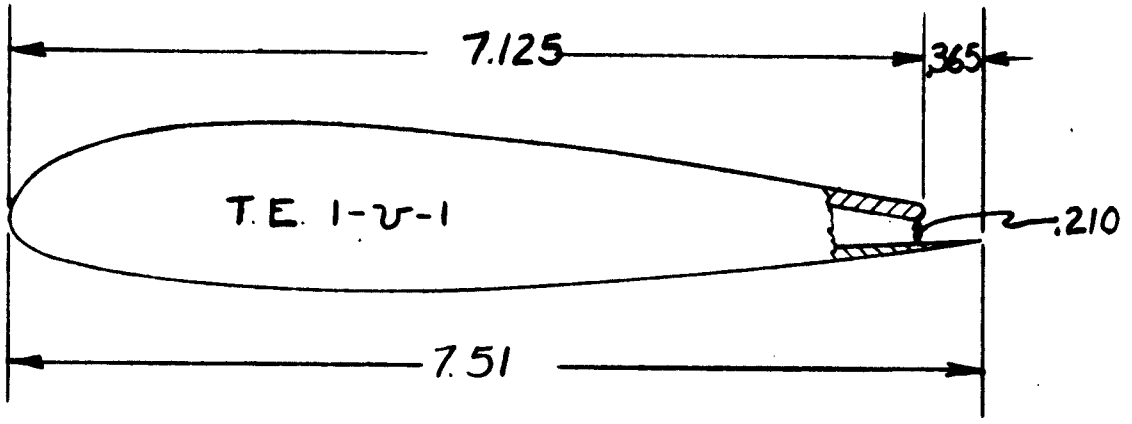

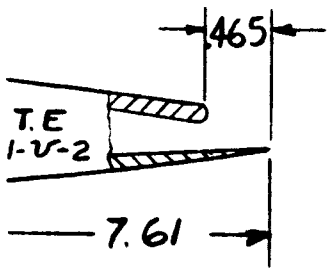

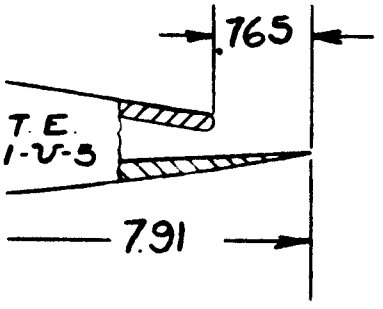

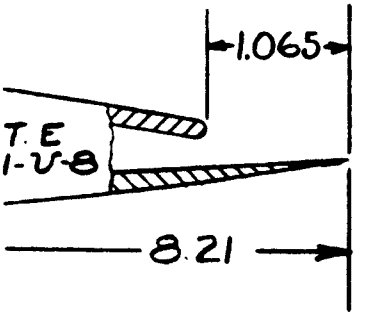

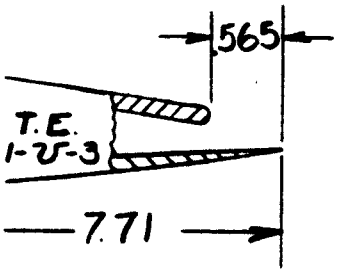

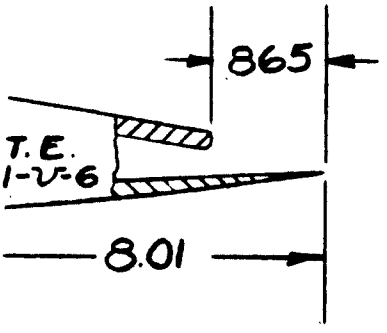

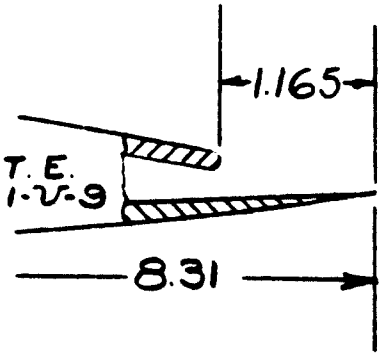

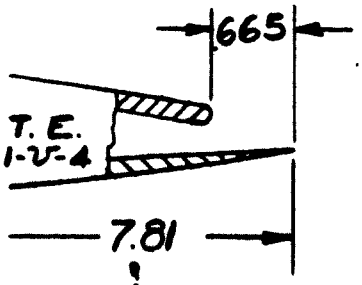

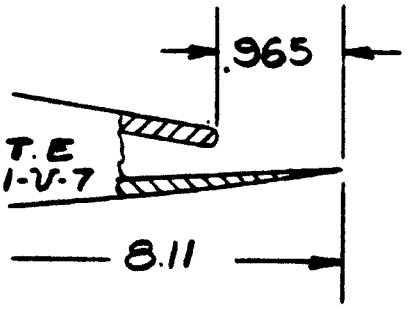

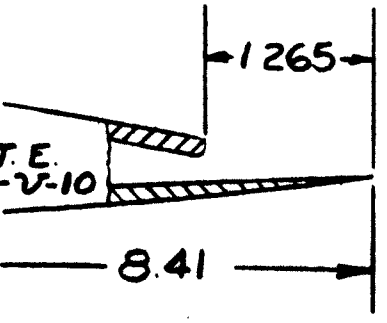

TWO DIMENSIONAL CHARACTERISTICS OF NACA 23015 AIRFOIL WITH NORMAL TRAILING EDGE 2-27-52

COMPARISON OF PRINCETON AND NACA LIFT DATA

FIG. 34

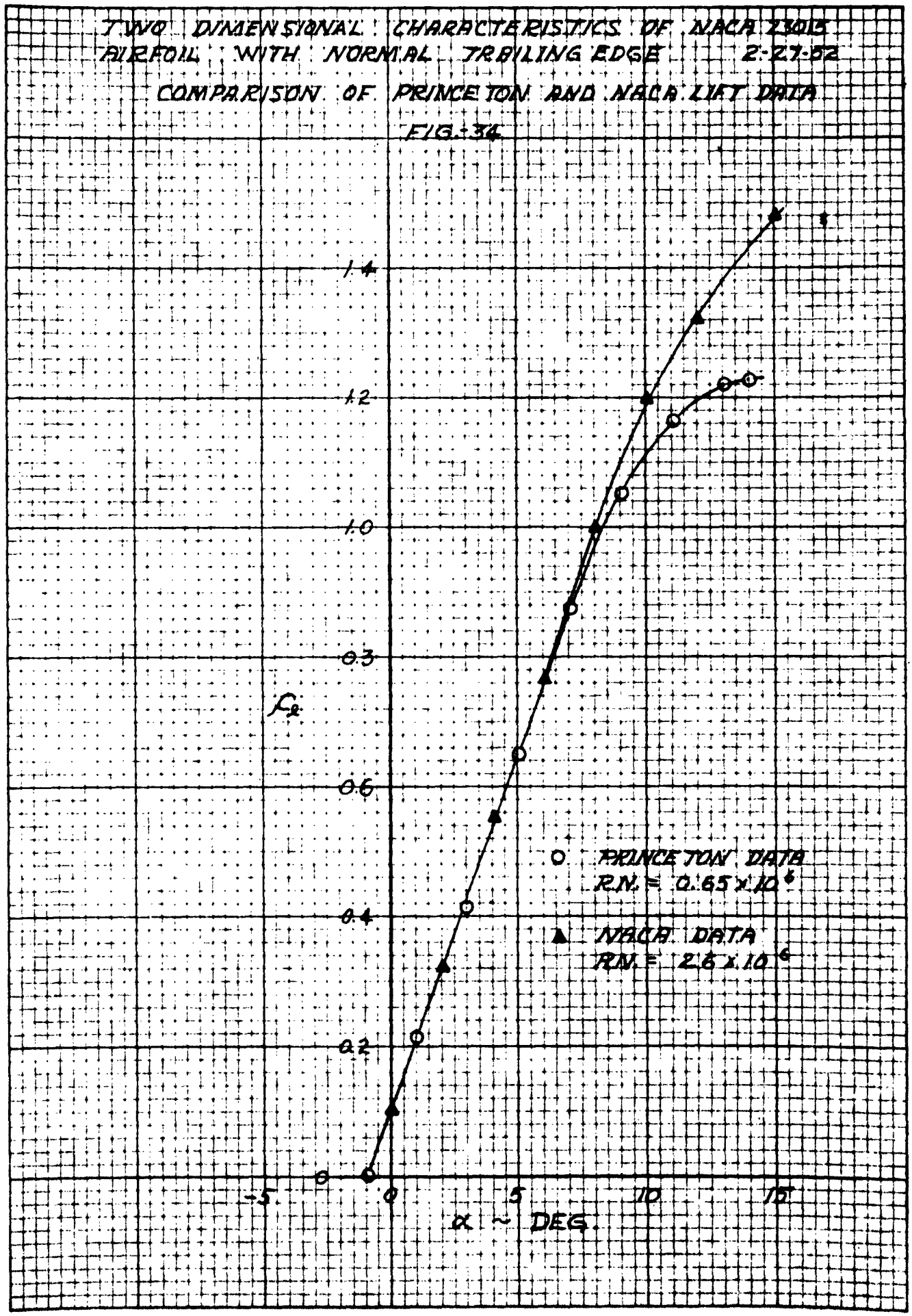

TWO DIMENSIONAL CHARACTERISTICS OF NACA 23015 AIRFOIL MODIFIED FOR TRAILING EDGE SUCTION

TRAILING EDGE 1/-2 , R.N. 1.690 x 10^6 , 4-23-42

C_l VS. α FOR SEVERAL VALUES OF C_Q

FIG.-35

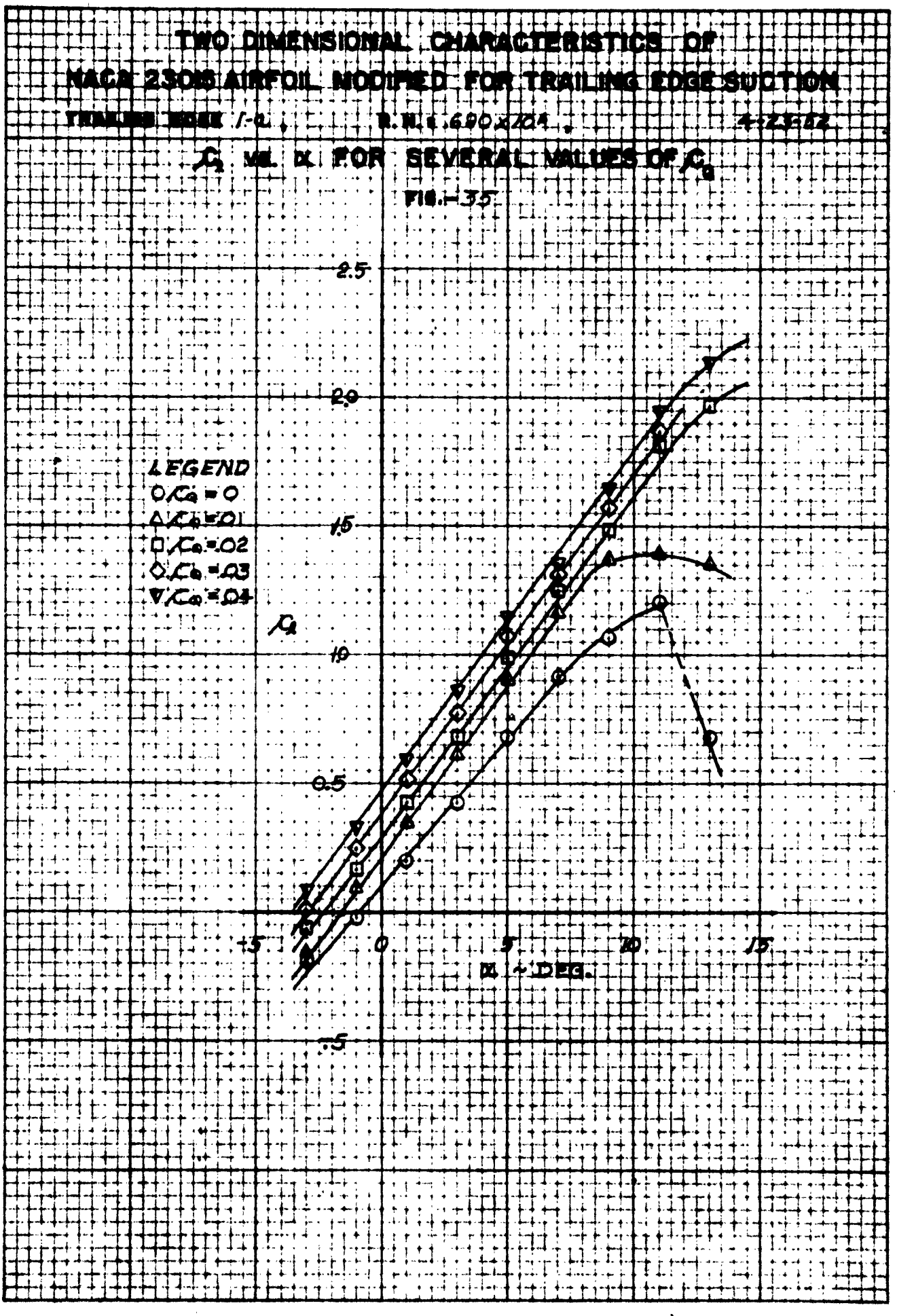

KEUFFEL & ESSER CO.
10 X 10 to the inch

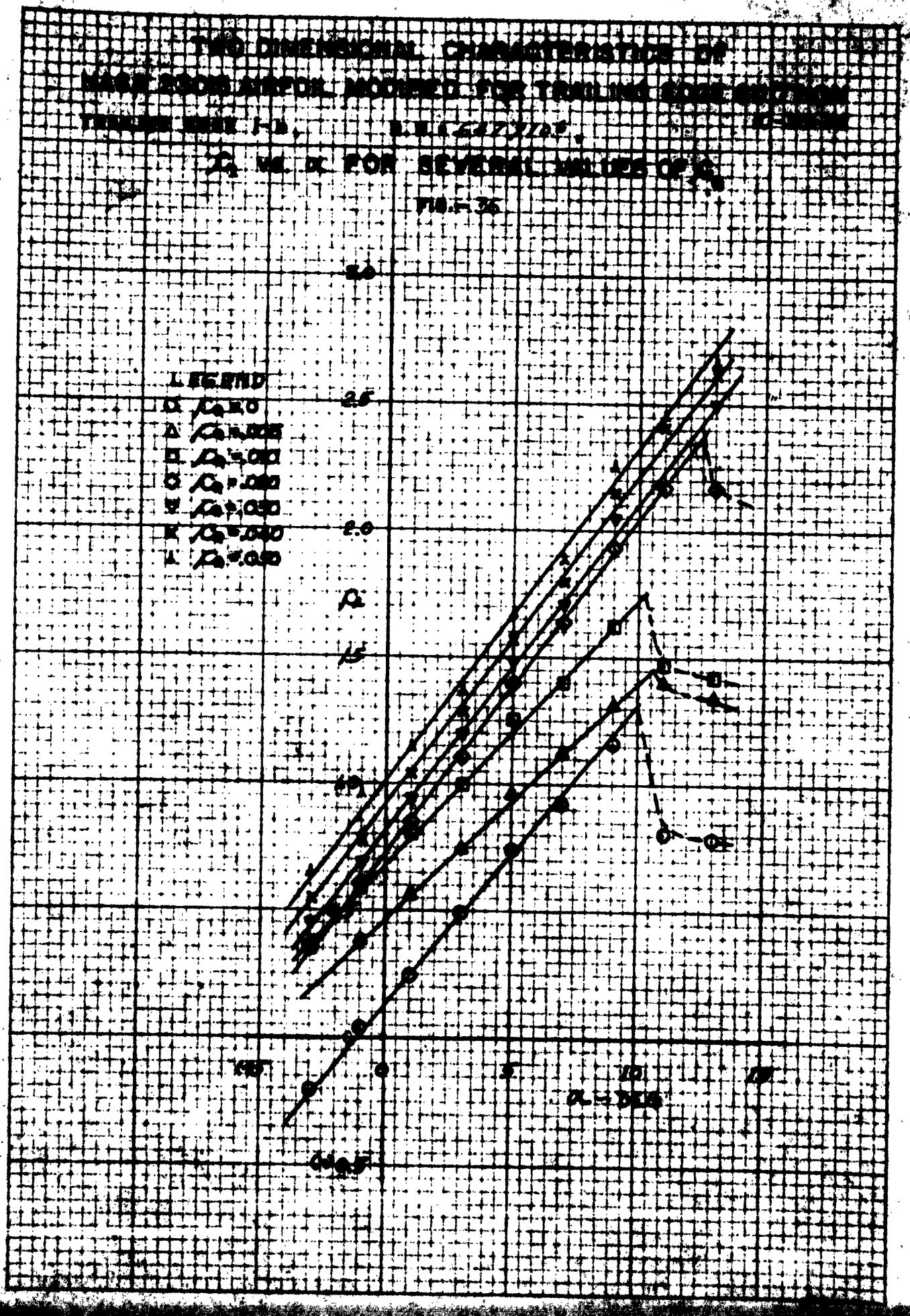
TWO DIMENSIONAL CHARACTERISTICS OF
NACA 23012 AIRFOIL MODIFIED FOR TRAILING EDGE FLAP
C_{l_α} VS. α FOR SEVERAL VALUES OF δ_f
FIG. 35
LEGEND
$\delta_f = 0$
$\delta_f = .005$
$\delta_f = .010$
$\delta_f = .020$
$\delta_f = .030$
$\delta_f = .040$
$\delta_f = .050$
2.6
2.0
C_{l_α}
1.6
1.2
.8
-10
0
10
α - DEG

TWO DIMENSIONAL CHARACTERISTICS OF NACA 2308 AIRFOIL MODIFIED FOR TRAILING EDGE SUCTION

TRAILING EDGE 1-C, R.N. = .561 X 10⁶, S.T. 7-52

C_l VS. α FOR SEVERAL VALUES OF C_q

FIG.-37

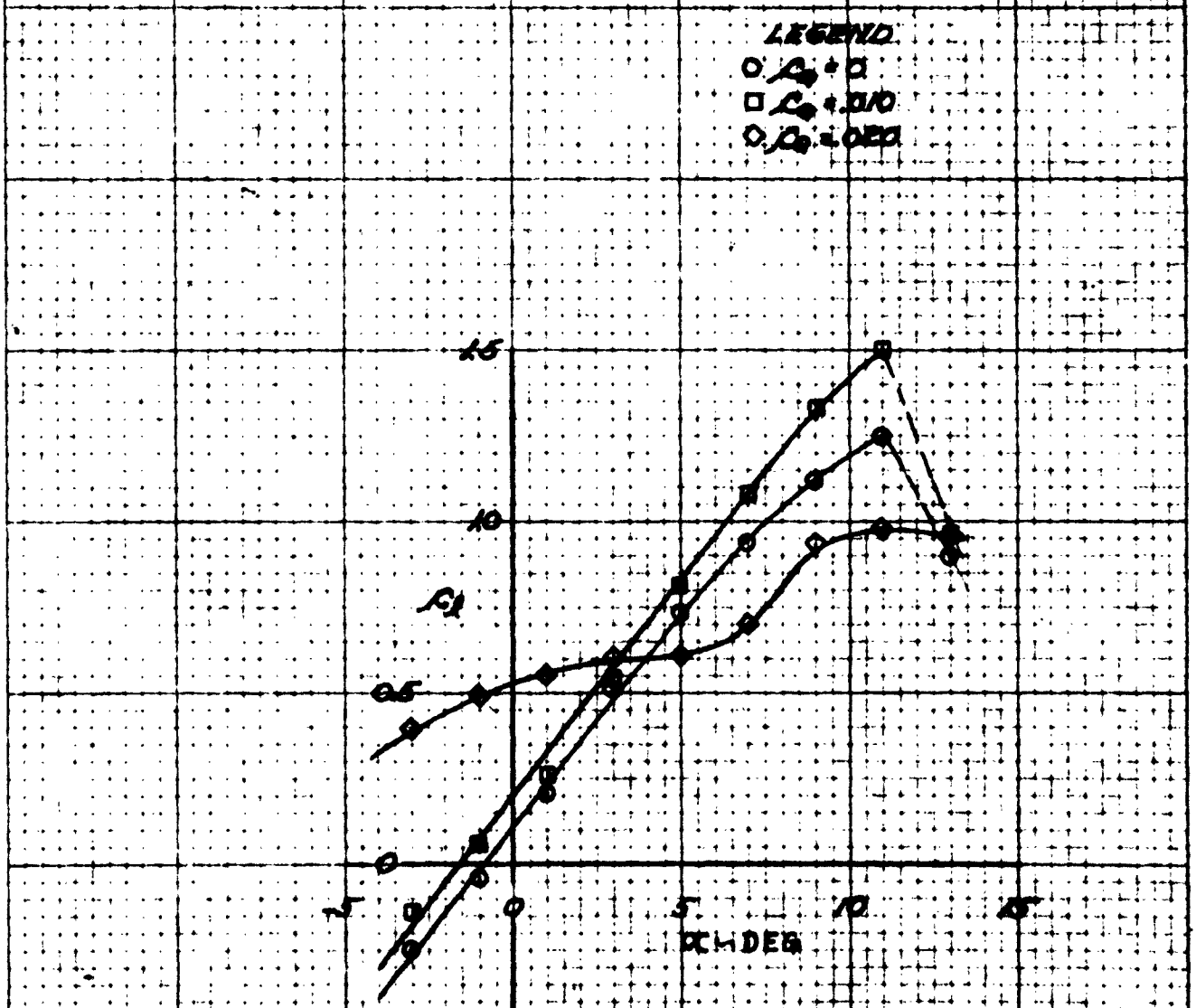

TWO DIMENSIONAL CHARACTERISTICS OF NACA 23018 AIRFOIL MODIFIED FOR TRAILING EDGE SUCTION

TRAILING EDGE 2-D, R.N. = 6M X 10⁶, 8-28-52

C_l VS. α FOR SEVERAL VALUES OF C_q

FIG. - 3B

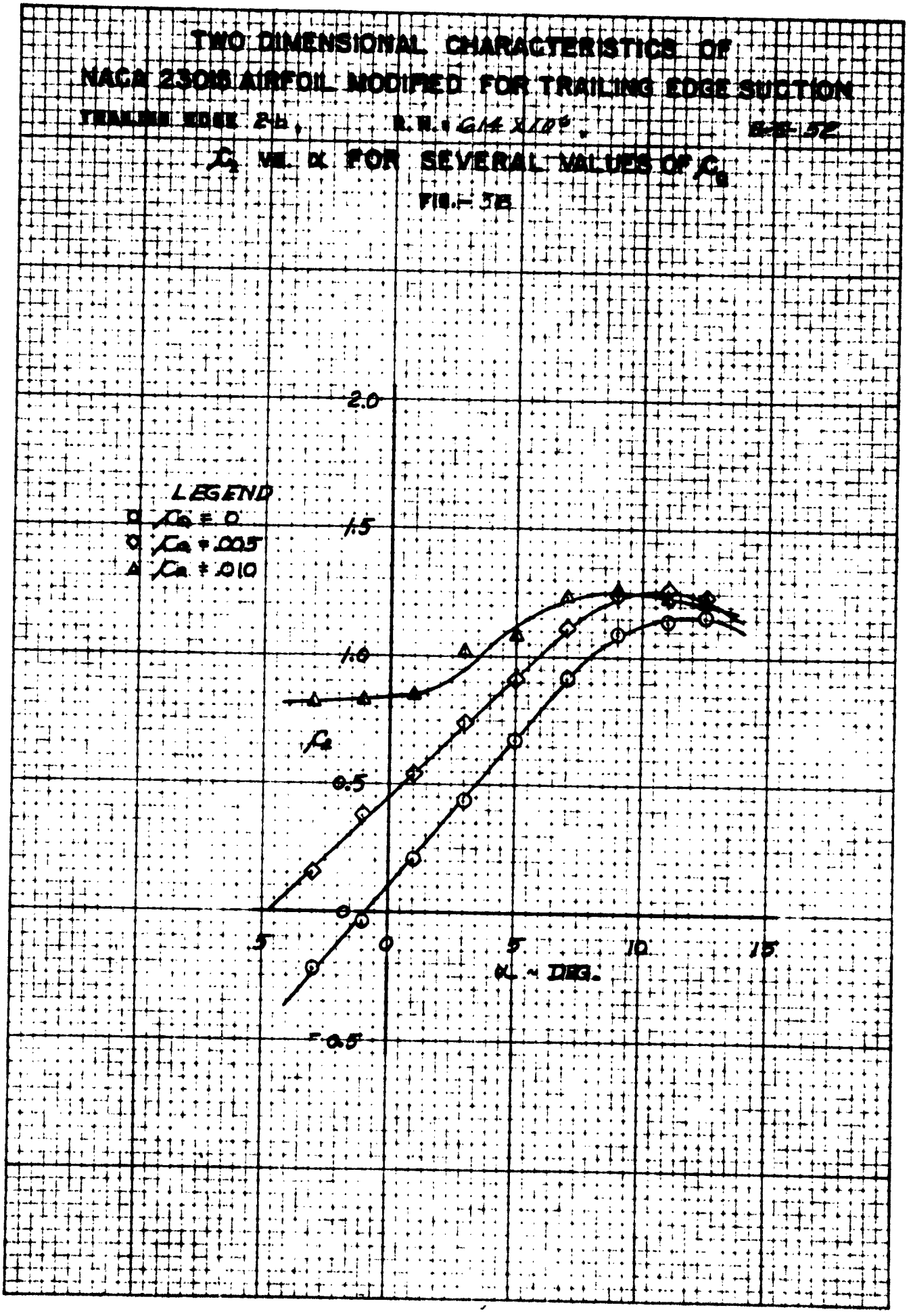

TWO DIMENSIONAL CHARACTERISTICS OF

MACH 2.30 AIRFOIL MODIFIED FOR TRAILING EDGE CONTROL

C_L VS. α FOR SEVERAL VALUES OF C_q

FIG. I-29

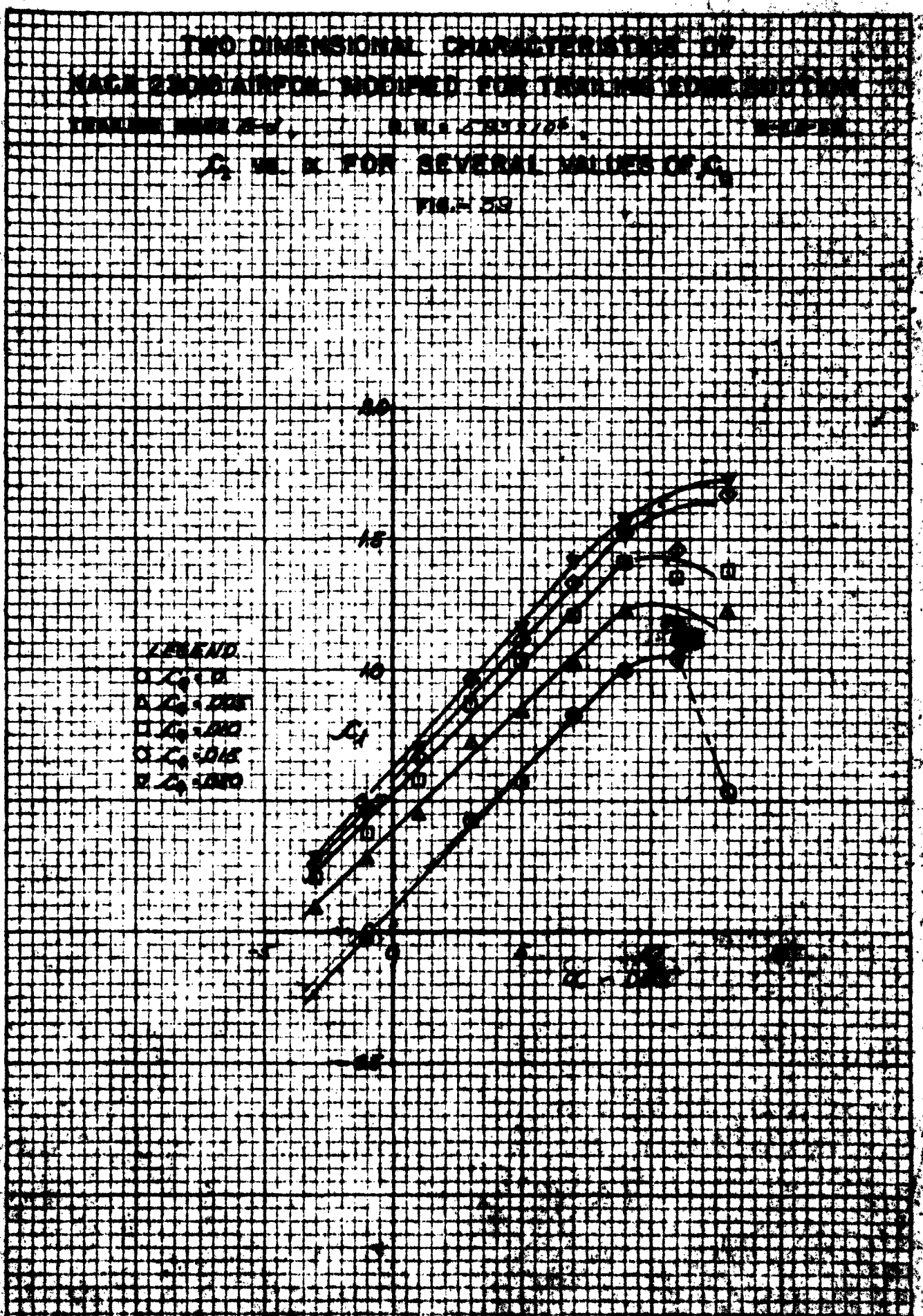

TWO DIMENSIONAL CHARACTERISTICS OF
NACA 23015 AIRFOIL MODIFIED FOR TRAILING EDGE SUCTION
TRAILING EDGE 2-C, R. N. = 593 X 10^6, [illegible]

C_l vs. α FOR SEVERAL VALUES OF C_Q

FIG.-70

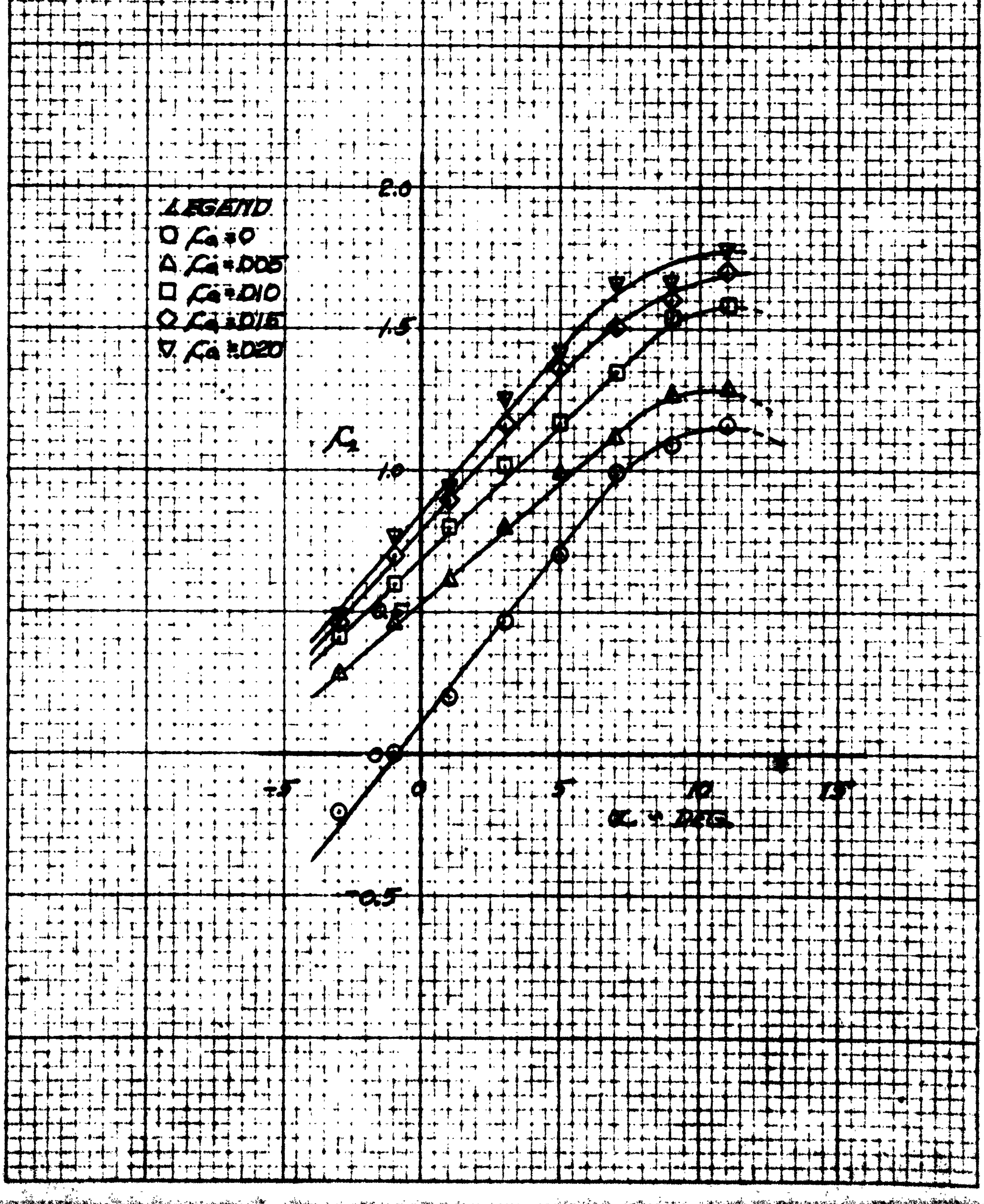

TWO DIMENSIONAL CHARACTERISTICS OF NACA 23015 AIRFOIL MODIFIED FOR TRAILING EDGE SUCTION

TRAILING EDGE 4-5 , R.N. = 6.14 x 10^6 , 10-7-52

C_l VS. α FOR SEVERAL VALUES OF C_Q

FIG. - 4-1

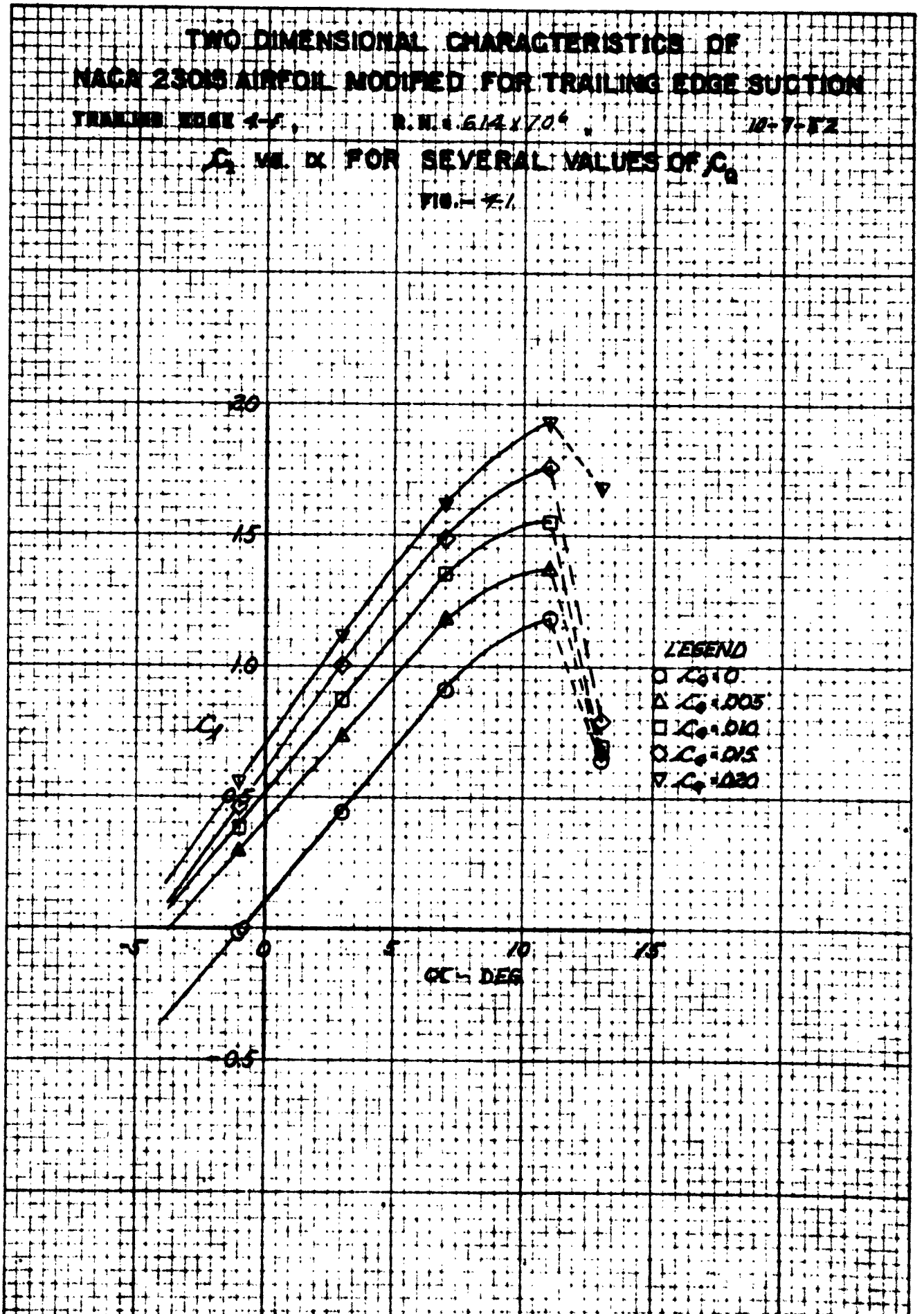

TWO DIMENSIONAL CHARACTERISTICS OF NACA 2305 AIRFOIL MODIFIED FOR TRAILING EDGE SUCTION

TRAILING EDGE 5-e, R.N. = .604 X 10⁶, M = .19 = 132

C_l VS. α FOR SEVERAL VALUES OF C_Q

FIG. 4.2

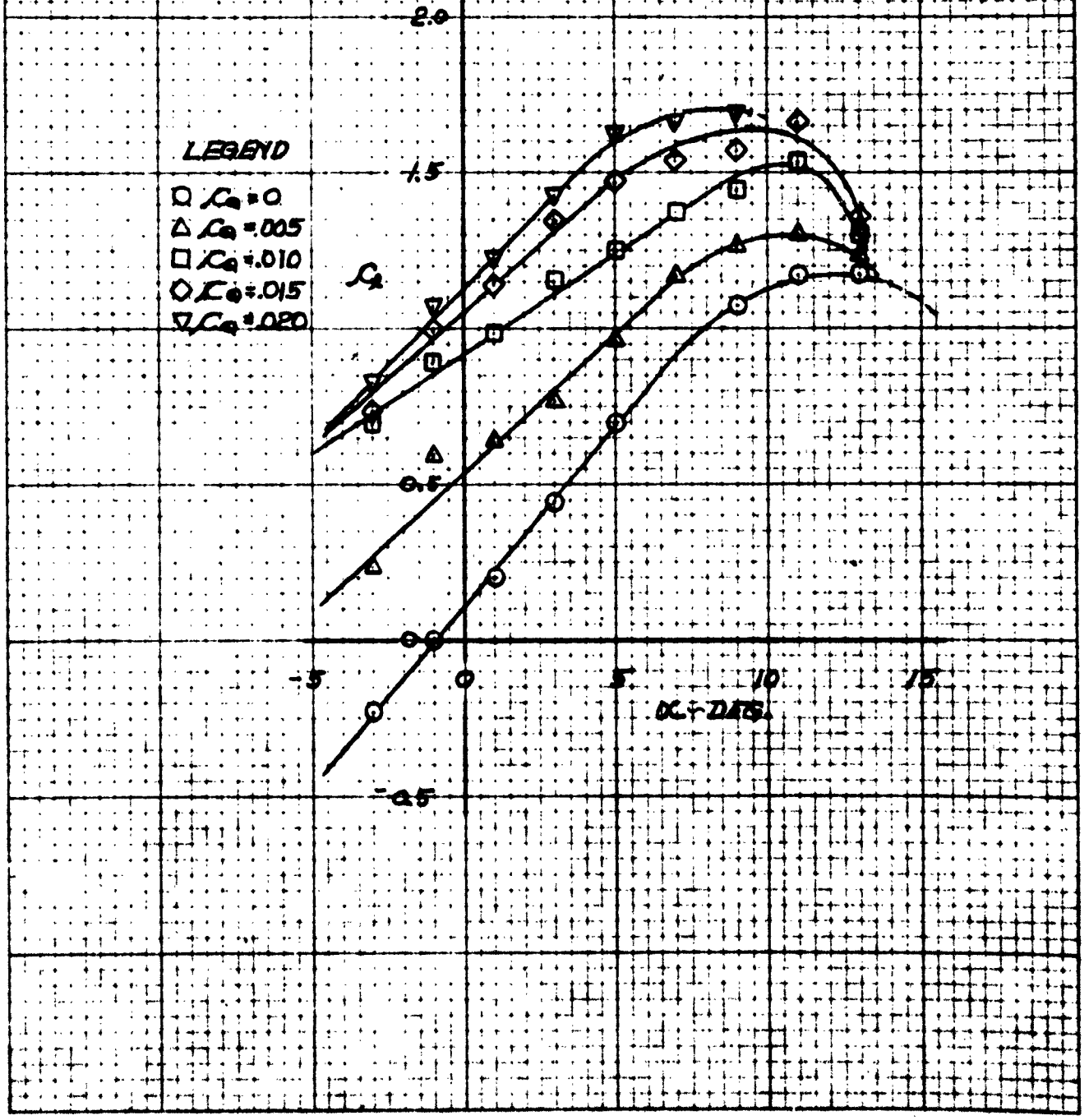

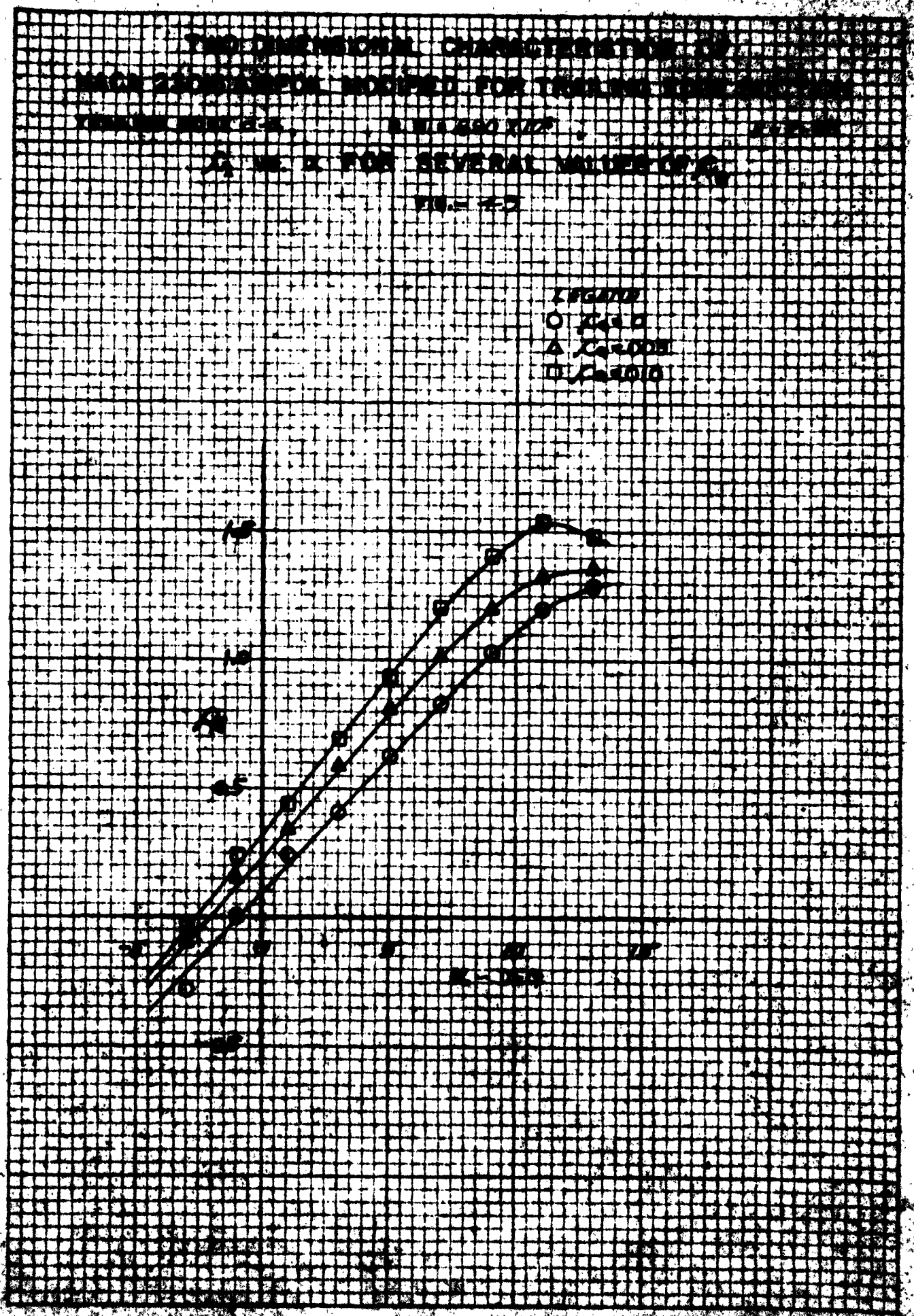
LEGEND
○ Cd-I
△ Cd-OOH
□ Cd-OIO

TWO DIMENSIONAL CHARACTERISTICS OF NACA 23015 AIRFOIL MODIFIED FOR TRAILING EDGE SUCTION

TRAILING EDGE 1-9, R.N. = 6.25 X 10⁶, 4-17-35

c_l VS. α FOR SEVERAL VALUES OF c_q

FIG. - 44

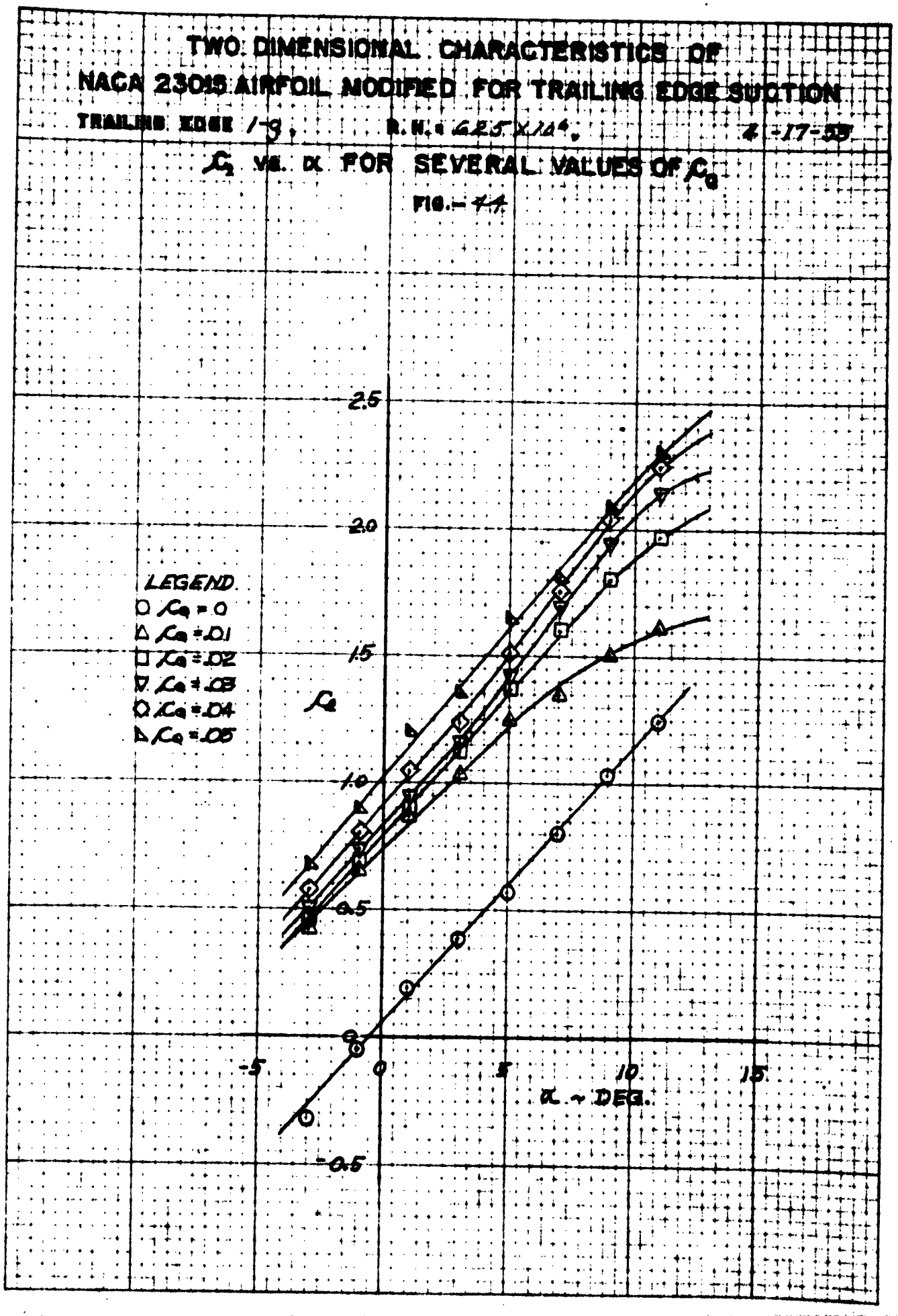

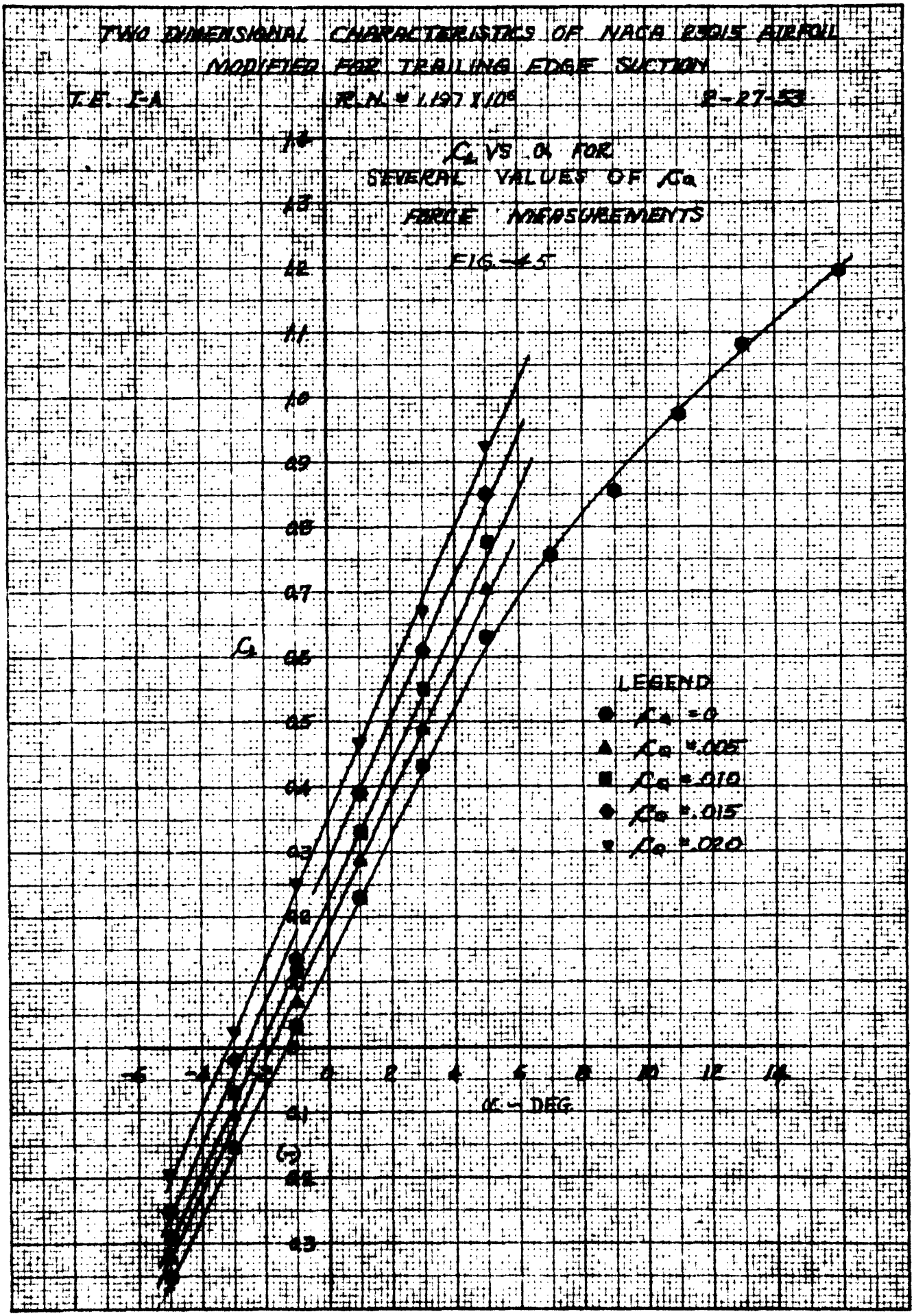
TWO DIMENSIONAL CHARACTERISTICS OF NACA 23015 AIRFOIL
MODIFIED FOR TRAILING EDGE SUCTION
T.E. I-A
R.N. = 1.197 X 10⁶
2-27-53
C_L VS α FOR
SEVERAL VALUES OF C_Q
FORCE MEASUREMENTS
FIG. -45
LEGEND
C_Q = 0
C_Q = .005
C_Q = .010
C_Q = .015
C_Q = .020
C_L
α - DEG
1.3
1.2
1.1
1.0
.9
.8
.7
.6
.5
.4
.3
.2
.1
0
-.1
-.2
-.3
-6
-4
-2
0
2
4
6
8
10
12
14

TWO DIMENSIONAL CHARACTERISTICS OF NACA 23015 AIRFOIL MODIFIED FOR TRAILING EDGE SUCTION

TRAILING EDGE 1-B, R. N. = 1.143 X 10^6, 4-10-42

C_l VS. α FOR SEVERAL VALUES OF C_Q

FIG.-16

FORCE MEASUREMENTS

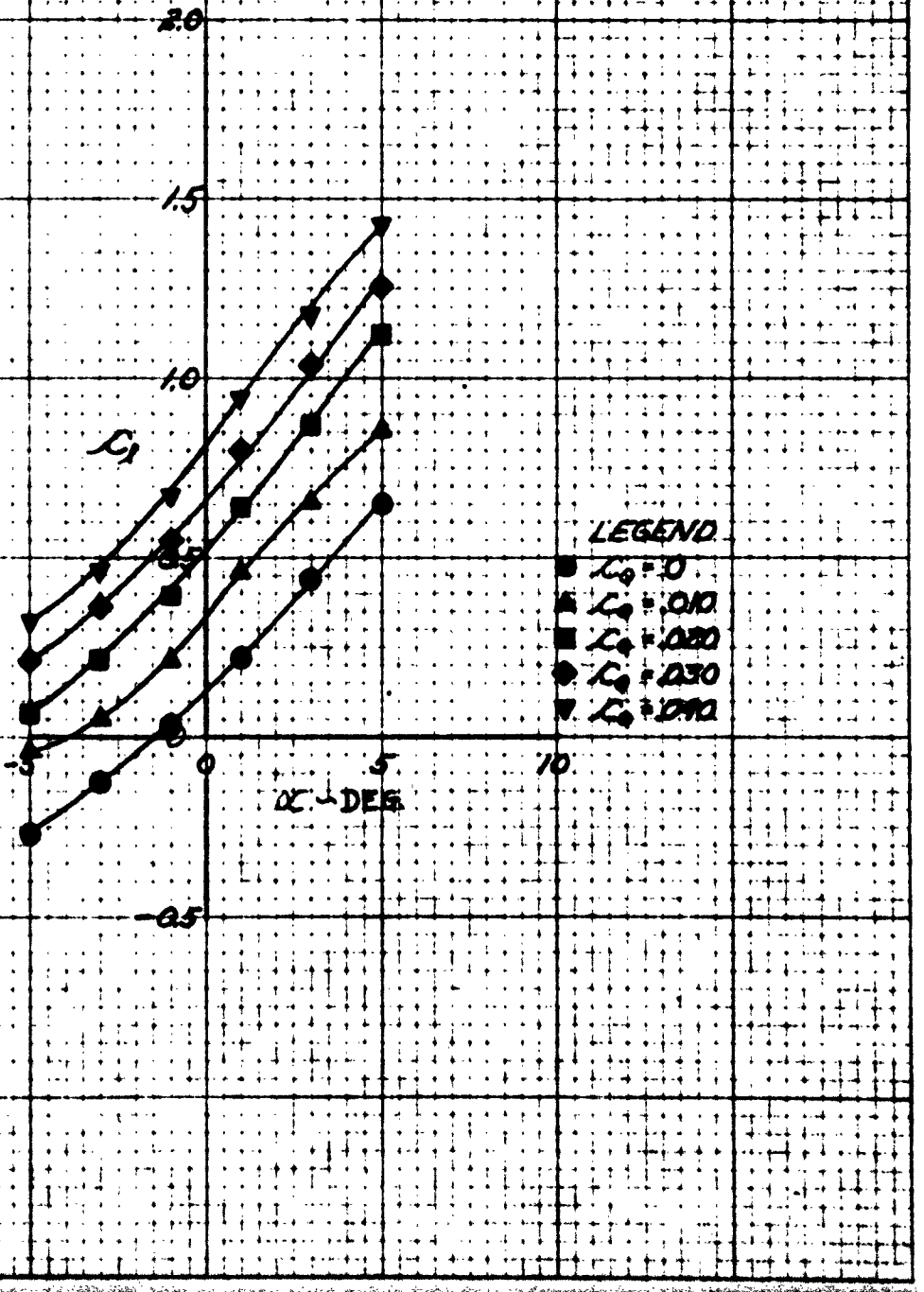

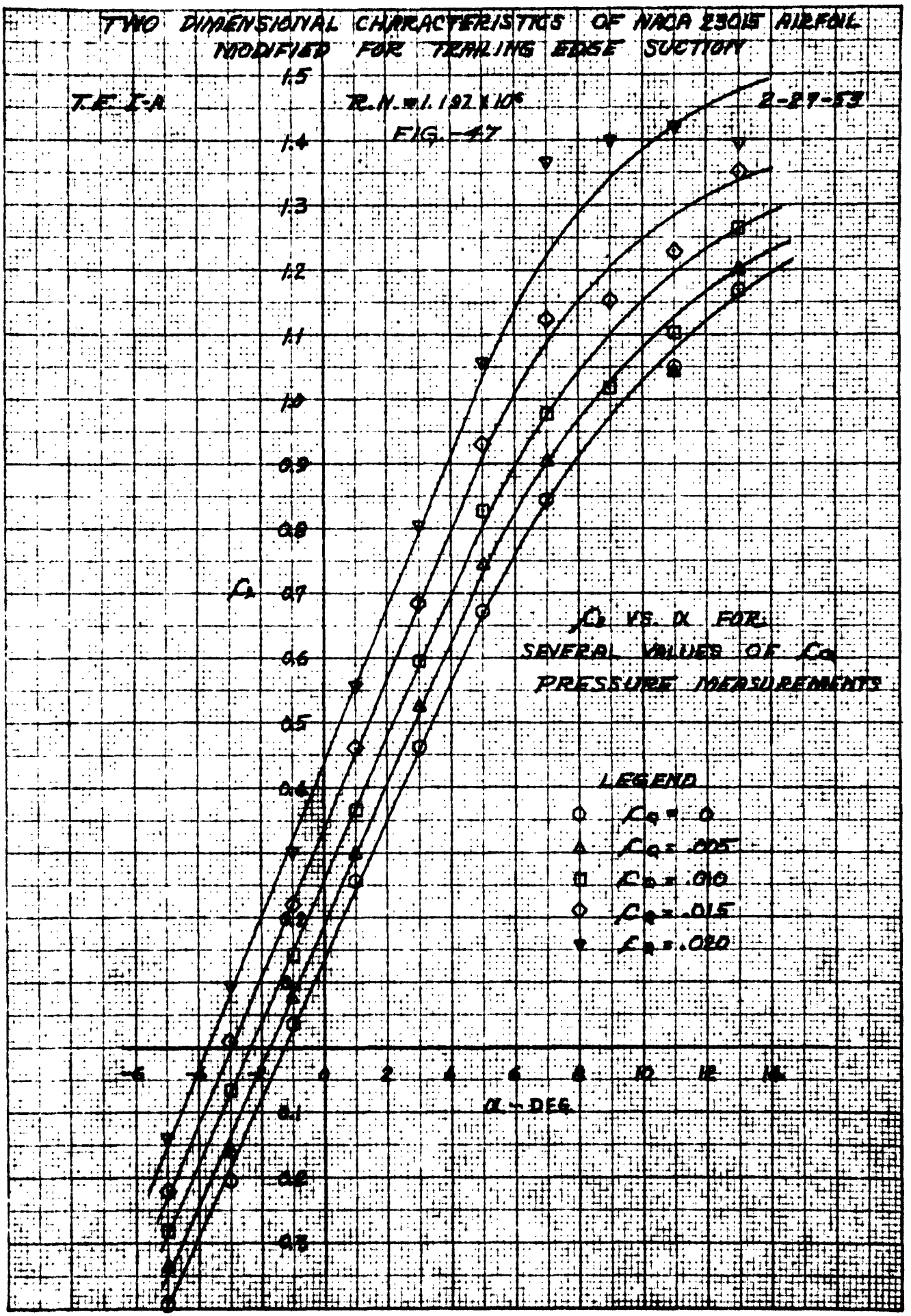
TWO DIMENSIONAL CHARACTERISTICS OF NACA 23015 AIRFOIL
MODIFIED FOR TRAILING EDGE SUCTION
T.E. I-A
R.N. = 1.192 X 10^6
FIG. 47
2-27-53
C_l VS. α FOR
SEVERAL VALUES OF C_Q
PRESSURE MEASUREMENTS
LEGEND
$C_Q = 0$
$C_Q = .005$
$C_Q = .010$
$C_Q = .015$
$C_Q = .020$
C_l
α - DEG.
1.5
1.4
1.3
1.2
1.1
1.0
0.9
0.8
0.7
0.6
0.5
0.4
0.3
0.2
0.1
-6
-4
-2
0
2
4
6
8
10
12
14

TWO DIMENSIONAL CHARACTERISTICS OF NACA 23015 AIRFOIL MODIFIED FOR TRAILING EDGE SUCTION

TRAILING EDGE 1-B, R.N. = 1.143 X 10⁶, 4-10-43

C_l VS. α FOR SEVERAL VALUES OF C_Q

FIG.-48

PRESSURE MEASUREMENTS

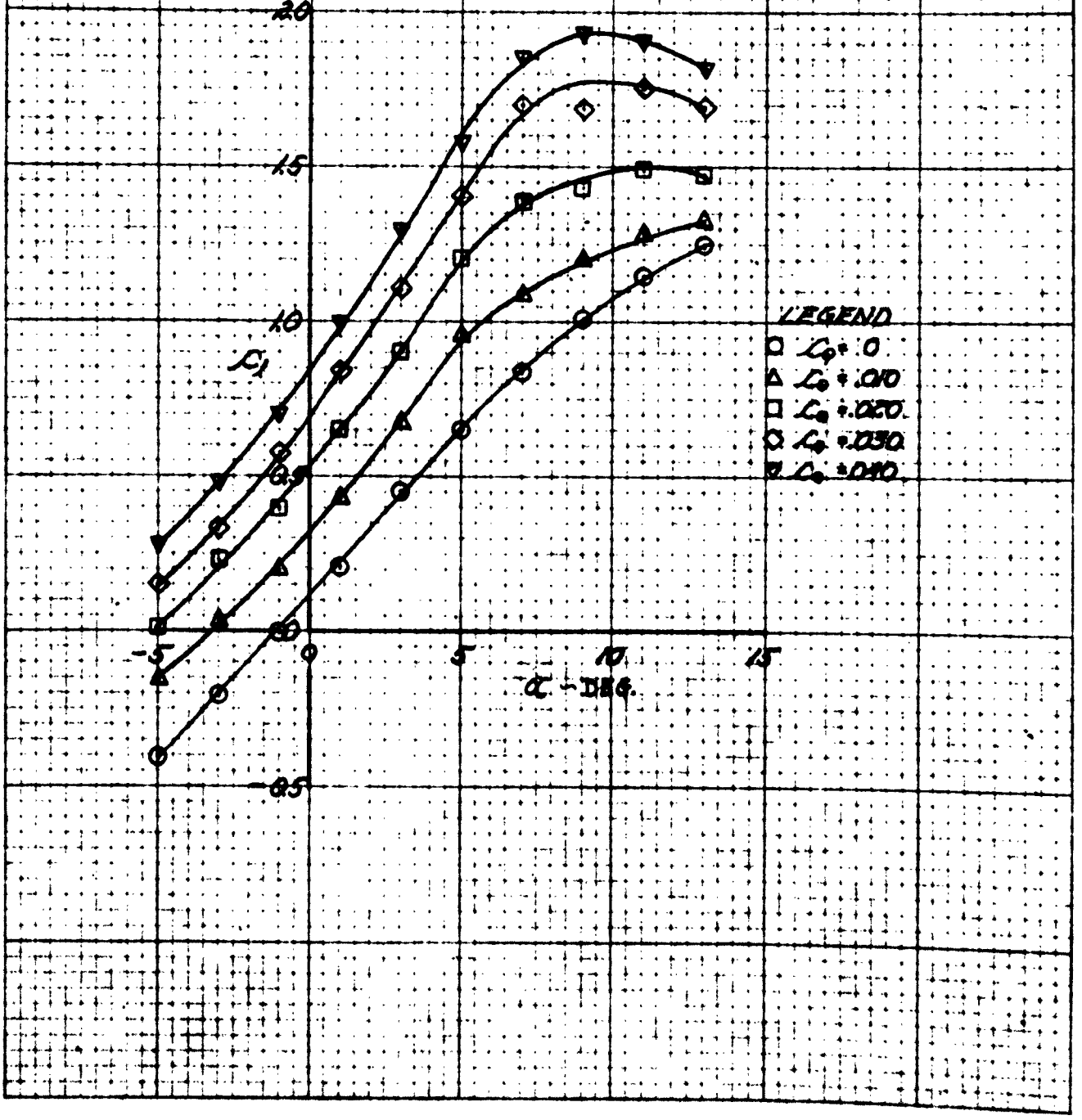

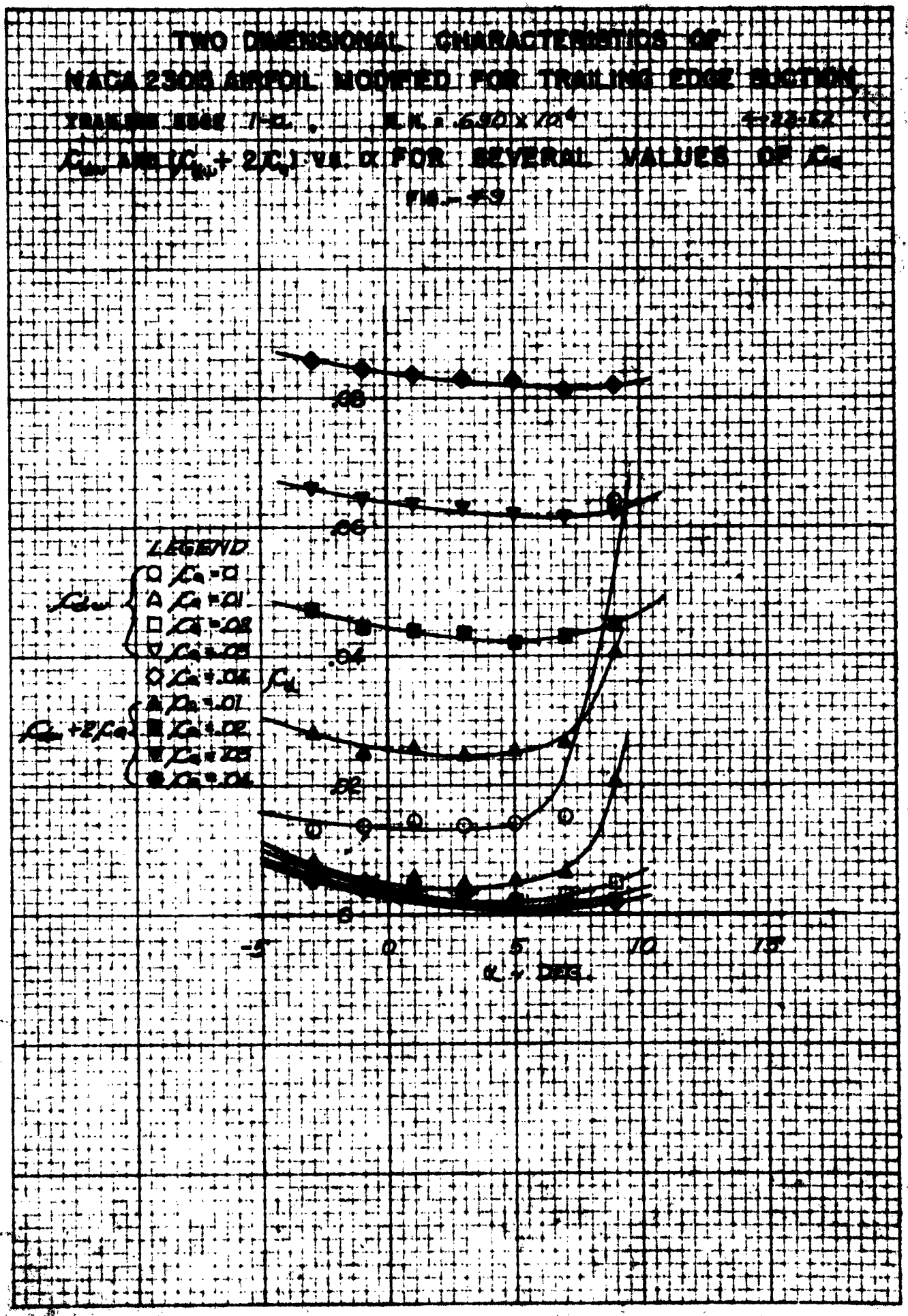
TWO DIMENSIONAL CHARACTERISTICS OF
NACA 2306 AIRFOIL MODIFIED FOR TRAILING EDGE SUCTION.
TRAILING EDGE 1-2%. R.N. = .630 x 10^6
$C_{l_{max}}$ AND $(C_{l_{max}} + 2C_q)$ VS. α FOR SEVERAL VALUES OF C_q
FIG. - 29
LEGEND
C_q = 0
C_q = .01
C_q = .02
C_q = .03
C_q = .04
C_q = .01
C_q = .02
C_q = .03
C_q = .04
$C_{l_{max}}$
$C_{l_{max}} + 2C_q$
.08
.06
.04
.02
0
-5°
0
5
10
15°
α, DEG.

TWO DIMENSIONAL CHARACTERISTICS OF NACA 23015 AIRFOIL MODIFIED FOR TRAILING EDGE SUCTION

TRAILING EDGE 1-a , R.N. = .647 X 10⁶

$C_{l_{max}}$ AND $(C_{l_{max}} + 2\Delta C_l)$ VS. α FOR SEVERAL VALUES OF C_q

FIG.- 50

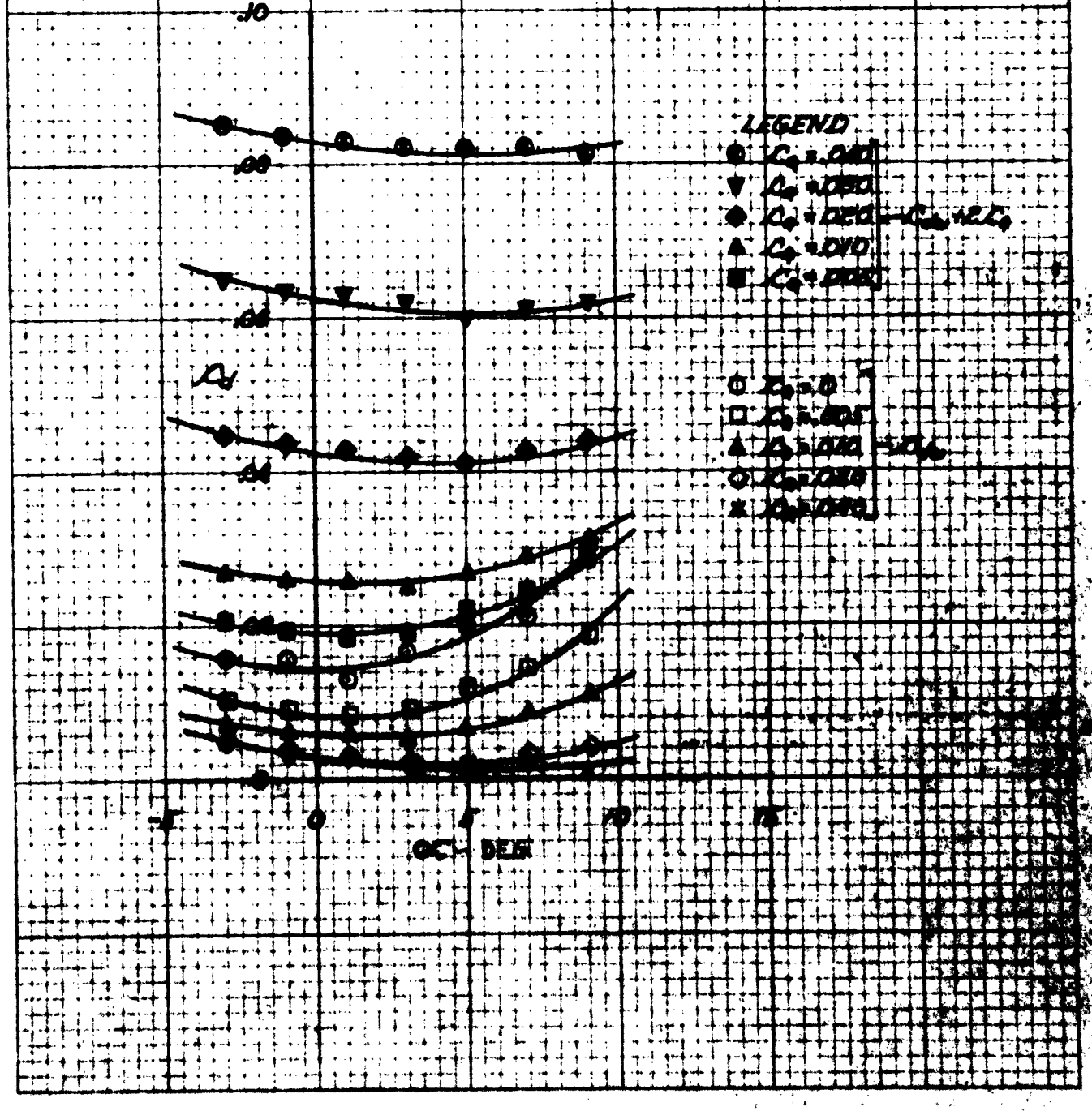

TWO DIMENSIONAL CHARACTERISTICS OF NACA 23015 AIRFOIL MODIFIED FOR TRAILING EDGE SUCTION

TRAILING EDGE: 1-C , R.N. = 5.61 X 10⁶ , 6-7-38

C_{d_w} AND $(C_{d_w} + 2C_q)$ VS. α FOR SEVERAL VALUES OF C_q

FIG. - 51

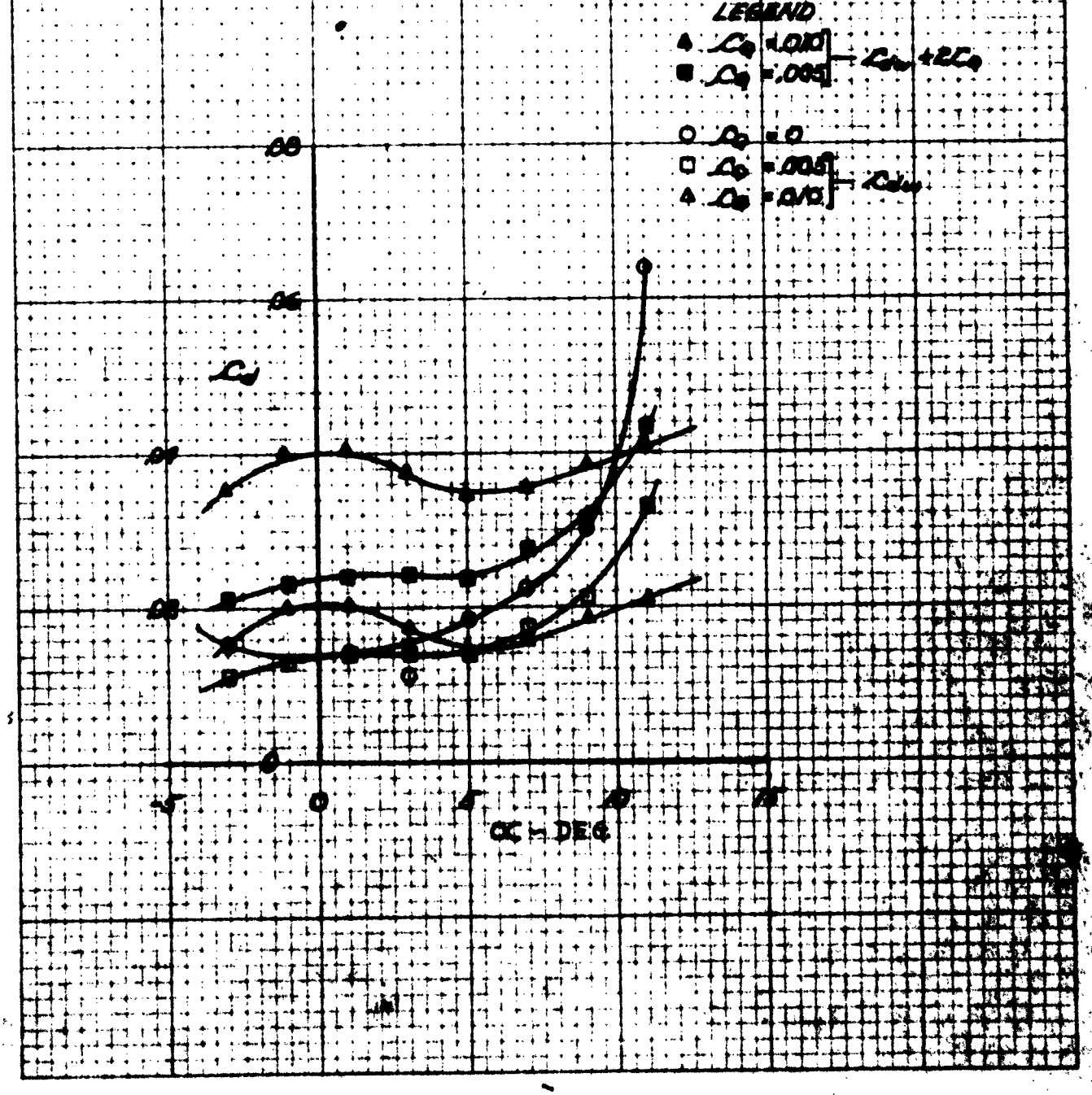

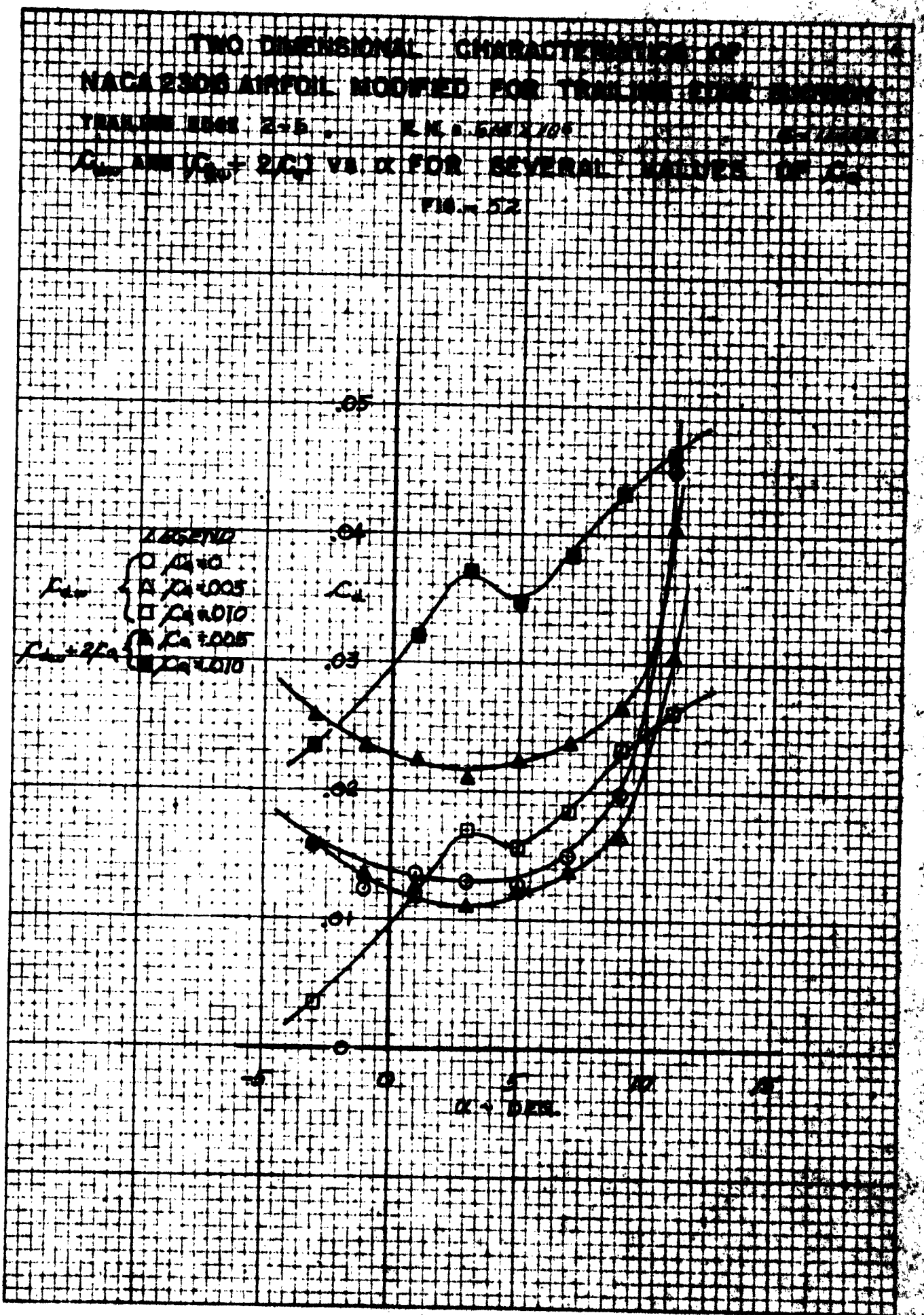
TWO DIMENSIONAL CHARACTERISTICS OF
NACA 2306 AIRFOIL MODIFIED FOR TRAILING EDGE FLAP
TRAILING EDGE 2.5%
FIG. 52
LEGEND
C_{f_0} = 0
C_{f_0} = .005
C_{f_0} = .010
C_{f_0} = .005
C_{f_0} = .010
$C_{l_{max}}$
$C_{l_{max}} + 2C_{f_0}$
.05
.04
.03
.02
.01
C_l
α = DEG.

TWO DIMENSIONAL CHARACTERISTICS OF NACA 23015 AIRFOIL MODIFIED FOR TRAILING EDGE SUCTION

TRAILING EDGE 2-d , R.N. = 5.93 X 10^6 5-25-52

c_{d_w} AND $(c_{d_{(w)}} + 2c_{q_j})$ VS. α FOR SEVERAL VALUES OF c_q

FIG.-53

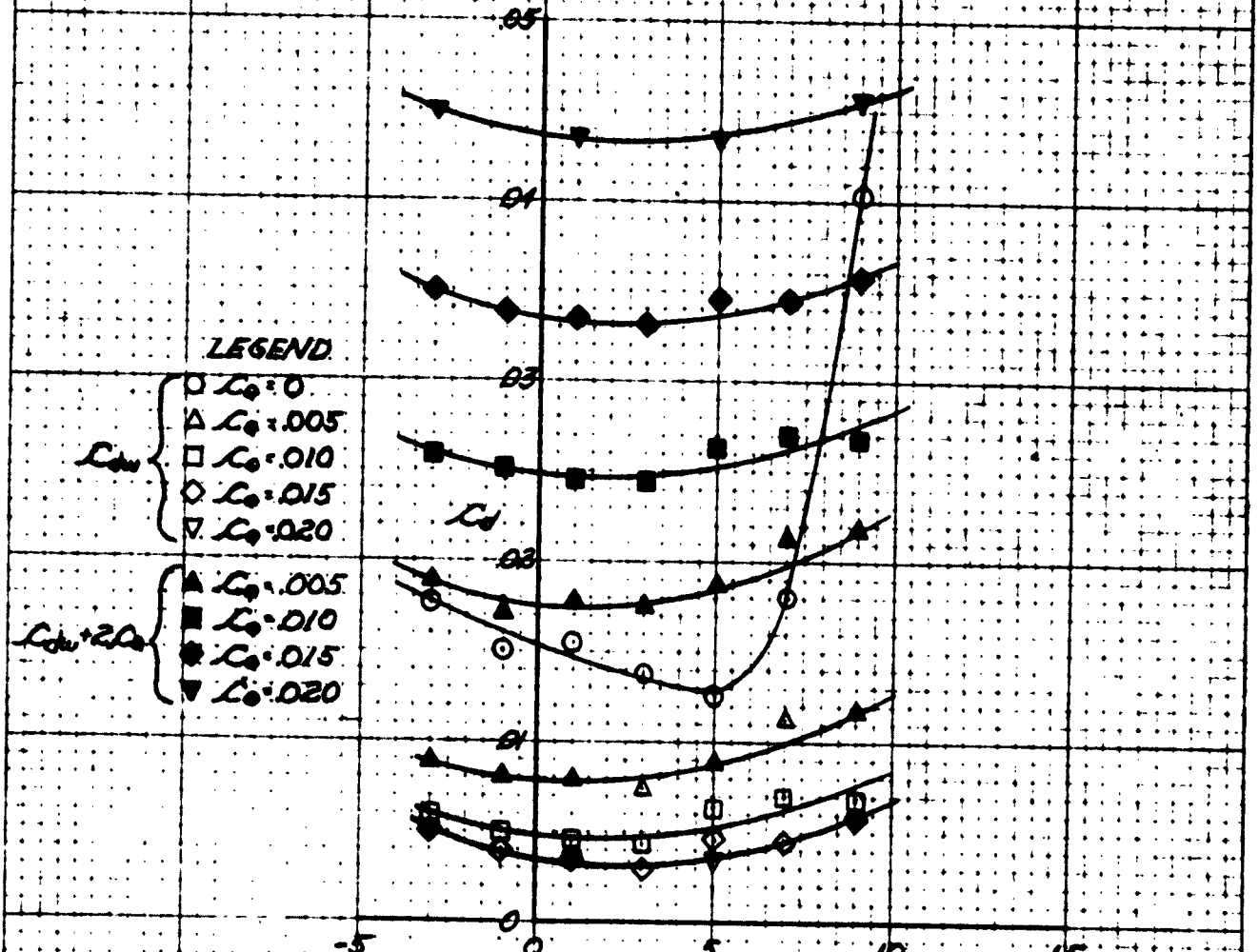

TWO DIMENSIONAL CHARACTERISTICS OF NACA 23015 AIRFOIL MODIFIED FOR TRAILING EDGE SUCTION

TRAILING EDGE 2-e , R.N. = .513 X 10⁶ 10-23-52

$c_{l_{dw}}$ AND $(c_{l_{dw}} + 2c_q)$ vs. α FOR SEVERAL VALUES OF c_q

FIG. – 5F

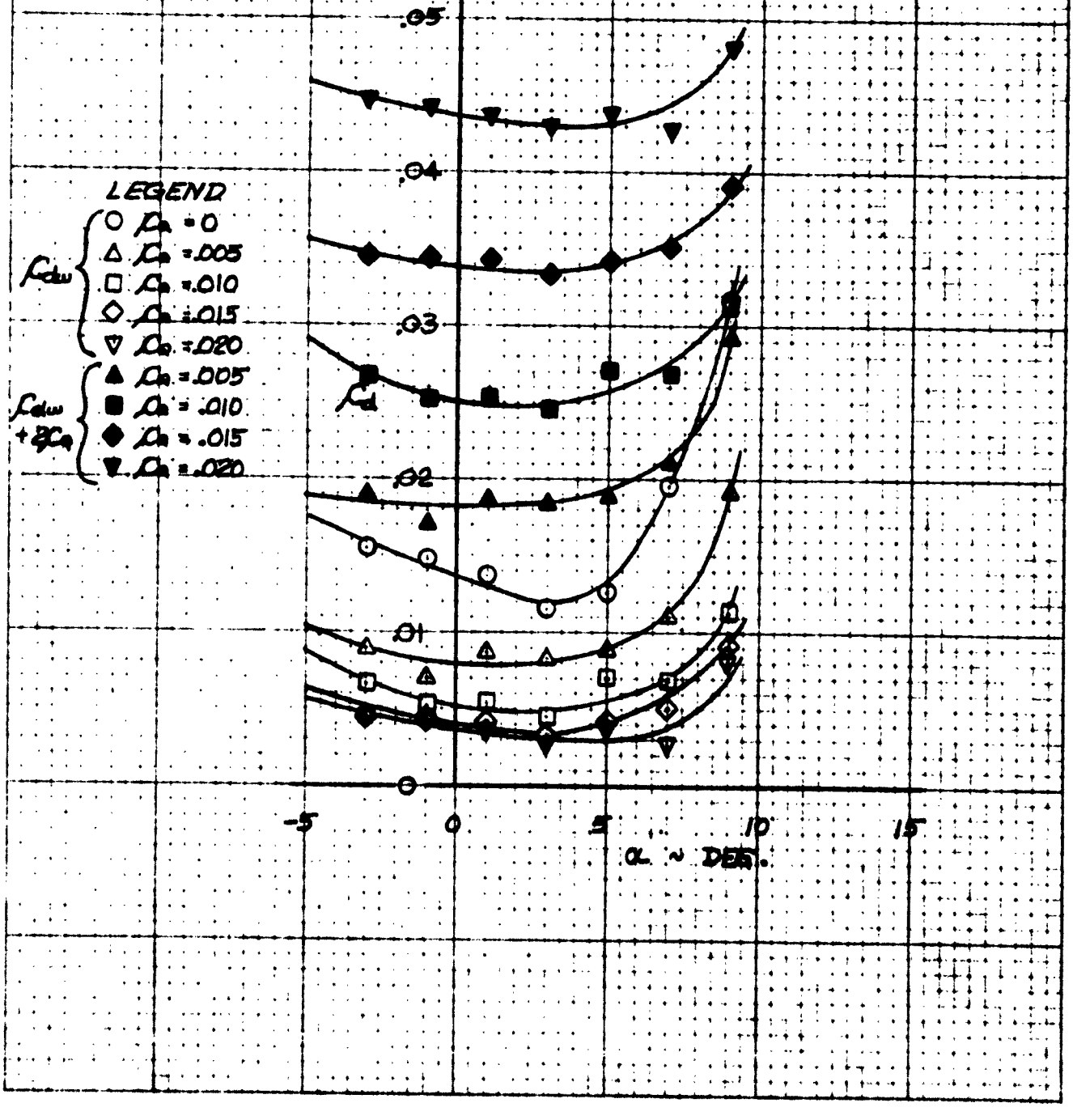

TWO DIMENSIONAL CHARACTERISTICS OF
NACA 23015 AIRFOIL MODIFIED FOR TRAILING EDGE SUCTION

TRAILING EDGE 4-F   R.N. = 6.14 x 10^6   10-7-52

C_{dw} AND $(C_{dw} + 2C_Q)$ VS. α FOR SEVERAL VALUES OF C_Q

FIG.-55

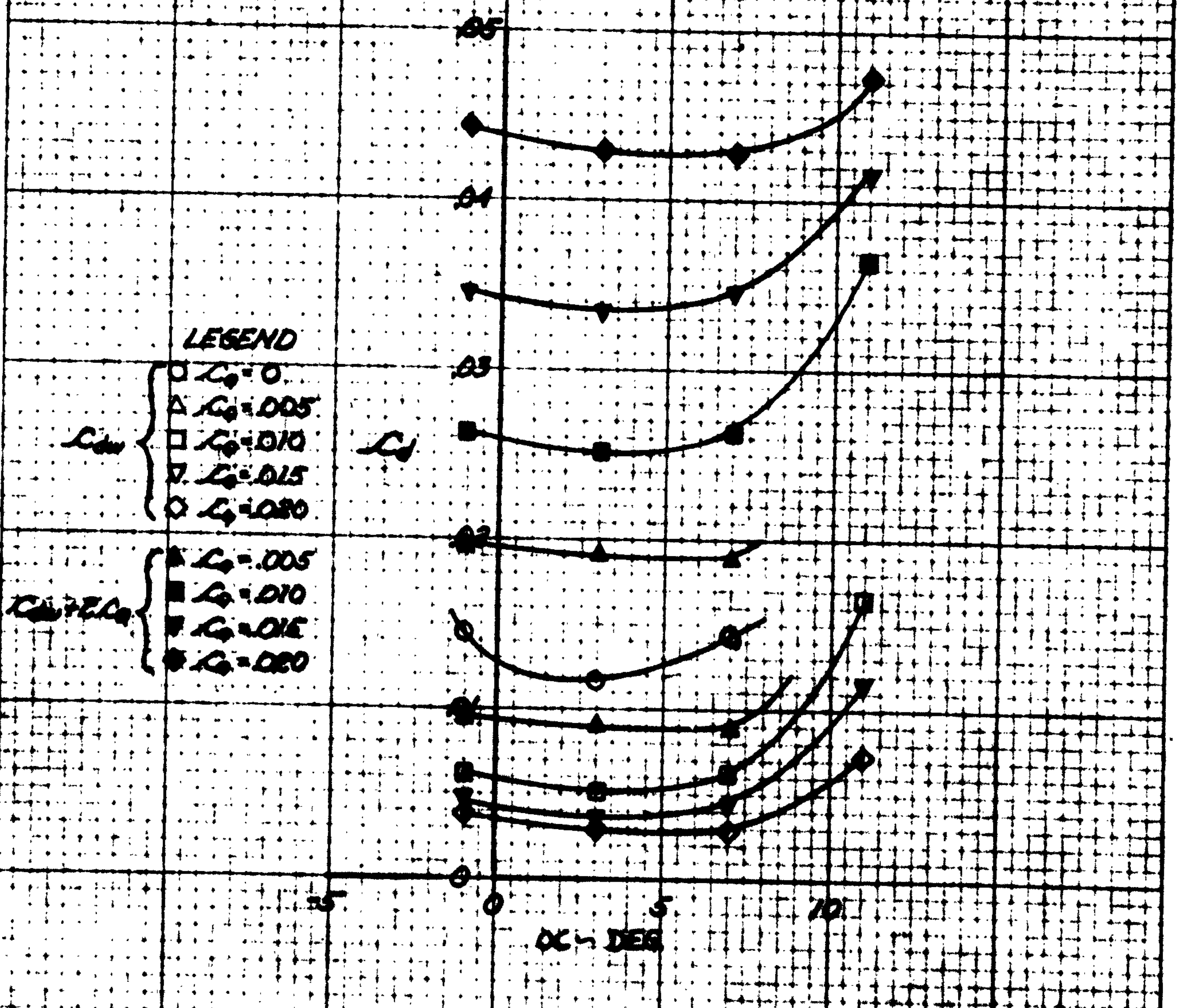

TWO DIMENSIONAL CHARACTERISTICS OF NACA 23015 AIRFOIL MODIFIED FOR TRAILING EDGE SUCTION

TRAILING EDGE δ-6 , R.N. = .604 X 10⁶ 11-19-53

c_{d_w} AND $(c_{d_w} + 2c_q)$ vs. α FOR SEVERAL VALUES OF c_q

FIG.- 56

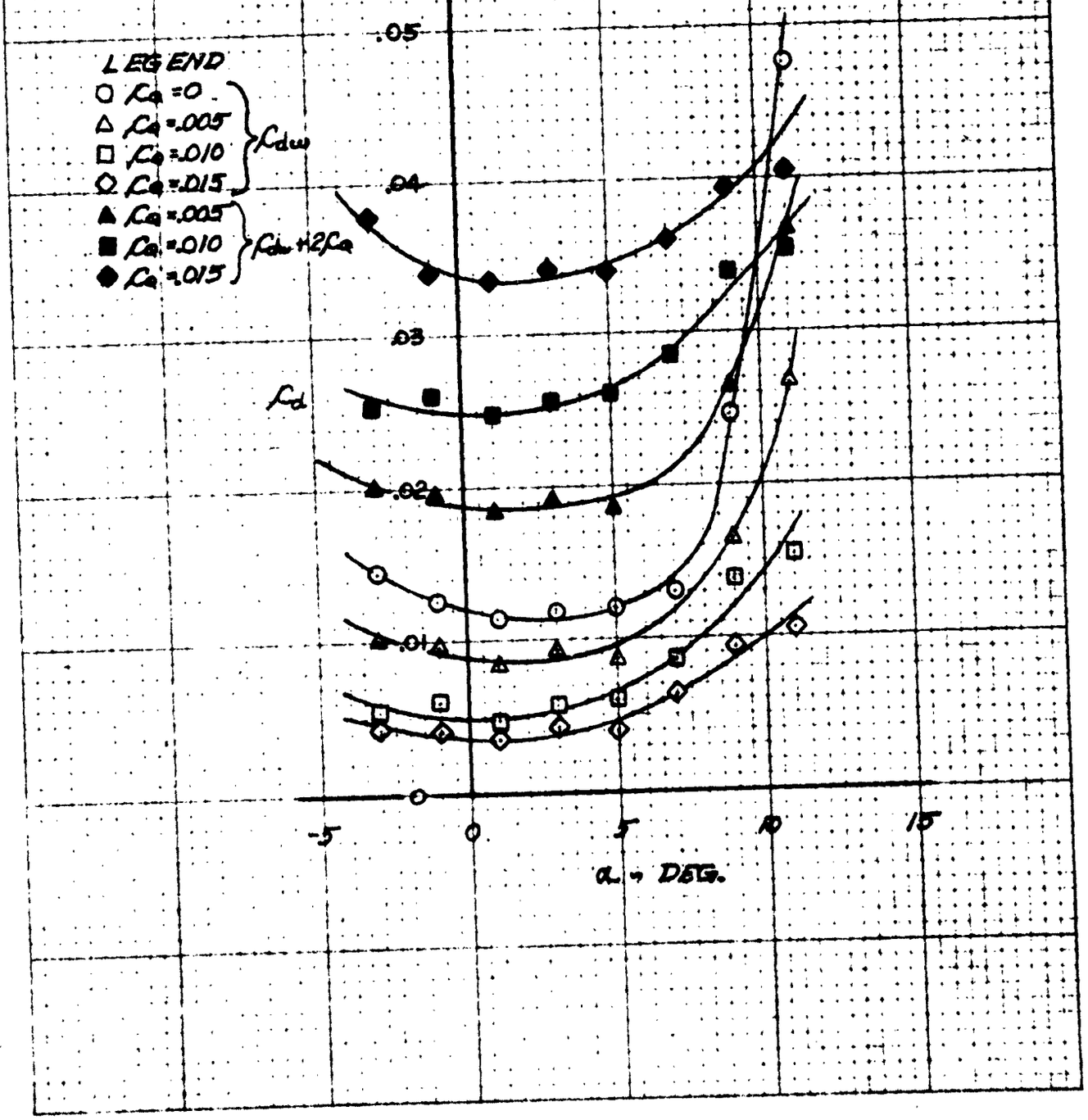

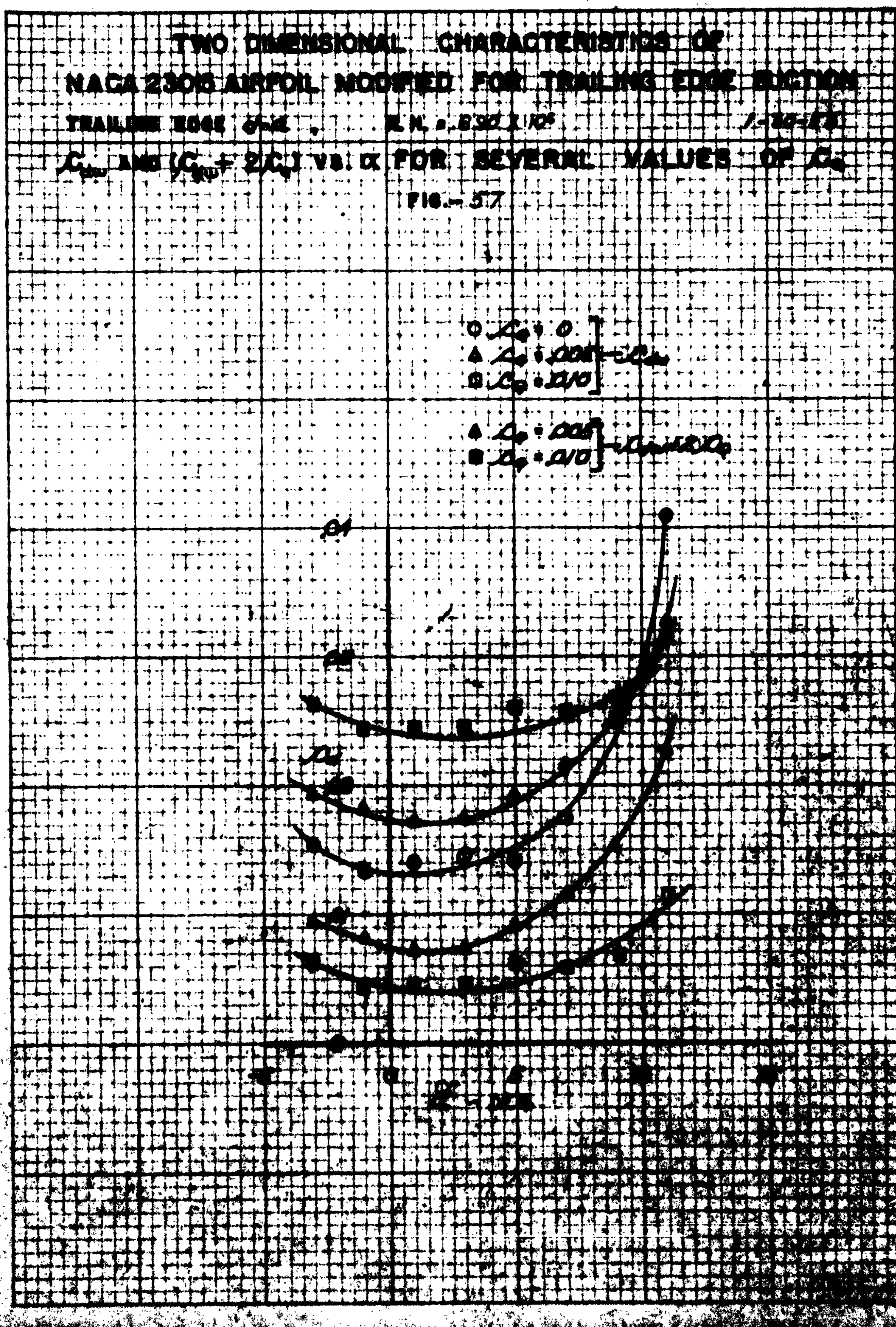
TWO DIMENSIONAL CHARACTERISTICS OF
NACA 23015 AIRFOIL MODIFIED FOR TRAILING EDGE SUCTION
FOR SEVERAL VALUES OF
FIG.— 57
α — DEG

TWO DIMENSIONAL CHARACTERISTICS OF
NACA 2308 AIRFOIL MODIFIED FOR TRAILING EDGE SUCTION

TRAILING EDGE 7-3 . R.N. = .6250 x 10⁶ 5-17-38

$C_{d_{min}}$ AND $(C_{d_{min}} + 2C_l)$ VS. α FOR SEVERAL VALUES OF C_q

FIG. 5B

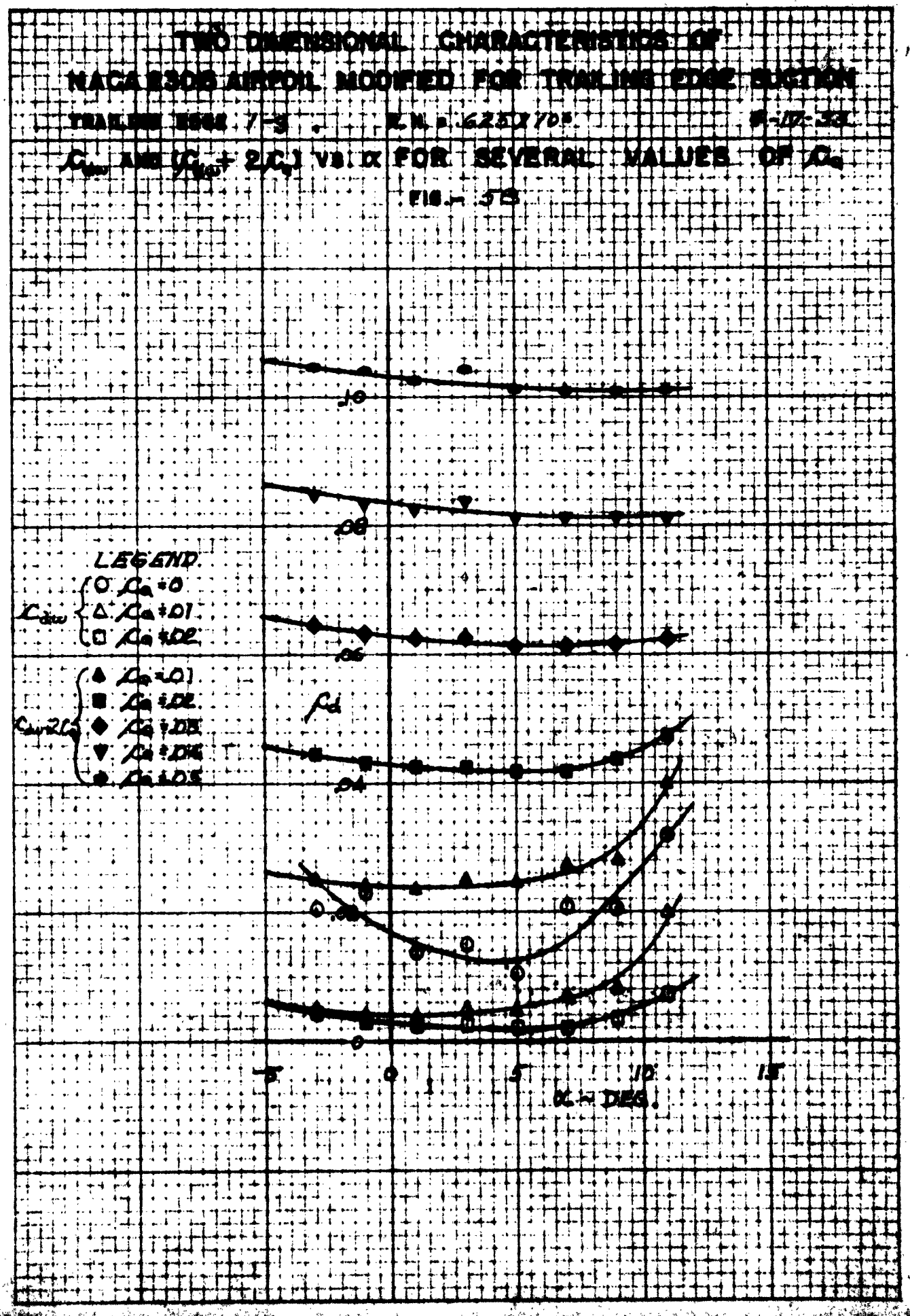

TWO DIMENSIONAL CHARACTERISTICS OF
NACA 2303 AIRFOIL MODIFIED FOR TRAILING EDGE SUCTION

TRAILING EDGE I-A R. N. = 1.97 x 10^6 2-25-38

C_{d_w} AND $[C_{d_{(w)}} + 2C_q]$ vs. α FOR SEVERAL VALUES OF C_q

FIG. - 59

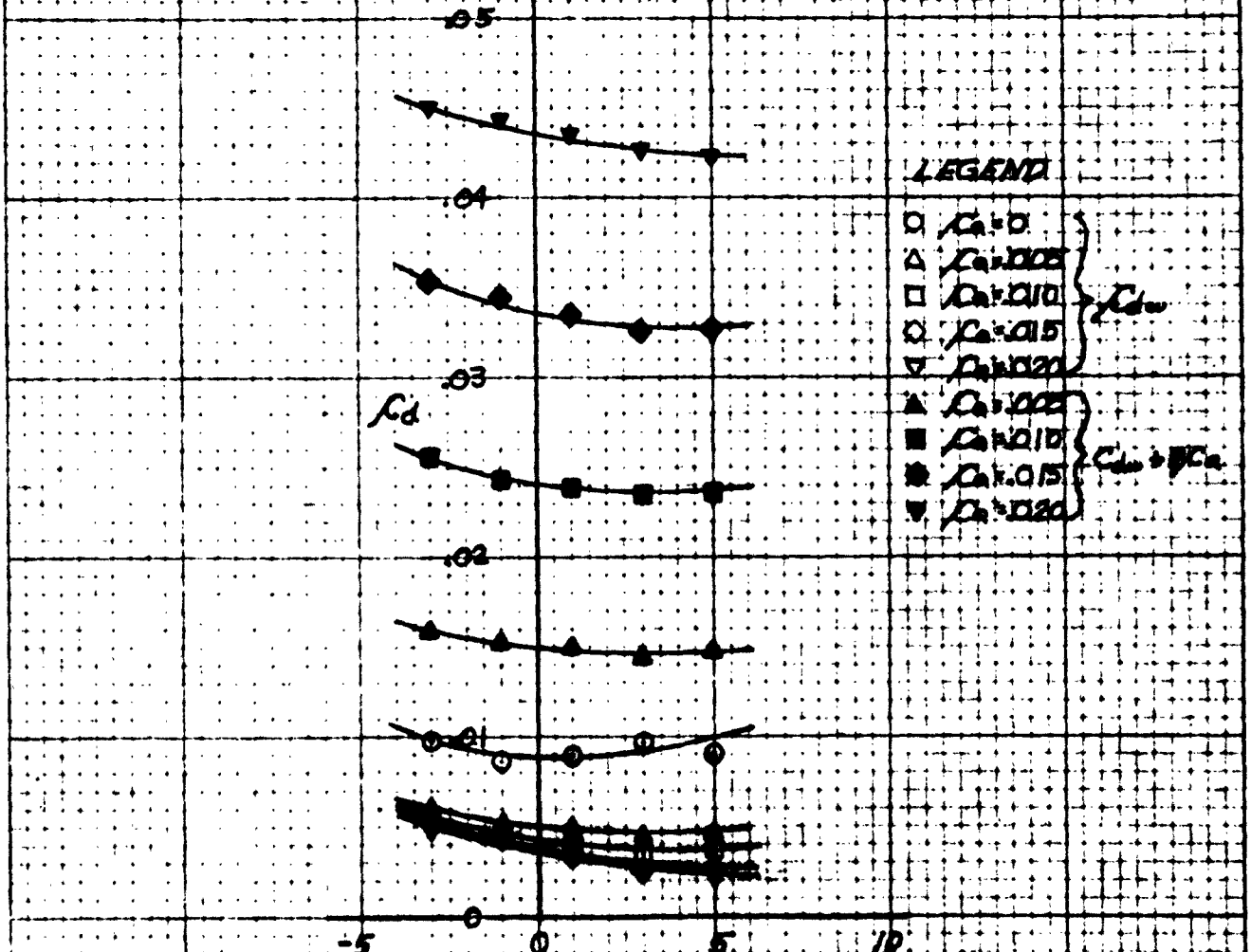

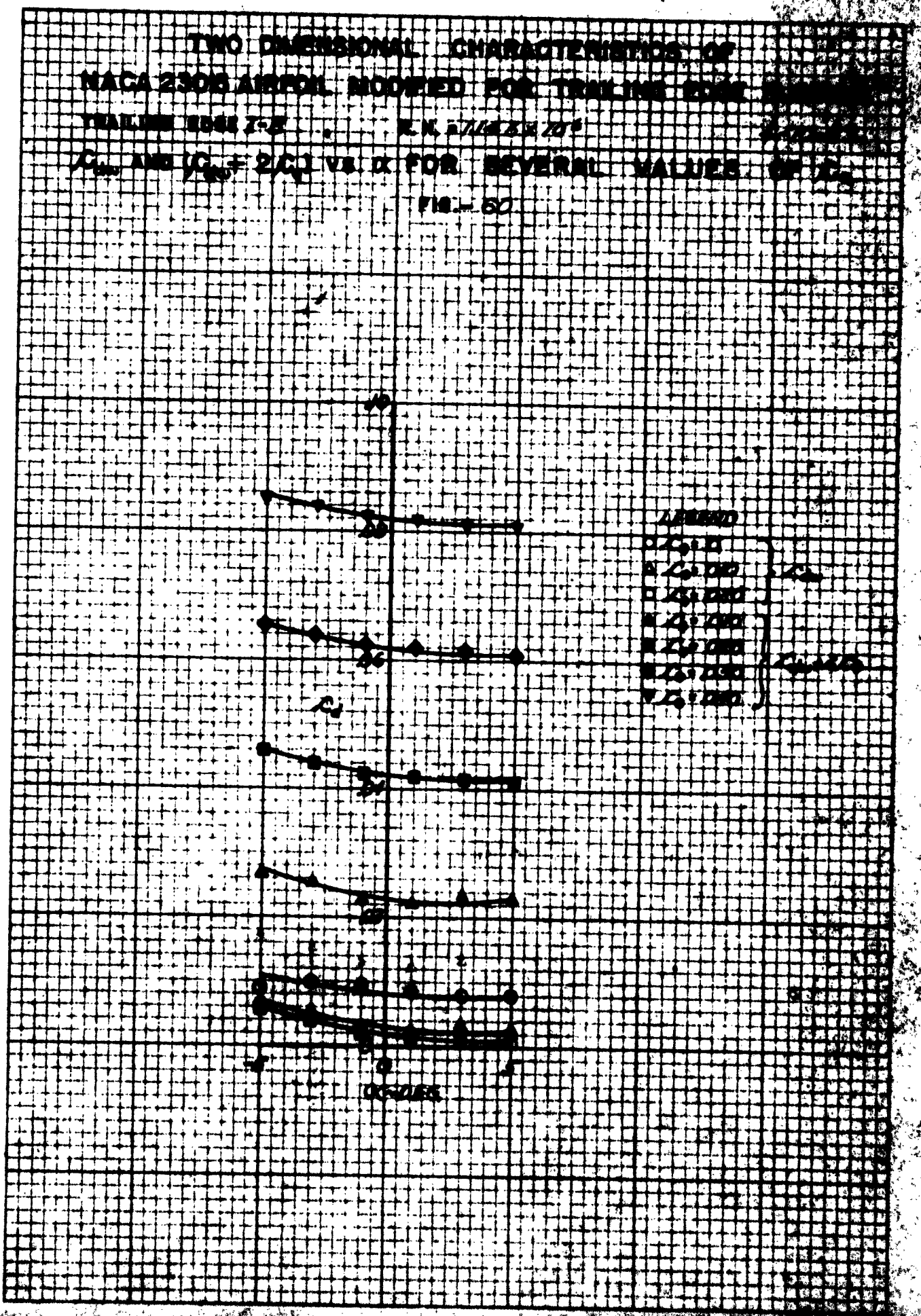
TWO DIMENSIONAL CHARACTERISTICS OF
NACA 2306 AIRFOIL MODIFIED FOR TRAILING EDGE
TRAILING EDGE 7.5%
$C_{l_{max}}$ AND $(C_{l_{max}} + 2C_{l_0})$ VS α FOR SEVERAL VALUES OF C_{l_0}
FIG. 60
$C_{l_{max}}$
$C_{l_{max}} + 2C_{l_0}$
C_{l_0}
$\alpha_{C_{l_{max}}}$

TWO DIMENSIONAL CHARACTERISTICS OF NACA 23015 AIRFOIL MODIFIED FOR TRAILING EDGE SUCTION

TRAILING EDGE /-d. R.N. = .690 x /0^6 4-23-52

$C_{m_{c/4}}$ vs. α FOR SEVERAL VALUES OF C_q

FIG. - 61

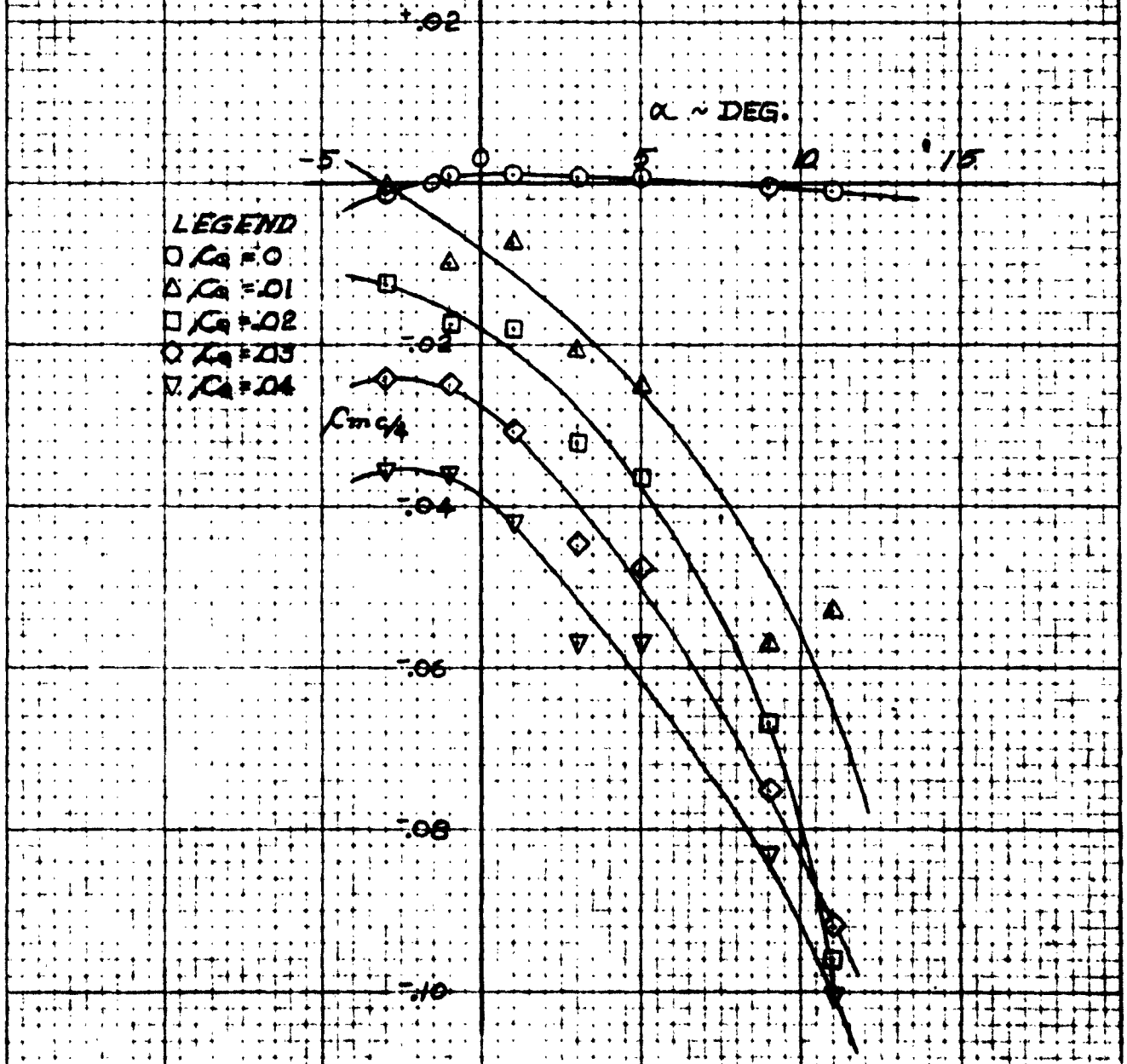

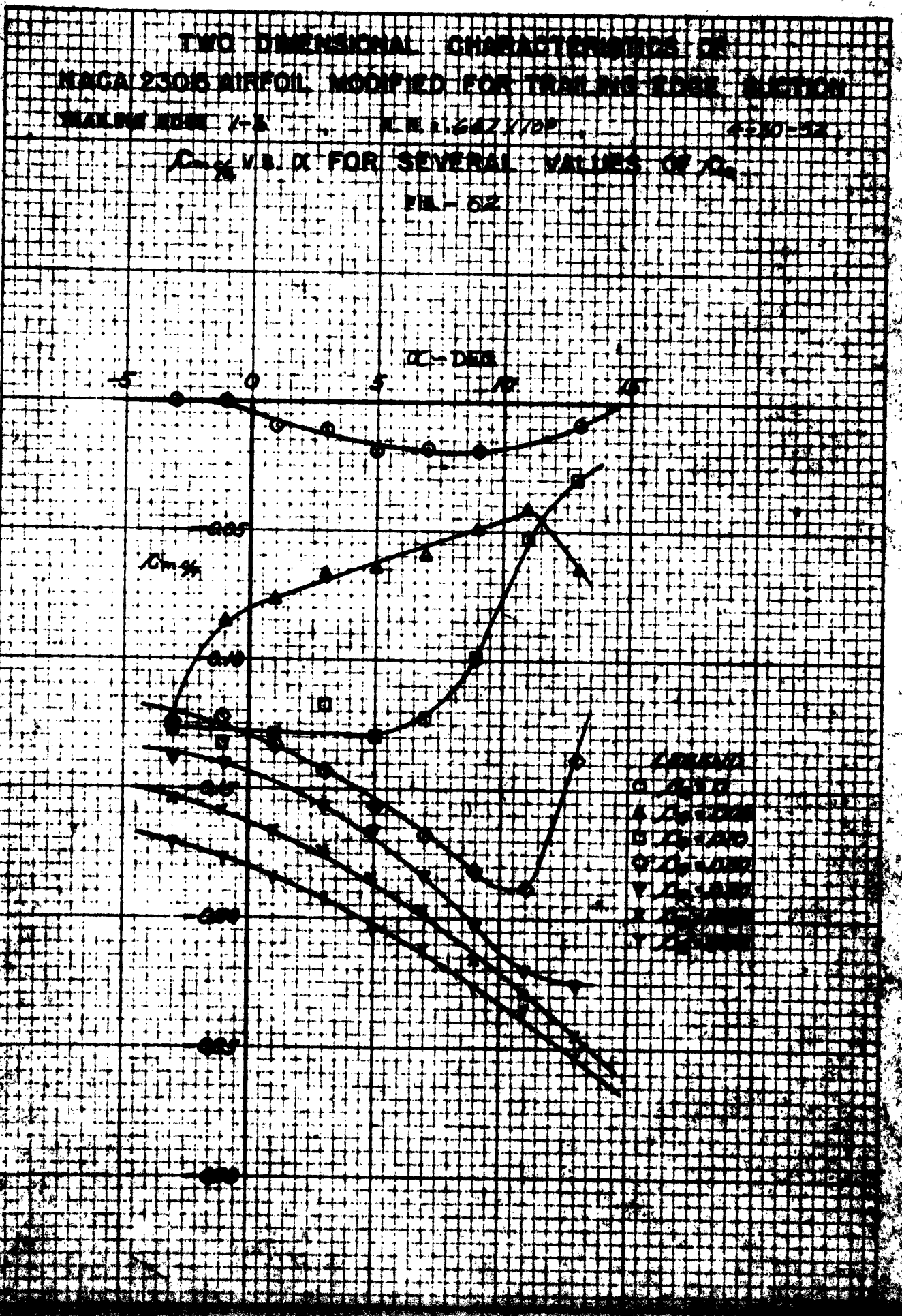
TWO DIMENSIONAL CHARACTERISTICS OF
NACA 23015 AIRFOIL MODIFIED FOR TRAILING EDGE SECTION
TRAILING EDGE V-A
R.N. 1.6 x 10^6
4-30-52
C_m vs. α FOR SEVERAL VALUES OF C_m
FIG. 52
α - DEG.
-5
0
5
10
15
0.05
C_m
0.10
0.15
0.20
0.25

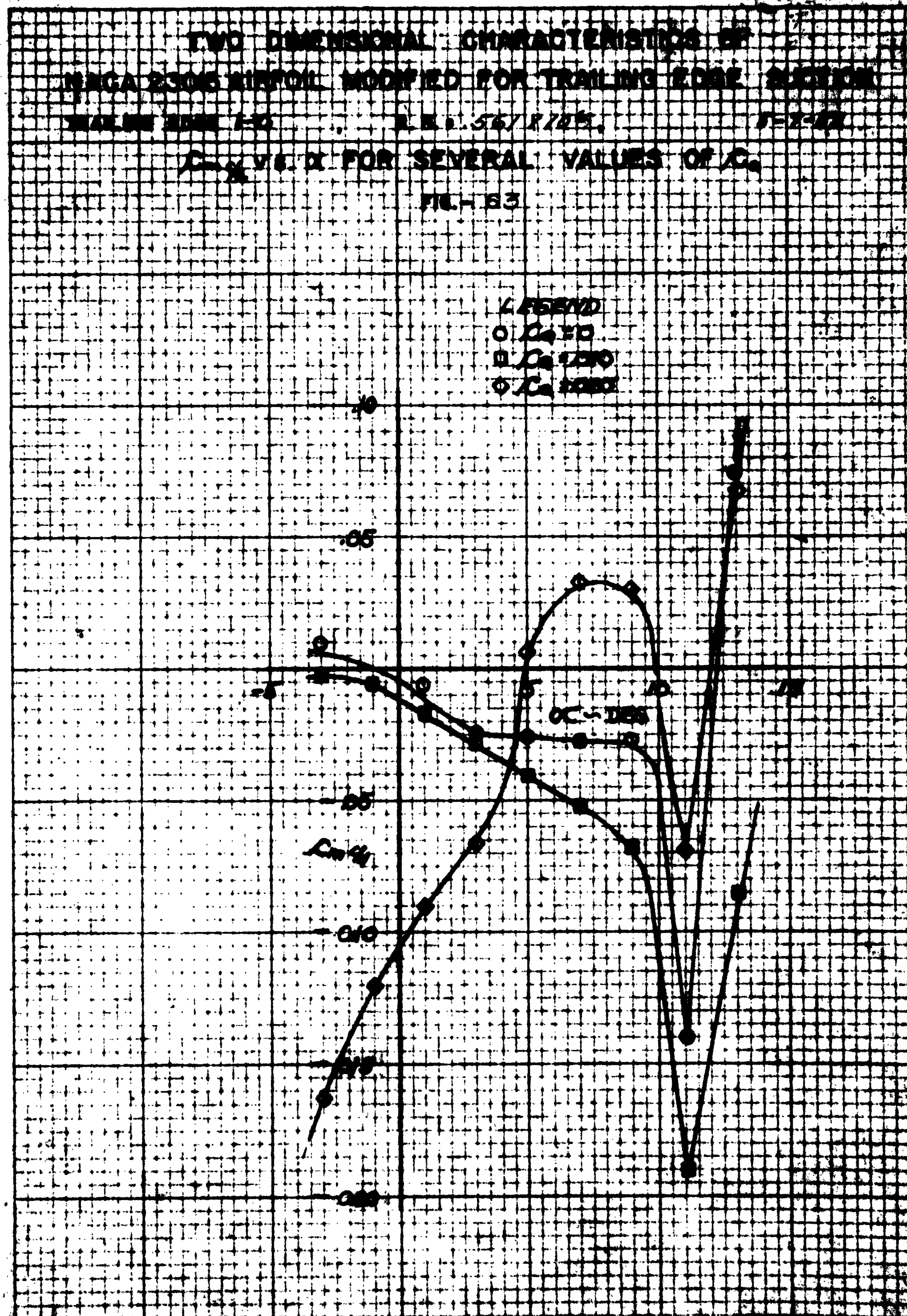

TWO DIMENSIONAL CHARACTERISTICS OF
AIRFOIL MODIFIED FOR TRAILING EDGE SUCTION
R.N. = .561 X 10^6
VS. α FOR SEVERAL VALUES OF
LEGEND
.10
.05
-.05
-.10
-.15
-.20
α ~ DEG

FIG.- 63

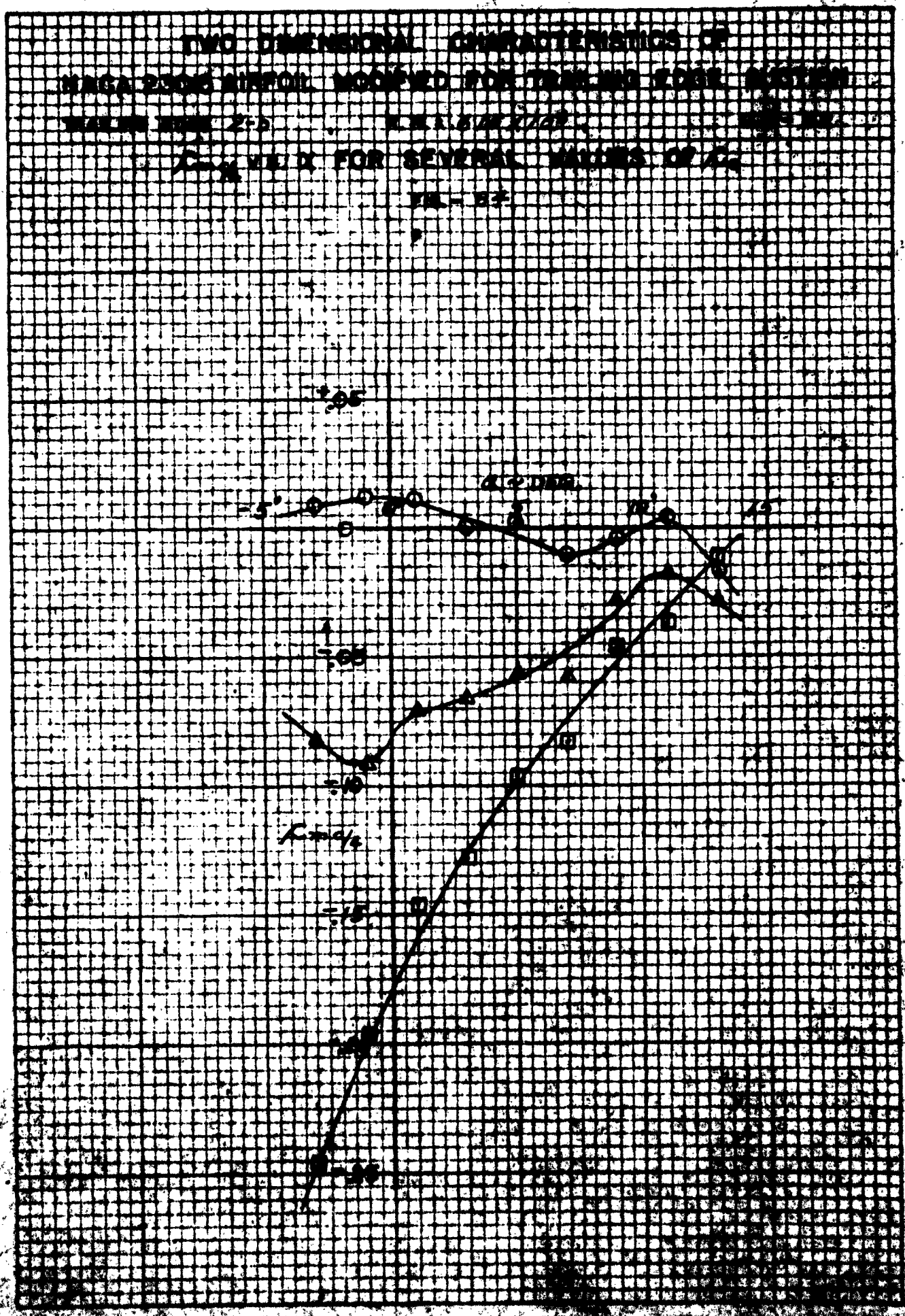

TWO DIMENSIONAL CHARACTERISTICS OF
NACA 23016 AIRFOIL MODIFIED FOR TRAILING EDGE SUCTION

TRAILING EDGE S-V . R.N. = 1.595 X 10⁶ . [illegible]

$C_{m_{c/4}}$ VS. α FOR SEVERAL VALUES OF C_Q

FIG. – 65

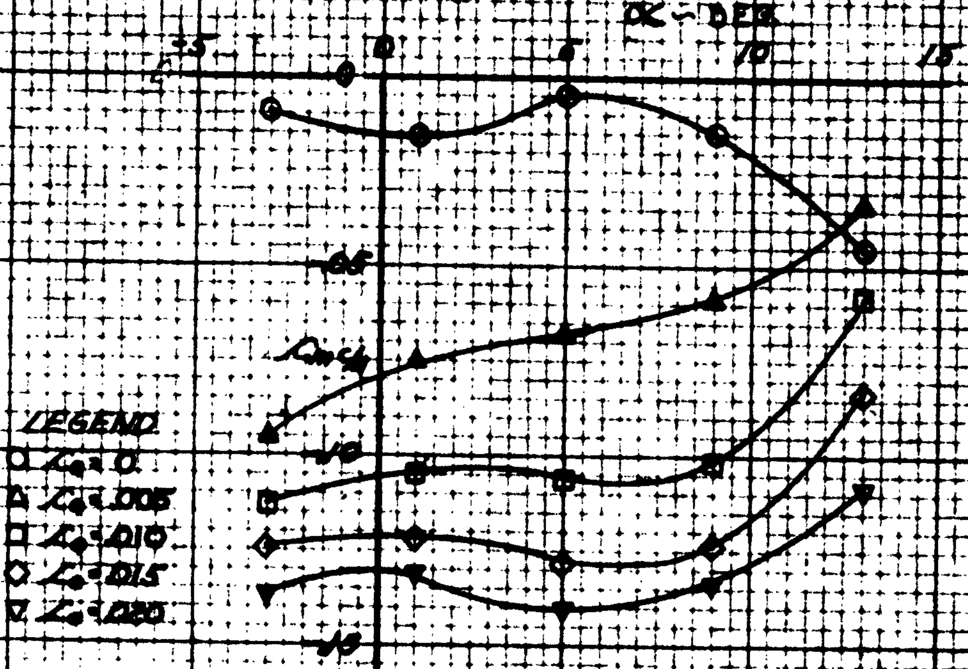

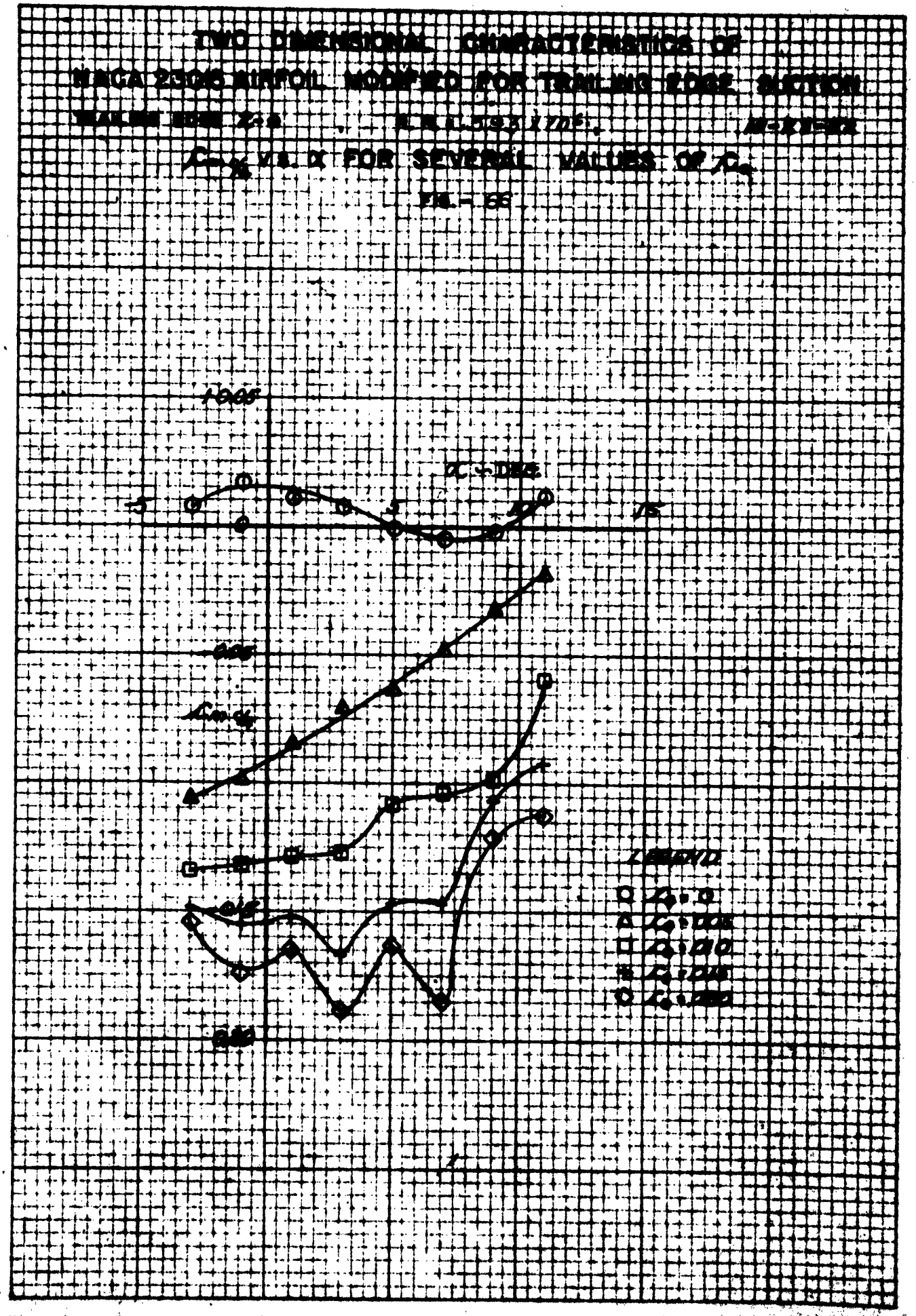
TWO DIMENSIONAL CHARACTERISTICS OF
NACA 23012 AIRFOIL MODIFIED FOR TRAILING EDGE SECTION
C_l - α VS. α FOR SEVERAL VALUES OF β_e
FIG. - 66
1.0
C_l
α - DEG.
LEGEND

TWO DIMENSIONAL CHARACTERISTICS OF NACA 23015 AIRFOIL MODIFIED FOR TRAILING EDGE SUCTION

TRAILING EDGE 1-F R.N. = 6.4 X 10⁶ 10-1-52

$C_{m\,c/4}$ vs. α FOR SEVERAL VALUES OF C_Q

FIG. - 167

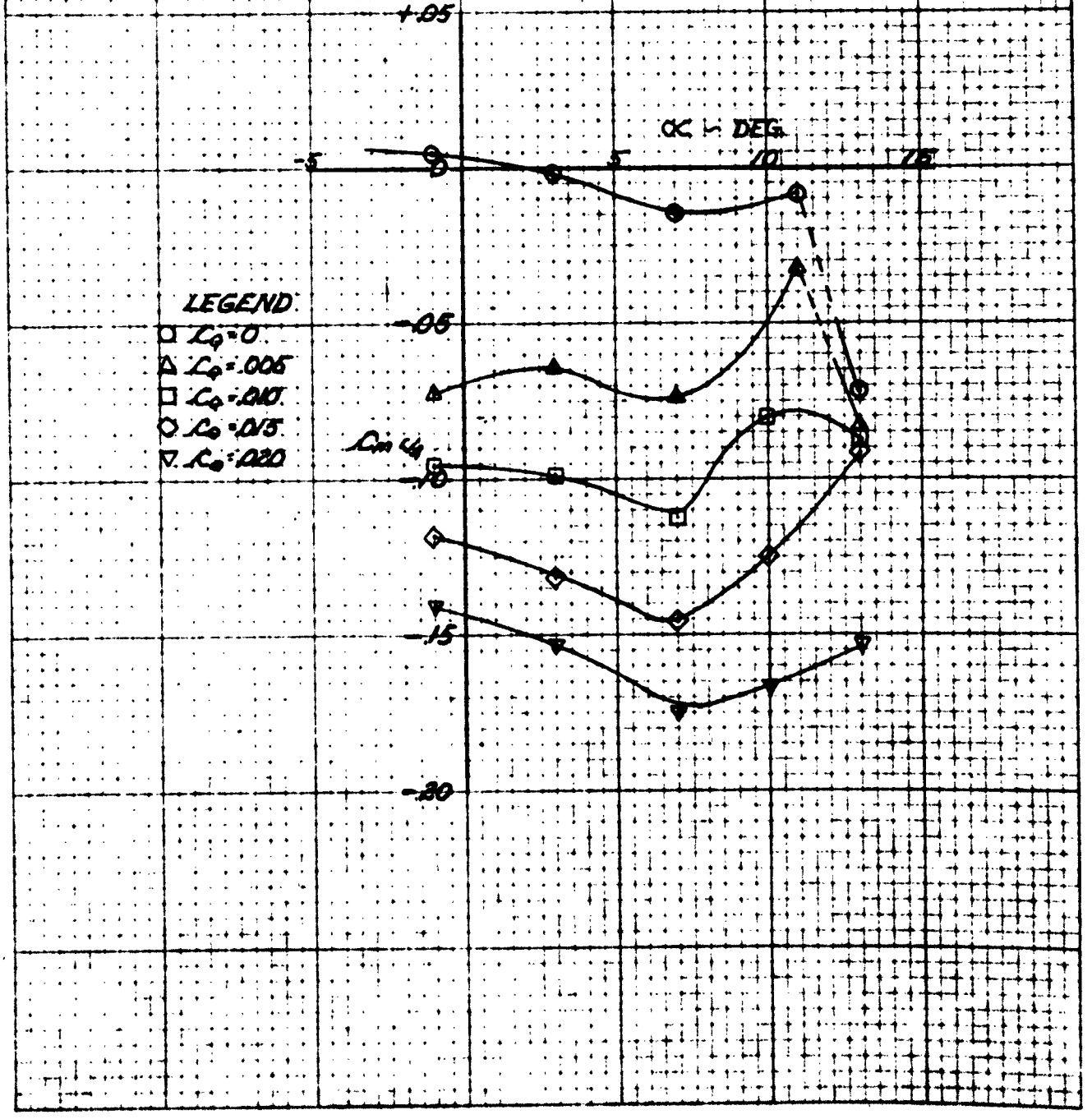

TWO DIMENSIONAL CHARACTERISTICS OF
NACA 23015 AIRFOIL MODIFIED FOR TRAILING EDGE SUCTION
TRAILING EDGE 5-B, R.N. = 6.0 × 10^5

$C_{m_{c/4}}$ VS. α FOR SEVERAL VALUES OF C_Q

FIG. – 123

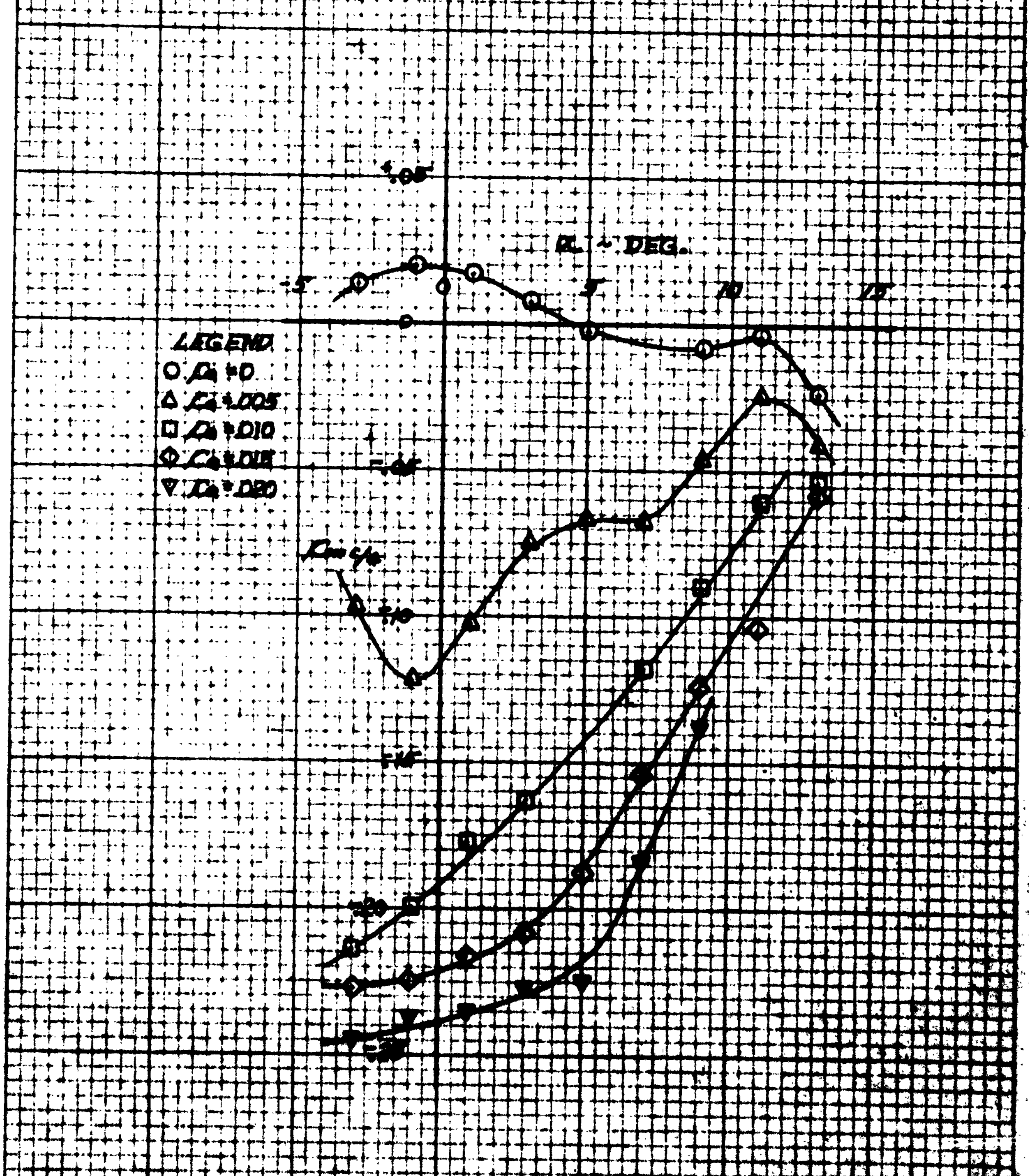

TWO DIMENSIONAL CHARACTERISTICS OF
NACA 2306 AIRFOIL MODIFIED FOR TRAILING EDGE SUCTION
TRAILING EDGE $\delta = 2$ . . . R.N. 1,680,000 . . . M = .17

$C_{L_{max}}$ VS. α FOR SEVERAL VALUES OF C_q

FIG. - 69

α - DEG

-5 0 5 10 15

C_L

$C_{L_{max}}$

LEGEND
□ $C_q = 0$
△ $C_q = .004$
○ $C_q = .008$

TWO DIMENSIONAL CHARACTERISTICS OF NACA 23015 AIRFOIL MODIFIED FOR TRAILING EDGE SUCTION

TRAILING EDGE 1-9 , R.N. = .625 X 10⁶ , 4-17-53

$C_{m_{c/4}}$ vs. α FOR SEVERAL VALUES OF C_q

FIG. - 70

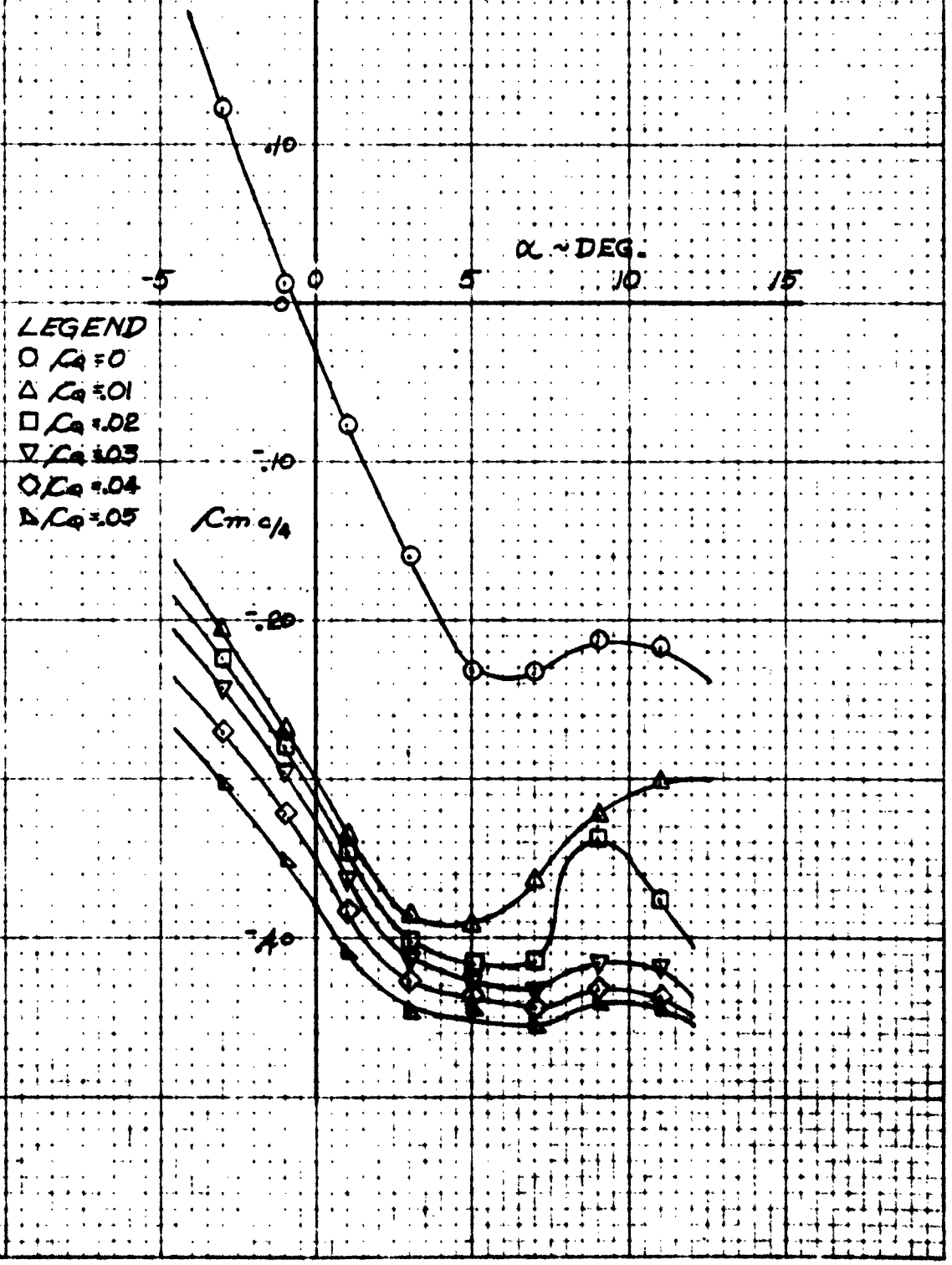

TWO DIMENSIONAL CHARACTERISTICS OF
NACA 2305 AIRFOIL MODIFIED FOR TRAILING EDGE SUCTION

TRAILING EDGE: 7-a, RN. = .690 x 10^6, DATE: 3-11-53

C_p VS. α FOR SEVERAL VALUES OF C_q

FIG. 21

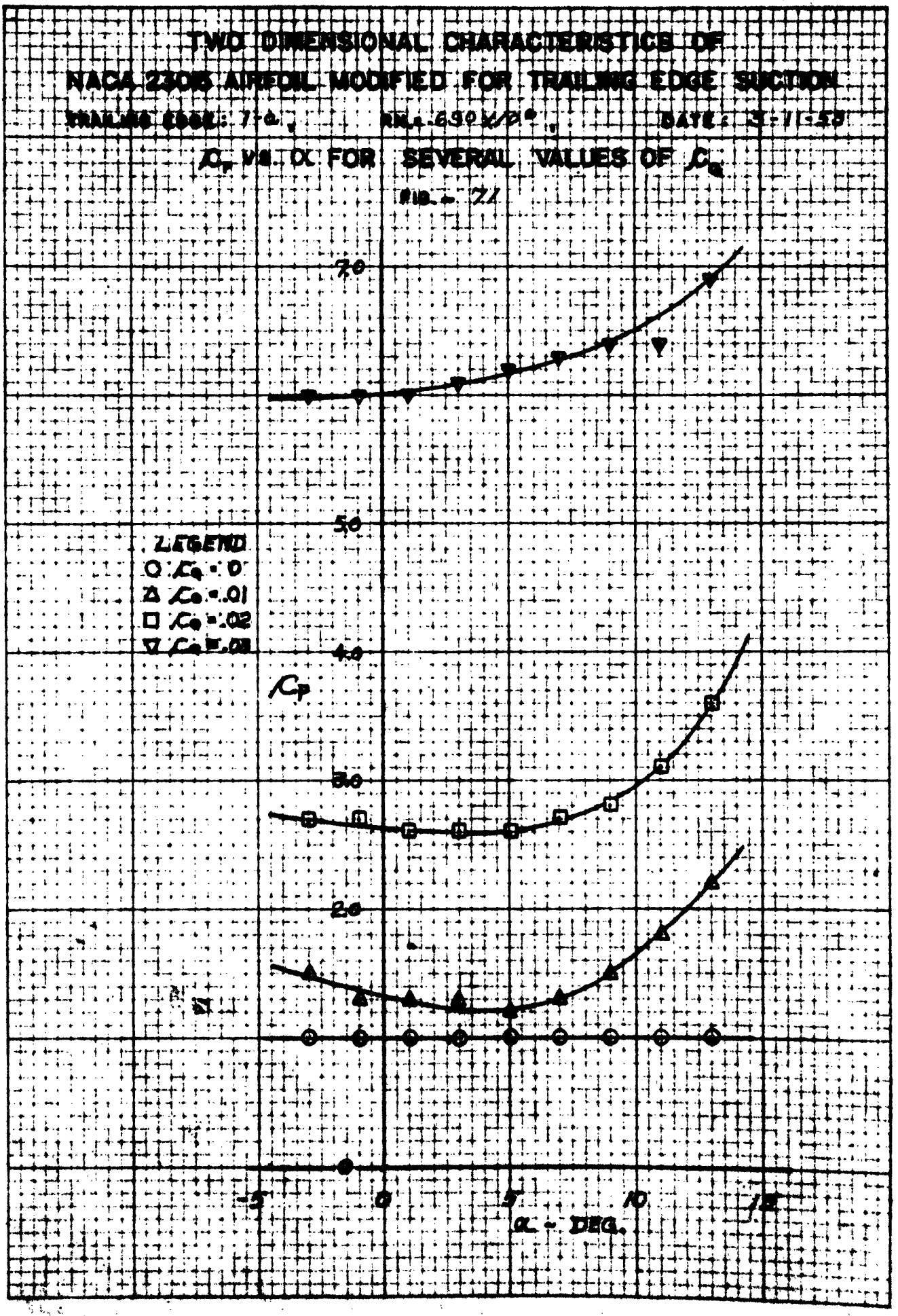

KEUFFEL & ESSER CO.
10 X 10 to the inch

TWO DIMENSIONAL CHARACTERISTICS OF NACA 23015 AIRFOIL MODIFIED FOR TRAILING EDGE SUCTION

TRAILING EDGE: 1-h, RN. = .647X10⁶, DATE: 12-31-52

C_p VS. α FOR SEVERAL VALUES OF C_q

FIG. - 72

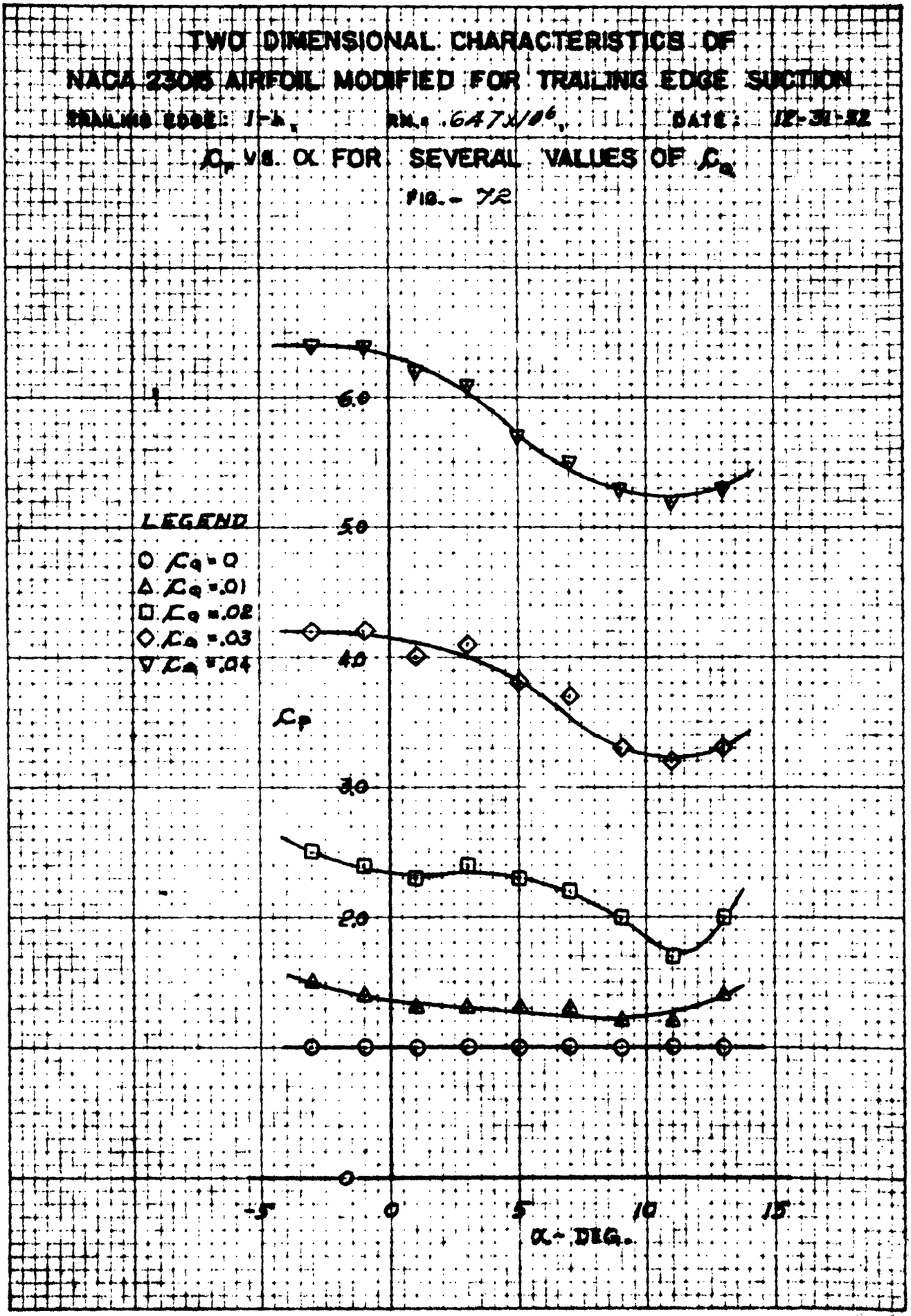

TWO DIMENSIONAL CHARACTERISTICS OF NACA 23015 AIRFOIL MODIFIED FOR TRAILING EDGE SUCTION

TRAILING EDGE: $I-C_q$ RN. 5.61×10^6, DATE: 2-16-53

C_p vs. α FOR SEVERAL VALUES OF C_q

FIG. - 73

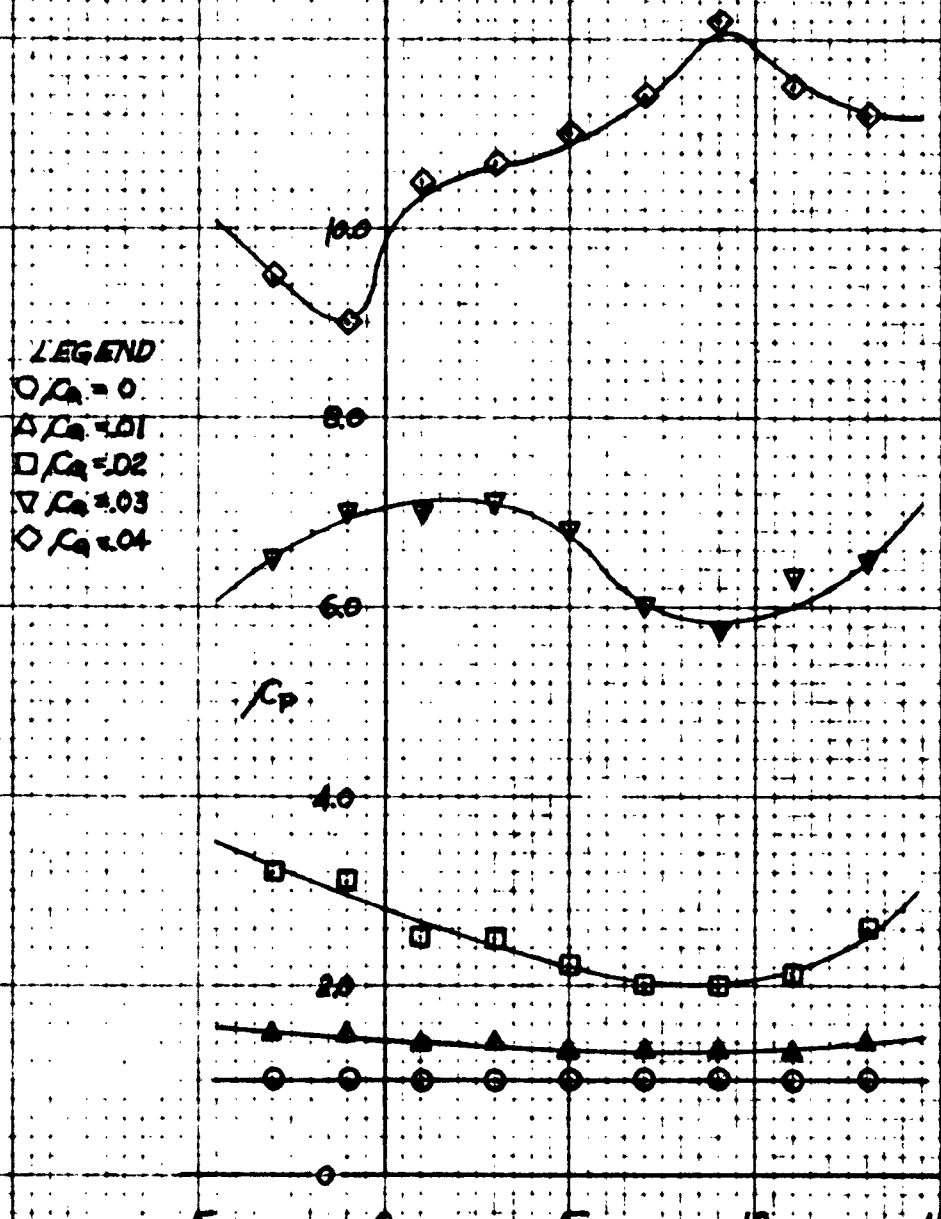

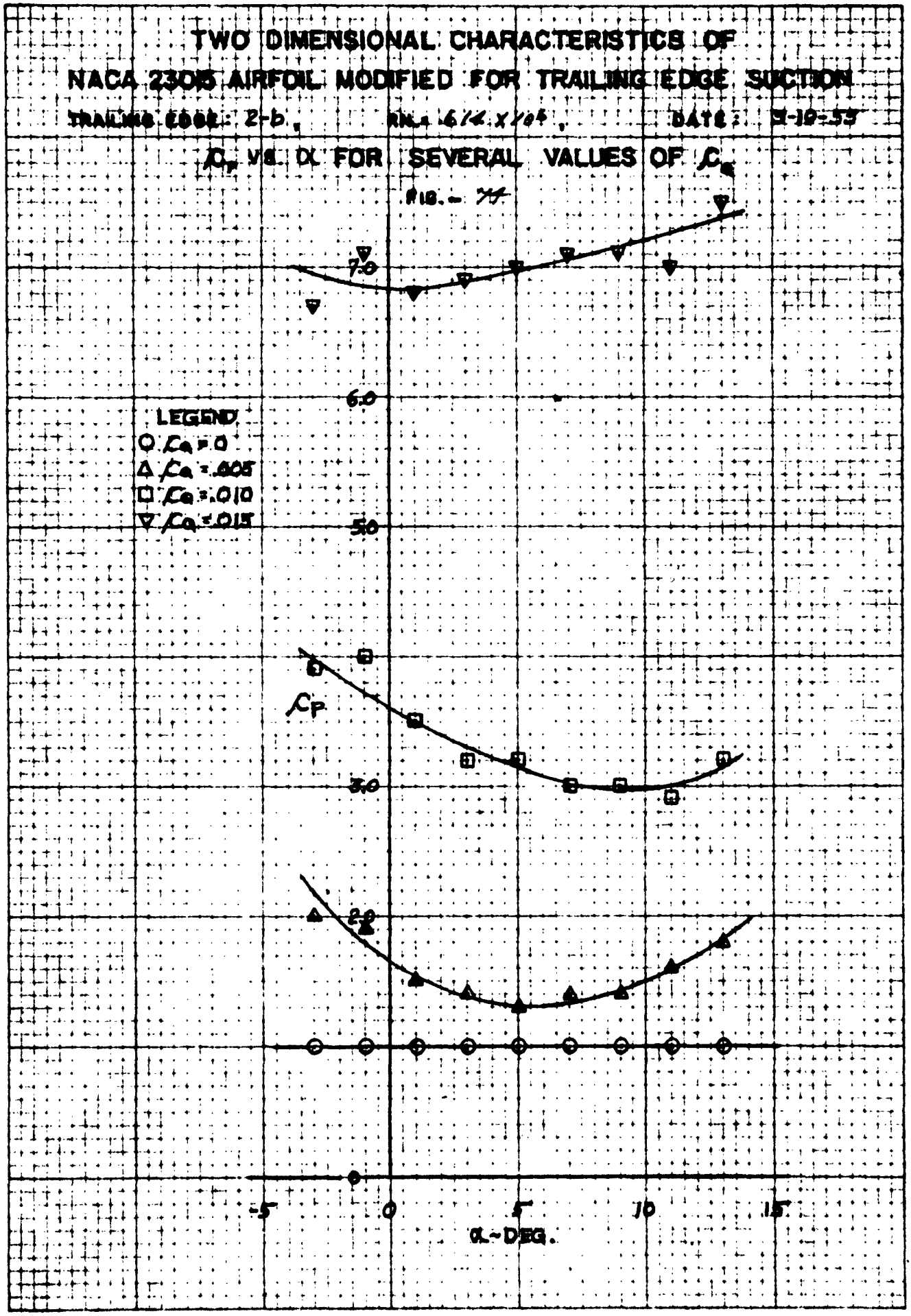
TWO DIMENSIONAL CHARACTERISTICS OF
NACA 23015 AIRFOIL MODIFIED FOR TRAILING EDGE SUCTION
TRAILING EDGE: 2-b, RN = .614 X 10⁶, DATE: 11-19-53
C_p VS. α FOR SEVERAL VALUES OF C_q
FIG. - 14
LEGEND
○ $C_q = 0$
△ $C_q = .005$
□ $C_q = .010$
▽ $C_q = .015$
7.0
6.0
5.0
4.0
3.0
2.0
C_p
-5
0
5
10
15
α - DEG.

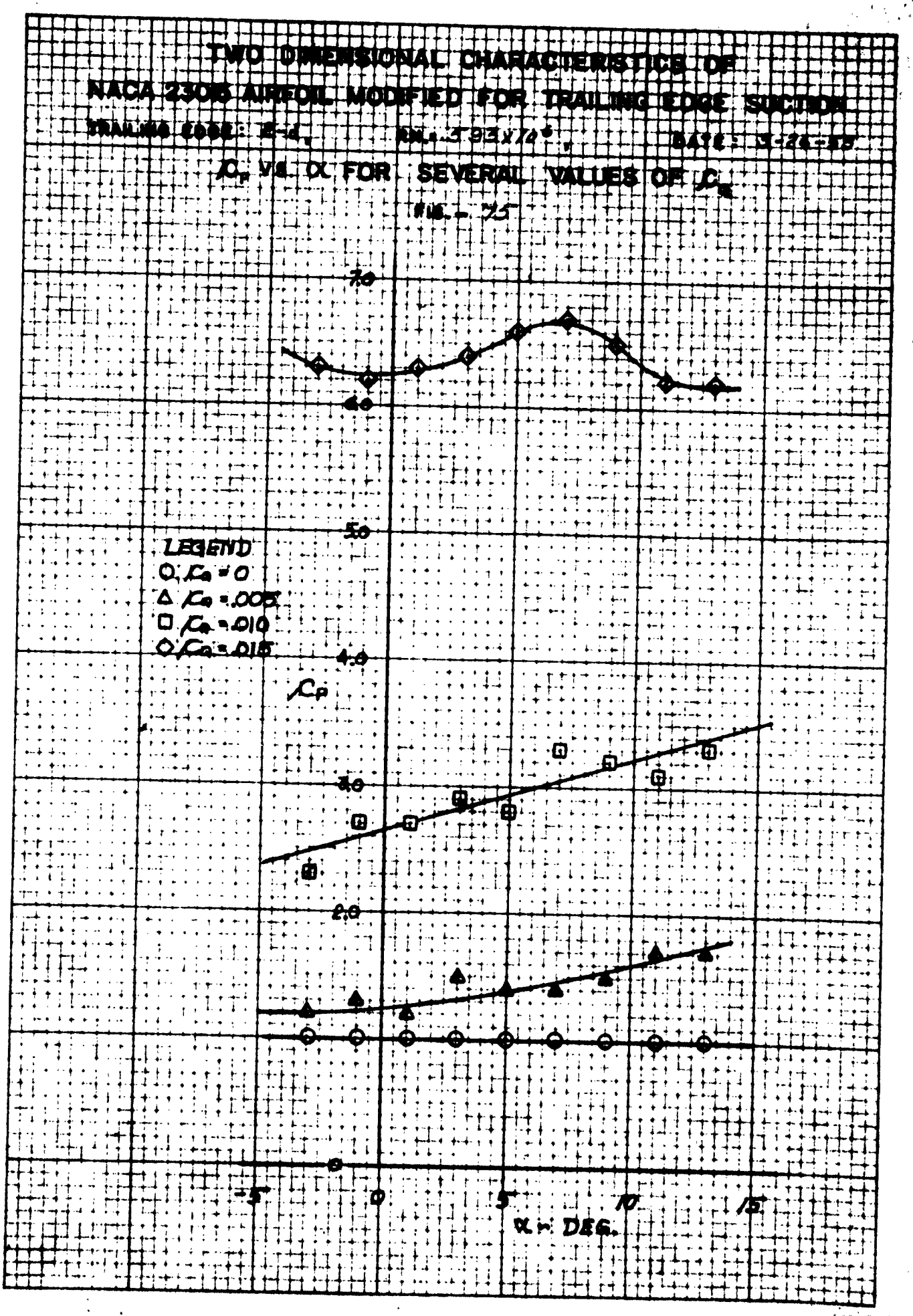
TWO DIMENSIONAL CHARACTERISTICS OF
NACA 2306 AIRFOIL MODIFIED FOR TRAILING EDGE SUCTION
TRAILING EDGE: 2-d, R.N. = 793 x 10^3, DATE: 3-26-35
C_p vs. α FOR SEVERAL VALUES OF C_q
FIG. - 25
LEGEND
○ $C_q = 0$
△ $C_q = .005$
□ $C_q = .010$
◇ $C_q = .015$
C_p
7.0
6.0
5.0
4.0
3.0
2.0
-5
0
5
10
15
α = DEG.

TWO DIMENSIONAL CHARACTERISTICS OF NACA 2305 AIRFOIL MODIFIED FOR TRAILING EDGE SUCTION

TRAILING EDGE: 2-Θ_t RN.= 5.93×10^6 DATE: 3-17-55

C_P VS. α FOR SEVERAL VALUES OF C_Q

FIG.- 76

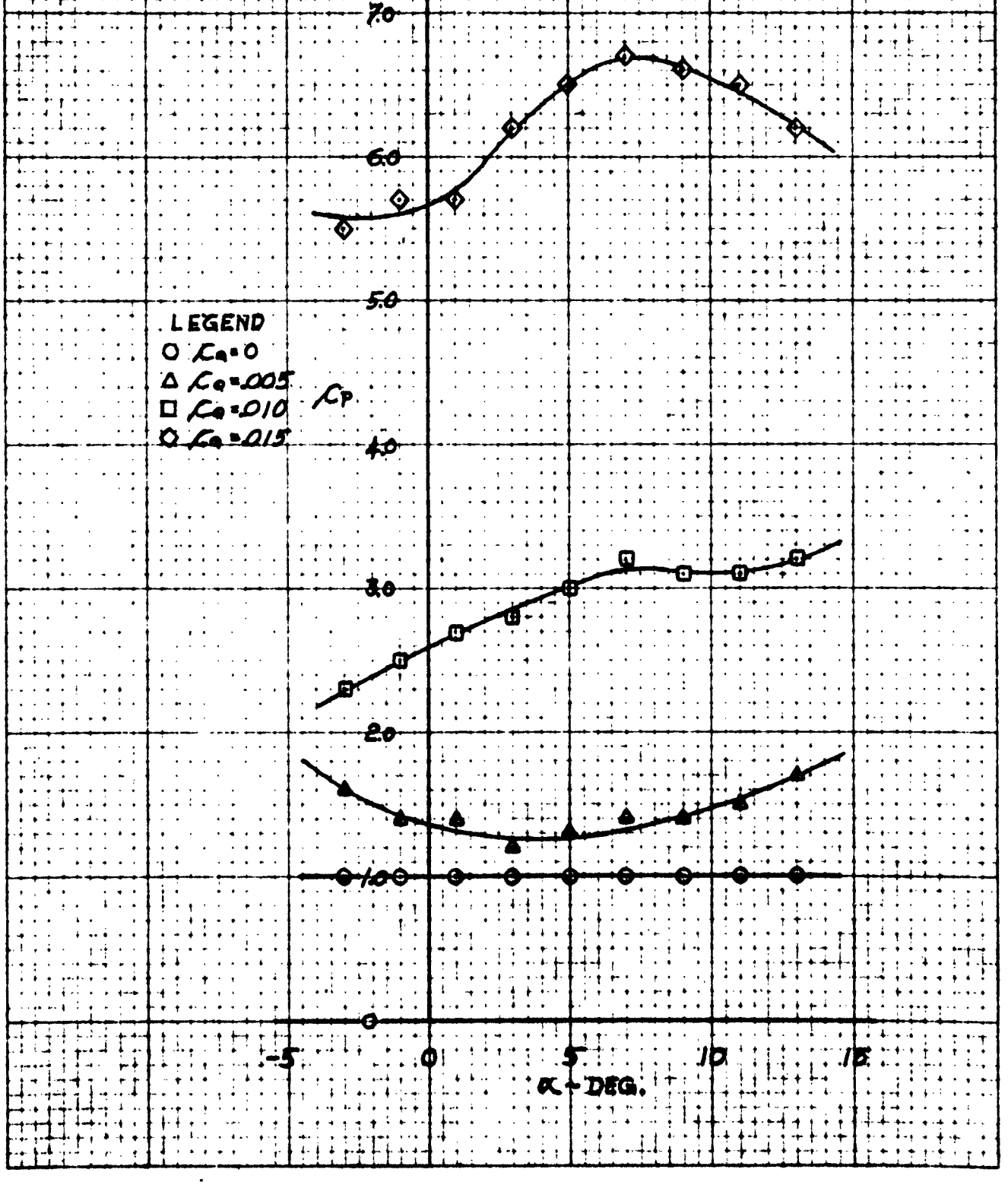

NACA 23015 AIRFOIL — ACTERISTICS OF TRAILING EDGE SUCTION

TRAILING EDGE: 4-f, RN. 6, DATE: 2-18-55

C_p vs. α FOR SEVERA VALUES OF C_q

FIG. - 7.7

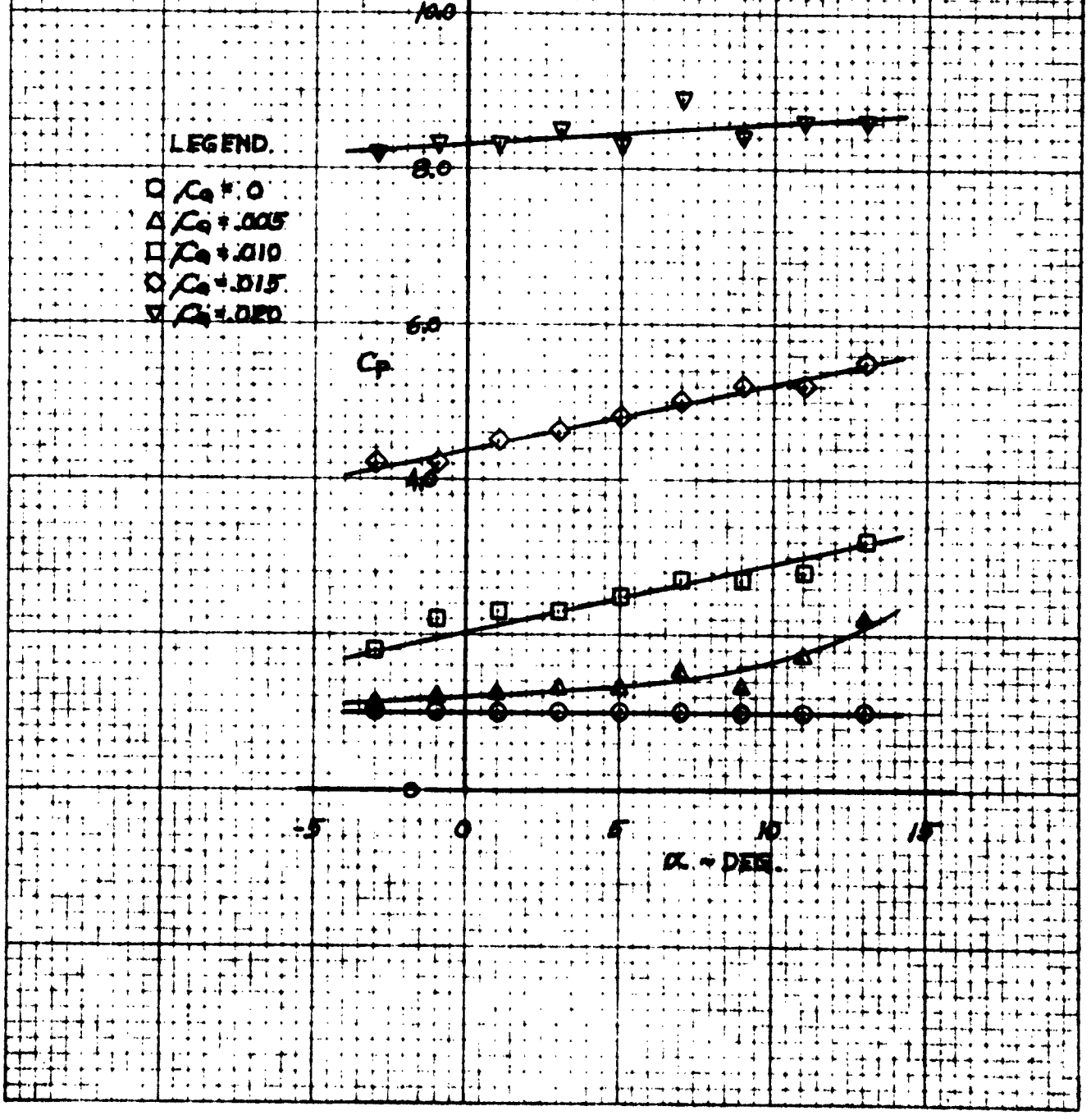

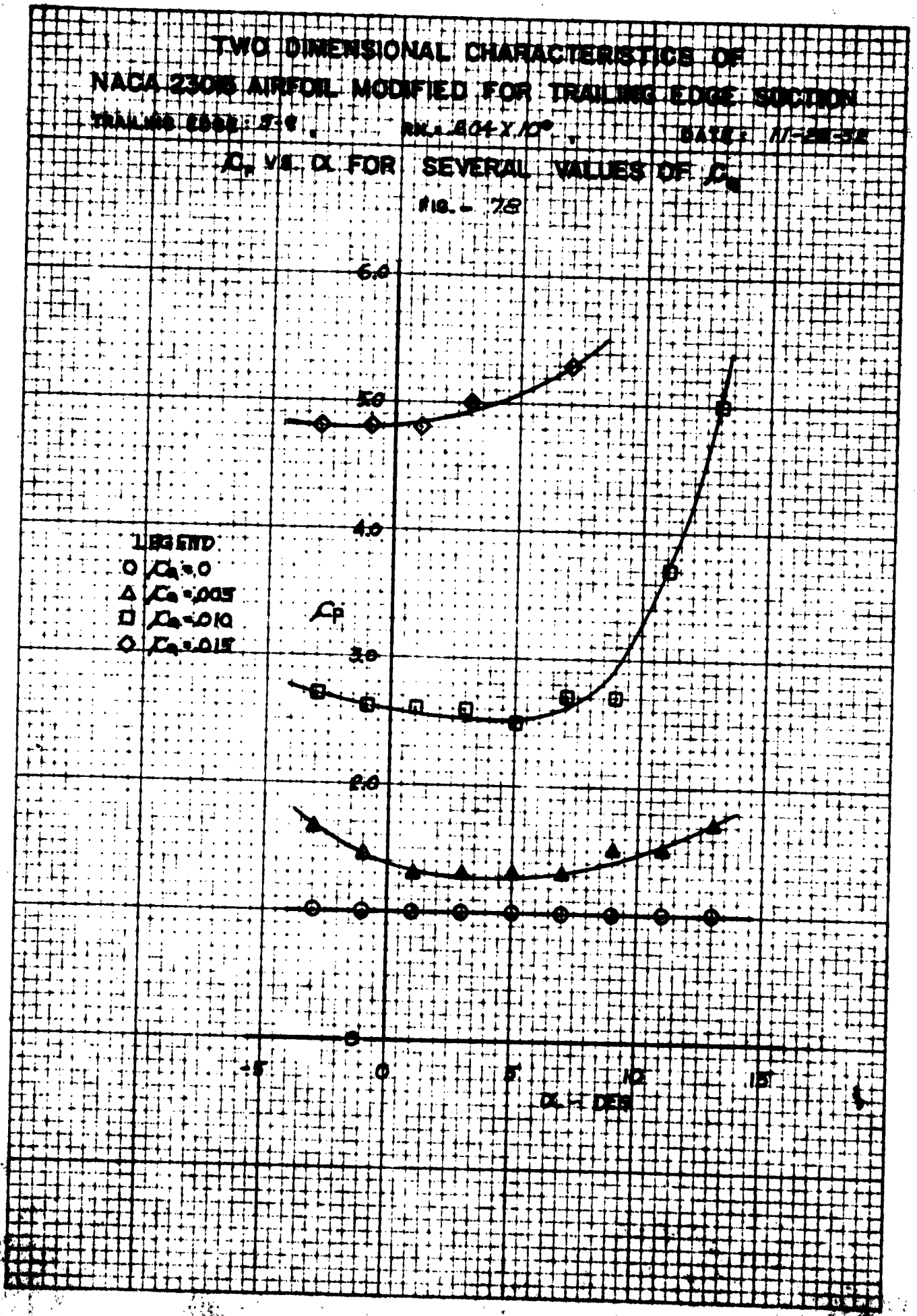
TWO DIMENSIONAL CHARACTERISTICS OF
NACA 23015 AIRFOIL MODIFIED FOR TRAILING EDGE SUCTION
TRAILING EDGE : 5% c
RN = .604 X 10^6
DATE : 11-28-52
C_p VS. α FOR SEVERAL VALUES OF C_q
FIG. - 7B
6.0
5.0
4.0
3.0
2.0
LEGEND
○ C_q = 0
△ C_q = .005
□ C_q = .010
◇ C_q = .015
C_p
-5°
0
5°
10°
15°
α - DEG

TWO DIMENSIONAL CHARACTERISTICS OF NACA 23015 AIRFOIL MODIFIED FOR TRAILING EDGE SUCTION

TRAILING EDGE: d-a, RN = .690 X 10^6, DATE: 2-2-53

C_p VS. α FOR SEVERAL VALUES OF C_q

FIG. - 79

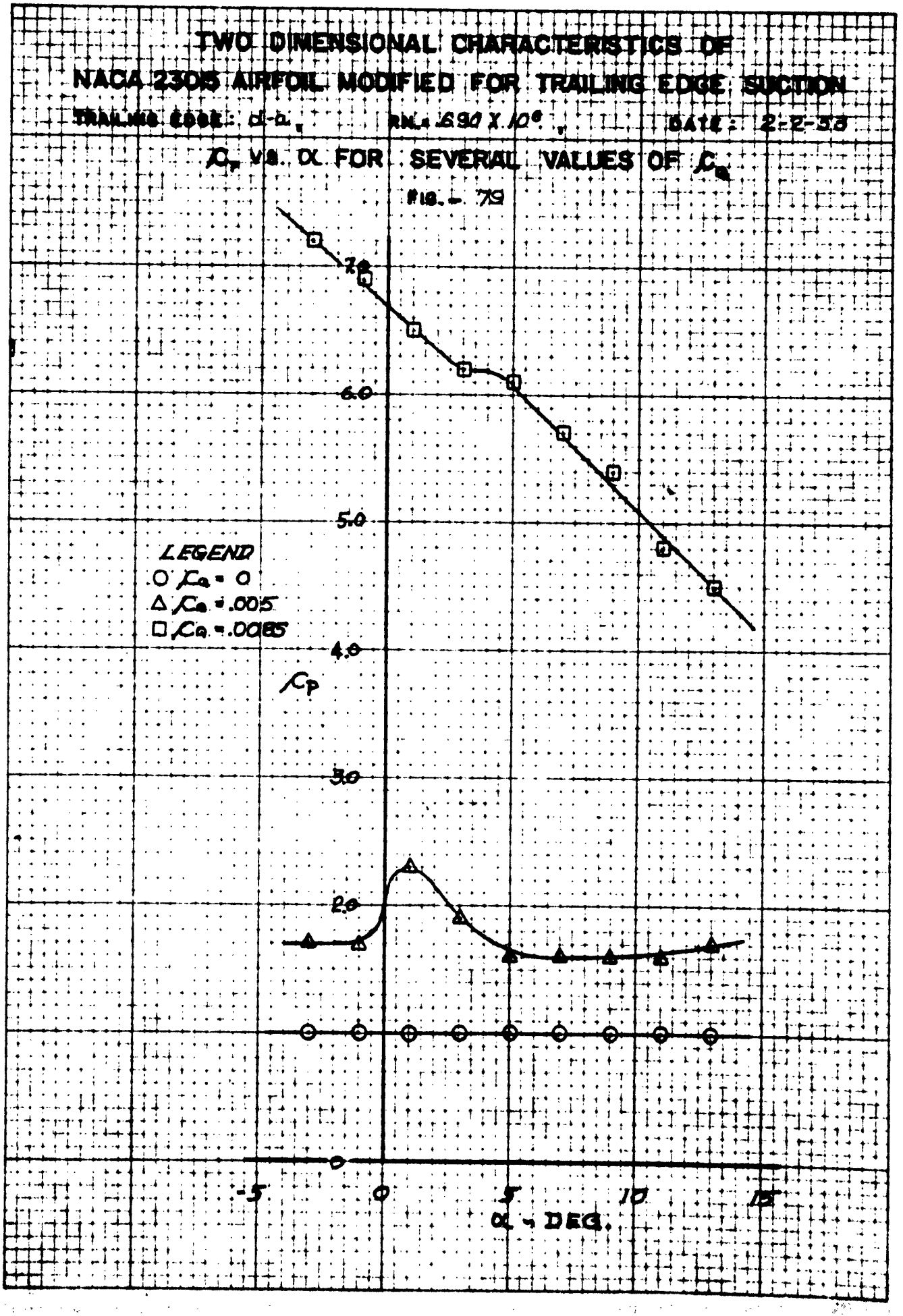

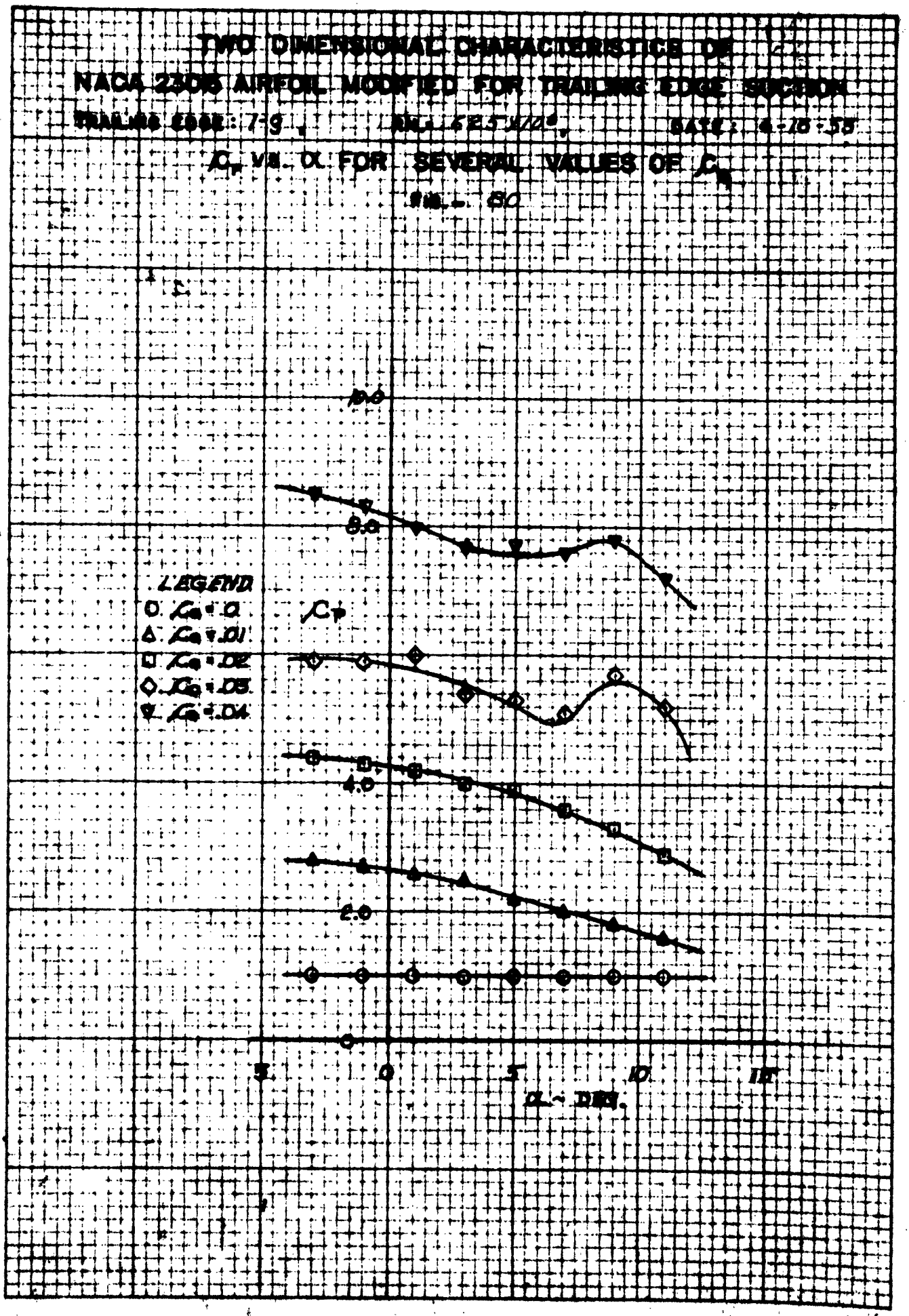
TWO DIMENSIONAL CHARACTERISTICS OF
NACA 2306 AIRFOIL MODIFIED FOR TRAILING EDGE SUCTION
TRAILING EDGE: 7-9
DATE: 4-16-35
C_p VS. α FOR SEVERAL VALUES OF C_q
FIG. 60
LEGEND
C_q = .0
C_q = .01
C_q = .02
C_q = .03
C_q = .04
C_p
10.0
8.0
4.0
2.0
-5
0
5
10
15
α ~ DEG.

SUMMARY OF LIFT CHARACTERISTICS OF THE VARIOUS CONFIGURATIONS TESTED

BASE AIRFOIL: NACA 23015, R.N. = .65×10⁶, 6-30-53

FIG. ~ 81

LEGEND
▲ α = 1°
▼ α = 7°
● α = 13°

1-a 1-b 1-c 1-g 2-b 2-d 2-e 4-f 5-e d-a

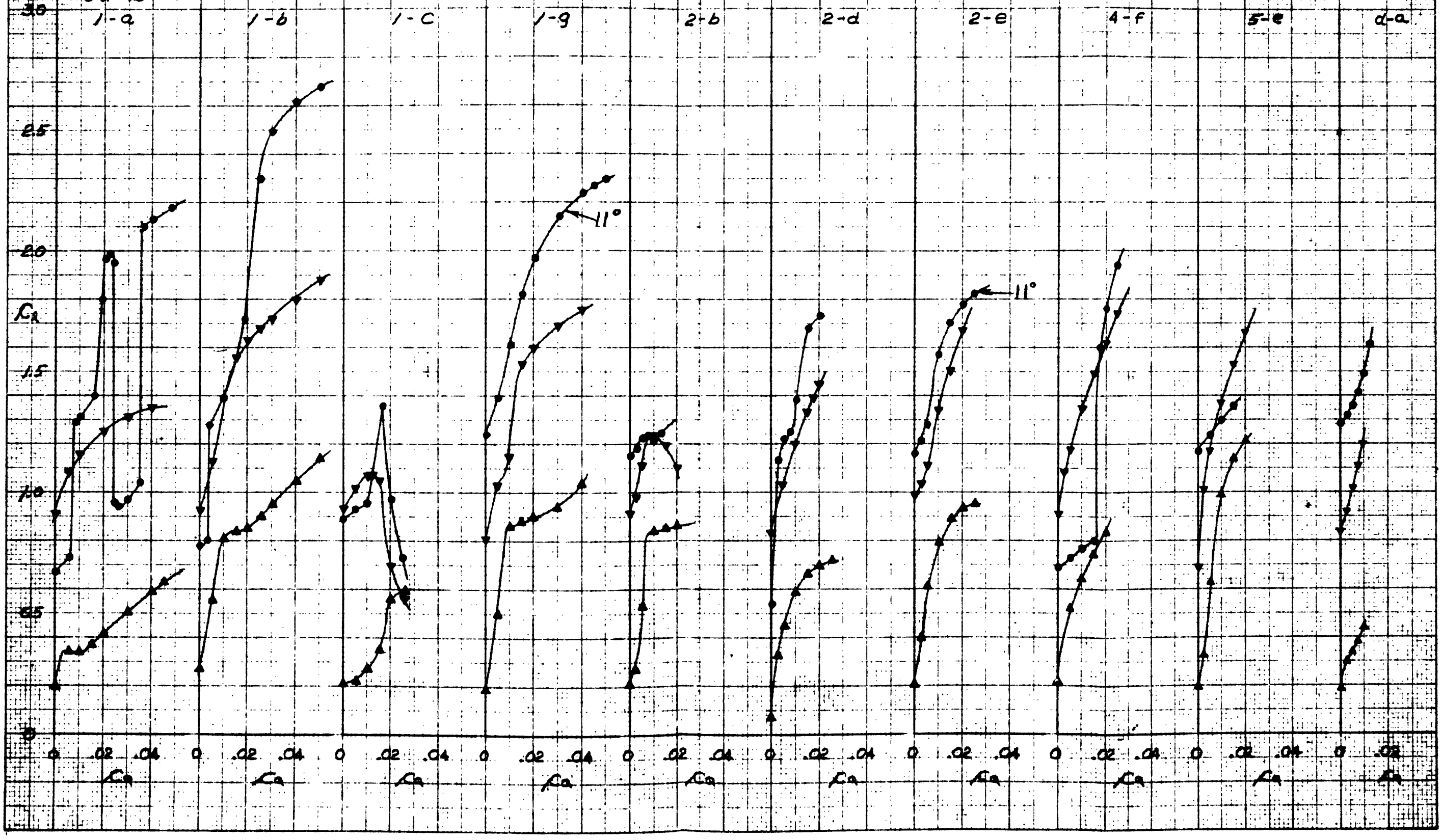

Summary Of Drag Characteristics Of The Various Configurations Tested

Base airfoil NACA 23015, R.N. = .65x10⁶, 6-30-53

Fig. ~ 8R

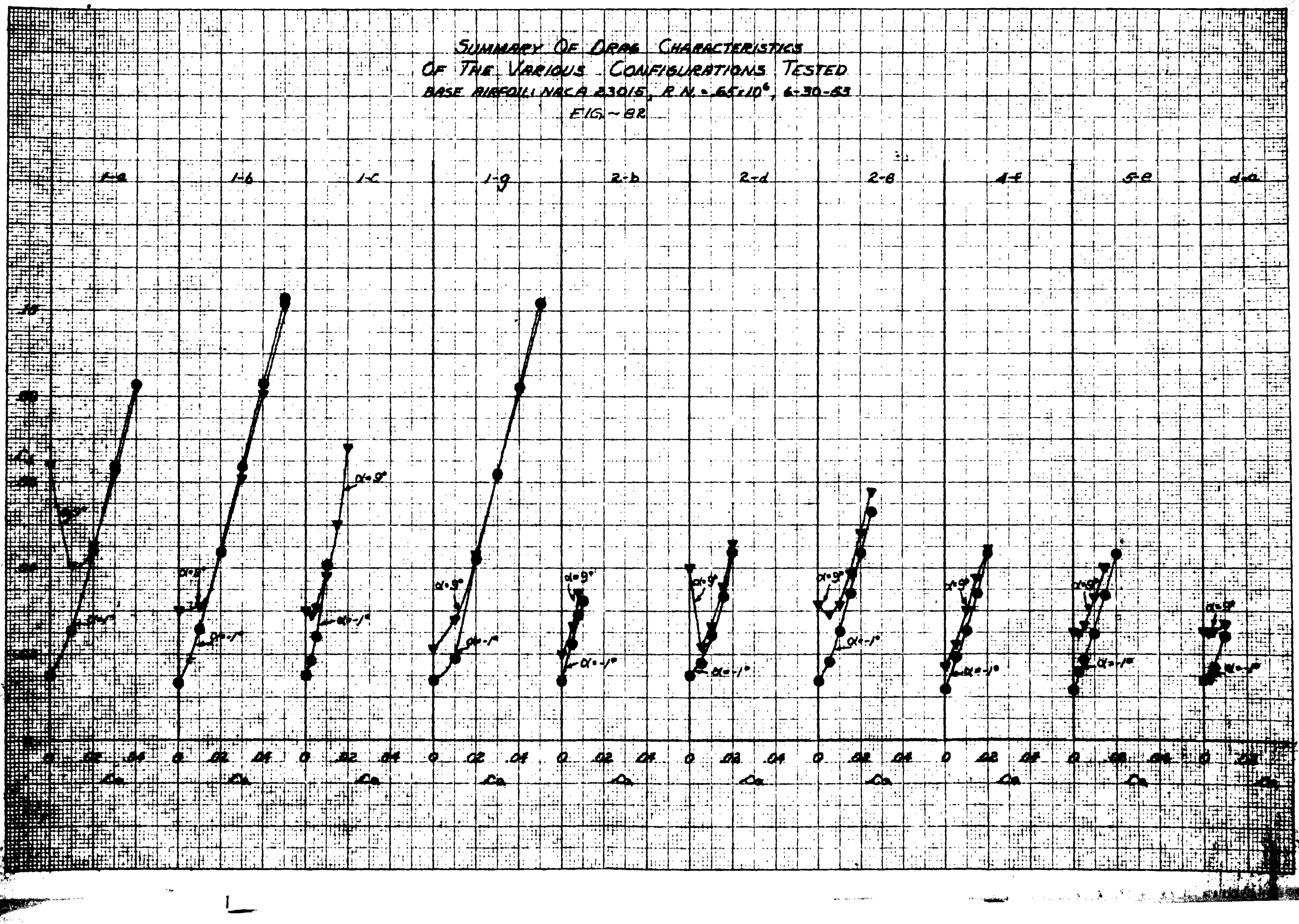

SUMMARY OF PITCHING MOMENT CHARACTERISTICS
OF THE VARIOUS CONFIGURATIONS TESTED
BASE AIRFOIL: NACA 23015, R.No. 6.5x10⁶, 6-30-53
FIG. ~ 83

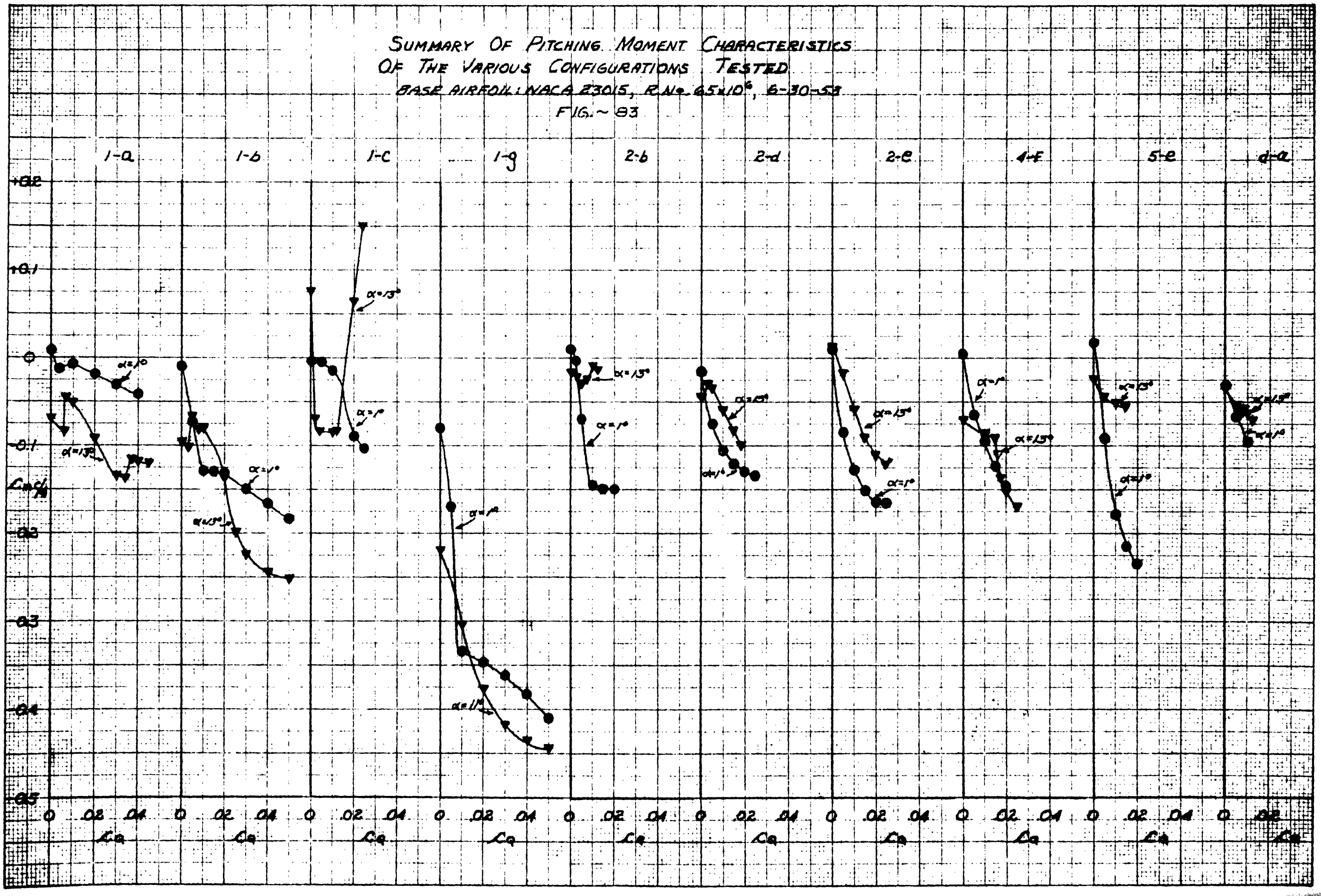

SUMMARY OF THE C_p CHARACTERISTICS OF THE VARIOUS CONFIGURATIONS TESTED

BASE AIRFOIL: NACA 23105, $R_N = .65 \times 10^6$, 6-30-53

FIG. ~ 84

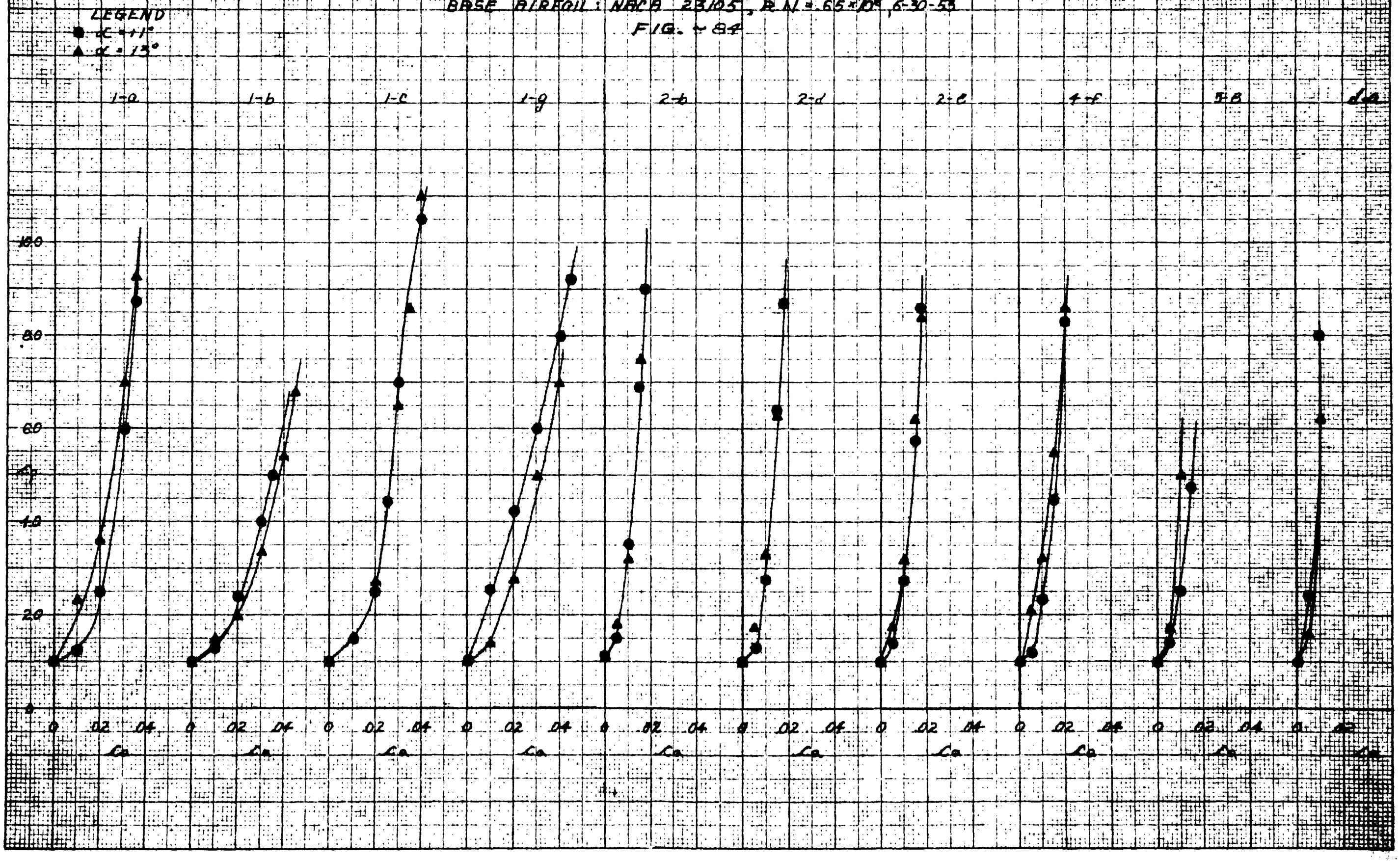

COMPARISON OF TOTAL DRAGS FOR THE SEVERAL CONFIGURATIONS

$R_N = 0.65 \times 10^6$ — ANGLE OF ATTACK = 9° — DATE: 8-20-53

TOTAL DRAG = (PROFILE DRAG + EQUIVALENT POWER DRAG), MOMENTUM DRAG ASSUMED TO BE ZERO, AND DUCT EFFICIENCIES ASSUMED AT 100%

FIG. 84-a

0.3 — 1-a — 1-b — 1-c — 2-b — 2-d — 2-e — 4-f — 5-e — d-a — f-a

--- REFERS TO C_L OF UNMODIFIED AIRFOIL AT SAME ANGLE OF ATTACK

0.2

C_d

0.1

0 0.2 0.4 0 0.2 0.4 0 0.2 0.4 0 0.2 0.4 0 0.2 0.4 0 0.2 0.4 0 0.2 0.4 0 0.2 0.4 0 0.2 0.4 0 0.2 0.4

C_L

Summary Of Lift Characteristics Of The Variable Trailing Edge Tested

Base Airfoil: NACA 23015, $R_N = .65 \times 10^6$, T-1-53

Fig. ~85

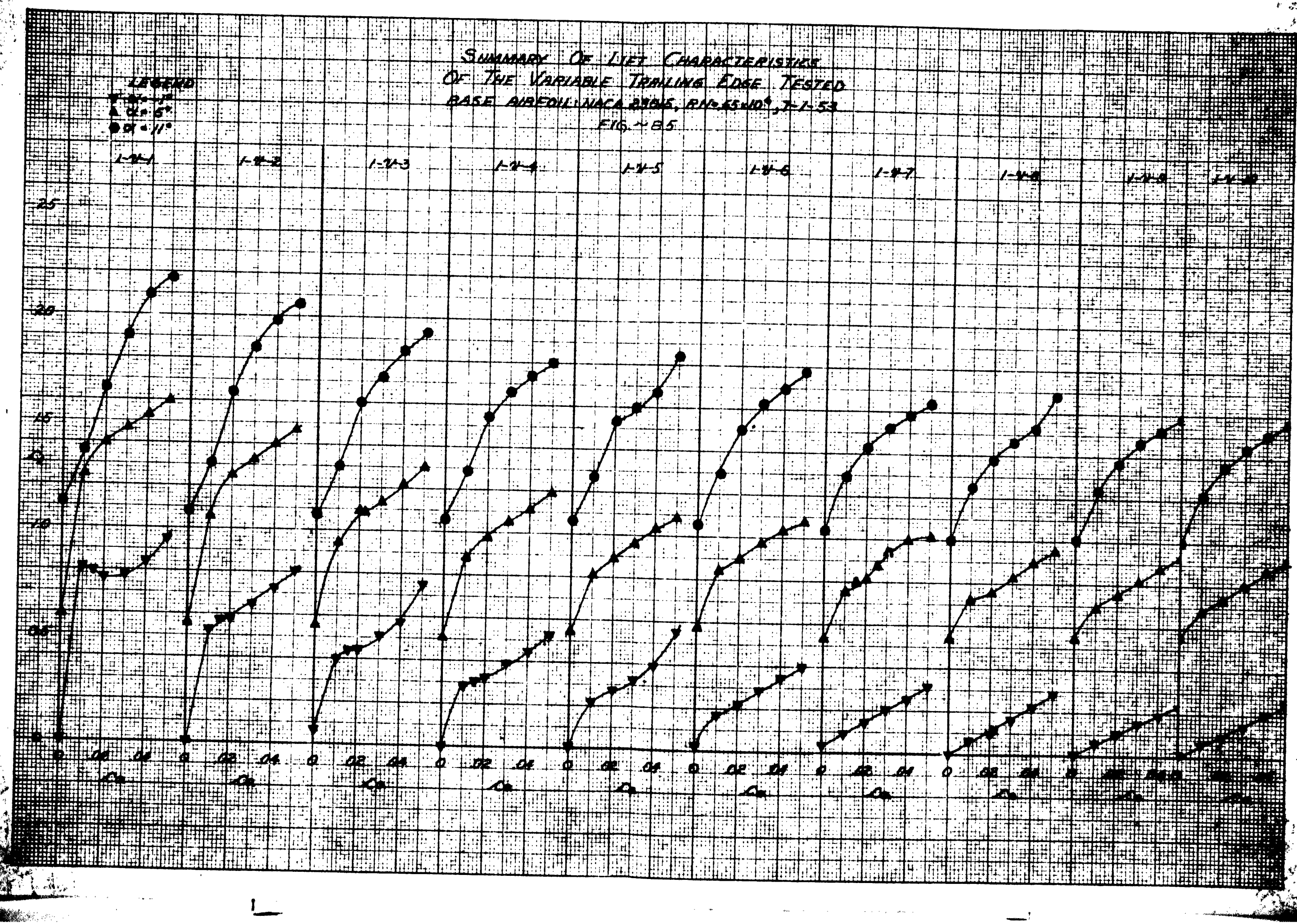

IDEALIZED EXPLANATION OF BOUNDARY LAYER REMOVAL

FIG 86

SIGNIFICANT BOUNDARY LAYER ON BOTH SURFACES

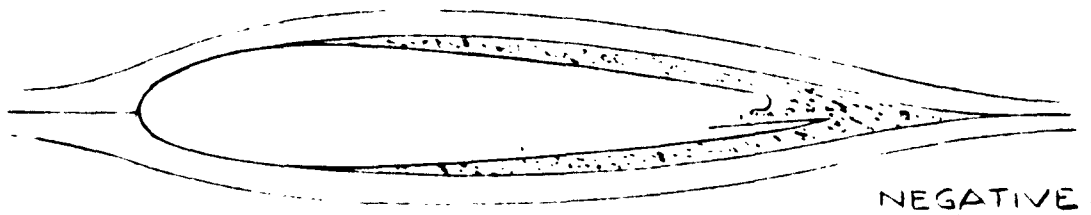

NEGATIVE α
$C_Q = 0$

BOUNDARY LAYER REMOVED FROM UPPER SURFACE
BUT STILL EXISTING ON LOWER SURFACE

NEGATIVE α
$C_Q = A$

BOUNDARY LAYER ESSENTIALLY REMOVED FROM BOTH SURFACES

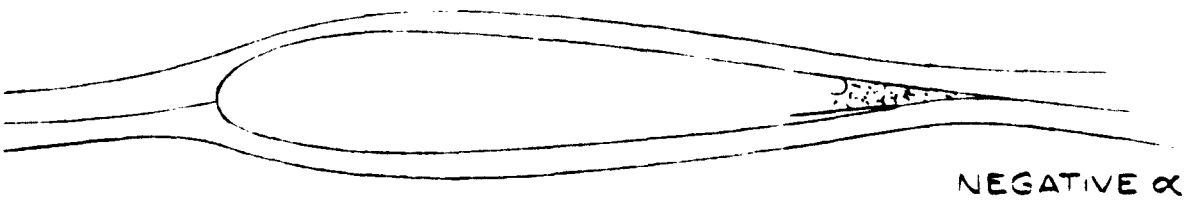

NEGATIVE α
$C_Q = B$

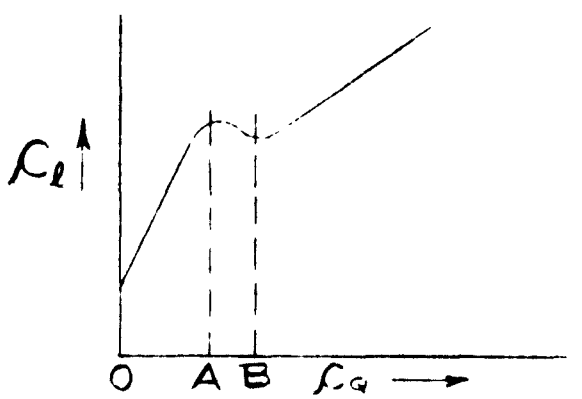

TWO DIMENSIONAL CHARACTERISTICS OF TRAILING EDGE 1-V
RELATING ΔC_l TO GEOMETRY PARAMETER a/c

RN =

DATE:

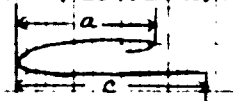

FIG - 87

$\alpha = 0°$ $\alpha = 5°$ $\alpha = 10°$

LEGEND
- ○ $C_a = .01$
- △ " .02
- □ " .03
- ◇ " .04
- ▽ " .05

ΔC_l

1.0
.8
.6
.4
.2
0

.85 .89 .93 a/c

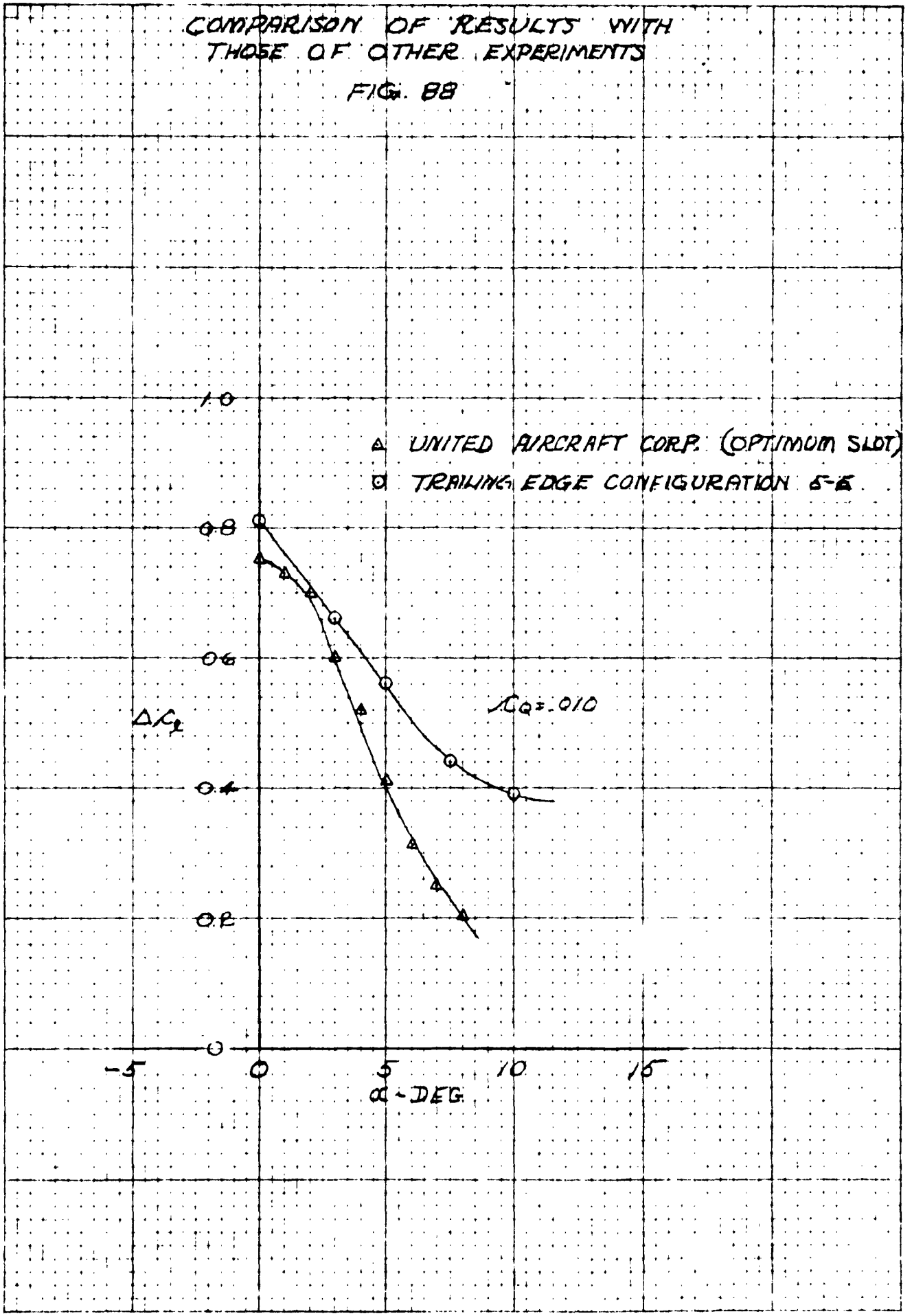
COMPARISON OF RESULTS WITH THOSE OF OTHER EXPERIMENTS
FIG. 88
UNITED AIRCRAFT CORP. (OPTIMUM SLOT)
TRAILING EDGE CONFIGURATION 6-6
C_Q=.010
ΔC_l
1.0
0.8
0.6
0.4
0.2
0
-5
0
5
10
15
α - DEG.

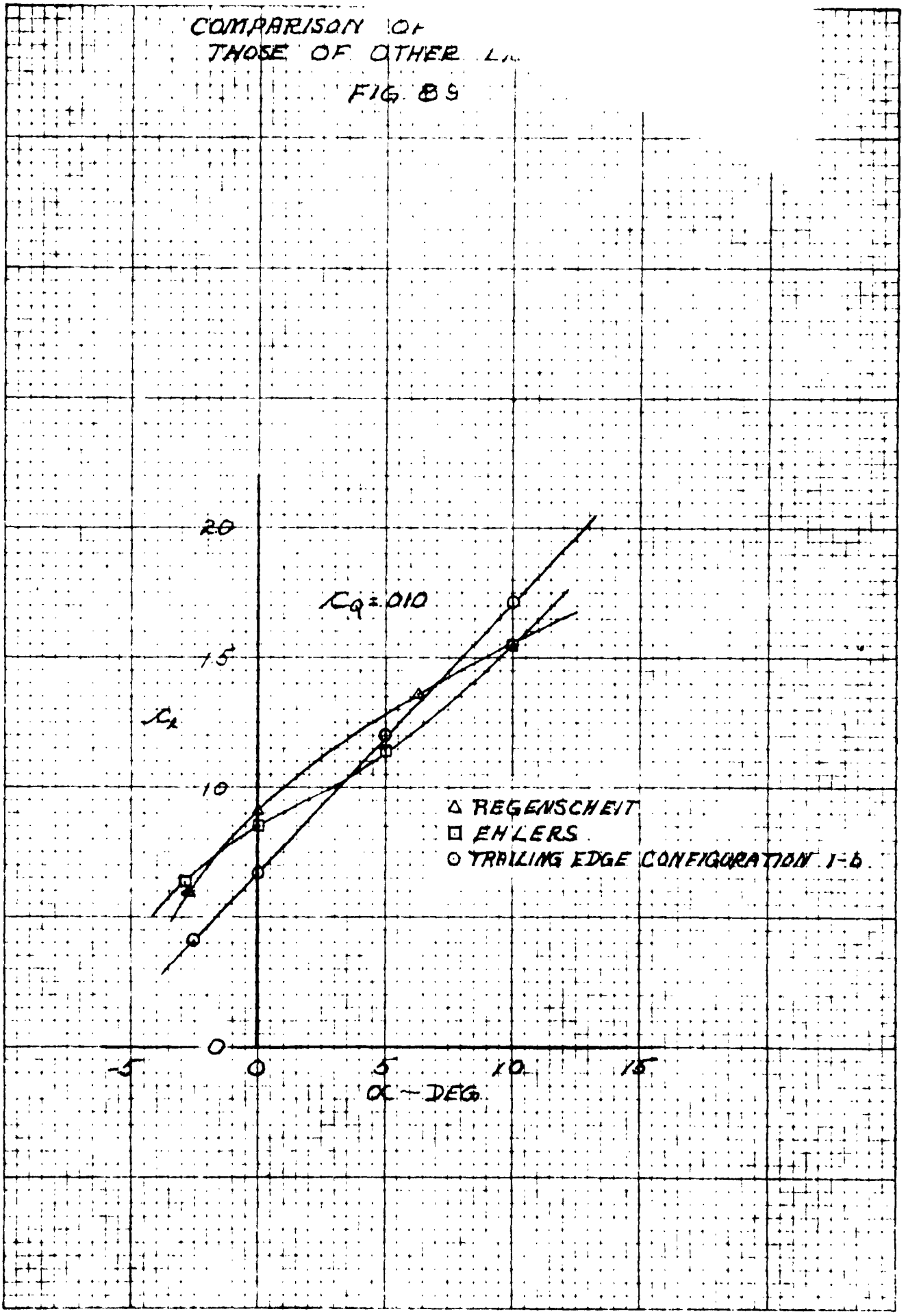
COMPARISON OF
THOSE OF OTHER
FIG. 89
20
15
10
0
C_L
$C_Q = .010$
△ REGENSCHEIT
□ EHLERS
○ TRAILING EDGE CONFIGURATION 1-b
-5
0
5
10
15
α - DEG.